COLLEGE DOCTORAL PAYS DE LA LOIRE

ED EDUCATION, COGNITION, LANGAGES, INTERACTIONS, SANTE

Nantes Université

# THESE DE DOCTORAT

NANTES UNIVERSITE

ECOLE DOCTORALE N° 603
*Education, Cognition, Langages, Interactions, Santé*
Spécialité : Sciences et Techniques des Activités Physiques et Sportives

Par
**Raphaël HAMARD**

## A neuromechanical approach to the coordination between the human *gastrocnemius medialis* and *gastrocnemius lateralis* muscles

**Thèse présentée et soutenue à Nantes, le 12 avril 2023**
**Unité de recherche : UR 4334, Laboratoire Motricité, Interactions, Performance**

**Rapporteurs avant soutenance** :

| | |
|---|---|
| Guillaume RAO | Professeur des Universités, Aix-Marseille Université |
| Olivier SEYNNES | Professor, Norwegian school of sport sciences |

**Composition du Jury :**

| | | |
|---|---|---|
| Président : | | |
| Examinateurs : | Guillaume RAO | Professeur des Universités, Aix-Marseille Université |
| | Olivier SEYNNES | Professor, Norwegian school of sport sciences |
| | Emilie SIMONEAU | Professeur des Universités, Université Polytechnique Hauts-de-France |
| | Vincent MARTIN | Professeur des Universités, Université Clermont Auvergne |
| Dir. de thèse : | François HUG | Professeur des Universités, Université Côte d'Azur |
| Co-dir. de thèse : | Taylor DICK | Senior Lecturer, The University of Queensland |
| | Jeroen AELES | Assistant Professor, Vrije Universiteit Brussel, Bruxelles |

## ABSTRACT

The three muscles within the *triceps surae* have large differences in volume, architecture and activation, resulting in distinct muscle behaviors. Even though the functional differences between the biarticular *gastrocnemii* and the monoarticular *soleus* are well established, the differences between the *gastrocnemius medialis* and *gastrocnemius lateralis* have been much less studied. Furthermore, the large majority of previous research on these two muscles has focused on their ankle plantar flexion role. Therefore, their behavior during their secondary role, i.e. knee flexion, remains poorly understood. The aim of this thesis was to provide a deeper understanding of muscle coordination between the *gastrocnemius medialis* and *gastrocnemius lateralis*. We used an approach that combines experimental measures and basic muscle modelling to explore muscle coordination across multiple scales, from the individual motor unit to the whole muscle. In this thesis, we performed three studies in healthy young individuals. Study #1 aimed to determine whether the differences in muscle activation between the *gastrocnemius medialis* and *gastrocnemius lateralis* during walking translate into differences in their contractile behavior. Study #2 aimed to estimate the individual distribution of force within the *gastrocnemii* during walking using an experimentally-informed Hill-type model. Study #3 aimed to determine whether the neural control of the *gastrocnemius medialis* and *gastrocnemius lateralis* differs between knee flexion and ankle plantar flexion. Four main results can be derived from this thesis. First, these two muscles have distinct neuromuscular behavior during walking. This results in a much higher production of force in the *gastrocnemius medialis* compared to the *gastrocnemius lateralis*. Second, our results highlight that a large inter-individual variability can be observed across multiple scales of the production of movement. Third, we present an approach combining subject-specific experimental measures with a muscle model that aims to consider the individual variability in muscle coordination. Fourth, the neural strategies to control the *gastrocnemius medialis* and *gastrocnemius lateralis* are robust across knee flexion and ankle plantar flexion. Together, these results demonstrate that the two muscles are distinct at the neural and biomechanical level, which results in distinct force outputs and highly inter-individual variable muscle coordination.



## KEYWORDS

B-mode ultrasonography; Hill-type model; Muscle force distribution; Neuromechanics; Surface electromyography; *Triceps surae*.

# PREFACE

The works presented in this PhD thesis result from the collaboration between the Motricité, Interactions, Performance lab from Nantes University and the Dr. Taylor Dick's lab from the University of Queensland. Although the initial project did not go as planned (to the delight of some lab members who found a way to make fun of me), I have always found great support from the people I have met. Using these few lines, I will try to express my gratitude to everyone who, from near or far, contributed to keep me happy and fulfilled during this PhD thesis.

First, I would like to thank the **Pr. Rao** and the **Pr. Seynnes** for accepting to review this PhD thesis. I am looking forward to reading your feedback. I extend my gratitude to **Pr. Simoneau** and **Pr. Martin** for accepting to be part of the jury. I am sincerely glad and honored to have your expert opinion on this work.

I also would like to express my sincere gratitude to the dream team of supervisors that I had during this PhD thesis. I realize that I am extremely lucky to have such supervisors during the three and a half years. You have once again demonstrated incredible professional and human qualities during the writing of this PhD thesis. I do not think that a PhD student can expect quicker and more comprehensive feedbacks from PhD supervisors. You deserved much more than these few line for the time, the patience and the support you have had for me. I learned so much by your side and I would like to sincerely thank you for everything you have done for me.

**Taylor**, I imagine that, given my English level, I was not always easy to follow. Yet, you have always been benevolent and positive with me. I thank you for all these exchanges where you transmitted to me part of your impressive expertise. One of the only regrets of this PhD thesis is not having been able to come in Brisbane to work with you. I hope we are going to fix that soon !

In a few year, I will likely remember **Jeroen** as the first Belgian that I met who did not like beer. It might be better this way because, when you drink you tend to propose crazy challenges and you include me in it. Sorry but I am still convinced that 30 km of rowing on an unsuitable boat is not a good idea. More seriously, I admire the passion that you have for sciences and research. I thank you for your always positive attitude and your great availability.

**François**, despite three years spent working under your supervision, I am still impressed by your efficacity. Knowing your proximity to the cycling world, I came to wonder if you did not get doping products from Maxime. You manage to associate all this work with an unwavering good humor which makes it a pleasure to work with you. Your passion and your work are an inspiration to me and, in addition, you have always been a great support for me. I could not have done all this work without you and I owe you a lot. Therefore, I would like to thank you sincerely.

I will move to French in order to thank people from France who have contributed to the smooth running of this PhD. J'aimerais globalement remercier l'ensemble du laboratoire MIP pour l'atmosphère bienveillante et propice au travail qui y règne. Nous avons toujours la possibilité de trouver de l'aide derrière chaque porte, ce qui est particulièrement appréciable pour un doctorant égaré. Un merci spécial à **Val**, **Aurélie**, **Véro** et maintenant **Gwen** pour les soutiens technique et administratif plus que performants !

Un grand merci à **Romain** et **Niki** pour l'aide sur les deux premières études et à **Simon** pour l'aide sur la dernière étude. Je voudrais également remercier les deux membres de mon comité de suivi de thèse, **Antoine** et **Guillaume**, pour leurs conseils tout au long de ces trois ans et demi. J'espère que le suivi du film à suspense « Mobilité en Australie » n'a pas été trop insoutenable pour vous. Notez que, même à la fin du doctorat, j'arrive encore à vous tenir en haleine avec un projet d'étude en Australie… To be continued !

Le laboratoire MIP est le lieu parfait pour réaliser un doctorat. J'ai découvert ce laboratoire en Master avec le commissaire **Bregeon** et son fidèle lieutenant **Archambault**. Je crois que nous pouvons dire que nous avons été très bien accueillis, particulièrement par l'ingénieur serbe à 80% de l'époque, **Doginov'**.

La suite en doctorat n'a pas été moins joyeuse avec une fantastique équipe de doc'. **Emilie**, **Eric**, **Marine** et **Marion**, ce fut un plaisir de pâtisser à vos côtés.

J'aimerais adresser un merci particulier à notre diffuseur officiel de courses de bicyclette, **M. Robin**. Bien que tes conseils vélo ne m'aient pas permis de devenir le nouveau van der Poel (comme tu as pu le constater un vendredi matin sur le terrain de beach du STAPS), j'ai toujours pu compter sur toi pour retrouver mon vélo et rentrer en bonne santé (la plupart du temps).

Je remercie également mon kiné personnel, **Antoine**, que je surcharge de travail. Sans ton expertise clinique, je serais probablement proche de l' « unijambisme ». J'imagine que nos syndromes de l'imposteur vont se manquer une fois que j'aurais quitté le bureau. Continue mon frouf, tu défonces tout !

Mon petit **Ju'**, je crois que je te trouve aussi bon à Matlab que mauvais aux fléchettes. C'est dire quelles considérations j'ai pour tes compétences en programmation. Je n'oublierai pas nos échanges, ton aide et ton attitude toujours positive.

**Jean**, tu l'as fait en 14,51 s ! 14,51 s. Je n'arrive pas à réaliser. Pour moi, ça restera ta performance la plus impressionnante, quoi qu'en pense le monde du triathlon.

**Iris**, championne, j'espère que tu frottes moins dans le peloton que sur les voitures en rentrant de chez **Marc**.

J'ai également une pensée pour la 'new gen' des docs, **Hugo** 'la demie marmule', **Julian** 'la marmule', **Val** 'la stat', **Tit'** 'l'homme tendon' et **Tristan** 'pasd'manip' (désolé, c'est tout ce qui me vient quand je pense à toi) et à tous ceux qui viennent faire leur pause dans le bureau PMU comme **Ricardo**. Vous avez tous grandement contribué au plaisir que j'avais à venir au laboratoire et je vous en remercie.

Je tiens également à remercier vivement tous les participants qui ont donné de leur temps et de leur unités motrices pour m'aider dans ce travail de thèse. Nombre d'entre eux sont des amis de longue date qui n'ont pas hésité à se rendre disponibles dès que j'en ai eu besoin. Je pense notamment aux copains du pays de la Mée ou des Jeunes d'Erbray. Bien que vous ayez parfois engendré des lundi matin compliqués, vous avez été d'un soutien inestimable.

J'ai également une pensée pour mon entourage proche, notamment mes parents qui ont toujours été d'un grand soutien. Je sais que je ne suis probablement pas assez démonstratif mais cela n'enlève en rien l'amour que je vous porte. J'espère ne jamais oublier votre éducation, votre humilité et vos valeurs.

Je consacre ces dernières lignes à **Noémie** qui a réalisé l'exploit de me supporter tout au long de cette thèse. Ta présence et ton oreille attentive m'ont permis de toujours voir le verre à moitié plein. Je te remercie sincèrement pour tout ce que tu m'apporte au quotidien.

## PUBLICATIONS AND PRESENTATIONS RELATED TO THIS PHD THESIS

### Published peer-reviewed articles

**Hamard, R.**, Aeles, J., Kelp, N. Y., Feigean, R., Hug, F. & Dick, T. J. (2021). Does different activation between the medial and the lateral gastrocnemius during walking translate into different fascicle behavior? *Journal of Experimental Biology*, *224*(12), jeb242626.

**Hamard, R.**, Hug, F., Kelp, N. Y., Feigean, R., Aeles, J. & Dick, T. J. (2022). Inclusion of image-based in vivo experimental data into the Hill-type muscle model affects the estimation of individual force-sharing strategies during walking. *Journal of Biomechanics*, *135*, 111033.

### Article currently submitted in peer-review journal

**Hamard, R.**, Aeles, J., Avrillon, S., Dick, T. J. & Hug, F. A comparison of neural control of the biarticular gastrocnemius muscles between knee flexion and ankle plantar flexion. *Journal of Applied Physiology* (submitted).

### Oral communications at international conferences

**Hamard, R.**, Aeles, J., Kelp, N. Y., Feigean, R., Hug, F. & Dick, T. J. (2021). Does different activation between the medial and the lateral gastrocnemius during walking translate into different fascicle behavior? 28th Congress of the International Society of Biomechanics (ISB). Stockholm, 25-29 July 2021.

**Hamard, R.**, Aeles, J., Kelp, N. Y., Feigean, R., Hug, F. & Dick, T. J. (2021). Does different activation between the medial and the lateral gastrocnemius during walking translate into different fascicle behavior? 19th Congress of the Association des Chercheurs en Activités Physiques et Sportives (ACAPS), Montpellier, 27-29 October 2021.

## LIST OF ABBREVIATIONS

| | |
|---|---|
| DTI | Diffusion Tensor Imaging |
| EMG | Electromyography |
| GL | *Gastrocnemius Lateralis* |
| GM | *Gastrocnemius Medialis* |
| MRI | Magnetic Resonance Imaging |
| MVC | Maximal Voluntary Contraction |
| PCSA | Physiological Cross-Sectional Area |

**TABLE OF CONTENTS**

# GENERAL INTRODUCTION

"*To move things is all that mankind can do, and for this task, the sole executant is a muscle, whether it be whispering a syllable or felling a forest*"

Charles Sherrington, 1924

Almost a century ago and a few years before receiving the Nobel prize, the famous British physiologist Charles Sherrington highlighted the omnipresence of movement in mankind. Extrapolating this beyond human life, we can say more generally that the ability to produce movements to interact with the environment is a key behavior for all animals. The need for efficient, maximal, rapid, adjustable or reliable movements likely plays a major role in driving the evolution of animals. For example, locomotion is the behavior that most conditions an animal's morphology and physiology (Dickinson et al., 2000). Muscles are the executing element of the motor system and are therefore central in animal movement.

The primary function of skeletal muscle is to enable animals to move. To do so, skeletal muscles convert chemical energy, i.e. energetic substrate, into mechanical force and work through cross-bridge cycling. The generated forces are then transmitted to bones, most often *via* tendons and the translational muscle force is then converted into rotation through joint moments. This essential, yet seemingly simple role hides a huge complexity. In reality, force production relies on the interaction between neurophysiological and biomechanical factors. Despite the fact that many of these factors were discovered several decades ago (Gordon et al., 1966; Hill, 1938; Huxley, 1974; Huxley & Niedergerke, 1954; Huxley & Simmons, 1971), they are still not fully understood today (Herzog, 2017).

The production of force is complex at the level of an individual muscle but even more complex when considering the level of the joint. Several muscles span each joint and numerous combinations of forces produced by the individual muscles are possible to achieve a motor task (Bernstein, 1967; Prilutsky & Zatsiorsky, 2002). Even a simple motor task such as a heel raise results from the complex coordination of many individual agonist and antagonist muscles (Crowninshield & Brand, 1981a), each with its own anatomical features and neuromechanical properties. Moreover, muscles can have more than one function if they span more than one joint. The central nervous system thus has to coordinate the behavior of muscles with different functional roles. This leads to the concept of muscle coordination that, in the scope of this thesis, we will define as the distribution of force among the muscles involved in a given motor task (Hug & Tucker, 2017). Although recent evidence has suggested that some muscle coordination patterns may favor performance (Avrillon et al., 2018) or be linked to the development and persistence of musculoskeletal disorder (Crouzier et al., 2019b; Hug & Tucker, 2017), the coordination of individual muscle forces still remains poorly understood (Herzog, 2017). This lack of knowledge is partly due to the absence of an experimental method to non-invasively measure individual muscle force *in vivo*.

Given this methodological limitation, a way to study muscle coordination is to indirectly estimate, rather than measure, the forces produced by muscles using models (Blemker et al., 2007; Buchanan et al., 2004; Delp et al., 2007; Zajac, 1989). However, models are often used with generic data which fails to consider the well-known inter-individual variability in muscle coordination and limits the accuracy of force estimation (Passmore et al., 2017). An option to overcome this limitation is to inform muscle models with personalized experimental data regarding activation and muscle architecture from measurement techniques such as electromyography (EMG), B-mode ultrasound or magnetic resonance imaging (MRI). Subject-specific muscle models are becoming an increasingly powerful tool to estimate individual forces (Blemker et al., 2007; Bolsterlee et al., 2015a; Charles et al., 2020; de Oliveira & Menegaldo, 2010; Passmore et al., 2017).

In this thesis, we focus on the *triceps surae* as it is a key muscle group for locomotion (Anderson & Pandy, 2003; Hamner & Delp, 2013). The *triceps surae* is composed of the biarticular *gastrocnemius medialis* (GM) and *gastrocnemius lateralis* (GL) and the monoarticular *soleus*. These three muscles have distinct volumes, architectures and therefore maximal force-generating capacity that likely lead to different functional behaviors. Although the neuromechanical differences between the biarticular *gastrocnemii* and the monoarticular *soleus* have been already investigated, differences between the GM and GL remain poorly understood. In many cases, the GM and GL are considered as similar muscles (Neptune et al., 2001), even though differences in muscle architecture and muscle activation, suggest that they may have different functional roles. Furthermore, nearly all studies on the *triceps surae* muscles have focused on their role in ankle plantar flexion. As a consequence, the behavior of the GM and GL during their secondary function, i.e. knee flexion, remains poorly understood.

The overall aim of this PhD thesis is to provide a deeper understanding of muscle coordination between the GM and GL, two muscles from the same anatomical group with the same function (i.e. knee flexion and ankle plantar flexion). For this purpose, we used a framework that combines experimental and modelling approaches and integrates neurophysiological and biomechanical measures. Throughout this work, we pay particular attention to the inter-individual variability as it is often overlooked by previous works examining muscle coordination.

This thesis contains four main chapters. Chapter 1 presents a literature review about (i) the production of muscle force, how to measure it and how we can get close estimations of it *in vivo*; (ii) the study of muscle coordination and (iii) the application of muscle coordination to a

muscle group, namely the *triceps surae*. Chapter 2 contains the overall experimental methods used for the three studies. Chapter 3 provides our contribution through the three studies that were performed during this PhD thesis. Chapter 4 consists of a general discussion about the implications and future perspectives derived from this work.

# CHAPTER 1: REVIEW OF LITERATURE

# Part 1: Individual muscle force

The force generated by skeletal muscle results from the interaction between the central nervous system and the muscular system. The production of active force requires the activation of the muscle by the central nervous system. To this end, information is conveyed, in the form of chemical and electrical signals from the central nervous system to the muscle (Loeb & Ghez, 2000). Then, the transmission of this information to the muscle results in the formation of cross-bridges between the actin and myosin filaments at the sarcomere level (Huxley, 1957; Huxley & Niedergerke, 1954). The length (Gordon et al., 1966) and the velocity (Hill, 1938) at which the muscle fibers operate, determines the number of cross-bridges attached and thereby the amount of active force that is generated. The active force transmitted from these cross bridges to the skeleton via elastic tissue finally depends on the number of muscle fibers activated by the central nervous system and their contractile properties. This section describes (i) the factors that contribute to individual muscle force production including the neural command, the maximal force-generating capacity, the force-length and force velocity relationships and (ii) methods to experimentally measure or to estimate muscle force.

## 1. Determinants of individual muscle force

### 1.1. Neural command

#### 1.1.1. Motor unit organization and function

As stated above, the production of active force originates from the actin-myosin cross-bridges. However, to enable the actin and myosin to link together, the central nervous system must excite the smallest functional neuromuscular units, i.e. the motor units (Sherrington, 1906). A motor unit consists of a motor neuron and the muscle fibers that it innervates. A motor neuron controls between a few to thousands of muscle fibers (Feinstein et al., 1955; Loeb & Ghez, 2000). Excitation of a single motor unit is an all-or-none event, such that when the central nervous system sends enough synaptic input to exceed the membrane potential of the spinal motor neuron body cell, a motor neuron action potential is generated. The motor neuron action potential propagates along the axon of the motor neuron towards the muscle fibers it innervates (Figure 1). It then reaches the neuromuscular junction at each innervated muscle fiber, where it induces an acetylcholine release. The acetylcholine stimulates the receptors of the muscle

fibers, which depolarizes the sarcolemma and consequently generates a muscle fiber action potential on each muscle fiber innervated by the motor neuron. The muscle fiber action potential propagates along the muscle fiber, from the neuromuscular junction to both ends of the fiber. Finally, the muscle fiber action potential causes an outflow of positive calcium ions from the sarcoplasmic reticulum which allows the formation of myosin and actin cross-bridges. The central nervous system controls the level of active force within a muscle via two mechanisms: (i) varying the number of motor units recruited, and (ii) regulating the discharge rate of the motor units (Duchateau & Enoka, 2011). Of note, as one motor neuron action potential results in one muscle fiber action potential in healthy individuals, the motor unit discharge rate provides direct information about its motor neuron excitation.

Motor units are often classified on the basis of their structure and contractile properties. Such classification is questioned as the motor unit properties are distributed continuously rather in distinct categories. However, for clarity purposes, in this thesis we consider two types of motor units. The slow motor unit produces lower forces and is more fatigue-resistant compared to the fast motor unit, which produces higher forces and is less fatigue-resistant (Duchateau & Enoka, 2011; Winter, 2009). These different types of motor units are generally orderly recruited as described by the size principle (Henneman, 1957). This principle states that to generate small force levels, the central nervous system recruits preferentially motor units with lower recruitment threshold (Figure 1). As the required force increases, the central nervous system progressively recruits motor units with higher recruitment threshold. Despite the size principle characterizing the motor unit recruitment well during progressively increasing voluntary contraction, it is less able to explain the motor unit recruitment in several other contexts such as ballistic and rapid movement (Desmedt & Godaux, 1977) or in the presence of pain (Tucker et al., 2009).

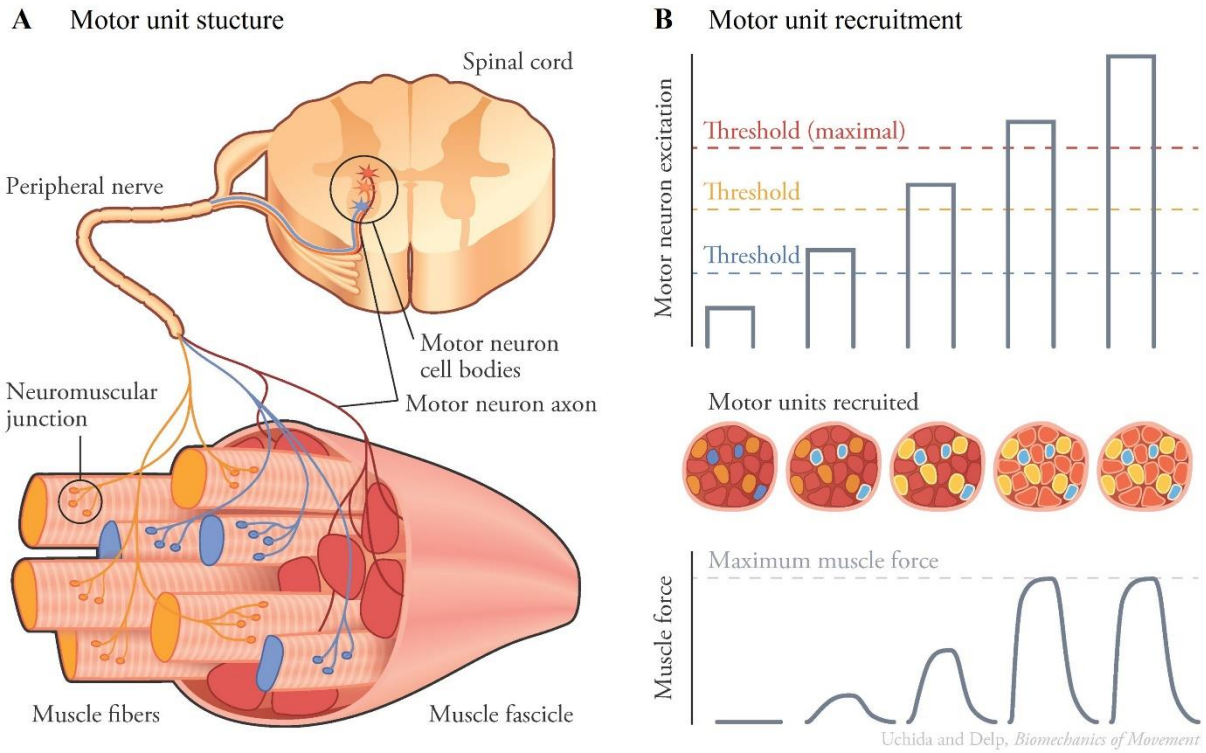


**Figure 1: The motor unit structure and recruitment.** A represents the general organization of a motor unit. Three motor units are represented in red, orange and blue. B: the top panel represents the motor neuron excitation and the individual threshold of the three motor units. The middle panel is a schematic representation of the motor units recruited depending on the motor neuron excitation. The bottom panel represents the production of muscle force which results of the motor units recruitment. From Uchida and Delp (2021).

The size of the motor unit, which is defined by the number of muscle fibers innervated by its motor neuron, varies greatly between motor units. Slow motor units are smaller, i.e. contain less muscle fibers than fast motor units (Duchateau & Enoka, 2011; Winter, 2009). A large diversity of motor units size is observed within a single muscle (Enoka & Fuglevand, 2001). For example, the size of motor units in the first dorsal interosseous muscle in humans varies between few tens to more than 1500 muscle fibers (Enoka & Fuglevand, 2001). This wide variety of motor unit size within a muscle results in a non-linear relationship between the number of motor neuron action potentials and the number of muscle fiber action potential (Enoka & Duchateau, 2015). The number of motor units, regardless of the motor unit size, varies also greatly between muscles (Feinstein et al., 1955). As a consequence, the relationship between the number of motor neuron action potentials and the number of muscle fiber action potentials is muscle-specific. Motor neuron action potentials and muscle fiber action potentials give two different pieces of information about the neural command. Neural drive refers to the sum of motor neuron action potentials (Enoka & Duchateau, 2019). It characterizes the strength of the motor command. Muscle activation refers to the sum of muscle fiber action potentials

(Enoka & Duchateau, 2019). In other words, muscle activation corresponds to the number of muscle fibers activated and their discharge rates (Besomi et al., 2020).

### 1.1.2. Electromyography

Active muscle force production originates from the neural command. Therefore, the measurement of this force determinant has long been and still is a key issue in biomechanics and motor control field (Adrian & Bronk, 1929; Besomi et al., 2019, 2020; De Luca, 1997; Martinez-Valdes et al., 2023; McManus et al., 2021). The easiest way to access the neural command is to measure the electrical activity from the muscle using EMG. Specifically, the EMG records the electrical activity of muscle fiber action potentials and therefore provides information about muscle activation. Different EMG methods exist. For example, intra-muscular EMG consists of inserting electrodes directly into the muscle. Intra-muscular EMG enables to directly identify the muscle fibers action potentials of some motor units. However, intra-muscular EMG signal informs only on the behavior of a small number of motor units from a small region of the muscle. Here, we present in more detail surface EMG, which is a non-invasive method that provides more representative information about the whole muscle activation compared to selective intra-muscular recordings (Besomi et al., 2019).

#### 1.1.2.1. Estimation of muscle activation using conventional surface EMG

As explained previously (Part 1, section 1.1.1), the muscle fiber action potential is generated at the level of neuromuscular junction and then propagates from the neuromuscular junction to both ends of muscle fibers. Although subcutaneous tissues reduce its amplitude, by acting as a natural low-pass filter, the action potential diffuses through these tissues to the skin. Surface electrodes placed over the skin of the target muscle are able to measure muscle fiber action potentials located within the detection volume of these electrodes (Figure 2). Therefore, Surface EMG records interferential signals from populations of motor units rather than individual motor units and provides information about global muscle activation from the region of interest. Thereby, this method is best suited for superficial and relatively large muscles (Besomi et al., 2019).

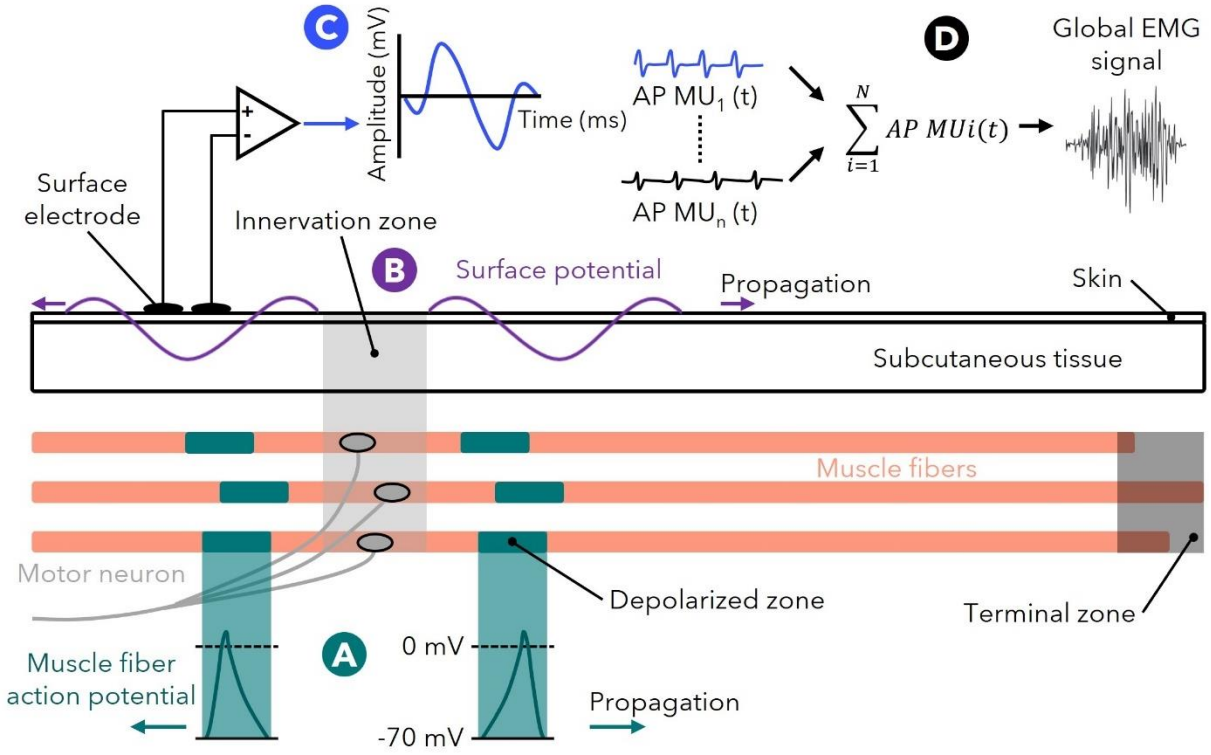


**Figure 2: Illustration of the muscle fiber excitation and electromyography recording.** The figure represents a motor unit composed of three muscle fibers. A muscle fiber action potential propagates along muscle fibers and through the subcutaneous tissue (A). Surface electrode records the surface action potential (B). The detected signal is amplified (C). All the detected action potentials are summed which results in the EMG signal (D). AP, muscle fiber action potential, MU, motor unit, N, number of motor unit, t, time. Adapted from Merletti et al. (2001).

Different configurations of surface electrodes exist. In monopolar mode, the signal from an individual electrode is compared to a reference electrode. In bipolar mode, the EMG signal is constructed from the difference between two electrodes placed over the targeted muscle. From EMG signals, researchers often extract information on the timing, the amplitude, or the time-varying profile of muscle activation to study muscle coordination.

Although surface EMG is relatively easy to implement, some factors can influence the EMG measurement and should be carefully considered. The factors that affects surface EMG can be non-physiological or physiological, (Farina et al., 2004a; Merletti et al., 2001). Non-physiological factors include (i) the detection system (e.g. skin-electrode contact, electrodes location, size, shape and inter-electrode distance); (ii) anatomical features (e.g. thickness of the subcutaneous tissue layers, size and distribution of the motor units); (iii) geometrical features (i.e. muscle fibers shortening or the shift of the muscle relative to the detection system); and

(iv) physical features (i.e. conductivities of the tissues and crosstalk from surrounding muscles). The physiological factors that affect EMG signals are either related to the fiber membrane properties (e.g. the muscle fiber conduction velocity and its distribution among the motor units or the shape of the muscle fiber action potentials) or the motor unit properties (e.g. the number of recruited motor units, the distribution of discharge rate or motor unit synchronization; Farina et al., 2004a). Methodological precautions could be used to limit the influence of some of these factors and improve the interpretability of the EMG signals (Besomi et al., 2020). However, some factors are intrinsic to the EMG method such as crosstalk and amplitude cancellation. These two factors are particularly important to consider when inferring neural strategies from surface EMG signals and are discussed below.

Crosstalk refers to the part of the recorded signal that is actually generated by surrounding muscles (De Luca & Merletti, 1988). The amount of crosstalk depends on the electrode location, the detection system (De Luca & Merletti, 1988), the thickness of the subcutaneous tissue (Solomonow et al., 1994) and the extinction of the muscle fiber action potential at the end of the muscle fibers (Farina, et al., 2004b). Some studies have suggested that crosstalk between calf muscles exists during walking (Campanini et al., 2007; Péter et al., 2019). For example, Péter et al. (2019) compared EMG amplitude from intra-muscular EMG and surface EMG. Intra-muscular EMG is known to be less prone to crosstalk contamination compared to surface EMG (Besomi et al., 2019) and was used as reference. Their results showed that surface EMG signals from the *soleus* and *tibialis anterior* muscles exhibited significant activity during specific phases of the gait cycle while intra-muscular EMG indicated inactivity (Figure 3). They also revealed that surface EMG appears to be suitable for the GM and GL. Although crosstalk is difficult to quantify, it can be reduced by a low skin-electrode impedance combined with a proper placement of the electrodes (Hug, 2011). Guidelines relative to the electrode placement are available and can be considered (Hermens et al., 2000; Stegeman & Hermens, 2007). However, these guidelines do not account for the inter-individual variability in the anatomy of muscles. To ensure a proper electrode placement for each participant, the determination of muscle boundaries using ultrasonography imaging is increasingly used (Crouzier et al., 2018; Crouzier et al., 2019a; Lacourpaille et al., 2017). This enables placement of the electrode in the center of the target muscle belly and away from the other muscles to limit the detection of their muscle fiber action potentials.

Amplitude cancellation corresponds to the reduced EMG signal due to the cancellation of positive and negative phases of muscle fiber action potentials (Farina et al., 2004a). Muscle

fiber action potentials are asynchronous as muscles fibers have different innervation zones, conduction velocities and discharge times. The large number of muscle fiber action potentials recorded by surface EMG increases the likelihood of action potential summation and therefore amplitude cancellation. Keenan et al. (2005) conducted a modelling study to assess the extent of amplitude cancellation on the EMG signal. They simulated a surface EMG signal and then compared two processing methods. The first method, where a large amount of amplitude cancellation is expected to occur, summed and then rectified the EMG signal. On the contrary, the second method rectified and then summed the EMG signal. Results highlighted that amplitude cancellation in the EMG signal can exceed 60% at maximal activation. Nevertheless, the amplitude cancellation can be reduced to less than 5% by normalizing the EMG signal with respect to maximal voluntary contraction (MVC; Keenan et al., 2005). Nevertheless, this normalization procedure can also induce a small (<13%) overestimation of muscle activation at intermediate levels of activation (Keenan et al., 2005). Despite crosstalk and amplitude cancellation, surface EMG has proven to be a suitable method to study muscle activation if methodological precautions are considered (Besomi et al., 2019, 2020; Hug, 2011).

Of note, as conventional surface EMG records an interferential signal, it does not provide information about individual muscle fiber action potentials; and therefore it cannot provide information about the neural drive sent to the muscle. Yet, neural drive estimation is useful to determine how the neural control of muscles is organized.

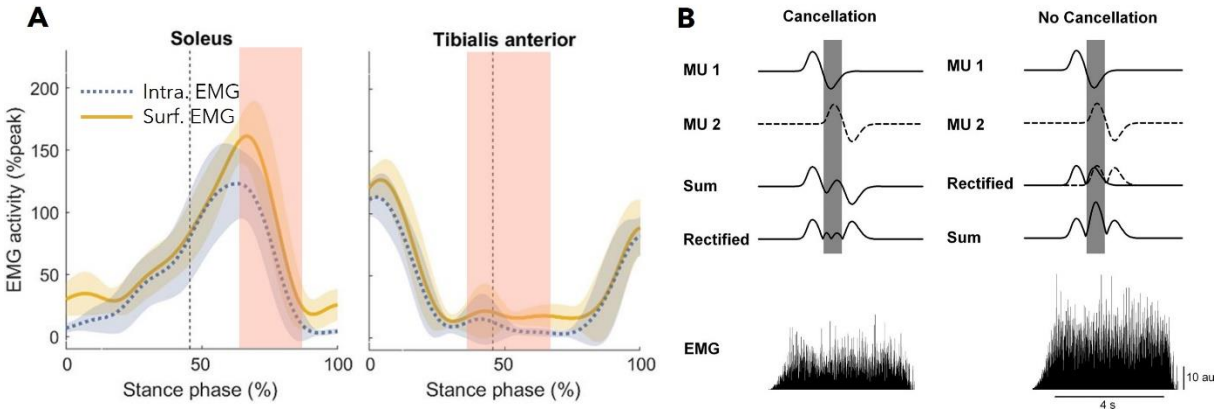


**Figure 3: Methodological considerations of surface electromyography.** A represents the intra-muscular electromyography (Intra. EMG) and electromyography EMG (Surf. EMG) from the *soleus* (left graph) and from the *tibialis anterior* (right graph) during walking. The red area represents the period where a statistical difference was found between intra-muscular EMG and surface EMG surve. The authors interpreted this difference as a crosstalk surface EMG activity. B represents the amplitude cancellation of EMG signal. An EMG signal is simulated after the action potential are summed and then rectified (cancellation) or rectified and then summed (no cancellation). au, arbitrary unit; EMG, electromyography; MU, motor unit. A adapted from Peter et al. (2019) and B from Keenan et al. (2005).

### 1.1.2.2. Estimation of neural drive using high-density surface EMG

To estimate the neural drive sent to a muscle, intra-muscular EMG or high-density surface EMG is required. High-density surface EMG refers to a matrix of at least four small-diameter electrodes that are closely spaced over the muscle, usually in the form of a linear array or an electrode grid (Gallina et al., 2022). The different electrodes enable to record the EMG signal from different locations (Figure 4). Although high-density surface EMG can also be used to assess muscle fiber properties (Merletti et al., 2003) and regional muscle activation (Watanabe et al., 2021a), it is a powerful technique to provide information on individual motor units activity (Holobar et al., 2010; Holobar & Zazula, 2007). As with intra-muscular EMG, the signal from the high-density grid of electrodes must be decomposed to observe individual motor unit activity. Compared to intra-muscular EMG, decomposition of high-density surface EMG signals is advantageous because it is less selective, non-invasive and it provides information on motor unit activity for a larger population of motor units per recording. The decomposition process consists of the separation of the muscle fiber action potentials from individual motor units that are contained within the overall high-density surface EMG signal (Farina et al., 2016). To decompose the high-density surface EMG signals into motor unit spiking activity, several methods exist however the most common is the blind source separation method (Holobar & Farina, 2014; Negro et al., 2016a). This method uses a semi-automated approach for detecting motor units, followed by manual editing of the individual each motor unit spike trains (Del Vecchio et al., 2020). The neural drive can be estimated at the muscle scale by calculating the cumulative spike train, i.e. the sum of the discharges of all the identified motor units.

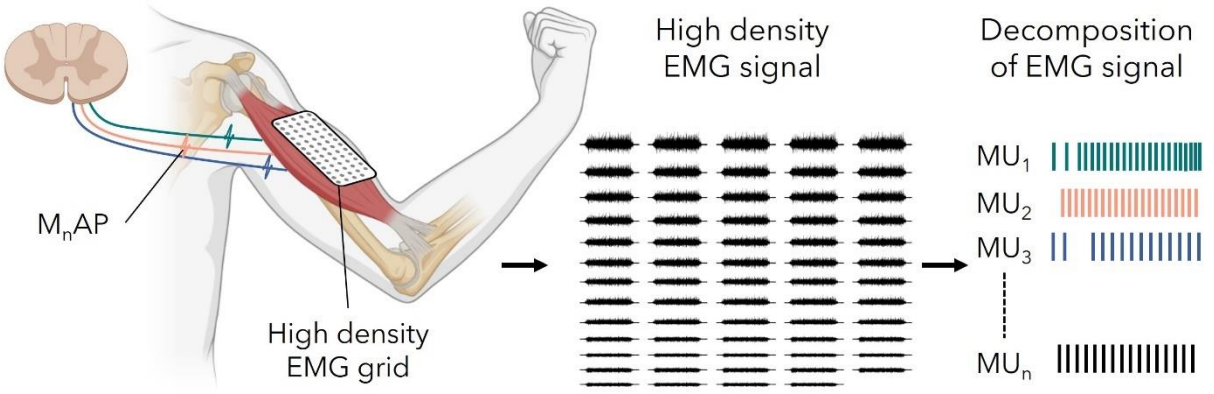


**Figure 4 : Illustration of the information provided by high-density surface electromyography.** Motor neuron action potentials ($M_nAP$) propagate throught three motor units to excitate a muscle. The high-density surface EMG recorded the sum of all the muscle fiber action potentials. This high-density surface EMG signal informs on the muscle activation. The high-density surface EMG signal can be decomposed into individual motor unit (MU) activity to inform on the neural drive.

The information provided by the decomposition of high-density surface EMG signal, i.e. individual motor unit activity, can be used to study how the central nervous system controls the motor units within a muscle or between muscles. For example, the simultaneous control of different muscles through motor modules is often proposed as a plausible option to reduce the dimensionality of motor control, i.e. the number of degree of freedom that need to be controlled by the central nervous system (Bizzi et al., 2008; Dominici et al., 2011). According to this concept, the central nervous system controls several muscles via a single command, i.e. a common neural drive. This motor module theory has been supported by animals studies where cortical (Overduin et al., 2012) or spinal microstimulation (Tresch & Bizzi, 1999) resulted in the generation of complex movement and multi-joint moment. Recent advancements in high-density surface EMG enable this theory to be tested, non-invasively in humans. The level of common neural drive can be estimated through the assessment of the common fluctuations of motor unit discharge rates in a low-frequency bandwidth (De Luca & Erim, 1994; Negro, et al., 2016b). The common neural drive can also be estimated by cross-correlating the smoothed discharge rate of individual motor units (De Luca & Erim, 2002; Rodriguez-Falces et al., 2017). Evidence suggests that motor units from the same muscle generally receive a high proportion of common neural drive (Negro, et al., 2016b). A high level of common neural drive can also be observed between motor units from different muscles such as *vastus lateralis* and *vastus medialis* (Avrillon et al., 2021; Laine et al., 2015). It has been suggested that the more that muscles are anatomically and functionally related, the more common neural drive they share (Gibbs et al., 1995; Kerkman et al., 2018). Nevertheless, this appears to depend on the muscle group studied, as a low level of common neural drive has been found within *triceps surae* muscles (Hug et al., 2021b).

## 1.2. Biomechanical factors

The force produced by a muscle also depends on several biomechanical factors such as maximal force-generating capacity, force-length relationship and force-velocity relationship. These factors are related to the highly organized structure of skeletal muscle. Sarcomeres are the basic force-generating units of muscle. They consist, in part, of the thin filament of actin proteins, the thick filament of myosin proteins and the titin protein. Sarcomeres are arranged in series to form a myofibril (Figure 5). Myofibrils are bundled, mostly in parallel, to make up muscle fibers which are themselves grouped into muscle fascicles. Finally, the different muscle fascicles make up the skeletal muscle (Barrett, 1962). Each substructure is enveloped by a

connective tissue. The aforementioned microscopic arrangement of the muscle appears very consistent within an organism and across skeletal muscles (Lieber & Fridén, 2000). Conversely, the macroscopic arrangement of the skeletal muscles, often referred to as muscle architecture, is highly variable between muscles. A wide diversity of muscle shapes and sizes, fascicle lengths and pennation angles (i.e. the angle between the muscle fascicles and the aponeuroses) can be observed within the human body (Lieber & Fridén, 2000). Importantly, the architecture of a muscle is intimately linked to its function. This section describes the influence of biomechanical factors on muscle force including: maximal force-generating capacity, force-length relationship and force-velocity relationship. We also discuss the methods that exist to experimentally measure these biomechanical factors *in vivo*.

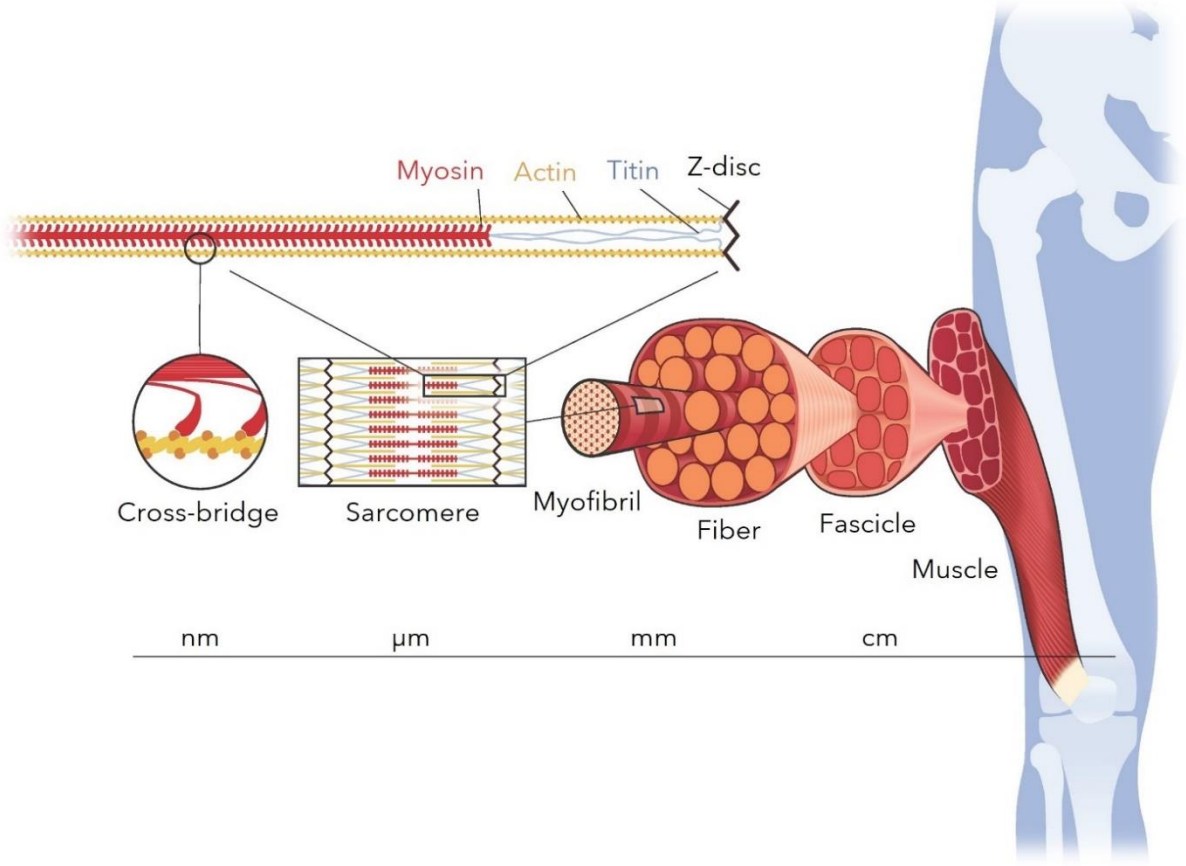


**Figure 5: Hierarchical organization of skeletal muscle.** The skeletal muscle is composed of different hierarchical structures from the sarcomere to the fascicle. The main proteins that compose the sarcomere are also represented. The cross-bridge between actin and myosin proteins is displayed on the left panel. From Uchida & Delp (2021).

## 1.2.1. Maximal force-generating capacity

### 1.2.1.1. Volume

The amount of muscle force produced depends on the maximal force-generating capacity. This refers to the force produced by a muscle maximally activated during isometric condition at its

optimal length. Maximal force-generating capacity is directly related to the number of muscle fibers arranged in parallel. Theoretically, when all other parameters are kept constant, the larger a muscle, the more muscle fibers it contains. As a consequence, for a given muscle architecture (i.e. same fascicle length and pennation angle), a given amount of intra-muscular fat and a given specific tension, a larger volume results in greater maximal force-generating capacity.

Muscle volume can be obtained either from cadaveric studies or from *in vivo* imaging. Cadaveric studies are often limited to small sample sizes and on older specimen (Ward et al., 2009). Therefore cadaveric data is often used as generic data to inform models or make predictions about function, it does not account for inter-individual variability in muscle volume that exists. For example, Albracht et al. (2008) reported *soleus* volumes ranging from 400 $cm^3$ to 600 $cm^3$ in 13 young males. The use of *in vivo* imaging techniques to measure muscle volume overcomes these problems. MRI is the gold-standard technique to measure volume (Albracht et al., 2008; Engstrom et al., 1991; Figure 6)). This technique provides a series of images with different contrast that are due to the specific molecular properties of each tissue. These different contrasts can be segmented on a series of transversal image to reconstruct muscle volume (Yushkevich et al., 2006). Although MRI remains the gold-standard technique, it is expensive and has a long acquisition time, and more affordable and portable alternatives have been developed such as freehand 3D ultrasound. The latter combines conventional B-mode ultrasound and synchronous tracking of the ultrasound transducer using 3D motion capture to image the muscle in 3D (Barber et al., 2009; Franchi et al., 2018). Although semi-automated segmentation procedures exist, the segmentation of MRI and freehand 3D ultrasound remains time-consuming.

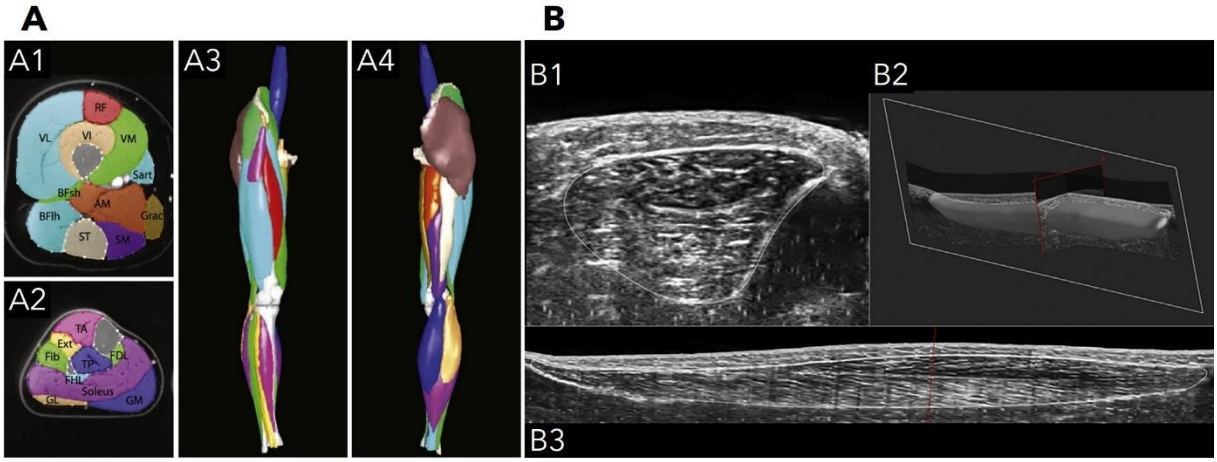


**Figure 6: Illustration of muscle volume measures.** A represents the 3D muscle volume of the lower limb from magnetic resonance imaging. Cross-section of the thigh (A1) and shank (A2) are depicted. An anterior view (A3) and a posterior view (A4) of the 3D reconstruction are also

depicted. B represents a transverse scan image (B1), an entire 3D reconstruction of (B2) and a sagittal view of the reconstruction (B3) of the *tibialis anterior* volume from freehand 3D ultrasound. A from Handsfield et al. (2014) and B from Franchi et al. (2018).

#### 1.2.1.2. Muscle architecture

Muscle architecture refers to the macroscopic arrangement of muscle fibers. Fascicle length and pennation angle are often use to quantify muscle architecture (Lieber & Fridén, 2000). Muscle architectures are very diverse, even within the human body. Muscle fibers can be arranged in designs that are parallel, unipennate, bipennate or multipennate. Muscle architecture is closely related to the muscle function (Figure 7). For a given volume, muscles characterized by relatively high pennation angles and thus shorter fascicle lengths pack more muscle fibers in parallel. This design is therefore best suited for the production of high amounts of muscle force. On the contrary, if in the same volume the muscle fascicles are less pennate and therefore longer, the number of muscle fiber decreases. In this case, the muscle can support larger excursions and higher shortening velocities but the muscle is less capable of producing large amounts of force. A wide variety of fascicle lengths, ranging from several mm to several hundred of mm, and pennation angles, ranging from 0° to 30° at rest can be observed within the human body (Lieber & Fridén, 2000). For example, the *triceps surae* muscles have relatively short and highly pennate fascicles, compared to other muscles such as the knee extensor muscles (Lieber & Fridén, 2000; Ward et al., 2009). On the contrary *sartorius* is designed for important movement excursion with its long and parallel fascicles.

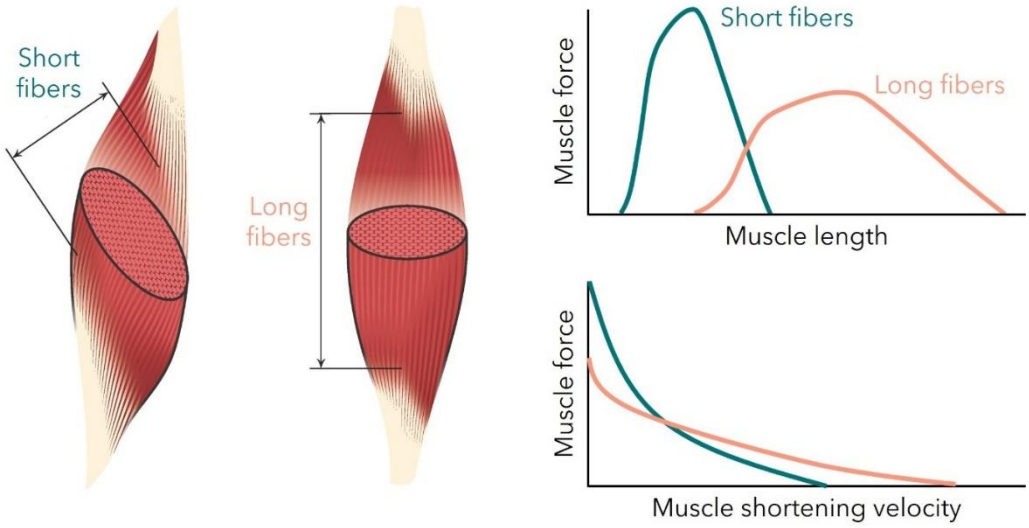


**Figure 7: The functional implication of different muscle architectures.** The left panel of the figure represents two muscles that have the same volume but different muscle architectures. The right panel of the figure represents the functional implication of the muscle architecture in terms of force and length (top graph) and in terms of force and velocity (bottom graph). Adapted from Lieber et Fridén (2000).

The most frequently used technique to measure human muscle architecture non-invasively is ultrasonography in B-mode configuration (Rutherford & Jones, 1992). This method uses the transmission of echo pulses from an ultrasound transducer placed on the skin. The amount of echo reflected back to and recorded by the transducer depends on the acoustic impedance. The muscle contractile tissue is mostly hypo-echoic (i.e. seen as dark) whereas connective tissues are hyper-echoic (i.e. seen as white). The connective tissue surrounding muscle fascicles combined with the hyper-echoic aponeuroses therefore allows us to obtain clear B-mode images of muscle architecture. From such an image, one or more fascicles can be traced to calculate the fascicle length and pennation angle relative to the aponeurosis (Figure 8). Measurements can be affected by the transducer orientation (Klimstra et al., 2007), the operator experience (Kwah et al., 2013) and the analysis method (Franchi et al., 2018). Nevertheless, suitable training for the operator and for analyses diminishes these issues and leads to reproducible (Aeles et al., 2017; Franchi et al., 2018) and valid measures (Bolsterlee et al., 2015b; Kwah et al., 2013). The main limitation of conventional B-mode ultrasound is its relatively small 2D field-of view, i.e. typically 4-6 cm, which is dependent on the transducer size. Although this field-of view is sufficient for some muscles such as the *triceps surae*, B-mode ultrasound is unable to completely image fascicles of other muscles that typically have long fascicles, such as the *vastus lateralis*. Extrapolations are then necessary to calculate the fascicle length when the fascicle extends beyond the field-of-view. However, the curvature of aponeurosis and fascicles may lead to inaccuracy in the extrapolated measure (Franchi et al., 2018). To address this limitation, the use of two transducers rigidly attached in series has been developed (Brennan et al., 2017). However, B-mode ultrasonography, whether using a single transducer or two transducers placed in series, captures only a limited part of the muscle and does not account for the muscle architecture regional variability.

Extended-field-of-view ultrasonography has been developed to take into account the spatial variability through the muscle (Weng et al., 1997). However, extended-field-of-view ultrasonography, as B-mode ultrasound, is a 2D technique which is unable to provide information about muscle architecture in 3D. Due to their ability to image the entire muscle in 3D, diffusion tensor imaging (DTI) and 3D freehand ultrasound are becoming increasingly popular. Here, we elaborate more on DTI as it is the technique that we used in this thesis. DTI is based on the fact that the Brownian motion of molecules, mostly water molecule, in the tissues are constrained by anatomical obstacles such as cell membrane. Water diffusion in our anisotropic muscles depends on the arrangement of the muscle fibers. DTI tracks the primary

diffusion gradient which is along the fiber length (Damon et al., 2002). This method exhibits reliable and robust measurements of the 3D muscle architecture (Bolsterlee et al., 2019). Although DTI allows for non-invasive 3D measures of *in vivo* muscle architecture, it remains limited to measuring muscle at rest or during very low level of contraction. B-mode ultrasonography remains the only method to dynamically image muscle architecture non-invasively *in vivo*.

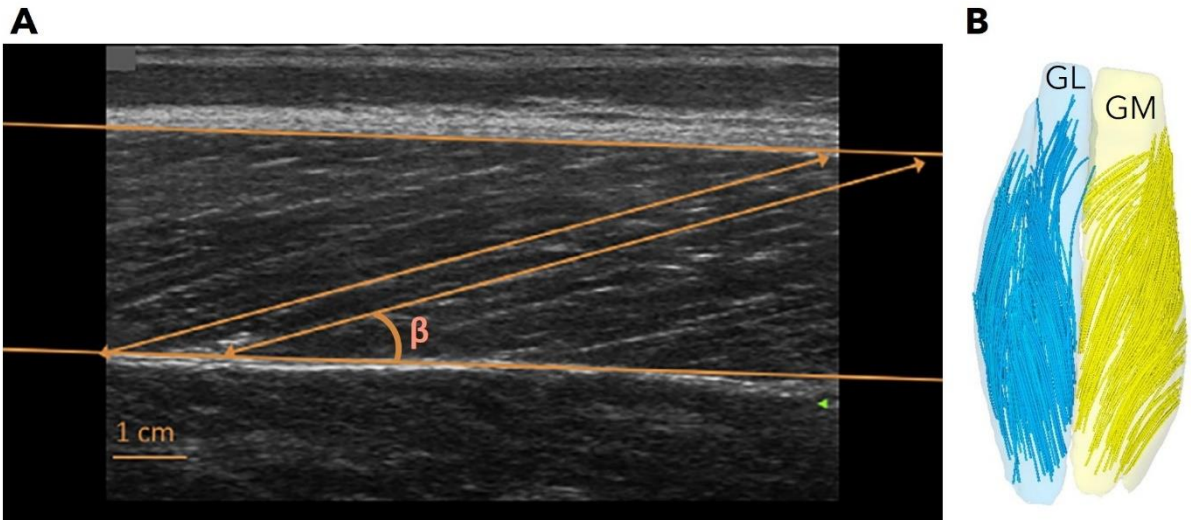


**Figure 8: Illustration of the measure of the muscle architecture**. A represents a B-mode ultrasonography image from the *vastus lateralis*. Two orange lines are drawn on the aponeuroses. Two muscle fascicles are represented by the orange arrows. The pennation angle (β) between a muscle fascicle and the deep aponeurosis is also depicted. B represents a 3D reconstruction of the GM and GL muscle fibers from diffusion tensor imaging. A is from Franchi et al. (2018) and B is from Bolsterlee et al. (2019).

#### 1.2.1.3. Physiological cross-sectional area

The number of muscle fibers arranged in parallel and therefore the maximal force-generating capacity depends on muscle volume and muscle architecture. These two parameters can be combined to estimate the physiological cross-sectional area (PCSA). Theoretically, the PCSA is defined as the sum of the cross-sectional areas of all muscle fibers in a whole muscle (Lieber & Fridén, 2000). Practically, the PCSA is often considered as the cross-sectional area of the whole muscle, perpendicular to its fibers (Lieber & Fridén, 2000; M. Narici et al., 2016). The latter definition is considered in this PhD thesis. For a parallel-fibered muscle, the PCSA is equal to the cross-sectional area. However, for pennate muscle, the cross-sectional area is smaller than the PCSA. The PCSA is calculated from muscle volume and fascicle length as described in the Equation 1:

$$PCSA = \frac{volume}{fascicle\ length}$$

Equation 1

Where PCSA is expressed in cm², volume in $cm^3$, fascicle length in cm. However, for pennate muscle, all of the force is not produced in the force-generating axis of the muscle (Haxton, 1944; Narici et al., 2016). A component of force is produced non-parallel to the force-generation axis. Therefore, the amount of functional force transmitted to the tendon can be estimated by the effective PCSA which takes into account the pennation angle:

$$Effective\ PCSA = PCSA \times \cos(pennation\ angle)$$

Equation 2

Where the effective PCSA is in cm² and pennation angle in radians. The effective PCSA appears to be a key factor to estimate muscle force-generation capacity (Lieber & Fridén, 2000). Powell et al., (1984) reported a strong positive relationship between the *in vitro* measures of maximal force-generating capacity and the maximal force-generating capacity estimated using PCSA in 10 guinea pig hindlimb muscles (Figure 9). The relationship between the PCSA and the maximal force-generating capacity was also indirectly studied in humans. Results suggested a positive and moderate correlation between the sum of the four quadriceps muscles effective PCSA and knee extension maximal voluntary torque ($r = 0.519$; $p = 0.047$; Massey et al., 2015). Nevertheless, this human study measured the torque rather than the force which likely explains the lower correlation compared to the study of Powell et al. (1984) on guinea pig muscles.

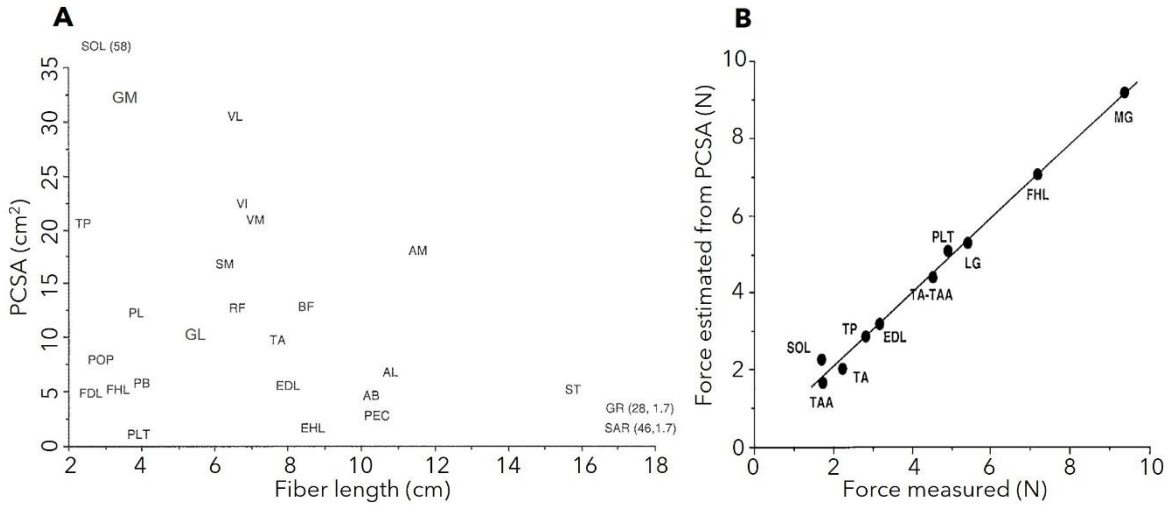


**Figure 9: Diversity of physiological cross-sectional area across human muscles and the relationship between physiological cross-sectional area and force.** A represents the wide diversity of muscle architecture within the human muscle system. B represents the relationship between muscle force estimated from physiological cross-sectional area (PCSA) and muscle force measured in 10 guinea pig muscles. AB, *adductor brevis*; AL, *adductor longus*; AM,

*adductor magnus*; BFl, *biceps femoris, long head*; BFs, *biceps femoris, short head*; EDL, *extensor digitorum longus*; EHL, *extensor hallucis longus*; FDL, *flexor digitorum longus*; FHL, *flexor hallucis longus*; GL, *gastrocnemius lateralis*; GM, *gastrocnemius medialis*; GR, *gracilis*; PB, *peroneus brevis*; PEC, *pectineus*; PL, *peroneus longus*; PLT, *plantaris*; POP, *popliteus*; RF, *rectus femoris*; SAR, *sartorius*; SM, *semimembranosus*; SOL, *soleus*; ST, *semitendinosus*; TA, *tibialis anterior*; TP, *tibialis posterior*; VI, *vastus intermedius*; VL, *vastus lateralis*; VM, *vastus medialis*. A from Lieber & Fridén (2000) and B adapted from Powell et al. (1984).

#### 1.2.1.4. Specific tension

The PCSA is an area which can indirectly estimate the number of muscle fibers arranged in parallel. However, the consideration of PCSA alone is unable to directly provide information about the amount of force. To estimate the level of force, PCSA should be multiplied by the force that each muscle area unit is able to produce, i.e. the specific tension:

$$F_{max} = PCSA \times Specific\ tension$$

Equation 3

Where $F_{max}$ is the maximal force-generating capacity in N, PCSA in cm² and specific tension in N.cm$^{-2}$. Specific tension refers to the maximal amount of force generated by muscle tissue for a given area. Specific tension can only be directly measured using invasive methods either at the individual muscle fiber scale or at the whole muscle scale. For an isolated muscle fiber, the specific tension corresponds to the peak force divided by the cross-sectional area of the fiber. *In vitro* studies suggest that the specific tension of individual fibers depends mainly on the contractile properties of the fiber (Bottinelli et al., 1999; Bottinelli & Reggiani, 2000). Fast muscle fibers have generally higher specific tension, i.e. between 15 and 30 N.cm$^{-2}$, compared to slow muscle fiber, i.e. between 10 and 20 N.cm$^{-2}$ (Bottinelli et al., 1996; Larsson & Moss, 1993; Stienen et al., 1996). Bottinelli & Reggiani (2000) suggested that this difference is related to the myosin properties of the muscle fibers.

The specific tension at the whole muscle scale is not necessarily proportional to the specific tension of the isolated fibers that compose the muscle. Muscle contains also non-contractile elements such as connective tissues and intra-muscular fat that affect the whole muscle specific tension. For example, older adults have higher levels of intra-muscular fat in *triceps surae* muscles despite similar muscle volumes compared to younger adults (Pinel et al., 2021). The higher level of intra-muscular fat in older adults is associated with lower muscle shear modulus during maximal isometric ankle plantar flexion contractions. Moreover, the consideration of the intra-muscular fat content in the PCSA enables to slightly increase the relationship between

PCSA and maximal plantar flexion torque. Taken together, these results suggest that whole muscle specific tension cannot simply be extrapolated from isolated muscle fibers specific tension.

The study of whole muscle specific tension *in vivo* in human is rare due to the difficulty to directly measure individual muscle force. Few studies have estimated individual muscle force during controlled contractions and derived the specific tension from the PCSA, the moment arm and the maximal isometric voluntary torque (Maganaris et al., 2001). However, such studies are based on questionable assumptions (Herzog, 2017). For example, this approach assumes an isometric behavior of the muscle fascicles during fixed-end maximal voluntary contraction whereas it is known that they have concentric behavior (Kelp et al., 2021). Moreover, this approach does not consider the contribution of antagonist muscles to the recorded torque. It remains experimentally impossible to directly measure whole muscle specific tension *in vivo* in human. As a consequence, the specific tension commonly used in the literature is taken from a single *in vitro* study on 10 hindlimb guinea pig muscles (Powell et al., 1984). Interestingly, this *in vitro* study reported similar specific tension, i.e. 22.5 $N.cm^{-2}$, for the different muscles, except for the *soleus* which had a specific tension of 15.7 $N.cm^{-2}$. In this PhD thesis, acknowledging its limitations, and as commonly done, we consider a specific tension of 22.5 $N.cm^{-2}$. PCSA and specific tension define the maximal force-generating capacity at optimal length and near-zero velocities. However, the length and velocity at which muscle operates also influence the production of force.

### 1.2.2. Force-length relationship and force-velocity relationship

When activated by the central nervous system, muscles generate active force through the interaction of actin and myosin proteins. The cross-bridge theory suggests that active force is generated by the cyclic action of actin and myosin forming cross-bridges (Huxley, 1957, 1974; Huxley & Niedergerke, 1954). The greater the number of cross-bridges, the greater the force generated. The cross-bridge formation is directly related to the sarcomere structure. A sarcomere is composed of a parallel arrangement of actin proteins that insert on Z-discs at the extremities of the sarcomere, and myosin proteins that originate from M-line in the middle of the sarcomere (Figure 10). Myosin proteins are also attached to the Z-discs via the elastic titin protein, which plays an important role in passive force generation (Wang et al., 1979). The cross-bridge theory explains most of the well-known properties of muscle such as the observed variation of force induced by a variation of muscle length (Gordon et al., 1966). Furthermore, this model is also able to explain why the velocity of muscle contraction influences the

interaction between actin and myosin and therefore the production of force (Hill, 1938). In this section, we introduce the force-length and the force-velocity relationships of muscle and describe approaches to measure time-varying changes in fascicle length and velocity *in vivo*.

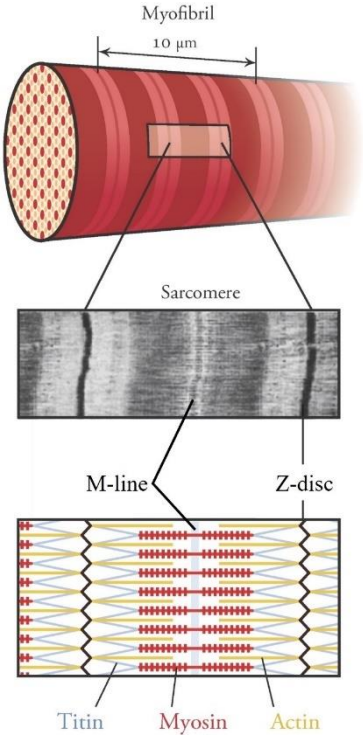


**Figure 10 : The sarcomere structure.** A myofibril is represent on the top panel. The magnified inset depicts a microscopic image of a sarcomere. The bottom panel represents a schematic structure of the sarcomere with the main proteins that contribute to the force production. From Uchida et Delp (2021) and based on (Huxley, 1957, 1974).

#### 1.2.2.1. Force-length relationship

The cross-bridge theory is also called the sliding filament theory owing to the fact that actin and myosin proteins slide past each other as the sarcomere changes length. The amount of overlap between actin and myosin, and thus the number of potential cross-bridge formations, depends on the sarcomere length (Gordon et al., 1966). As a consequence, the force that can be produced is directly affected by sarcomere length (Figure 11). More recently, we have learned that sarcomere length also affects the lattice spacing between actin and myosin, which in turn has an effect on the force (Rockenfeller et al., 2022; Williams et al., 2013). When muscle fibers shorten, they must expand radially to maintain a quasi-constant volume. This radial expansion increases the distance between actin and myosin and thereby reduces the ability to form cross-bridges (Williams et al., 2013). The force-length relationship is typically divided into three regions: (i) the ascending region where an increase in sarcomere length results in an increase in force due to excessive initial overlap of the thin actin elements which prevents the formation of

many cross-bridges; (ii) a small plateau region where the sarcomere length is considered optimal and where the force remains at its maximum; and (iii) the descending region where the force decreases with an increase in sarcomere length which decreases the amount of overlap between actin and myosin (Gordon et al., 1966; Rassier et al., 1999). Due to the hierarchical organization of skeletal muscle, the force-length relationship can be observed at all organizational scales, i.e. the sarcomere scale, muscle fiber scale and whole muscle scale.

In addition to the active component described above, the force-length relationship has a passive component. Even without any activation, muscle generates passive force exponentially when it is stretched beyond its optimal fiber length (Figure 11). The passive component of the force-length relationship mostly arises from the titin protein at the microscopic sarcomere scale and from the elastic properties of the connective tissue surrounding the muscle fibers, fascicles and entire muscle. For example, titin has low stiffness when the sarcomere is short, but when the sarcomere lengthens, titin stretches and its stiffness increases (Labeit et al., 2003). Moreover, recent evidence has shown that titin stiffness and force are regulated by activation (Powers et al., 2014). The total force produced by a muscle corresponds to the sum of active and passive component (Figure 11).

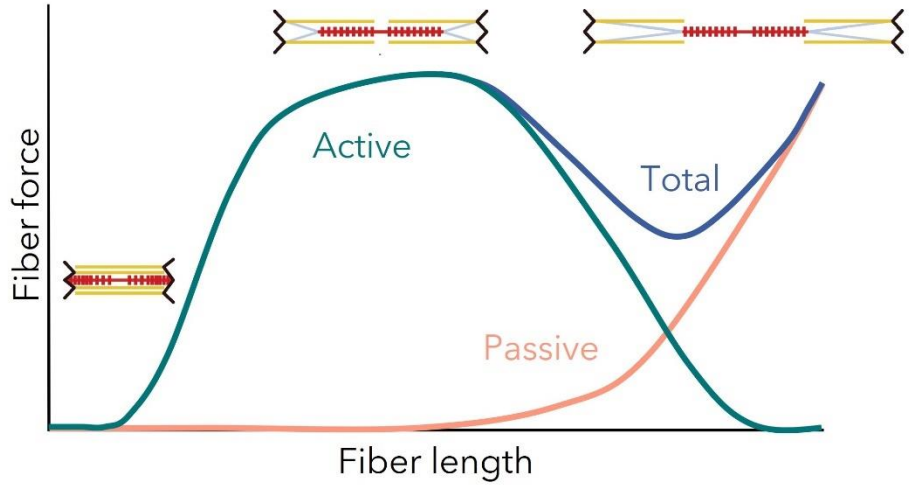


**Figure 11 : Schematic representation of the force-length relationship.** The figure represents the relationship between the muscle fiber length and the passive (orange), active (green) and total (blue) forces. The figure displays also three schematic representations of the sarcomere at three different lengths. Adapted from Gordon et al. (1966).

### 1.2.2.2. Force-velocity relationship

The force produced by a muscle depends not only on its length but also on the rate at which the length is changing, i.e. the velocity (Hill, 1938). Similar to the force-length relationship, the force-velocity relationship is related to the attachment and detachment of cross-bridges

(Huxley, 1974). To generate force, myosin heads cyclically bind with and pull on the actin protein. The myosin needs time to execute this process. Therefore, when the shortening velocity increases, the number of cross-bridges that can be formed, and thus the force generated in the sarcomere, decreases. Theoretically, at maximal shortening velocity, no active force is generated because the actin and myosin proteins slide past each other faster than the myosin head is able to form cross-bridges (Huxley, 1974; Piazzesi et al., 2007). As a consequence, for a given activation level and a given length, there is an inverse relationship between force and velocity whereby higher shortening speeds are associated with lower forces (Figure 12). Conversely, during eccentric contractions, sarcomeres are stretched. The lengthening strains the cross-bridges before the myosin heads fully detach from the actin and this then also results in the production of force (Huxley, 1974).

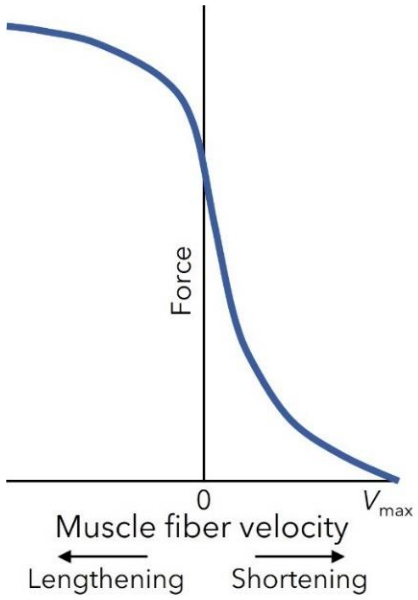


**Figure 12: Schematic representation of the force-velocity relationship.** The figure represents the change in muscle fiber force depending on the shortening or lengthening velocity. At the theoretical maximal velocity ($V_{max}$), a muscle fiber does not produce force. Adapted from Huxley (1974).

### 1.2.2.3. Measure of dynamic muscle length and velocity

The force-length and force-velocity relationships have been widely investigated *in vitro* (Bottinelli et al., 1996; Bottinelli & Reggiani, 2000; Piazzesi et al., 2007). However, *in vivo* studies are less common, primarily because of the challenge to measure these relationships non-invasively (Herzog, 2017). The *in vivo* determination of force-length and force-velocity relationships require the simultaneous recording of length or velocity and muscle force. However, there is a lack of non-invasive methods to measure individual muscle forces. As a

consequence, most of the *in vivo* human studies examining the force-length and force-velocity relationships have estimated individual muscle forces from joint torque. However, several muscles contribute to a joint torque. An option to provide information on the individual muscle force in human is to combine the joint torque with the moment arm and the relative PCSA of the muscle within the muscle group (de Brito Fontana & Herzog, 2016; Hauraix et al., 2017; Hessel et al., 2021; Ichinose et al., 2000; Maganaris, 2003). For example, this method enables to estimate the force of *vastus lateralis* at different lengths (de Brito Fontana & Herzog, 2016) and velocities (Hauraix et al., 2017) through the use of B-mode ultrasonography. Rubenson et al. (2012) used similar methods to study the force-length relationship of the human *soleus*. In this study B-mode ultrasound was further used to image the fascicle contractile behavior during locomotion. The authors reported that the *soleus* operates on the ascending region of the force-length curve during both walking and running (Rubenson et al., 2012). Nevertheless, in a similar way to the *in vivo* measure of specific tension, such measure of force are based on assumptions that are debated. For example, different activation between the muscles spanning the joint or antagonist muscle activity could influence the force-length or force-velocity relationships but are not considered.

Although it remains challenging to measure *in vivo* force-length and force-velocity properties, the assessment of muscle operating lengths and velocities does provide information about muscle function. For example, fascicle velocity measurements during locomotion revealed that the walk to run transition enables the GM fascicles to operate at slower velocities where they can theoretically produce more force (Farris & Sawicki, 2012). To non-invasively measure the dynamic muscle architecture, B-mode ultrasound is the best suited method (Cronin & Lichtwark, 2013; Franchi et al., 2018; Loram et al., 2006). B-mode ultrasound has been first used to measure the muscle architecture changes during isometric contraction (Fukunaga et al., 1997) and then during shortening and lengthening contraction (Reeves & Narici, 2003). Later, B-mode ultrasound has been widely used to study the muscle fascicle contractile behavior during locomotion (Farris & Raiteri, 2017; Fukunaga et al., 2001; Ishikawa et al., 2005; A. Lai et al., 2015; Lichtwark & Wilson, 2006). The recent development of automatic and semi-automatic tracking software has made the fascicle tracking process during movement less time-consuming and more objective (Farris & Lichtwark, 2016; Seynnes & Cronin, 2020). These software packages allow valid and reliable measurement of the fascicle length and pennation angle during different tasks (Gillett et al., 2013; Kwah et al., 2013).

# 2. *In vivo* measure and estimation of muscle force

## 2.1. Measures of muscle force from invasive experimental techniques

Although there have been studies that measure muscle force *in vivo,* these experiments are highly invasive and not common in most biomechanics laboratories today. Walmsley et al. (1978) pioneered the use of buckle-type transducers for measuring *in vivo* time-varying muscle forces in animals. Buckle transducers consist of a strain gauge surgically implanted onto the tendon of interest (Figure 13). The tendon force informs directly on the muscle force due to the in series arrangement of the muscle and tendon. Buckle transducers are able to provide reliable tendon force measurements (Ginn et al., 1993) and their use has advanced our knowledge on basic muscle function (Daley & Biewener, 2003; Roberts, 1997), muscle-tendon interactions and the role of elastic energy (Biewener et al., 1998a; Biewener & Blickhan, 1988) or muscle coordination (Biewener & Corning, 2001; Herzog et al., 1993). Although less common, studies using buckle-type force transducers in human do exist. Komi and colleagues developed the use of buckle-type transducers in the human Achilles tendon (Komi, 1990; Komi et al., 1984). Using this method, Komi et al. (1990, 1992) observed that the Achilles tendon undergoes a very high amount of force during running, around 12 times the body weight,. The Achilles tendon force measurement from buckle-type force transducer has also been applied to human walking (Komi et al., 1992), cycling (Gregor et al., 1987) and jumping (Fukashiro et al., 1995).

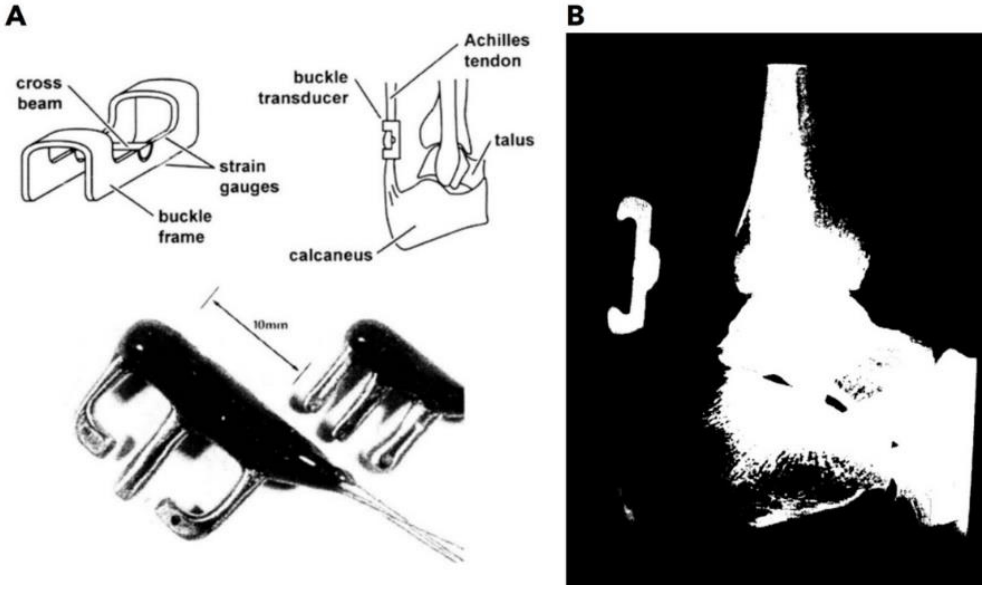


**Figure 13: Illustration of the buckle-type force transducer.** A represents the shape of a buckle-type force transducer. B represents a X-ray side view of an Achilles tendon with a buckle-type force transducer. A from Herzog et al. (1999) and B from Komi (1990).

Later, optic fiber techniques were developed to avoid the considerable surgical procedure inherent to the buckle-type force transducer method (Finni et al., 1998; Komi et al., 1996). To measure the forces, an optic fiber is inserted in the tendon of interest. The geometric properties, and thereby the intensity of light within the optic fiber is mechanically changed when force is applied to the tendon providing information about force. This method was first validated on the calcaneal tendon in rabbits (Komi et al., 1996) and later used to measure Achilles tendon forces in humans during walking (Finni et al., 1998) and jumping (Finni et al., 2000) as well as patellar tendon forces during jumping (Finni et al., 2000).

However, both the buckle-type force transducer and the optic fiber technique are invasive methods and have several drawbacks. First, they require a medical intervention to insert the sensor, which results in ethical consideration. Second, the invasive intervention induces pain and healing reactions that probably affect motor function. Third, they need either *in vitro* calibration or complex calibration procedures that are challenging to maintain during the *in vivo* measurement. Finally, they are unable to provide individual muscle force information when tendons from different muscles are merged such as in the human Achilles tendon. Yet, to our knowledge, there are no studies that have used these techniques on a tendon from an individual muscle. Taken together, these limitations explain why *in vivo* individual force measurement has not been performed in human. This has led researchers to use alternative methods to indirectly estimate individual muscle forces.

## 2.2. Estimation of muscle force from non-invasive imaging techniques

Non-invasive imaging methods have been used to estimate muscle forces. For example, B-mode ultrasound can be used to estimate the tendon force from tendon length changes during contraction. To this end, the muscle-tendon junction needs to be tracked during contraction. This method was used to investigate the Achilles tendon force during one-legged hopping (Lichtwark & Wilson, 2005) and cycling (Dick et al., 2016). Both studies combined tendon length changes, a subject-specific determination of the Achille tendon stiffness and a moment arm estimation to calculate the Achilles tendon force. Using this technique, Lichtwark and Wilson (2005) revealed that the Achilles tendon undergoes forces around 3000 N to 5000 N during single leg hopping depending on the individual. Shear wave tensiometry is another method to indirectly estimate force applied on a tendon. A shear wave tensiometer consists of a mechanical tapping device and accelerometer array in series (Keuler et al., 2019). The tapping

device generates a shear wave, which propagates along the tendon length. The accelerometer array is then able to detect the shear wave propagation. The fundamental basis of this method is the proportional relationship between the squared tendon wave speed and the axial stress in tendinous tissue (Martin et al., 2018). The tendon force can be calculated using the ratio between the measured tendon stress and the tendon cross-sectional area. However, these two methods based on tendon properties require time-consuming calibration procedures and are limited to superficial tendons. Furthermore, these tendon-based techniques are often applied to tendons that merge several individual muscles. For example, tendon length changes and shear wave tensiometry have been mainly use to estimate the Achilles tendon force (Dick et al., 2017; Ebrahimi et al., 2020; Lichtwark & Wilson, 2005; Slane et al., 2017). These techniques, as the invasive techniques described above, are unable to inform on the individual contribution of each muscle attached to the tendon.

Shear-wave elastography has also been proposed to estimate individual muscle force (Bouillard et al., 2011; Hug et al., 2015c). This method relies on the linear relationship between muscle stiffness and muscle force (Hug et al., 2015c). Bouillard et al (2011) showed a strong relationship between the torque produced during isometric contraction and the shear elastic modulus with a $R^2$ of, in average, 0.986 ± 0.007 for the human *first dorsal interosseous* and 0.977 ± 0.016 for the human *abductor digiti minimi*. However, shear wave elastography cannot provide information on the absolute level of force. It only estimates the relative changes in muscle force. Moreover, this method has a limited temporal resolution which limits its use in several contexts such as locomotion. As a consequence, the three techniques described above provide interesting information on the force produced by a group of muscles, but are not able to estimate individual muscle forces.

## 2.3. Estimation of muscle force from biomechanical modelling

Biomechanical modelling remains the most widely used method to estimate time-varying individual muscle forces. Modelling is a powerful approach to gain insights on parameters that researchers cannot measure. Different biomechanical approaches exist to estimate muscle force. A first approach combined musculoskeletal models with either inverse dynamics or forward dynamics to estimate joint moment and individual muscle force. For the musculoskeletal models that used inverse dynamics, the latter enables to calculate a net joint moment from external force measurements such as ground reaction force. The net joint moment calculated represents the sum of all the moments from individual muscles crossing the joint. Then, the

individual muscle force can be calculated using static optimization techniques (Penrod et al., 1974; Seireg & Arvikar, 1973, 1975). Optimization techniques consist of minimizing an objective function such as the muscle stress (Crowninshield & Brand, 1981b) or the metabolic cost (Prilutsky & Zatsiorsky, 2002). However, combining inverse dynamics and optimization techniques has a high computational cost (Challis, 1997; Erdemir et al., 2007). To address the limit of optimization-based inverse dynamics, a second computational approach called forward dynamics can be used. On the contrary to inverse dynamics, forward dynamics rely on kinematics. This approach consists of estimating the individual muscle activation from the experimental kinematics data. Forward dynamics iteratively updates the muscle activation to find the solution that best reproduce the kinematics data. Even though the forward dynamics approach is computationally more affordable compared to the inverse dynamics approach, both methods have crucial limitations such as inaccuracies or a lack of validation (Ait-Haddou et al., 2004; Challis, 1997; Herzog & Leonard, 1991). As a consequence, the ability of musculoskeletal models associated to inverse dynamics or forward dynamics appears limited to estimate individual muscle force.

An alternative approach to estimate muscle force consists of combining experimentally-determined EMG with forwards dynamics (Piazza & Delp, 1996) or, most often, both inverse dynamics and forward dynamics (Amarantini & Martin, 2004; Buchanan et al., 2004). The inverse dynamics is used to determine the joint moment. Then, forward dynamics calculate the moment produced by each muscle from (i) the activation dynamics based on experimental EMG; (ii) the contraction dynamics based on muscle model; and (iii) the muscle-tendon geometry determined by a musculoskeletal model based on experimental kinematics. Finally, the resultant joint moment predicted by the forward dynamics is compared to the reference joint moment determined by inverse dynamics. This approach has three main advantages. First, its computational cost is limited. Second, these EMG-driven models use information from experimental EMG to estimate individual muscle force. Therefore, these models do not require the optimization of objective functions and are free from any assumption. Third, the subject-specific EMG input enables to consider the individual differences in muscle activation strategy.

Forwards dynamics and EMG-driven models use muscle model to predict force. Different muscle models exist, all based on the neuromechanical determinant previously described. For example, the Huxley-type cross bridge model simulates the dynamics of cross-bridge cycling (Huxley & Niedergerke, 1954; Lemaire et al., 2016). This model has been mainly used to study phenomena at the sarcomere or single fiber level and is particularly powerful to assess the

relationship between metabolic cost and mechanical behavior. The Hill-type model predicts whole muscle force using few parameters based on sarcomere to muscle simplifications. The muscle behavior has been also modelled using continuum mechanics and finite element to mainly characterized the force-length relationship (Dao & Tho, 2018; Heidlauf et al., 2017; Röhrle et al., 2012). Recently, titin clutch models have also integrated an activation-dependant spring to consider the contribution of titin to the production of force (Nishikawa, 2020).

Among these different existing muscle models, the Hill-type model is the most popular. The Hill-type model has a lower computational cost compared to the Huxley-type cross-bridge model, the titin clutch model or the continuum model. Despite its computational and conceptual simplicity, the Hill-type model is able to capture with enough accuracy the dynamic biological complexity of force production (Schmitt et al., 2019). As a consequence, the Hill-type model is often considered as the best suitable compromise between model complexity and accuracy (Buchanan et al., 2004; Perreault et al., 2003). Moreover, this model is embedded in user-friendly biomechanical simulation software such as Opensim (Delp et al., 2007), which makes it even more accessible.

Various arrangements of the Hill-type model exist. The more conventional Hill-type model represents the whole muscle-tendon unit with a contractile element that produces active force and two linear springs that are responsible for passive force. One of these springs, is arranged in series to the contractile element, i.e. the series elastic element, and the other is arranged in parallel to the contractile element, i.e. the parallel elastic element. The contractile element represents the active force generated from the actin-myosin cross-bridges. The series elastic element corresponds to the tendon and aponeuroses whereas the parallel elastic element refers to the other connective tissues within and surrounding the muscle and the microstructures that generate passive forces such as the titin protein. The combination of contractile element, parallel elastic element and series elastic element is generally represented as shown in Figure 14:

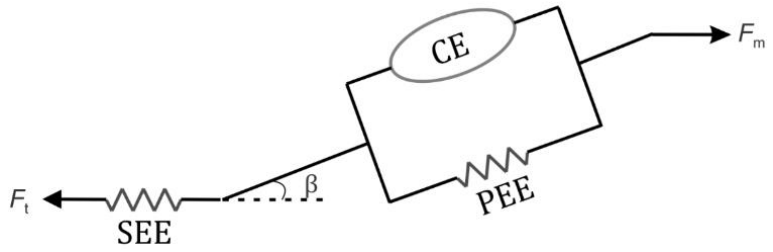


**Figure 14: The schematic representation of a conventional Hill-type model.** The contractile element (CE) produces the active force. The parallel elastic element (PEE) and the series elastic element (SEE) generate the passive force. $\beta$ represents pennation angle. $F_m$ and $F_t$ represent the resultant force in the muscle and tendon, respectively.

The Hill-type model includes all the main determinants of force described above, i.e. activation, maximal force-generating capacity, force-length relationship and force-velocity relationship (Zajac, 1989). The most common form of the Hill-type model is formulated as follow:

$$F_m = F_{max}\left[\hat{a}(t)\widehat{F_a}(l_f)\widehat{F_a}(v) + \widehat{F_p}(l_f)\right]\cos\beta$$

Equation 4

Where the muscle force $F_m$ in N depends on maximal force-generating capacity $F_{max}$ in N, normalized level of activation $\hat{a}(t)$, normalized active $\widehat{F_a}(l_f)$ and passive $\widehat{F_p}(l_f)$ forces as determined from the force-length relationship and normalized force $\widehat{F_a}(v)$ as determined by the force-velocity relationship. The muscle force generated by the contractile element and parallel elastic element is then multiplied by the cosine of the pennation angle $\beta$ to obtain $F_m$ which corresponds to the effective force.

Hill-type models have been widely used to study individual muscle force during walking (Anderson & Pandy, 2003) and running (Hamner et al., 2010). Although Hill-type models are ubiquitous in biomechanics, there are only few studies that have compared the accuracy of the model prediction to measured muscle forces *in situ* in animal (Lee et al., 2013; Perreault et al., 2003; Sandercock & Heckman, 1997) or to *in vivo* force estimated from tendon length changes in human as described above (Dick et al., 2017). For example, Lee et al. (2013) assessed the Hill-type model accuracy by comparing the predicted force to *in vivo* measured force from buckle-type force transducer inserted on the GM and GL tendons of goat during walking, trotting and galloping. They observed that the Hill-type model captures the force changes well and reported root mean square errors between 9% and 17% during walking (Figure 15).

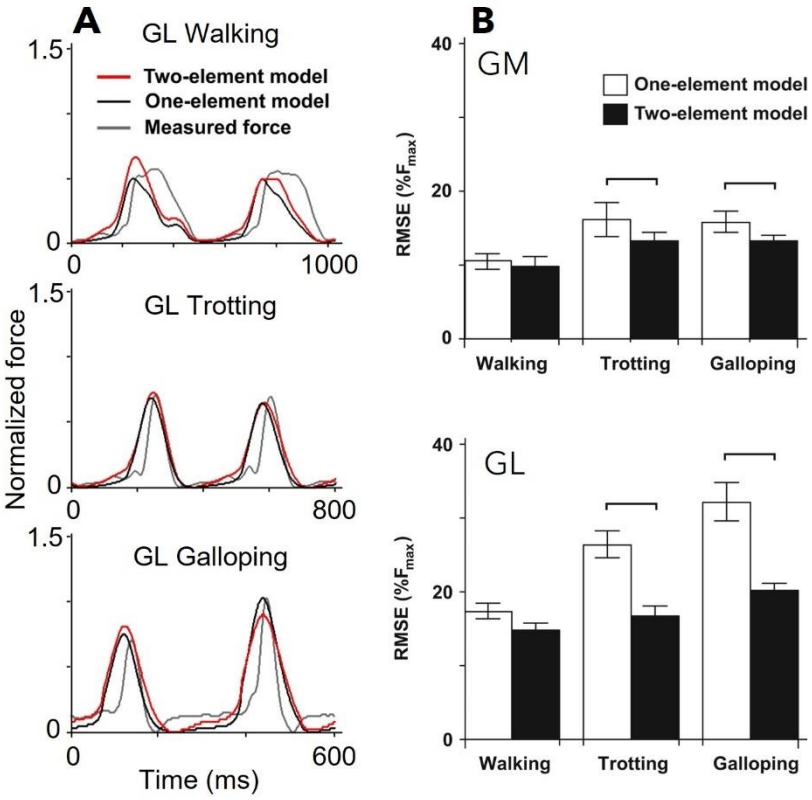


**Figure 15: Comparison of predicted force from a Hill-type model to measured force using buckle-type force transducer in goat.** A represents the force profiles of the *gastrocnemius lateralis* (GL) measured using buckle-type force transducer (grey), estimated from a conventional Hill-type model (one-element model; black) or estimated from a Hill-type model that accounts for slow and fast motor units (two-element model; red). B represents the root mean square error (RMSE) between the measured force and the estimated force from the Hill-type models for the *gastrocnemius medialis* (GM) and GL. From Lee and al. (2013).

One of the drawbacks of the Hill-type models, used for example in forwards dynamics, is that it is often informed with generic data (Blemker et al., 2007). Although the Hill-type model has been informed with experimentally determined muscle activation in EMG-driven models for two decades (Ai et al., 2016; Amarantini & Martin, 2004; Buchanan et al., 2004; Perreault et al., 2003), the other muscle parameters are often based on mean values provided in the literature. For example, maximal force-generating capacity is often calculated from muscle volume and muscle architecture based on literature values. The use of generic inputs enable to simplify the experimental data collection but it also conceals the inter-individual variability and leads to inaccuracies in the individual muscle force prediction (Passmore et al., 2017). To address this limitation, researchers have recently added more subject-specific inputs based on experiments to inform Hill-type models (Charles et al., 2020; Dick et al., 2017; Gerus et al., 2015; Modenese et al., 2016). For example, Gerus et al. (2012 & 2015) used B-mode ultrasound to determine subject-specific series elastic element properties by determining the aponeurosis and tendon

force-strain relationships. They demonstrated that the integration of these subject-specific series elastic element properties into the Hill-type model led to a better agreement between force predictions and measured ankle torques when compared to generic data (Gerus et al., 2012). Later, the same authors added the subject-specific muscle architecture to calibrate the Hill-type model and further improve the accuracy of the prediction (Gerus et al., 2015). Dick et al. (2017) personalized the Hill-type model with subject-specific time-varying fascicle lengths, fascicle velocities and pennation angles recorded during a cycling task (Figure 16). They reported satisfying RMSE values (between 8% and 22%) when comparing predicted force from the Hill-type model to forces estimated from ultrasound-based measures of tendon strains and tendon mechanical properties (Dick et al., 2017). Even though the Hill-type model has limitations such as the inability to account for history-dependent phenomena, it currently remains a key method to estimate individual muscle forces, especially when it is informed with subject-specific data.

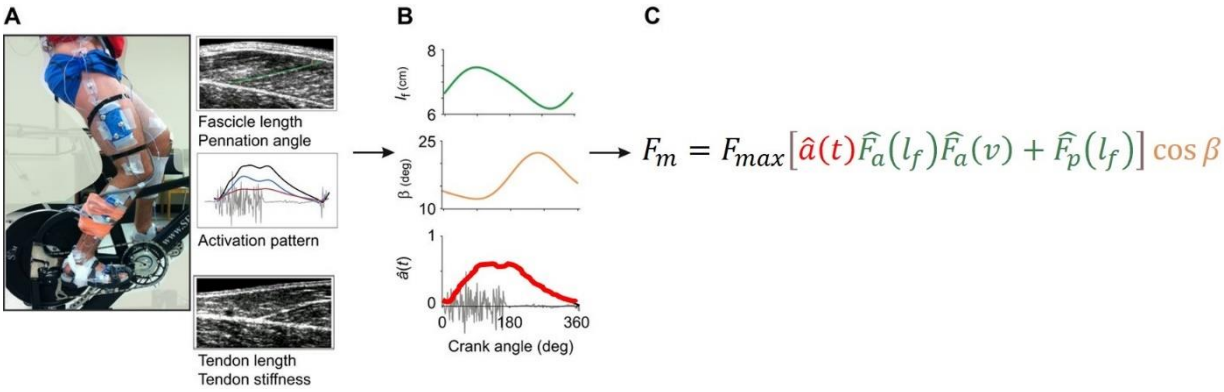


**Figure 16: Illustration of the inclusion of ultrasound-based subject-specific input in a Hill-type model**. The force was estimated during a cycling protocol illustrated with the left image (A). The participants pedalled on a stationary bike while the authors measured tendon lengths from tracked muscle-tendon junctions, fascicle lengths ($l_f$) and pennation angles (β) from ultrasound images, and activation patterns (â) derived from surface electromyography from the *gastrocnemius medialis* and *gastrocnemius lateralis* (B). The subject-specific time-varying activation and muscle architecture was then used into a Hill-type model. Adapted from Dick et al. (2017).

# Individual muscle force

—

# Summary

The production of force arises from the interplay between the neural command sent to a muscle and several biomechanical factors. Specifically, once excited by the neural command, a muscle produces active force, the magnitude of which depends on several biomechanical determinants. First, the muscle force is determined by the muscle's maximal force-generating capacity which is related to its volume, architecture and specific tension. Second, the length and the velocity at which muscle operates influence the muscle force production.

Although we are able to collect rich sources of neurophysiological and biomechanical data with modern tools, there remains no technique to measure individual muscle force. Invasive buckle-type force transducers and optic fibers have been used to measure muscle force in humans, but these techniques are not common practice and do not differentiate individual muscle forces from those measured in a common tendon.

Alternatively, muscle models can be used to estimate muscle force. However, most musculoskeletal models rely on generic inputs, which limits the accuracy of their predictions. Later, studies extended the possibilities of modelling by using muscle models informed with subject-specific inputs. This improves the accuracy of model predictions while accounting for the inter-individual variability in muscle force production. Muscle models informed with subject-specific inputs appears to be a key approach to estimate individual muscle force.

# Part 2: Muscle coordination

Muscle coordination refers to the distribution of muscle force among the muscles involved in a given motor task (Hug & Tucker, 2017), and is therefore equivalent to the notion of muscle force-sharing strategy. The large number of muscles that cross a joint results in numerous possible muscle coordination strategies to produce the required joint moment. The reasons underlying the use of specific muscle coordination among the numerous possibilities remain poorly understood. Muscle coordination has been studied using animal models or using alternative approaches to estimate individual muscle force. This section first outlines the theoretical concepts underlying the study of muscle coordination, and second, describes the different methods that have been used to study muscle coordination.

## 1. Distribution problem

### 1.1. Muscle redundancy

The contribution of individual structures crossing a joint to the joint moment, i.e. the "distribution problem", is a fundamental issue in biomechanics and motor control (Herzog, 2017). Although it was established more than 50 years ago (Bernstein, 1967) and has been extensively studied ever since, the distribution problem is still not fully understood. The distribution problem emerges from the muscle redundancy. The number of muscles (>600) contained within the human body largely exceeds the number of degrees of freedom (244) offered by our joints meaning that our musculoskeletal system is redundant (Bernstein, 1967; Prilutsky & Zatsiorsky, 2002). This large redundancy of the musculoskeletal system implies that numerous combinations of individual muscle forces are theoretically able to achieve a given joint moment. Moreover, most of the muscles span more than one joint and therefore produce moments at multiple joints. This further increases the complexity of motor control. Crowninshield and Brand (1981a) illustrated muscle redundancy at the knee joint. They highlighted that this joint has three degrees of freedom (flexion-extension; internal rotation-external rotation; abduction-adduction) whereas 14 muscles (*rectus femoris*, *vastus lateralis*, *vastus medialis*, *vastus intermedius*, *biceps femoris*, *semi-membranosus*, *semi-tendinosus*, *tensor fascia latae*, *sartorius*, *gracilis*, *popliteus*, GM, GL, *plantaris*) span the knee and contribute to its moment (Figure 17; Crowninshield & Brand, 1981a). Similar redundancy is

observed at the ankle which has also three degrees of freedom: plantar flexion-dorsal flexion; inversion-eversion; abduction-adduction. However, 13 muscles (*Tibialis anterior; Extensor digitorum longus; Extensor hallucis longus; Fibularis longus; Fibularis brevis; Fibularis tertius; Tibialis posterior; Flexor digitorum longus; Flexor hallucis longus;* GM; GL; *Soleus; Plantaris*) span the ankle and are able to contribute to its moment. Therefore, from a motor control perspective, the numerous muscles spanning a joint constitutes a complex system for the central nervous system.

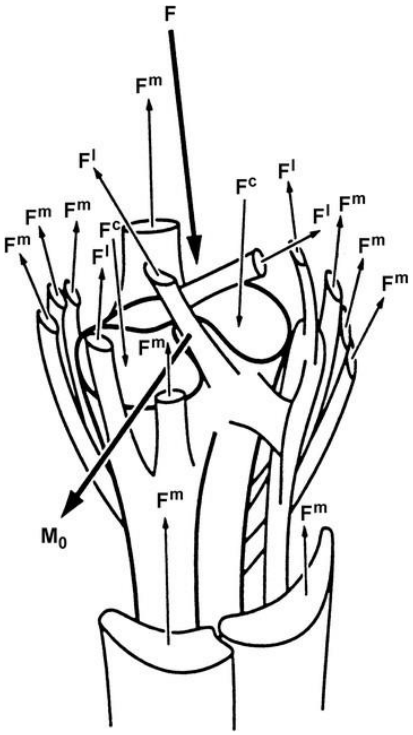


**Figure 17: Illustration of the different forces acting on the human knee.** Muscle force ($F^m$), ligament force ($F^l$) and bony contact force ($F^c$) influence the joint moment ($M_0$). From Herzog et al. (2017) based on Crowninshield and Brand (1981a).

## 1.2. Individual muscle force and the joint moment

A joint moment corresponds to the sum of the moments produced by each structure that spans this joint. The contribution to the joint moment of blood vessels, nerves, joint capsule, ligament and bony contact force are typically assumed to be low (Andrews, 1974; Herzog, 1996, 2017). Moreover, the central nervous system does not control these structures. As a consequence, for a sake of clarity, in this section we considered that the joint moment can be computed as:

$$M^0 = \sum_{i=1}^{m} (f_i^m \times r_i^m)$$

Equation 5

Where $M^0$ is the joint moment; $f_i^m$ designates the force in the i$^{th}$ muscle; $r_i^m$ represents the moment arm of the the i$^{th}$ muscle; m is the number of muscles spanning the joint.

Even this simplified equation that considers only the muscle structures is an indeterminate system which, theoretically, has an infinite number of solutions. In other words, an infinite number of muscle coordination can produce the same joint moment. This raises the question of why the central nervous system selects a particular muscle coordination among all the possible alternatives. Although the fact that the central nervous system has to choose between several solutions remains unquestioned, recent studies highlighted mechanical and neural constraints, which drastically reduce the number of solutions.

## 1.3. Feasible force set

### 1.3.1. Mechanical constraints

The feasible force set refers to the space that contains all muscle coordination possibilities (Kutch & Valero-Cuevas, 2011). This feasible force set theoretically has an infinite number of muscle coordination strategies. However, when taking into account the mechanical and neural constraints that act on muscles involved in a specific task, this feasible force set is reduced (Kutch & Valero-Cuevas, 2011). First, mechanical constraints limit the muscle coordination strategies that can physiologically be used to reach a given joint moment. In a cadaveric study, Kutch and Valero-Cuevas (2011) determined the feasible force set for an isometric abduction contraction of the index finger. They resected cadaver arms and connected the proximal tendons of all 7 muscles controlling the index finger (i.e. *flexor digitorum profundus, flexor digitorum superficialis, extensor indicis, extensor digitorum communis, first lumbricals, first forsal interosseous and first palmar interosseous*) to motors. This set up allowed the authors to control the individual muscle force and to simultaneously measure the resultant joint moment. The results showed that when the task required a mechanical constraint such as a specific force direction, the set of feasible coordination strategies is greatly limited. Specifically, the 7 muscles must be activated in a very restrained range of activation. The authors extended these results to multi-joint tasks such as walking using computational simulation (Figure 18). They found that 84% of the feasible force set area was vulnerable to the loss of any one muscle. For example, the *gastrocnemii* seemed to be necessary to produce a vertical force to support the body weight during walking whereas the hamstrings were necessary to produce a force oriented posterior (Kutch & Valero-Cuevas, 2011).

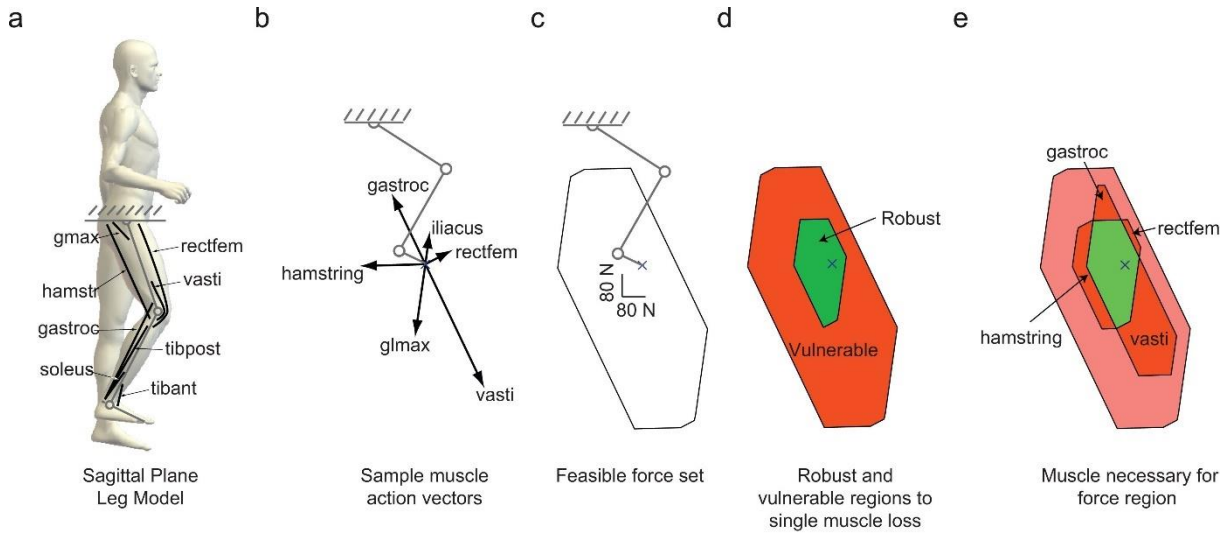


**Figure 18: Illustration of the mechanical constraints that can limit the muscle redundancy.** A represents the model considered with 14 muscles groups (only 8 are represented for a clarity purpose). B represents the force vector of each muscle group. C represents the feasible force set generated by these vectors. D displays the regions that are robust or vulnerable to the loss of any muscle. E displays the regions vulnerable to the loss of only one muscle. Gastric, *gastrocnemii*; gmax, *gluteus maximus*; rectfem, *rectus femoris*; tibant, *tibialis anterior*; tibpost, *tibialis posterior*; vasti, *vastii*. From Kutch & Valero-Cuevas (2011).

### 1.3.2. Neural constraints

Neural constraints also limit the muscle coordination possibilities. Synergist muscles within a muscle group generally receive a certain amount of common neural drive (De Luca & Erim, 1994). The muscles that share a high level of common neural drive cannot be controlled fully independently by the central nervous system which influence the muscle coordination possibilities. Hug et al. (2014) studied the neural constraints within the quadriceps muscles. In this work, participants were asked to voluntarily reduce the activation of *vastus medialis* or *rectus femoris* while maintaining a knee extension torque of 20%. Participants succeeded to voluntarily reduce the activation for *rectus femoris*, by increasing the force produced by the *vastii*. However, they failed to reduce the *vastus medialis* activation while maintaining the required knee extension torque. These results are likely explained by the fact that *rectus femoris* is controlled mostly independently from the *vastus lateralis* and *vastus medialis*, whereas the *vastus lateralis* and *vastus medialis* receive a high level of common neural drive (Laine et al., 2015). The shared neural command between muscles therefore reduces the number of possible muscle coordination strategies. Taken together, the mechanical and neural constraints suggest that the muscle redundancy initially established by Bernstein (1967) is more limited than

previously suggested. Nevertheless, several muscle coordination strategies are still possible, and the central nervous system has to solve the distribution problem.

# 2. Study of muscle coordination

## 2.1. Insights from animal studies

Muscle coordination has been studied in animals using buckle-type force transducers placed on the tendon of the muscles of interest (Biewener & Corning, 2001; Herzog et al., 1993; Kaya et al., 2003; Walmsley et al., 1978). Using this approach, Walmsley et al. (1978) quantified the force produced during locomotion by implanting two buckle-type force transducers on the GM and *soleus* tendons in cats. They observed that the *soleus* produces more force than the GM during normal walking and slow trotting. Moreover, the force production of the *soleus* appeared to be consistent across speed and locomotor tasks whereas the GM force varied according to the mechanical demands of the task. The authors suggested that these between-muscle differences are likely due to the muscle fiber composition of each muscle. The cat *soleus* is mainly composed of slow muscle fibers whereas cat GM has a more mixed muscle fiber population. The *soleus* may be preferentially activated during low intensity tasks to take advantage of its fatigue-resistant muscle fibers. The GM activation was instead modulated to match the intensity of the task (Walmsley et al., 1978). This pioneering work was later extended by additionally measuring the *plantaris* muscle, whose shape, structure and muscle fiber composition are similar to those of the GM (Herzog et al., 1993). In this study, muscle coordination between the GM, *soleus* and *plantaris* was measured in freely moving cat during various tasks and locomotion speeds. They showed that *plantaris* force, similarly to the GM force, increased with the movement intensity whereas the *soleus* force remained similar across tasks. Surprisingly, muscle coordination across the different tasks that were studied covered a wide spectrum of possibilities. For example, during quiet standing, the cat *soleus* produced substantial force whereas the GM was not active. On the contrary, when paw-shaking or jumping, cats exhibited substantial GM force and small if no *soleus* force (Figure 19). Between these two extremes cases, the different gaits and speeds have a specific muscle coordination strategy (Herzog et al., 1993).

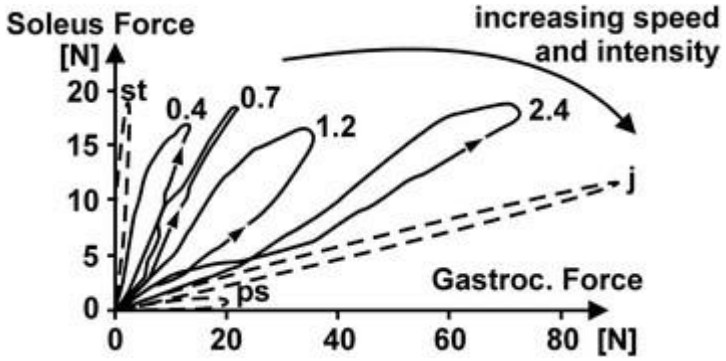


**Figure 19: Illustration of muscle coordination between the *gastrocnemius medialis* and *soleus* of cat.** The authors reported a large flexible in the muscle coordination depending on the task. Different tasks were examined: standing still (st); paw shake (ps); jumping (j); 0.4, 0.7 and 1.2 are the speeds of walking in $m.s^{-1}$, 2.4 is the speed of trotting. Gastroc, *gastrocnemius medialis.* From Herzog (2017).

Muscle coordination between the GM and GL has also been studied, namely in the mallard duck during swimming and terrestrial locomotion. The results showed that GM generated half the force of the GL during swimming (5 N and 10 N, respectively) whereas terrestrial locomotion was associated with more balanced muscle force distribution whereby the relative contribution of GM increased (GM and GL generated 14 and 20 N respectively; Biewener & Corning, 2001). Taken together, these animal studies revealed that muscle coordination is flexible, and varies with the mechanical demands of the task. The central nervous system might consider the muscle properties such as the muscle fiber composition when distributing the force among synergists muscles.

## 2.2. Insights from human studies

### 2.2.1. Experimental estimation of muscle coordination strategies

In the absence of non-invasive methods to directly measure individual muscle force, an alternative strategy has been developed to experimentally study muscle coordination in humans. This approach consists of combining muscle activation from EMG and experimentally-determined biomechanical features to estimate muscle coordination during controlled tasks. As described in Part 1, section 1., the main determinants of muscle force are muscle activation, PCSA, specific tension, and the force-length and force-velocity relationships. During isometric contractions, especially at relatively low submaximal intensities, the fascicle velocity is low and the influence of the force-velocity relationship on force production is therefore limited. Moreover, specific joint angles can place different synergist muscles at similar length relative to their specific force-length relationships. The use of these specific joint angles could therefore

minimize the impact of the force-length relationship on muscle coordination. Furthermore, if the muscles considered have similar muscle fiber composition such as the *gastrocnemii* (Johnson et al., 1973), we can assume that their specific tensions are similar. More generally, as specific tension cannot be experimentally determined, this parameter is often passed over by considering a similar specific tension across muscles. As a consequence, during isometric contractions at specific muscle length, the distribution of force between synergist muscles can be estimated using an index of force based on experimental activation and PCSA.

Hug et al., (2015a) used this approach and determined the PCSA of the *vastus lateralis* and *vastus medialis* muscle using measured muscle volumes and fascicle lengths from MRI and freehand 3D ultrasound, respectively. They also recorded muscle activation during submaximal isometric knee extension using bipolar EMG. Finally, they used the product of muscle activation and PCSA as an index of force, which was used to assess the distribution of force between the *vastus lateralis* and *vastus medialis* muscles. The results revealed that the *vastus lateralis* produces in average higher force compared to the *vastus medialis* during a knee extension of 20% and 50% of MVC. Interestingly, this study also reported a high level of inter-individual variability in the distribution of force. For example, within the quadriceps at 20% of knee extension MVC, some participants produced much more force with the *vastus lateralis* compared to the *vastus medialis* whereas others used the reverse strategy (Hug et al., 2015a). Furthermore, the observed individual distribution of activation was positively correlated to the individual distribution of maximal force-generating capacity (Figure 20). In other words, the greater the PCSA of *vastus lateralis* compared to *vastus medialis*, the stronger the bias of muscle activation towards the *vastus lateralis*. This results aligns with a previous study highlighting that the muscle activation was modulated to take advantage of biomechanical characteristics such as moment arm (Hudson et al., 2009). The central nervous system might bias the activation to the muscle with the greater maximal force-generating capacity, in order to decrease the activation cost (Crouzier et al., 2018). However, this neuromechanical coupling became moderate and non-significative for a knee extension of 50% of MVC.

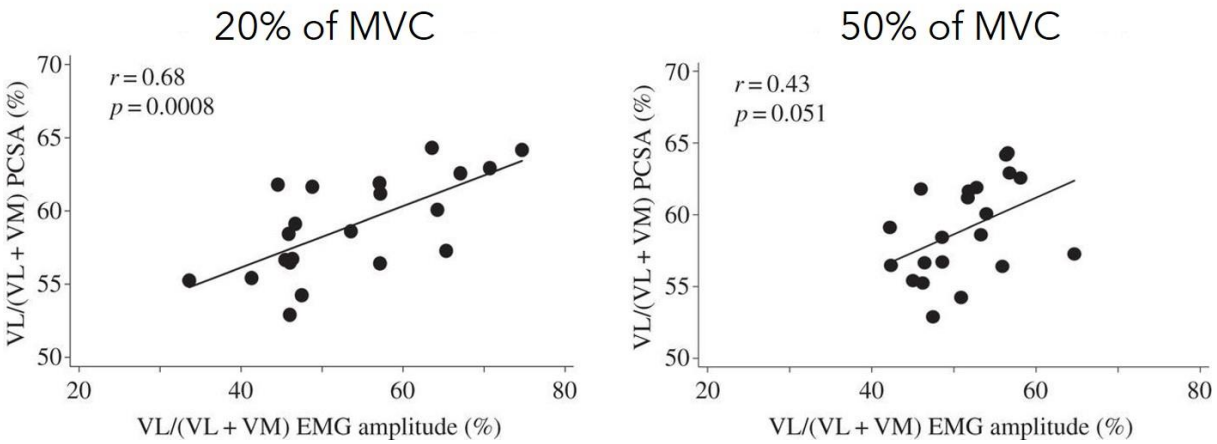


**Figure 20: The neuromechanical coupling between the physiological cross-sectional area and the muscle activation of the *vastus lateralis* and *vastus medialis*.** The correlation was strong and significant at 20% of maximal voluntary contraction (MVC; left graph) but only moderate and non-significant at 50% of MVC (right graph). EMG, electromyography, PCSA, physiological cross-sectional area, VL, *vastus lateralis*; VM, *vastus medialis*. From Hug et al. (2015a).

A similar approach was used in the hamstrings (Avrillon et al., 2018, 2020). The authors were interested in the torque-generating capacity of the muscle and therefore they additionally experimentally determined the moment arm. Large inter-individual variability in muscle coordination was observed within the hamstrings suggesting the presence of individual strategies (Figure 21). Specifically, the contribution of *biceps femoris*, *semimembranosus* and *semitendinosus* to the overall torque ranged from 20% to 55%, from 25% to 65% and from 5% to 45%, respectively during a knee flexion at 20% of MVC (Avrillon et al., 2018). Moreover, results suggested that individual muscle coordination strategies can be related to motor performance (Avrillon et al., 2018). Specifically, the participants that had a more evenly distributed muscle coordination within the hamstring muscles were able to sustain longer a time-to-exhaustion exercise. The same researchers later showed that previous injury can also affect muscle coordination. The contribution of the previously injured *biceps femoris* to total knee flexion torque was lower compared to the non-injured leg and compensated by a greater contribution of the *semimembranosus* (Avrillon et al., 2020). Of note, the neuromechanical coupling, found earlier in the *vastii*, was not found between the torque-generating capacity and activation within the hamstrings muscle group (Avrillon et al., 2018).

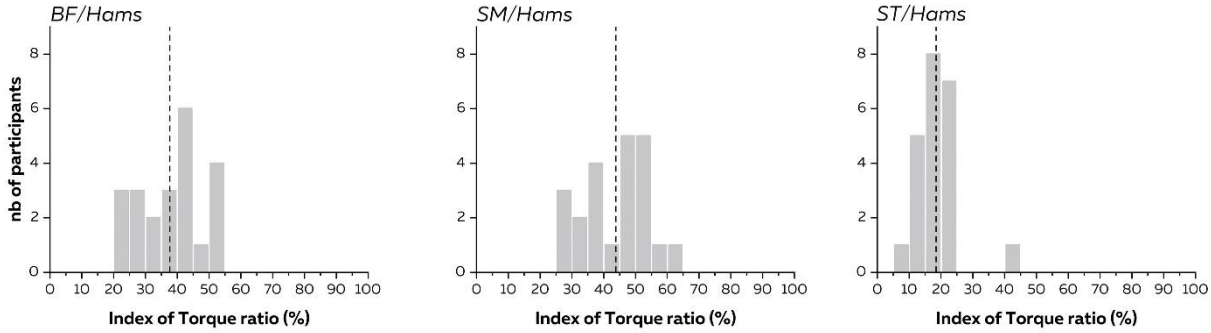


**Figure 21: Inter-individual variability in the distribution of torque within the hamstring muscles.** The contribution of biceps femoris (left panel), semimembranosus (middle panel) and semitendinosus (right panel) to the overall hamstring torque are displayed. The dashed vertical line represents the average torque ratio for each muscle. A large inter-individual can be observed. BF, *biceps femoris*; Hams, hamstrings; SM, *semimembranosus*; ST, *semitendinosus*. From Avrillon et al. (2018).

The contribution of individual *triceps surae* muscles to plantar flexion moment is also highly variable between individuals. The contribution of the GM, GL and *soleus* to the overall *triceps surae* force ranged from 5% to 50%, from 5% to 15% and from 40% to 85%, respectively, during an ankle plantar flexion at 20% of MVC (Crouzier et al., 2018). Furthermore, Crouzier et al. (2018) observed an association between the distribution of activation between the GM and GL and the distribution of PCSA between the GM and GL. This confirmed the neuromechanical coupling previously observed between the *vastii* (Hug et al., 2015a). Later, using similar approach, the same authors reported an association between musculoskeletal disorders and altered muscle coordination in the *triceps surae*, which echoes the previously mentioned work on hamstring muscles. Specifically, results revealed that the GL contributed less to the *triceps surae* force in participants with Achilles tendinopathy compared to healthy controls (Crouzier et al., 2019b).

Taken together, this series of studies revealed that muscle coordination varies between individuals. Evidences suggest that this inter-individual variability emerges from the neuromechanical coupling between the activation a muscle receives and its biomechanical characteristics, such as PCSA. As a consequence, the central nervous system might consider the muscle features to optimize the distribution of activation among synergist muscles. Moreover, the large inter-individual variability observed seems to have functional consequences. Specifically, the individual muscle coordination strategy was associated with motor performance and the presence of musculoskeletal disorder. Although combining an experimentally determined PCSA and muscle activation provides insights into muscle coordination, this approach is limited to isometric contractions. During less controlled tasks

such as locomotion, the influence of force-length and force-velocity relationships should be considered. As a consequence, in these tasks, the estimation of muscle coordination requires another approach.

### 2.2.2. Estimation of muscle coordination using biomechanical models

Since the distribution problem was established, researchers have used biomechanical modelling to estimate muscle forces (Penrod et al., 1974; Seireg & Arvikar, 1973, 1975). The combination of inverse dynamics and static optimization techniques was initially used to determine muscle coordination. The relevance of the inverse dynamics-based prediction to study muscle coordination seemed dependent of the objective function used. The first attempts using this approach were unrealistic (Penrod et al., 1974; Seireg & Arvikar, 1973, 1975). For example, during walking, models predicted that only a few synergist muscles were simultaneously activated. Moreover, muscles with small PCSA such as tibialis anterior, produced high amounts of force whereas larger muscles produced almost no force (Seireg & Arvikar, 1975). The use of more physiological objective functions that considered the mechanical properties of muscle (Crowninshield et al., 1978; Crowninshield & Brand, 1981a, 1981b) or the muscle fiber composition (Dul et al., 1984) resulted in more reasonable predictions. Moreover, these later study predictions agreed with empirical EMG recordings. The results from these studies suggested that the central nervous system preferentially activates the muscles with the larger PCSA and the higher proportion of slow muscle fiber to minimize the energetic cost and fatigue. This is in agreement with the neuromechanical coupling found in the *vastii* and *gastrocnemii* (Crouzier et al., 2018; Hug et al., 2015a). Studies using forward dynamics approaches to determine the contribution of individual muscles are less numerous than inverse dynamics studies (Erdemir et al., 2007). For instance, this approach has been used to determine that the *gastrocnemii* and *soleus* had opposite energetic effects on the leg and trunk during the single-leg stance phase to ensure support and forward progression (Neptune et al., 2001). Despite the improvements made over the years, important limitations in these approaches remain such as a lack of validity and accuracy (Ait-Haddou et al., 2004; Challis, 1997; Herzog & Leonard, 1991). Although these two approaches use experimentally-determined external kinetics or kinematics, none consider any subject-specific determinant of force as input. Taken together, these limits has led researchers to use alternative models such as EMG-driven models that consider subject-specific inputs.

Traditional EMG-driven models have been used to determine individual muscle force. For instance, Menegaldo & Oliveira (2011) observed that muscle coordination within the quadriceps remained unchanged after 13 weeks of knee flexion strength training. This approach was also used to suggest that muscle coordination was maintained with the aging process (Oliveira et al., 2017). The lower limb muscle force was also estimated during walking for healthy patients (Lloyd & Besier, 2003) and for stroke patients (Shao et al., 2009). Despite these models used subject-specific EMG, the other parameter of the muscle model such as maximal force-generating capacity, the dynamic fascicle behavior or the tendon properties are generic and could lead to inaccuracies. Recent studies extended the possibilities of muscle models by adding more experimental inputs than solely EMG. For example, the tendon-aponeurosis properties (Gerus et al., 2012) and muscle architecture (Gerus et al., 2015) determined using B-mode ultrasound enabled to improve the muscle force prediction of the Hill-type model. However, these studies were performed in only one muscle (the GM), which does not provide information on between-muscle coordination. Another study used time-varying fascicle length, fascicle velocity and pennation angle to estimate individual force from the GM and GL during cycling (Dick et al., 2017). The authors showed that GM and GL produced similar level of force relative to their maximal force-generating capacity during cycling (Figure 22). As the GM had higher maximal force-generating capacity, the distribution of force between GM and GL was unbalanced towards the GM (Dick et al., 2017). Nevertheless, some parameters of the Hill-type model remained generic such as the maximal-force generating capacity of muscle. Yet, recent studies suggested that the use of subject-specific maximal-force generating capacity could improve the accuracy of models (Charles et al., 2018, 2020). To our knowledge, there is no study that used subject-specific EMG, fascicle contractile behavior and maximal force-generating capacity inputs to investigate muscle coordination.

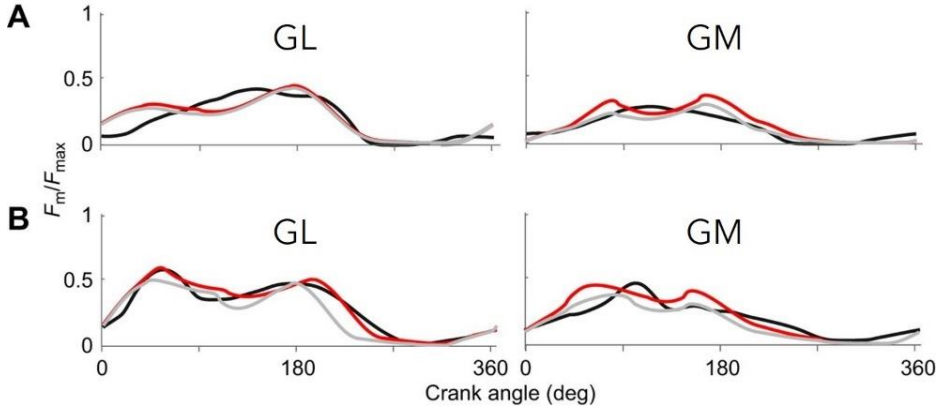


**Figure 22: Forces produced by the human *gastrocnemius medialis* and *gastrocnemius lateralis* during cycling.** The figure represents the time-varying forces estimated from ultrasound measures of tendon strain (black), predicted by a conventional Hill-type model

(grey), and predicted by a Hill-type model that accounts for the independent contributions of slow and fast motor units (red). Muscle force ($F_m$) is normalized to the maximum isometric force ($F_{max}$). A represents the *gastrocnemius medialis* (GM) and *gastrocnemius lateralis* (GL) forces during pedalling at 60 rpm cadence at 44 Nm crank torque. B represents the GM and GL forces during pedalling at 100 rpm cadence at 26 Nm crank torque. From Dick et al., (2017).

# Muscle coordination

—

# Summary

Muscle coordination refers to the distribution of force among individual muscles to produce a given joint moment. The number of muscles that cross a joint largely exceeds the number of degrees of freedom available at the joint. This means that the musculoskeletal system is redundant. Thereby, numerous muscle coordination strategies exist to produce a given joint moment. Even though muscle redundancy means that there is theoretically an infinite number of muscle coordination strategies available to produce a given joint moment, mechanical and neural constraints limit these possibilities. Nevertheless, the central nervous system has to select particular muscle coordination among the numerous alternatives.

Muscle coordination has been studied in various animals to understand the mechanisms underlying the use of a particular muscle coordination strategy. Studies in cats revealed that muscle coordination is highly flexible and depends on the mechanical demands. Despite the lack of an experimental method to measure individual muscle forces in humans, some studies have used alternative approaches to provide information about the distribution of force across human muscles. Evidence has shown that the human central nervous system preferentially activates muscles with the larger PCSA. Nevertheless, information about muscle coordination in humans are sparce and further studies are required to better understand muscle coordination, especially during locomotion.

# Part 3: Application to the *triceps surae*

The *triceps surae* is a muscle group located in the posterior compartment of the lower leg. It comprises the biarticular GM and GL and the monoarticular *soleus*. The three muscles have independent origins, but distally, their respective tendons combine to form the common Achilles tendon which inserts into the posterior calcaneus. The primary function of the *triceps surae* is to generate ankle plantar flexion torque, thereby playing a fundamental role in locomotion (Dorn et al., 2012; Hamner & Delp, 2013). Nevertheless, the *triceps surae* contains biarticular muscles that span the knee and thus also contribute to knee flexion. In this section, we first describe the functional anatomy of the *triceps surae* muscles. Then, we discuss the distribution of activation between the *triceps surae* muscles. Finally, we elaborate on the functional interplay between muscle activation and the muscle architecture.

## 1. Functional anatomy of the *triceps surae*

### 1.1. *Triceps surae* muscles

The GM and GL are biarticular and superficial muscles (Figure 23). They originate from the medial and lateral femoral condyles, respectively. Thereby, the *gastrocnemii* are both knee flexors and ankle plantar flexors. The GM and GL have a unipennate muscle architecture. Of note, although some studies reported two or three compartments in the GL (Johnson et al., 1973; Segal et al., 1991), most consider that GL is constituted of one unipennate compartment. Importantly, as the GM and GL are biarticular, their lengths and therefore their ability to produce force with respect to the force-length relationship depends on both knee angle and ankle angle (Cresswell et al., 1995). The *triceps surae* also contains a monoarticular muscle, the *soleus*. This large muscle lies deep to the *gastrocnemii* and originates from the posterior surfaces of the fibula and tibia to insert on the calcaneus via the Achilles tendon. In contrast to the GM and GL, the *soleus* is only a plantar flexor muscle. Another property that distinguishes the *soleus* from the GM and GL is its complex 3D architecture that comprises four compartments (i.e. antero-medial; antero-lateral; postero-medial and postero-lateral). The compartments are separated by an intra-muscular aponeurosis in the transverse plane and by the medial septum in the sagittal plane (Wickiewicz et al., 1983). The unipennate posterior compartments wrap around the radially bipennate anterior compartments. The overall *triceps*

*surae* muscles represent roughly 73% and 80% of the total plantar flexor volume and PCSA, respectively (Fukunaga et al., 1996).

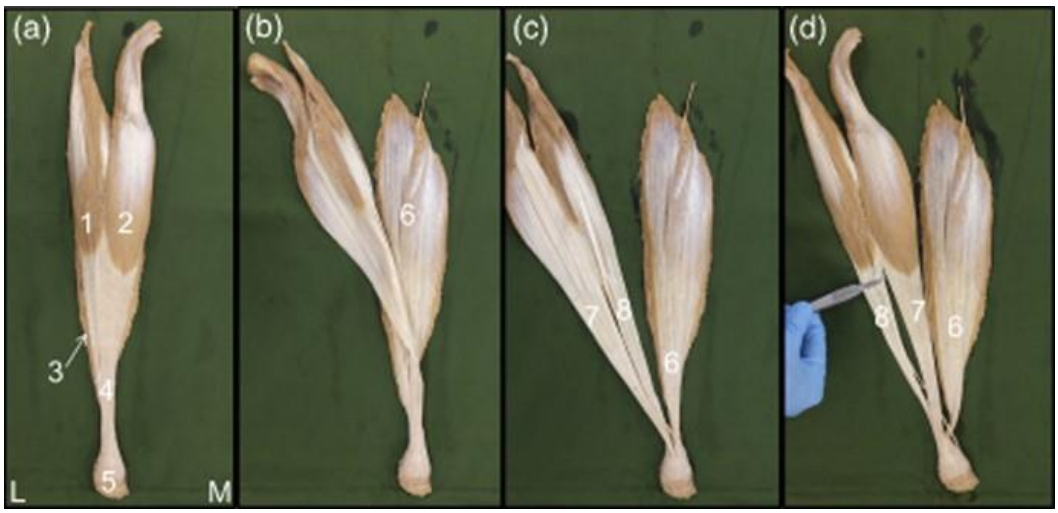


**Figure 23: Dissection of the *triceps surae***. Different step of the dissection process are represented in (a), (b), (c) and (d). 1, *gastrocnemius lateralis* (GL); 2, gastrocnemius medialis (GM); 3, *soleus*; 4, Achilles tendon; 5, calcaneus; 6, fascicle from the *soleus;* 7, fascicle from the GM; 8, fascicle from the GL; L, lateral; M, medial. From Edama et al. (2015).

Muscle volume is not evenly distributed between the three heads of the *triceps surae*. The GM, GL and *soleus* volumes are respectively ~30%, ~17% and ~53% of the total *triceps surae* volume (Table 1). The resting muscle architecture is also quite different between the muscles. The GL has the longer fascicle length followed by the GM and the *soleus* (Table 1). Of note, a recent study used DTI to determine the 3D architecture of the plantar flexors and reported no differences between the GM and GL fascicle length (Aeles et al., 2021a). This discrepancy could be related to the selectivity of the 2D B-mode ultrasound compared to the DTI which provides fascicle length estimation from the whole muscle. The GL is also characterized by a smaller pennation angle compared to the GM and *soleus* which exhibit similar values (Kawakami et al., 1998; Morse et al., 2005a).

**Table 1: Review of muscle volume, architecture, and muscle fiber composition of the *triceps surae* muscles.** All Muscle volume, architecture and physiological cross-sectional area (PCSA) data reported in this table were measured *in vivo* on healthy subjects. For the fascicle length and pennation angle, the measure was performed at rest in anatomical position (knee angle at 180° and ankle angle at 90°). For the PCSA, we reported only the studies that did not integrate the pennation angle in the PCSA calculation. Data are reported as mean ± s.d. or mean [range]. GM, *gastrocnemius medialis*; GL, *gastrocnemius lateralis*.

| | GM | GL | *Soleus* | Reference |
|---|---|---|---|---|
| **Volume ($cm^3$)** | 285 ± 45 | 146 ± 23 | 477 ± 66 | Albracht et al., 2008 |
| | 274 ± 75 | | | Barber et al., 2009 |
| | | | 362 ± 59 | Bolsterlee et al., 2018 |
| | 251 ± 64 | 137 ± 50 | 448 ± 193 | Bolsterlee et al., 2019 |
| | 230 ± 48 | 128 ± 35 | 461 ± 108 | Charles et al., 2019 |
| | 250 ± 54 | 138 ± 40 | 420 ± 98 | Crouzier et al., 2018 |
| | 244 ± 42 | 155 ± 33 | 451 ± 58 | Crouzier et al., 2019b |
| | 244 ± 33 | 141 ± 28 | 489 ± 65 | Fukunaga et al., 1992 |
| | 250 ± 14 | 145 ± 9 | 504 ± 23 | Fukunaga et al., 1996 |
| | 247 ± 17 | 130 ± 7 | 430 ± 12 | Kinugasa et al., 2005 |
| | 303 ± 65 | 178 ± 39 | 520 ± 114 | Morse et al., 2005a |
| | 234 ± 67 | 145 ± 42 | 416 ± 127 | Pinel et al., 2021 |
| **Fascicle length (cm)** | 5.7 ± 0.7 | 6.6 ± 0.7 | 3.9 ± 0.9 | Albracht et al., 2008 |
| | 5.7 ± 0.9 | | 4.2 ± 1.0 | Cronin et al., 2008 |
| | 5.4 ± 0.8 | 6.4 ± 0.7 | 3.9 ± 0.8 | Crouzier et al., 2018 |
| | 5.9 ± 0.7 | 6.7 ± 0.8 | 4.0 ± 0.7 | Crouzier et al., 2019b |
| | 5.4 ± 0.7 | 6.3 ± 1.0 | 4.6 ± 0.9 | Geremia et al., 2019 |
| | 5.2 ± 0.7 | 5.6 ± 0.8 | 3.8 ± 0.4 | Kawakami et al., 1998 |
| | 4.4 ± 0.9 | 4.2 ± 0.7 | 3.0 ± 1.1 | Martin et al., 2001 |
| | 6.3 ± 1.2 | 7.0 ± 1.4 | 4.3 ± 0.8 | Morse et al., 2005a |
| | | 5.5 ± 1.1 | | Morse et al., 2005b |
| | 5.5 ± 0.3 | | | Muramatsu et al., 2002 |
| | 5.1 ± 0.4 | | | Narici et al., 2016 |
| | 5.1 ± 0.7 | 5.7 ± 0.7 | 3.5 ± 0.8 | Pinel et al., 2021 |
| | 4.8 ± 0.7 | | 4.1 ± 1.0 | Stenroth et al., 2012 |
| **Pennation angle (°)** | 10 ± 4 | 9 ± 3 | 12 ± 2 | Charles et al., 2019 |
| | 27 ± 8 | | 23 ± 4 | Cronin et al., 2008 |
| | 20 ± 4 | 11 ± 3 | 20 ± 7 | Crouzier et al., 2018 |
| | 18 ± 2 | 13 ± 2 | 23 ± 4 | Crouzier et al., 2019b |
| | 21 ± 2 | 12 ± 1 | 18 ± 2 | Geremia et al., 2019 |
| | 24 ± 2 | 13 ± 1 | 21 ± 3 | Kawakami et al., 1998 |
| | 19 ± 4 | 16 ± 3 | 24 ± 6 | Martin et al., 2001 |
| | 22 ± 3 | 14 ± 2 | 25 ± 3 | Morse et al., 2005a |
| | | 18 ± 4 | | Morse et al., 2005b |
| | 17 ± 3 | | | Narici et al., 1996 |
| | 21 ± 3 | 15 ± 4 | 20 ± 3 | Pinel et al., 2021 |
| | 25 ± 4 | | 20 ± 5 | Stenroth et al., 2012 |
| **PCSA ($cm^2$)** | 51 ± 10 | 24 ± 5 | 131 ± 31 | Albracht et al., 2008 |
| | | | 102 ± 19 | Bolsterlee et al., 2018 |
| | 49 ± 6 | 26 ± 5 | 128 ± 26 | Morse et al., 2005a |
| | | 32 ± 6 | | Morse et al., 2005b |
| **Slow muscle fiber proportion (%)** | | 54 | | Coggan et al., 1992 |
| | 50 [16-86] | 52 [37-62] | 70 [12-95] | Edgerton et al., 1975 |
| | | 60 [45-82] | 80 [64-100] | Gollnick et al., 1974 |
| | | 49 ± 3 | | Green et al., 1981 |
| | | | 78 ± 17 | Harridge et al., 1996 |
| | 51 | 47 | 88 | Johnson et al., 1973 |
| | 50 ± 20 | | | Moss, 1992 |
| | | 54 ± 16 | | Rice et al., 1988 |
| | | 54 ± 3 | 71 ± 5 | Secher et al., 1982 |

These between-muscle differences in volume and architecture lead to large difference in PCSA between the GM, GL and *soleus*. The *soleus* has a PCSA more than twice that of the GM which itself has a PCSA twice as large as the GL. Specifically, the GM, GL and *soleus* PCSAs are respectively ~26%, ~14% and ~60% of the total *triceps surae* PCSA. The different muscles from the *triceps surae* have very different force-generating capacities. Moreover, the muscle volume, muscle architecture and PCSA vary greatly between individuals. For example, in young and healthy participants, the individual contribution of each muscle to the overall *triceps surae* PCSA ranged from 17.9% to 33.1%, from 8.8% to 19.5% and from 50.6% to 68.5% for the GM, GL and *soleus*, respectively (Crouzier et al., 2018; Figure 24).

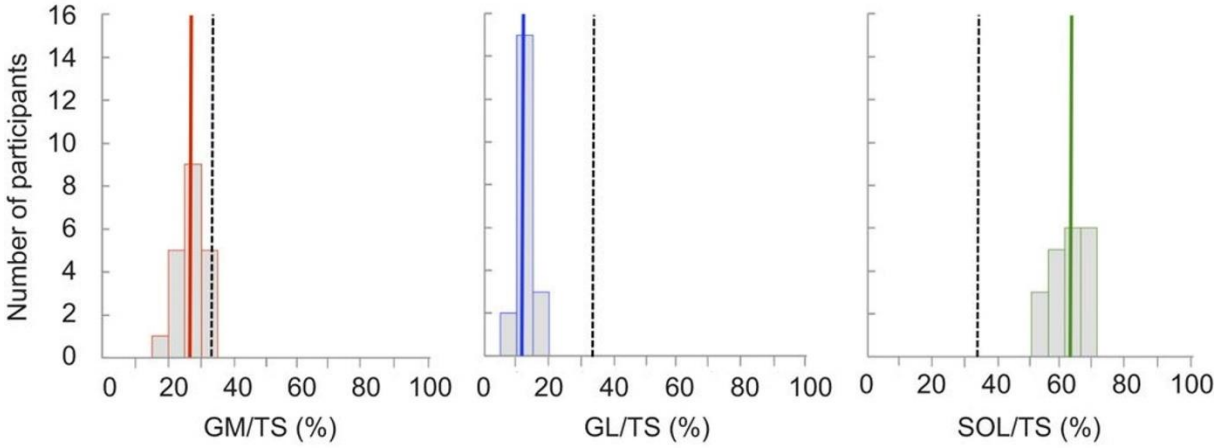


**Figure 24: Inter-individual variability in the distribution of physiological cross-sectional area within the *triceps surae*.** The dashed vertical line represents an evenly distributed physiological cross-sectional area (PCSA) among the three muscles. The thick vertical line represents the mean PCSA ratio for each muscle. GL, *gastrocnemius lateralis*; GM, *gastrocnemius medialis*; Sol, *soleus*; TS, *triceps surae*. From Crouzier et al. (2018).

As explained in Part 1, section 1.2.1.4., the specific tension cannot be experimentally measured in humans but it is mainly related to the muscle fiber composition of the muscle. Therefore, muscle fiber type can provide indirect information about specific tension. Cadaveric studies reported that both the GM and GL are composed of around 50% of slow muscle fibers (Edgerton et al., 1975; Johnson et al., 1973). These studies also reported higher percentages, i.e. 70-90%, of slow muscle fiber, for the *soleus* compared to the *gastrocnemii* (Edgerton et al., 1975; Johnson et al., 1973). These percentages are confirmed by studies on living human using biopsy. For example, Secher et al. (1982) found that the GL and *soleus* contains respectively 54% and 71% of slow muscle fibers. Taken together, these studies suggest that the specific tension of the GM and GL is likely similar and higher compared to the specific tension of the *soleus*.

## 1.2. The Achilles tendon

The Achilles tendon corresponds to the connective tissue that connects the distal end of the *triceps surae* muscles to the calcaneus. The Achilles tendon is the largest and strongest tendon in the human body (Pang & Ying, 2006), allowing it to tolerate high stresses and high strains. Within the Achilles tendon, the proximal section and the free section are commonly distinguished. The proximal section of the Achilles tendon contains only the tendons from the GM and GL due to their proximal locations and longer tendons compared to the *soleus*. Then, from the *soleus* myotendinous junction, the *gastrocnemii* tendons merge with the *soleus* tendon to form the free Achilles tendon (Edama et al., 2015; Szaro et al., 2009, 2020). The proximal section and free section represent roughly 75% and 25% of the total Achilles tendon length, respectively (Pękala et al., 2017). Tendon fibers arising from each muscle are grouped into subtendons (Handsfield et al., 2016). These subtendons can be anatomically distinguished and separated (Edama et al., 2015; Pękala et al., 2017; Szaro et al., 2009; Figure 25). Subtendons are arranged in parallel in the proximal section of the tendon and then, in the free tendon, twist counter-clockwise for the right leg and clockwise for the left leg. The degree of twist is highly variable between participants (Edama et al., 2015; Funaro et al., 2022; Szaro et al., 2009). Different hypotheses have been established about the role of the Achilles tendon twist. It has been suggested to enhance the ability to store and release energy, to optimize the length of each muscle, or to regulate the intra-tendinous stresses and strains within the Achilles tendon (Bojsen-Møller & Magnusson, 2015).

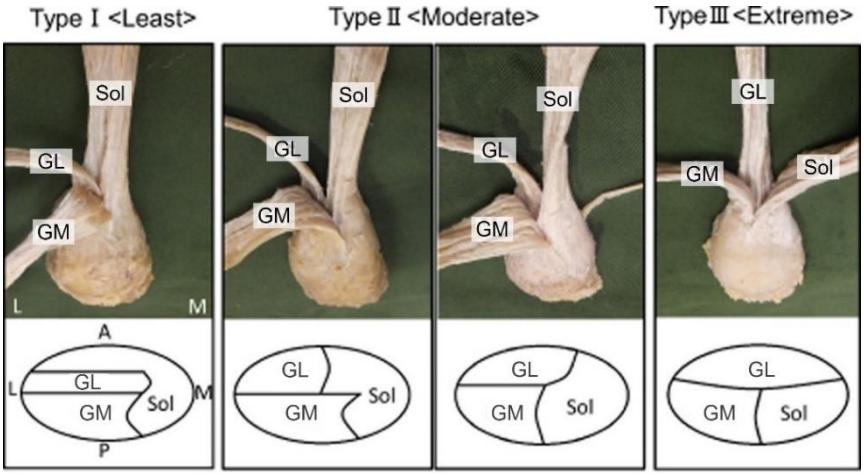


**Figure 25: The subtendons structure and twist and the Achilles tendon**. Postero-superior view of human Achilles tendons dissected. Three patterns of twist, from least twisted (left panel) to extremely twisted (right panel) are represented. The lower diagrams represent the transverse cross-section through the left Achilles tendon 1 cm above the insertion of the Achilles tendon on the *calcaneus*. A, anterior; GL, g*astrocnemius lateralis*; GM, *gastrocnemius medialis*; L, lateral; M, medial; P, posterior; Sol, *soleus*. from Edama et al. (2015).

Evidence reported that the high level of lubricin in the inter-fascicular matrix of the Achilles tendon enables sliding between subtendons (Sun et al., 2015). Each subtendon could therefore behave in an independent manner. Although *in vivo* approaches to measure the behavior of each subtendon within the free Achilles tendon remains lacking, indirect evidence supports this hypothesis. Several studies have employed speckle tracking techniques to demonstrate non-uniform displacements within the free Achilles tendon during passive movement (A. Arndt et al., 2012), isometric contractions (Clark & Franz, 2018; Farris et al., 2013), eccentric contractions (Slane & Thelen, 2015) and walking (Franz et al., 2015). Cadaveric (A. Arndt et al., 1999), animal (Finni et al., 2018; Maas et al., 2020) and modelling (Handsfield et al., 2017) studies have confirmed the partially independent behavior of individual subtendons and revealed that the individual subtendon behaviors are related to the distribution of forces within the *triceps surae*, i.e. the muscle coordination strategies (Figure 26).

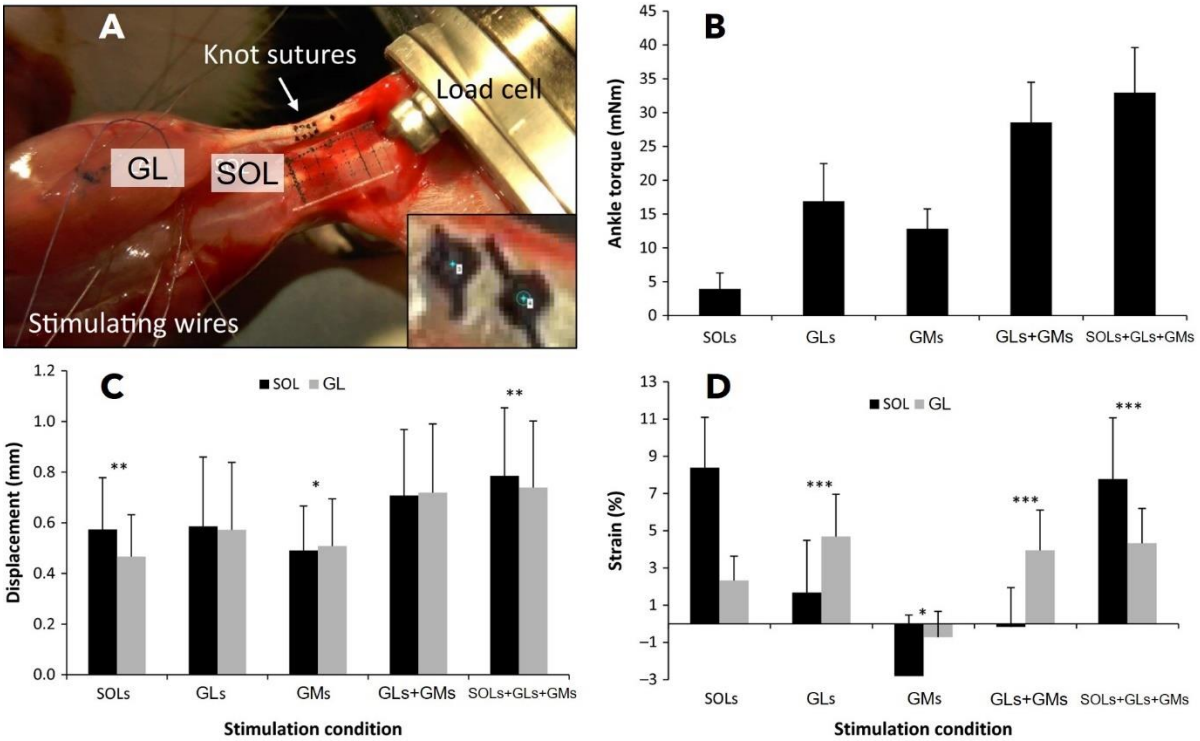


**Figure 26: Interplay between specific muscle stimulation and subtendon behavior of the rat Achilles tendon**. A represents the experimental setup with the sutured Achilles tendon, the load cell used to record the torque, the *gastrocnemius lateralis* (GL) and the *soleus* (Sol). The other panels represent the ankle torque (A), the GL and *soleus* tendon displacements (C) and the GL and *soleus* tendon strains (D) depending of different stimulation conditions. They authors found that the GL and soleus subtendons can have distinct displacements and can undergo distinct strains depending of the stimulation condition. From Finni et al. (2018).

Due to their viscoelastic nature, tendons can have a variety of mechanical roles (Roberts & Azizi, 2011; Figure 27). First, tendon plays a role in energy conservation. For example, tendon store and return elastic energy, thereby enabling the contractile element to undergo smaller length changes than the whole muscle-tendon unit. This allows to the muscle fibers to operate at more optimal length and velocity (Roberts & Azizi, 2011). Second, tendons can play an important role in power amplification, via the slow storage and quick release of energy. The work released by the tendon is nearly equal to the muscle work, but it is released in a shorter time to generate higher power outputs (Alexander et al., 1982; Biewener et al., 1998a; Wilson et al., 2003). Third, tendons play a role in energy dissipation. For example, when a muscle-tendon unit undergoes rapid stretch, much of the length change occurs in the tendon which protects muscle fibers from potential damaging strains (Konow et al., 2011; Proske & Morgan, 2001; Roberts & Konow, 2013). Finally, tendons play an important role in movement stability during unexpected environmental perturbations. Specifically, the spring-like behavior of the tendon can address unexpected changes in running or hopping surface stiffness in humans (Moritz & Farley, 2004) and in guinea fowl (Daley et al., 2006). The tendon is therefore a flexible structure that can serve diverse functions depending on the muscle activation.

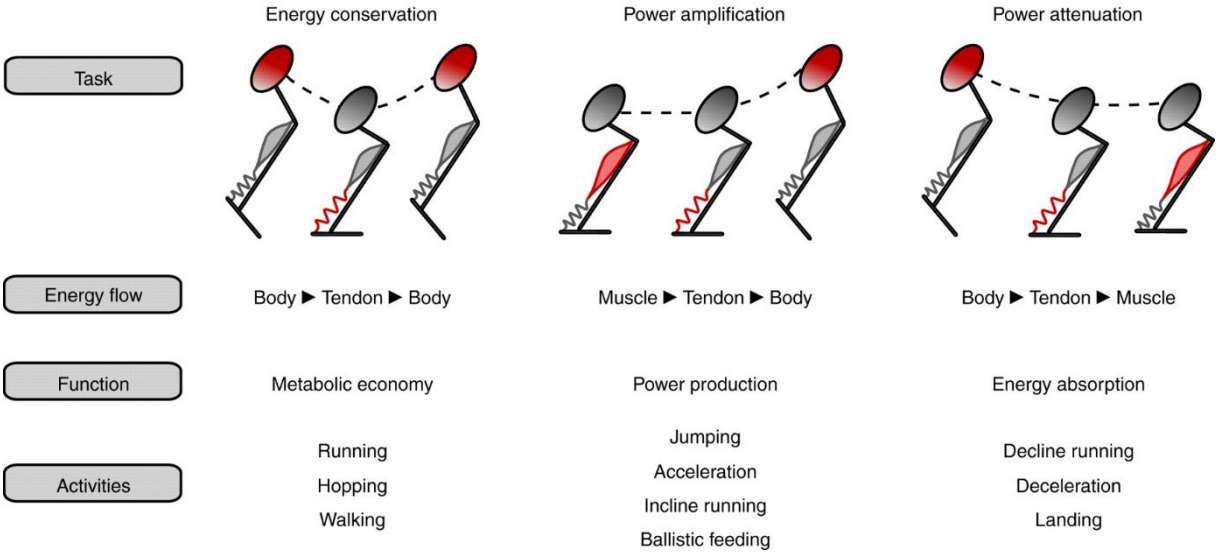


**Figure 27: Schematic illustration of different roles of tendons.** The energy conservation role (left panel), the power amplification role (middle panel) and the power attenuation role (right panel) of tendon are depicted. Each panel displays a schematic illustration, the directional flow of energy, the main function and examples of activity where this main function is used. From Roberts & Azizi (2011).

# 2. The distribution of muscle activation within the *triceps surae*

Muscle activation is not evenly distributed between the muscles of the *triceps surae* as revealed by EMG (Crouzier et al., 2019a; Lacourpaille et al., 2017; Masood et al., 2014), positron emission tomography (Masood et al., 2014) and functional MRI (Kinugasa et al., 2005) techniques. For example, EMG data revealed higher activation in the GM compared to the GL with no statistical differences between the GM and *soleus* or between the GL and *soleus* during an ankle plantar flexion at 30% of MVC (Masood et al., 2014). Later, a study confirmed this by showing that the contribution of GM activation (36.3 ± 11.4%) and *soleus* activation (44.8 ± 8.9%) to the overall *triceps surae* activation were higher than the contribution of GL activation (18.8 ± 6.4%) during an ankle plantar flexion at 20% of MVC (Crouzier et al., 2018). The distribution of muscle activation within the *triceps surae* during walking is similar to that observed during isometric ankle plantar flexion. Specifically, the GL was less activated compared to the GM (Ahn et al., 2011; Crouzier et al., 2019a) and compared to the *soleus* (Crouzier et al., 2019a) during walking at various speed ranging from 0.3 $m.s^{-1}$ to 1.5 $m.s^{-1}$. Interestingly, the distribution of activation within the *triceps surae* varies greatly between participants during both isometric ankle plantar flexion contractions (Crouzier et al., 2018; Crouzier et al., 2019a) and walking (Ahn et al., 2011; Crouzier et al., 2019a; Figure 28). For example, the GM, GL and *soleus* activation contribution relative to the overall *triceps surae* activation ranged, respectively, from 19.1% to 57.0%, from 7.3% to 31.6% and from 26.4% to 61.0% (Crouzier et al., 2018).

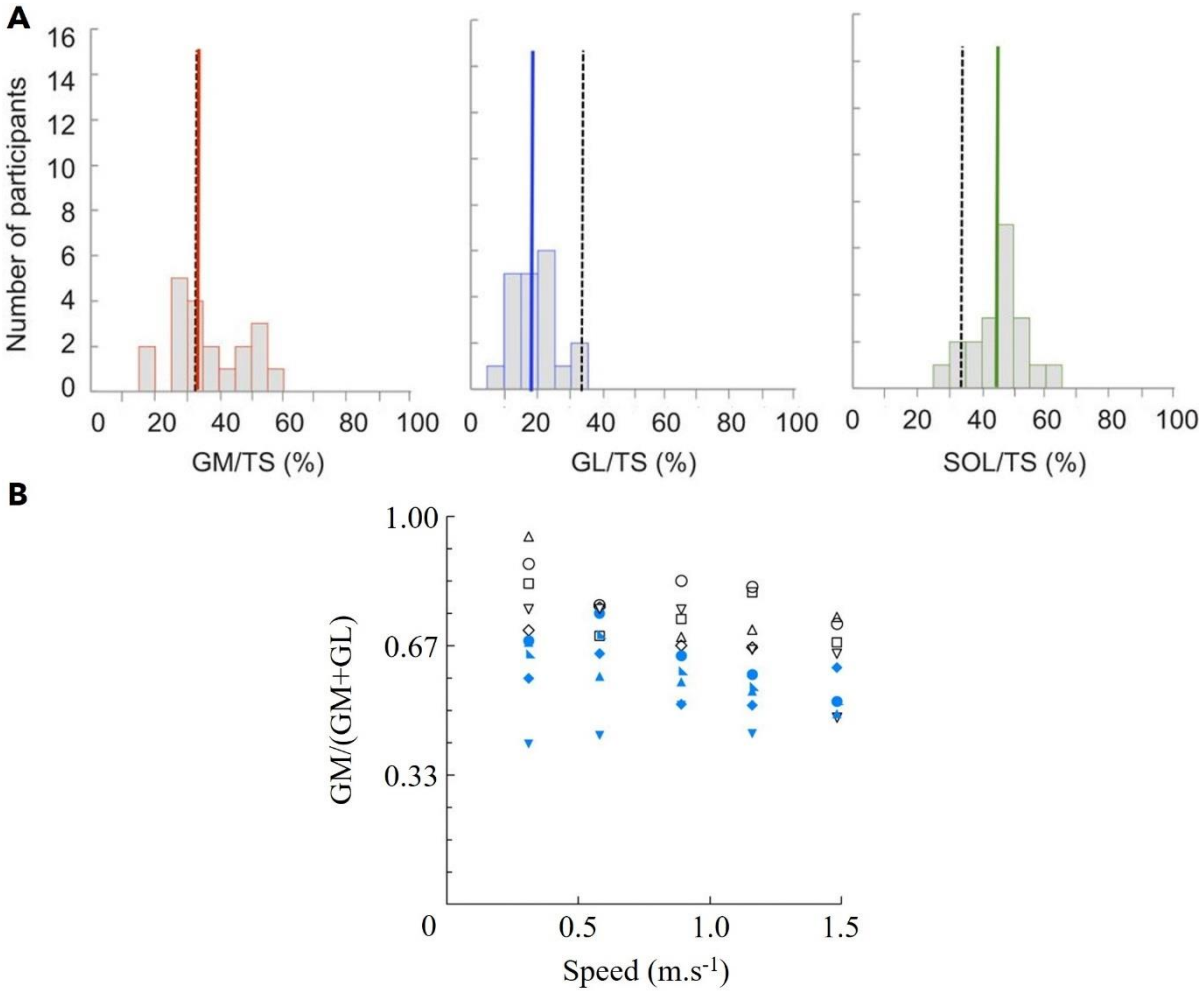


**Figure 28: Inter-individual variability in the distribution of muscle activation within the *triceps surae*.** A represents the muscle activation within the *triceps surae* during an isometric ankle plantar flexion at 20% of MVC. The dashed vertical line represents an evenly distributed physiological cross-sectional area (PCSA) among the three muscles. The thick vertical line represents the mean PCSA ratio for each muscle. B represents the distribution of activation between the *gastronemii* during walking. The open symbols represents the individuals who exhibited the highest GM activation compared to the GL whereas the blue symbol represents the participants that had a more balanced activation. GL, *Gastrocnemius lateralis*; GM, *Gastrocnemius medialis*; Sol, *soleus*; TS, *triceps surae*. A from Crouzier et al. (2018) and B from Ahn et al. (2011).

The highly individual distribution of activation within the *triceps surae* during isometric ankle plantar flexion was reliable across different days (Crouzier et al., 2019a). Moreover, this distribution of activation within the *triceps surae* was also consistent between isometric ankle plantar flexion, walking and pedalling tasks (Crouzier et al., 2019a). This robustness of individual distribution of muscle activation within the *triceps surae* across days and across tasks suggests that the variability is not random but rather that each individual uses their own unique coordination strategy across different tasks. Hug et al. (2019) confirmed this hypothesis and

showed that muscle activation is much like a signature, i.e. a distinctive patterns robust across time by which someone can be identified. In this study, the authors used a machine-learning approach to demonstrate the uniqueness of activation patterns. Based on the EMG profiles from 8 muscles during walking, this approach was able to identify the different participants with 99% accuracy (Hug et al., 2019). A follow up study revealed that the unique muscle activation signature is related to specific portions of the EMG profile (Aeles et al., 2021b). The individual activation signature might originate from the neuromechanical coupling between the PCSA and muscle activation (see Part 2, section 2.2.1; Crouzier et al., 2018). The central nervous system might activate muscles in an individual way to take advantage of the PCSA and musculoskeletal properties that vary greatly between individuals. This assumption needs to be confirmed and further works are required to better understand the origin and consequences of individual muscle activation strategies.

# 3. Functional interplay between muscle architecture and muscle activation

## 3.1. Overall muscle-tendon unit function

The human *triceps surae* muscle-tendon units have short pennate fibers connected to a long and compliant tendon. These features are typical of the distal limb and are shared by numerous species (Biewener et al., 1998b; Biewener & Roberts, 2000; Roberts, 1997, 2002). On the one hand, compared to a muscle with long and parallel muscle fiber, a muscle with short and pennate muscle fibers activates a smaller volume to generate a given force (Figure 29; Roberts et al., 1998). Thereby, such muscle architecture limits the metabolic cost. On the other hand, long and compliant tendons decouple muscle length changes from muscle-tendon unit length changes. This favors economical force production by allowing the muscle fibers to work at more optimal length and velocity (Biewener, 1998a). The energetic benefit of this minimization of changes in muscle fascicle length is however questioned (Holt et al., 2014). Other works rather suggest that the benefit of a long tendon is related to the concentration of the muscle mass proximally within the limb which contributes to reduce the inertia and therefore swing costs (Browning et al., 2007; Tickle et al., 2010). Taken together, these features make the *triceps surae* primarily designed for efficient force production (Biewener, 1998a, 2016; Roberts, 1997). Nevertheless, the muscle-tendon unit function is also flexible and depends, for example on the timing of activation relative to muscle length changes (Roberts & Azizi, 2011; Sawicki et al., 2015).

Muscle-tendon unit function can be broadly characterized into four distinct behaviors: (i) a motor that mainly generates positive work by active shortening; (ii) a spring that stores and releases elastic strain energy; (iii) a strut that can sustain substantial force with minimal length change; and (iv) a damper that absorbs energy by lengthening (Dickinson et al., 2000).

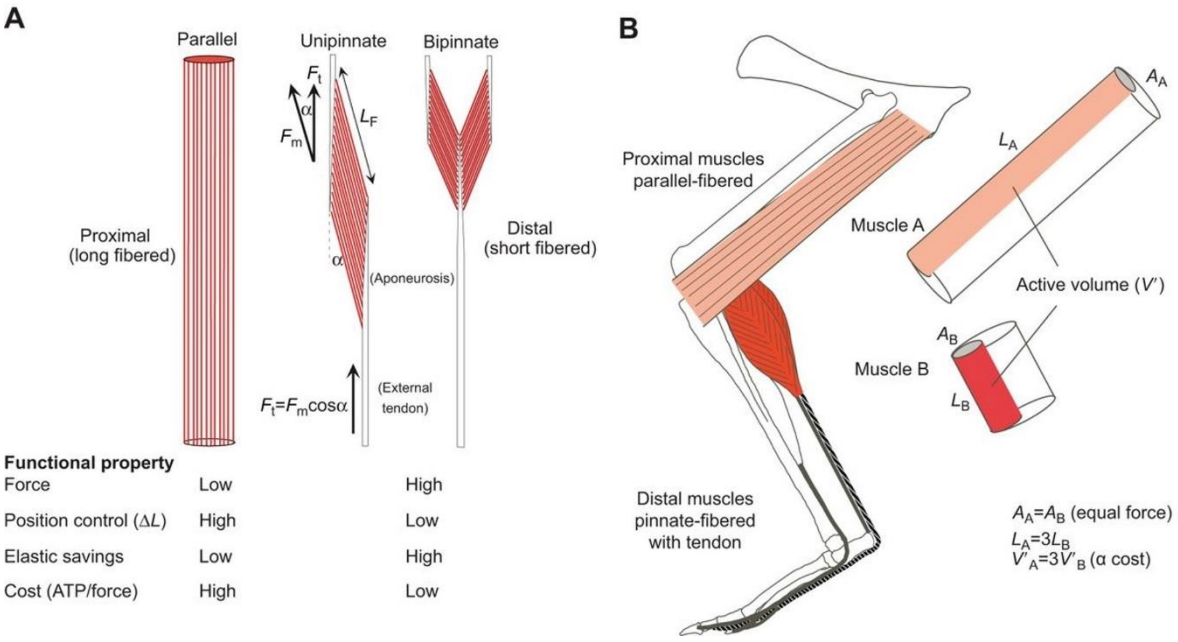


**Figure 29: Functional property of muscle architecture.** A displays a comparison of the functional property between parallel and pennate muscles. B represents the functional cost of activation for a parallel muscle and for a pennate muscle. α, pennation angle; Δ*L*, length changes; $A_A$, area of muscle activated for the muscle A; $A_B$, area of muscle activated for the muscle B; ATP, adenosine triphosphate; $F_t$, tendon force; $F_m$, muscle force; $L_A$, length of the muscle fibers activated for the muscle A; $L_B$, length of the muscle fibers activated for the muscle B; $L_F$, fascicle length; *V'*, active volume. From Biewener et al. (2016).

Walking can be used to illustrate the primary function of the *triceps surae* muscle-tendon units and its flexibility. On the one hand, the *triceps surae* fits the mold of highly compliant muscle-tendon units useful for efficient locomotion. About 20 years ago, human studies using B-mode ultrasound and motion capture revealed that, during the first part of the stance phase, the muscle-tendon units lengthens while muscle fascicles act nearly isometrically (Fukunaga et al., 2001; Ishikawa et al., 2005). Through lengthening of the muscle-tendon units, the tendon is slowly stretched to store elastic potential energy (Figure 30). Then, during the late stance, the elastic energy is returned through elastic recoil of the tendon, allowing the entire muscle-tendon units to rapidly shorten (Ishikawa et al., 2005; Lichtwark & Wilson, 2006). This so-called catapult effect, i.e. a slow stretch of the tendon followed by its rapid recoil, allows us to walk efficiently by increasing the power production while limiting the work of the muscle fiber

(Alexander, 2002; Wilson et al., 2003). As a consequence, during steady state level walking, the *triceps surae* muscle-tendon units have mainly a spring-like and a strut-like behavior (Lai et al., 2019).

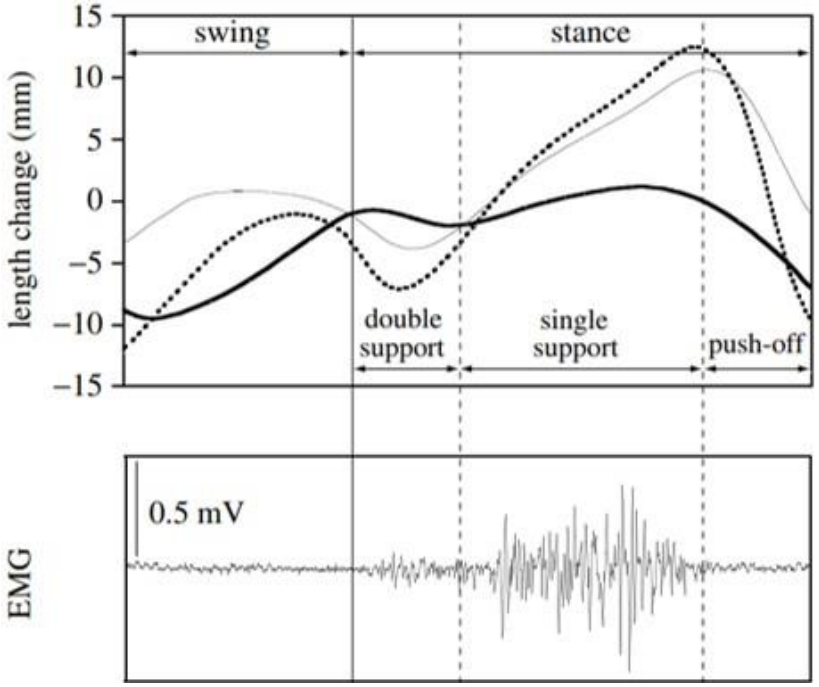


**Figure 30: Time-varying length changes and muscle activation of the *gastrocnemius medialis* during walking.** The top panel represents the length of the fascicle (thick line), muscle-tendon unit (dashed line) and tendon (thin line). An entire gait cycle is represented with first the swing phase and then the stance phase. EMG, electromyography. From Fukunaga et al. (2001).

On the other hand, there is increasing evidence that the muscle–tendon interaction can be modulated to fulfil different functions. For example, during accelerative walking, the muscle-tendon interaction is adjusted to behave like a motor (Farris & Raiteri, 2017). Accelerative walking is associated with longer and higher activation of the GM and *soleus* compared to steady-state walking. This induces greater active shortening and therefore greater production of muscle fiber work. In a similar way, incline walking requires greater GM activation (Lichtwark & Wilson, 2006). The manipulation of the mechanical demand using horizontal aiding or impeding forces during walking also influences the activation and fascicle contractile behavior to produce different amount of positive work (Clark et al., 2020). Taken together, these studies highlight that even though the *triceps surae* muscles are primarily designed to economically produce force, these muscle-tendon units are flexible and have the ability to sustain different roles.

## 3.2. Functional behavior of the individual *triceps surae* muscles

The studies described in the previous section are useful to appreciate the mechanisms that enable the efficiency of human locomotion. However, the majority of these studies have measured the function of one muscle of the *triceps surae* and thus do not provide information about the functional differences between the GM, GL and *soleus*. However, the large differences in PCSA and in muscle activation between muscles suggest that the *triceps surae* muscles can have distinct functional behaviors. Moreover, the GM and GL are biarticular muscles whereas the *soleus* is monoarticular. This leads to different functions during complex movements (van Ingen Schenau et al., 1990, 1995). Evidence suggests that the biarticular muscles are able to transfer the force and the power between the joints that they span (van Ingen Schenau et al., 1990) whereas monoarticular muscles are more involved in work production (van Ingen Schenau et al., 1995). For example, the GM and GL transfer the work produced by the knee extensors to the ankle joint during a counter movement jump. This enables to take advantage of the ability of proximal muscles, such as the knee extensor, to generate work (van Ingen Schenau et al., 1987).

A handful of studies have examined the between-muscle differences in neuromechanical behavior during locomotion. Ishikawa et al. (2005) compared the GM and *soleus* contractile behavior during walking. They showed that the *soleus* fascicles undergo greater active fascicle lengthening during the single support phase of walking and less fascicle shortening during the subsequent push off phase, when compared to the GM fascicles (Ishikawa et al., 2005). Cronin et al. (2013) demonstrated that the *soleus* fascicles undergo slower shortening velocities than the GM fascicles during the push-off phase of walking (Figure 31). Similar results were found during the stance phase of running (Lai et al., 2018). Moreover, the *soleus* displays a more consistent contractile behavior across walking speeds and walking durations (Cronin et al., 2013). The authors hypothesized that this more consistent behavior of the *soleus* compared to the GM is likely owing to a muscle-specific modulation in activation (Cronin et al., 2013). Recently, a study combined imaging and musculoskeletal simulation to show that the *soleus* had more consistent contractile behavior across different mechanical demands compared to the GM and GL (Clark et al., 2020). The s*oleus* also produces the greatest amount of fascicle positive work and fascicle net work, followed by the GM and the GL (Clark et al., 2020; Farris & Raiteri, 2017). Taken together, these studies highlight substantial differences between the *gastrocnemii* and the *soleus* during locomotion. The *soleus* is the main work generator within the *triceps surae*, which is consistent with its monoarticular function. The GM and GL are less

involved in the work production and have a more flexible behavior to transfer power and work between the knee joint and the ankle joint depending on the task intensity.

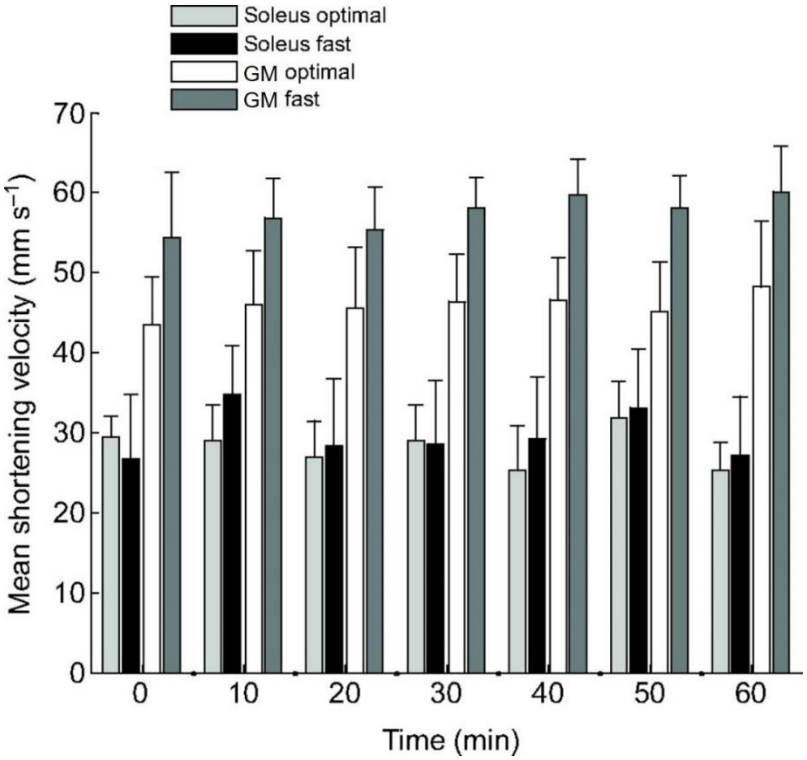


**Figure 31: G*astrocnemius medialis* and *soleus* shortening velocities during walking.** The data reported represents the mean fascicle shortening velocities calculated during the push-off phase of walking at optimal speed or fast speed (20% faster than the optimal speed). Data are presented for both the *gastrocnemius medialis* (GM) and *soleus*. From Cronin et al. (2013).

The aforementioned studies have focused on the differences between the *gastrocnemii* and the *soleus*. However, only few studies have recorded experimental data from both the GM and GL. To our knowledge, only one study recorded the contractile behavior of both *gastrocnemii* muscles during walking (Farris & Raiteri, 2017) and only one during running (Lai et al., 2018). The GM and GL are generally considered as two heads of the same muscles (Landin et al., 2016; Neptune et al., 2001; van Ingen Schenau et al., 1987). As a consequence, researchers often record only one muscle and generalize the results to both the GM and GL. Moreover, studies that have measured the neuromechanical behavior of both the GM and GL have focused on differences between the biarticular *gastrocnemii* and monoarticular *soleus*. For example, Clark et al. (2020) recorded the EMG activity from the GL and *soleus* and imaged the contractile behavior from the GM and *soleus*. As a consequence, the functional differences between the GM and GL remain poorly understood. Yet, different results suggest potential differences between the GM and GL: (i) The distribution of activation between these two muscles is biased towards the GM during both isometric contractions and locomotion. During standing balance,

the GL is even not active whereas the GM is. It is likely that the difference between the GM activation and GL activation results in different contractile behavior and muscle function; (ii) the GM and GL play distinct roles in ankle joint stabilization in the frontal plane (Lee & Piazza, 2008; Vieira et al., 2013); (iii) On the contrary to other muscles from the same anatomical group such as the *vastii*, the GM and GL do not a share high level of common drive (Hug et al., 2021b). This suggests that the central nervous system has the possibility to independently control these two muscles; and (iv), although the comparisons between the GM and GL are limited, evidence suggests certain differences in the contractile behavior of the two muscles (Héroux et al., 2016; Wolfram, 2017; Wolfram et al., 2020). For example, during isometric ramped contraction, the pennation angle increased more for the GM compared to the GL (Héroux et al., 2016). Taken together, these factors suggest that the GM and GL may have distinct neuromechanical behaviors during movement. To characterize these neuromechanical differences is important to better understand muscle coordination within a muscle group and the functional role of individual muscle.

## Application to the *triceps surae*

—

## Summary

The *triceps surae* is composed of the biarticular GM and GL and the monoarticular *soleus*. These three muscles have different volumes and muscle architectures. Even though their respective distal tendons merge to form the long and compliant Achilles tendon, they have individual subtendons that allows the muscles to exert forces independently. In addition to their distinct anatomy, the *triceps surae* muscles are activated at different levels during isometric task and walking.

The *triceps surae* muscle-tendon units are designed for economical force production. Nevertheless, evidence highlights that the function of these muscle-tendon units is also flexible. The *triceps surae* muscle-tendon units have the ability to sustain different roles depending on muscle activation timing.

Although the overall behavior of the *triceps surae* during functional tasks is relatively well established, the neuromechanical differences between *triceps surae* muscles are not fully understood. Yet, the between-muscle differences in PCSA and activation suggest that the *triceps surae* muscles can have distinct functional behavior. Although a few studies have investigated the differences between the *gastrocnemii* and the *soleus*, studies examining the difference between the GM and GL are lacking. However, the distinct neural command, anatomy and muscle architecture of the GM and GL could lead to potential neuromechanical differences between the two muscles. These functional differences remain to be established.

# Aims and hypotheses

The production of movement is associated with a high complexity. First, at the individual muscle scale, the production of force arises from the interaction between neural activation and several biomechanical factors. Second, numerous muscles typically span a joint and are involved in the production of the joint moments that generate movement (Bernstein, 1967). Therefore, an additional level relating to the distribution of force between different muscles should be considered. The study of each of these two scales in humans is limited by the lack of experimental methods to measure individual muscle forces non-invasively. Such major constraints explain why muscle coordination still remains poorly understood despite this problem having been studied for more than 50 years (Herzog, 2017). The use of models such as the Hill-type model has therefore become a common alternative approach for estimating muscle forces *in vivo*. Nevertheless, these models are often used with generic data, which conceals inter-individual variability and likely limits the accuracy of individual force predictions and ultimately our understanding of muscle coordination.

In this thesis, we focused on the *triceps surae* as this muscle group plays a major role in human locomotion (Dorn et al., 2012; Hamner & Delp, 2013). Researchers have primarily studied the differences between the biarticular *gastrocnemii* and the monoarticular *soleus*. On the contrary, structured and in-depth comparisons between the GM and GL are lacking. Nevertheless, several factors, such as distinct activations, suggest potential functional differences between the GM and GL during movement. Studies are therefore required to understand the individual functional role of the GM and GL. Moreover, it would be of particular interest to determine the differences between these two synergist muscles, which share two primary functions, i.e. knee flexion and ankle plantar flexion. This comparison is critical to further improve our understanding of muscle coordination. Taken together, these elements led our team to undertake a thorough investigation into the neuromechanical differences between these two muscles.

The neural and contractile behavior of the *gastrocnemii* are mostly studied during ankle plantar flexion. Thereby, the secondary function of the GM and GL, i.e. knee flexion, remains poorly understood. This generates a gap in our understanding of the control and function of the *gastrocnemii,* and more broadly of biarticular muscles. Even though a recent study merely suggested that a joint-specific neural control is possible for the GM (Watanabe et al., 2021b), this remains to be experimentally determined. In the same way, the joint-specific modulation

of shared neural drive between the GM and GL, and more generally between biarticular synergist muscles, remains unexplored.

The overall aim of this PhD thesis was to provide a deeper understanding of muscle coordination between the GM and GL, two muscles from the same anatomical group with the same function (i.e. knee flexion and ankle plantar flexion). Specifically, we first aimed to examine the mechanical consequences of the distribution of activation between these two muscles in terms of contractile behavior and muscle force production during walking. Second, we aimed to determine the influence of different mechanical constraints (i.e. knee flexion or ankle plantar flexion) on muscle coordination between the GM and GL. Throughout the different studies, we used an approach that combined muscle modelling, neurophysiological recordings (global EMG and motor unit activity), biomechanical features at rest (muscle volume and architecture) and dynamic *in vivo* imaging of the contractile behavior (time-varying fascicle lengths, fascicle velocities and pennation angles). Moreover, we focused strongly on the inter-individual variability throughout the three studies that compose this entire PhD project.

The aim of Study #1 was to determine the neuromechanical difference between the GM and GL and more specifically the difference in the interplay between muscle activation and fascicle contractile behavior during walking. To address this aim, we recorded muscle activation using surface EMG and fascicle contractile behavior using B-mode ultrasound during walking. We hypothesized that the GM and GL each have distinct fascicle contractile behavior based on the established differences between the two muscles in muscle activation during walking.

The aim of Study #2 was to estimate the individual distribution of force between the GM and GL during walking. To this end, we used a Hill-type model informed with *in vivo* data. We first determined the muscles' PCSA experimentally using MRI and DTI measures. Then, we recorded muscle activation, fascicle lengths, fascicle velocities and pennation angles during walking. A secondary aim of Study #2 was to assess the effect of a subject-specific maximal force-generating input compared to a generic input, based on scaled data, on the force prediction. Due to the greater force-generating capacity and activation in the GM compared to the GL, we hypothesized that the GM would produce more force compared to GL during walking. Moreover, we hypothesized that the generic and subject-specific Hill-type models would lead to a different distribution of force between the GM and GL at an individual level.

The aim of Study #3 was to determine whether the neural control of the GM and GL differs between knee flexion and ankle plantar flexion. On the contrary to the Study #1 and Study #2, we used isometric contractions to isolate knee flexion and ankle plantar flexion actions. We

simultaneously investigated both the muscle activation and neural drive using high-density surface EMG. We hypothesized that the distribution of activation would be robust across knee flexion and ankle plantar flexion whereas the shared neural drive would be lower during knee flexion compared to ankle plantar flexion.

# CHAPTER 2: MATERIAL AND METHODS

# 1. Summary of the data collection

## 1.1. Participants characteristics

The participants involved in the three studies were young and healthy (Table 2). They had no lower limb injury during the 6 months preceding any of the experimental sessions. For Study #1, we recruited 20 participants, including males and females. Five participants were excluded during post-analyses due to low quality of the ultrasound images. Study #2 was performed on the same participants as Study #1, except for three participants, who were excluded from analysis due to technical issues with the DTI data. For Study #3, we recruited only male participants due to the challenge in decomposing high-density surface EMG signals from female participants. This methodological issue could be related to the higher level of subcutaneous fat in female participants, although this still remains unknown (Souza de Oliveira et al., 2022).

## 1.2. Summary of the experimental protocols

The three studies of this PhD thesis focused on the GM and GL muscles. In Study #1, we collected bipolar surface EMG and B-mode ultrasonography images to determine the interplay between muscle activation and fascicle contractile behavior during walking, the most common form of human locomotion. In Study #2, we used the data collected in Study #1 and additional experimental muscle volume and muscle architecture measures as input into a Hill-type muscle model to predict the individual distribution of force between the GM and GL during walking. In Study #3, we collected high-density surface EMG signals from the GM and GL to investigate the differences in neural control between knee flexion and ankle plantar flexion. Thereby, the use of isometric knee flexion and ankle plantar flexion on an ergometer was required to isolate each task (Table 2).

**Table 2: Participant characteristics and data collected for the three studies.** All participants were young and healthy. The data were collected on the *gastrocnemius medialis* and *gastrocnemius lateralis*. Study #1 investigated the interplay between the muscle activation and fascicle contractile behavior of the *gastrocnemius medialis* and *gastrocnemius lateralis* during walking. Study #2 examined the distribution of force between the *gastrocnemius medialis* and *gastrocnemius lateralis* during walking. Study #3 investigated the difference of the neural control of the *gastrocnemius medialis* and *gastrocnemius lateralis* between knee flexion and ankle plantar flexion. MVC, maximal voluntary contraction.

| | Study #1 | Study #2 | Study #3 |
|---|---|---|---|
| **Number of participants** | 20 recruited, 15 conserved | 20 recruited, 12 conserved | 21 |
| **Sex** | 5 females and 10 males | 5 females and 7 males | 21 males |
| **Age** (years) | 25.9 ± 3.9 | 25.0 ± 3.5 | 27.3 ± 4.3 |
| **Height** (m) | 1.73 ± 0.10 | 1.71 ± 0.10 | 1.76 ± 0.24 |
| **Weight** (kg) | 75.2 ± 14.6 | 75.4 ± 16.4 | 77.1 ± 12.9 |
| **Data collected** | **Isometric MVCs**<br>Myoelectrical activity<br>**Walking**<br>Myoelectrical activity<br>Fascicle length<br>Fascicle velocity<br>Pennation angle<br>Kinematics | **Isometric MVCs**<br>Myoelectrical activity<br>**Walking**<br>Myoelectrical activity<br>Fascicle length<br>Fascicle velocity<br>Pennation angle<br>Kinematics<br>**Muscle volume**<br>**Resting fascicle length** | **Isometric knee flexion MVCs**<br>Torque<br>Myoelectrical activity<br>**Isometric ankle plantar flexion MVCs**<br>Torque<br>Myoelectrical activity<br>**Submaximal isometric knee flexion**<br>Torque<br>Myoelectrical activity<br>**Submaximal isometric ankle plantar flexion**<br>Torque<br>Myoelectrical activity |

# 2. Experimental tasks

## 2.1. Maximal Voluntary Contraction

We used MVC tasks in the three studies composing this PhD thesis. The aim of the MVCs was to assess the maximal EMG level activity. In the three studies, we estimated the muscle activation during submaximal tasks using either bipolar surface EMG in Study #1 and Study #2 or differentiated signal from high-density surface EMG in Study #3. As described in Part 1,

section 1.1.2.1, a normalization step is necessary to avoid amplitude cancellation of the EMG signal (Keenan et al., 2005). More generally, EMG normalization is required to make comparisons between muscles, between participants and between sessions (Besomi et al., 2020). The aim of the normalization procedure consists of recording the maximal EMG activity level from each muscle of interest to then express the submaximal level of activity with respect to this maximal EMG activity. Several methods exist to determine the maximal EMG activity. For example, the submaximal EMG can be normalized to the peak EMG during the task of interest, to the maximal M-wave or to the maximal voluntary performance during the task of interest (Besomi et al., 2020). We chose to use the most common method which consists of assessing the maximal EMG level during standardized isometric MVC. This method requires that the participants maximally activate the muscles of interest during the isometric MVC. The twitch interpolation technique could also be used during the MVC to ensure that participants reach the maximal voluntary activation level. Previous studies from our group used the twitch interpolation techniques during MVC and revealed that the healthy participants reached a level of maximal activation of more than 98% (Crouzier et al., 2018). This level of activation is satisfactory for our objective. Therefore, we performed the same MVC protocol with a similar population and we assumed that the maximal activation level was reached based on the study of Crouzier et al. (2018).

For each study, the experimental sessions began with a warm-up followed by a standardized isometric MVC protocol. For Study #1 and Study #2, participants performed three ankle plantar flexion MVCs with 120 s of rest between each MVC. We recorded bipolar surface EMG signals during these MVCs to determine the maximal EMG level. For Study #3, participants performed three knee flexion MVCs and three ankle plantar flexion MVCs while we recorded HDsEMG signals. Similarly, participants rested for 120 s between each MVC. For the three studies, each MVC contraction lasted between 3 s and 5 s. Participants were instructed to produce as much force as possible. Moreover, during the MVC contraction, we strongly encouraged the participants to do their best to produce the maximal torque using verbal feedback.

## 2.2. Walking

The single experimental session for Study #1 and Study #2 used walking as the main task of interest. Participants walked barefoot on a treadmill (Nautilus Trimline T345). After a familiarization period, the preferred walking speed of each participant was determined using standardized procedures (Dal et al., 2010). On average, the preferred walking speed was 1.1 ±

0.1 $m.s^{-1}$. Then, participants walked at their preferred walking speed under two conditions in a randomized order: level walking (0% grade) and incline walking (10% grade). Four trials were performed for each condition, two with EMG electrodes on the GM and GL and two with two ultrasonography transducers placed on the GM and GL. For each trial, participants walked for 60 s.

## 2.3. Submaximal isometric contraction

For Study #3, the main task of interest consisted of submaximal isometric contractions to produce either knee flexion or ankle plantar flexion. The submaximal isometric contraction was a trapezoidal contraction which consist of a 5 s ramp-up, 20 s of steady-state plateau and a 5 s ramp-down. Participants performed several (~5) practice trials to become familiar with the task. The number of familiarization trials realized depended on the ability of the subject to perform steady-state torque plateau. Following this, participants were instructed to match a visual torque target at 30%, 40% and 50% of MVC torque for knee flexion and 20%, 30% and 40% of MVC torque for ankle plantar flexion. Of note, this protocol aimed to match the average activation of the GM and GL between knee flexion and ankle plantar flexion tasks. Therefore, we used three different intensities for each task to ensure the conditions covered a range of activation levels to match between knee flexion and ankle plantar flexion during the post-processing step. These contraction levels were informed from pilot testing, whereby we observed that the *gastrocnemii* are less activated during knee flexion than ankle plantar flexion for the same relative peak torque. For this reason, we use higher contraction intensities for knee flexion. Participants performed three trapezoidal contractions per intensity separated by 60 s of rest. Consequently, participants did 60 s of plateau per intensity. A monitor placed in front of the participant displayed the torque target and the torque produced by the participant.

# 3. Neural control measures

## 3.1. Estimation of muscle activation using bipolar surface electromyography

For Study #1 and Study #2, we recorded myoelectrical activity from the GM and GL of the dominant leg using bipolar surface EMG. First, we determined the boundaries of the muscle bellies using B-mode ultrasound (v11.0, Aixplorer, Supersonic Imagine, Aix-en-Provence, France). This ensured we placed the electrodes in the center of the muscle bellies to limit

crosstalk. B-mode ultrasound was also used to identify the fascicle orientation to align the electrodes in the direction of the fascicles. Before placing the wireless electrodes (Trigno Delsys Inc., Natick, MA, USA; 10 mm inter-electrode distance), the participant's skin was shaved, abraded and cleaned with alcohol. This step was intended to reduce the skin-electrode impedance. We ensured that the skin-electrode contact was maintained throughout the entire experiment by using elastic bandages. The bipolar EMG signals were amplified, digitized at 2048 Hz, band-pass filtered (20-500 Hz) and recorded in Spike2 (V7, CED Ltd, Cambridge, UK).

The EMG analysis of Study #1 and Study #2 was performed on 15 gait cycles per trial. Analyses were performed in Matlab (R2018b, The MathWorks, Natick, MA) using custom-written scripts. We first band-pass filtered the signal between 20 Hz and 500 Hz using a second-order Butterworth filter. All the filtered data were then visually checked to detect noise and movement artefacts. We rectified the filtered signals and used a low-pass filter (12 Hz) to obtain the EMG envelope. We used the maximal EMG value obtained during the MVC trials to normalize the EMG signals during walking. The data from each gait cycle were interpolated to 100 data points. Finally, we averaged the 15 gait cycles within a trial and then averaged the two trials to obtain a representative cycle. From the normalized EMG of this representative cycle, we extracted the peak EMG, the average EMG during the step cycle and the average EMG during the stance phase. The distribution of activation between the GM and GL was estimated by calculating the GM/(GM+GL) ratio from the normalized peak EMG, average EMG and average EMG during stance.

## 3.2. Estimation of muscle activation using high-density surface electromyography

We measured the myoelectrical activity of the right GM and GL in Study #3 using HDsEMG. The latter consists of a two-dimensional adhesive grid of 64 electrodes (13×5 electrodes with one electrode absent on a corner, gold-coated, inter-electrode distance: 8 mm; GR08MM1305 OT Bioelettronica, Italy). Similar to the experimental session of Study #1 and Study #2, we first determined the location of muscle boundaries and the muscle fascicle orientation of the GM and GL from the right leg using B-mode ultrasound. The skin was shaved and then cleaned and abraded with an abrasive gel. We used a disposable biadhesive foam layer to hold the grids on the skin. To ensure the skin-electrodes contact, the cavities of the biadhesive foam were filled with a conductive paste (SpesMedica, Battipaglia, Italy). We placed a reference electrode

(Kendall Medi-Trace, Canada) over the right tibia and a strap electrode, dampened with water, as ground electrode around the left ankle. We secured the whole set-up with elastic bandages to maintain the skin-electrode contact and to avoid movement artefacts. The monopolar signals were band-pass filtered between 10 Hz and 500 Hz, digitized at a sampling rate of 2048 Hz and recorded in a multichannel high-density surface EMG acquisition system (EMG-Quattrocento, 400 channel EMG amplifier; OT Bioelettronica, Italy).

Similar to Study #1 and Study #2, analyses were performed in Matlab using custom-written scripts. We first band-pass filtered the data with a second-order Butterworth filter (20-500 Hz). Then, we visually checked the signal to remove channels that contained noise or artefacts. When we excluded an electrode due to noise or artefacts, a new signal was linearly interpolated from all the adjacent electrodes (i.e. between two and four electrodes depending of the electrode location). We calculated the differential signals from the 64 channels as the difference between two adjacent electrodes in the proximo-distal direction. This resulted in 59 differentiated signals. The signals from the MVC trials were averaged over the whole grid of electrodes and then rectified. We determined the maximal EMG during MVCs as the maximal value from a 500 ms moving mean over the three MVCs. The differentiated signals from the submaximal trials were rectified and normalized to the maximal EMG from ankle plantar flexion MVCs. We only used the maximal EMG activity from ankle plantar flexion MVCs because this value was systematically higher than the maximal EMG activity recorded during knee flexion. It was required to use a single value to normalize both condition as our aim was to compare EMG amplitude across tasks within an individual and muscle (Besomi et al., 2020). Then, we calculated the average EMG from each channel and each plateau. Finally, we determined the EMG value from the submaximal conditions by first averaging the three plateaus and second by averaging all the channels. Consistent with Study #1, we estimated the distribution of activation by calculating the GM/(GM+GL) ratio. We also used the normalized EMG value from each channel to determine the regional activation for each muscle and for each task. To do this, we calculated the barycenter of the normalized EMG amplitude across the 2D EMG grid.

## 3.3. Estimation of motor unit activity using high-density surface electromyography

In Study #3, we decomposed the HDsEMG signal into single motor unit activity using the convolutive blind source separation method (Negro et al., 2016a). This method automatically

identifies and decomposes motor unit activity. We performed the automatic decomposition on the plateau of the trapezoidal contraction that exhibited the highest EMG amplitude among the three trapezoidal contractions. Following this automatic decomposition, manual editing of the identified motor units was required. For the manual editing, we followed previously published procedures (Del Vecchio et al., 2020; Hug et al., 2021a). This consisted of visually checking the motor unit spikes identified by the automatic decomposition to remove the incorrectly identified false positive spikes. Moreover, we added all the false negative spikes that were not identified by the automatic processing. Then, the motor unit filters derived from the processing of this plateau were reapplied on the other two plateaus. Of note, this manual editing of motor units is highly reliable across operators (Hug et al., 2021a). Only the motor units with a pulse-to-noise ratio above 30 dB were retained for further analyses (Figure 32).

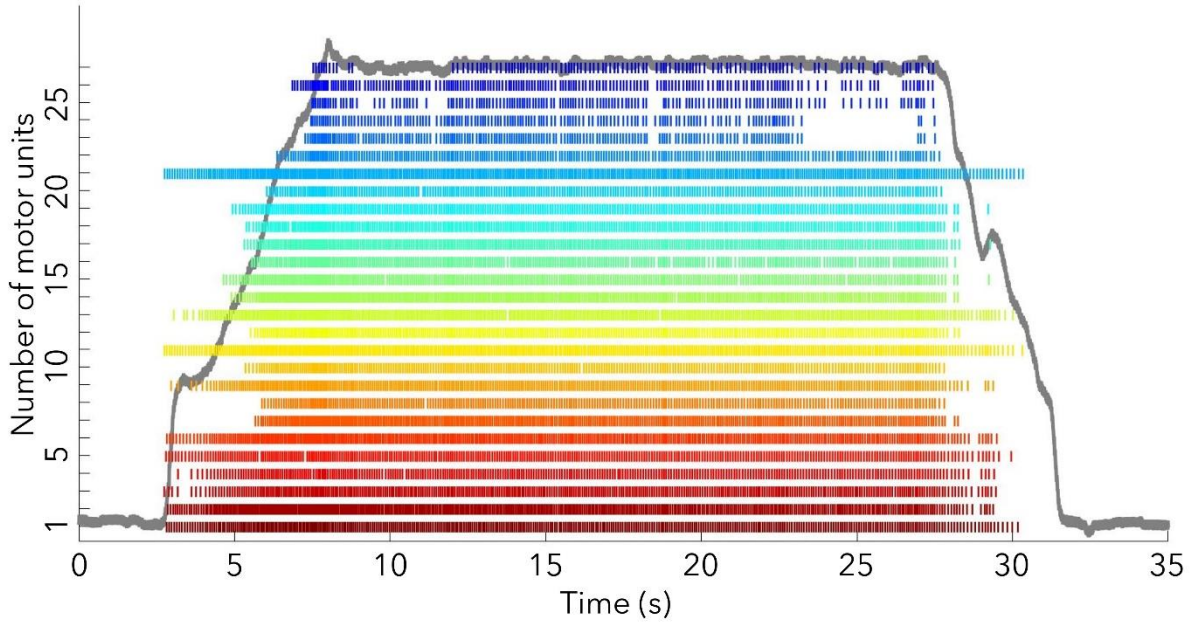


**Figure 32: Example of the motor units spike train after manual edition.** This example depicts the motor units spike trains of the *gastrocnemius medialis* during ankle plantar flexion. Each colored line corresponds to a motor unit. Within a motor unit, each individual spike represents a motor unit action potential. The trapezoidal grey curve represents the ankle plantar flexion torque produced by the participant. The torque plateau corresponds to a contraction level of 40% maximal isometric voluntary contraction.

After the manual editing, we checked for crosstalk by ensuring that each identified motor unit for a muscle did not originate from the other muscle. To do this, we used spike-trigger averaging technique consistent with previously studies (Del Vecchio & Farina, 2019; Hug et al., 2021b). Specifically, we extracted the firing time of each motor unit to locate each motor unit action potentials in all of the 59 differential EMG channels of the grid for each of the two muscles. Based on the muscle fiber action potential waveform, we calculated the maximal peak-to-peak

amplitude for each channel and for each HDsEMG grid. Finally, the maximal peak-to-peak amplitudes of each grid were compared. We assumed that the action potential amplitude should be largest in the signal from the electrodes closest to the discharging muscle fibers. Therefore, we considered a motor unit as a crosstalk motor unit when the maximal peak-to-peak amplitude was higher in the neighbouring muscle. When it was the case, the motor unit was removed from further analyses (Aeles et al., 2023; Del Vecchio et al., 2019).

To gain information about the neural command of individual motor units, we calculated the discharge rate and the spatial location of each motor unit. The average discharge rate of motor units was calculated over each plateau for both the knee flexion and ankle plantar flexion tasks. The values from the three plateaus were then averaged to obtain a single value for each task. We also determined the spatial location of the action potential over the grid of electrodes for each motor unit. To do this, we used the spike-trigger averaging technique to determine the shape of the motor unit action potentials. Then, we determined the peak-to-peak amplitude of the motor unit action potential for each channel over the EMG grid. Finally, we calculated the barycenter of the peak-to-peak amplitude for each muscle.

We also determined the proportion of motor units that were identified during both the knee flexion and ankle plantar flexion tasks. Similar to previous studies, we used the spatio-temporal properties of the action potential waveforms within the 2D grids to match the motor units across tasks (Del Vecchio & Farina, 2019; Martinez-Valdes et al., 2017). Specifically, we determined the motor unit action potential waveform on the differentiated signal using the spike-triggered averaging technique previously described. The motor unit waveforms from the 59 electrodes were concatenated. Then, normalized 2D cross-correlations between the waveforms of motor units were used to compare the motor unit action potentials. Motor units were considered as matched across tasks when they exhibited a correlation coefficient higher than 0.75 (Martinez-Valdes et al., 2017). We ensured the quality of the matching by visually checking the action potential shape and the action potential distribution over the grid between the two motor units identified (Figure 33).

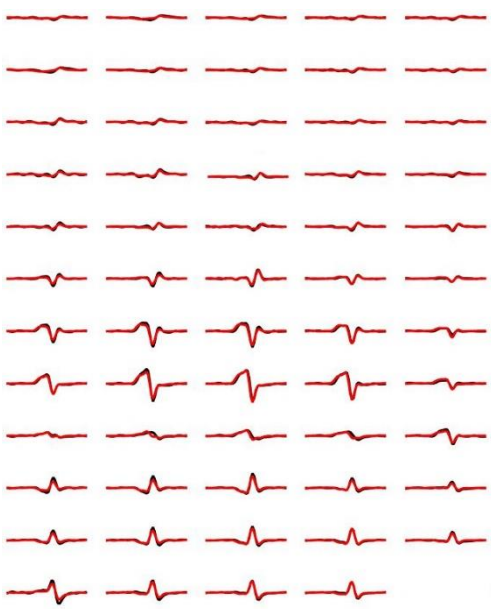

**Figure 33: Example of a motor unit matched across knee flexion and ankle plantar flexion tasks.** The figure depicts the distribution of the motor unit action potentials over the grid of electrodes during knee flexion (black curve) and ankle plantar flexion (red curve) for a *gastrocnemius lateralis* motor unit.

## 3.4. Estimation of common synaptic input using high-density surface electromyography

For Study #3, we assessed the amount of common synaptic input between the GM and GL using a coherence analysis. The coherence analysis was performed on the muscles cumulative motor unit spike trains. To determine the cumulative spike trains, we maximized the number of motor units and the duration for each participant. For this purpose, we discarded the portions of the signal where not enough motor units were discharging simultaneously. We also discarded the motor units that had discharge patterns that were too intermittent during the torque plateau (inter-spike interval > 500 ms). The same duration was considered for both tasks within a participant because the duration can affect the coherence calculation. We used the Welch periodogram with nonoverlapping windows of 1 s to calculate the magnitude-squared coherence on two equal-sized groups of cumulative spike trains. As the number of motor units considered can affect the level of coherence, we used a constant number of motor units to calculate the cumulative spike trains for each muscle. Therefore, the cumulative spike trains are calculated as the sum of the binary spike trains of three motor units. Nevertheless, we considered all the motor units in the coherence analysis as we tested all the unique combinations of three motor units from each participant's entire available motor unit pool, with the maximal number of permutations set to 100. This pool of 100 random permutations was used for further

analysis. We considered the level of coherence within the delta band (0-5 Hz) as it reflects the presence of common synaptic input relevant for force modulation (Del Vecchio et al., 2019; Laine et al., 2015). Similar to previous studies (Del Vecchio et al., 2019; Laine et al., 2015; Laine & Valero-Cuevas, 2017) a standard z-score was calculated from the coherence value:

$$\mathrm{COH}\ z\ \mathrm{score} = \sqrt{2L} \times \alpha\tanh\sqrt{\mathrm{COH}} - \mathrm{bias}$$

Equation 6

Where COH is coherence, L is the number of time segments considered in the coherence analysis, and bias is calculated as the mean COH z score between 250 Hz and 500 Hz where no coherence is expected.

# 4. Estimation of muscle volume and architecture

## 4.1. Estimation of muscle volume using magnetic resonance imaging

For Study #2, we determined the PCSA using experimental data. First, we measured the muscle volume. For this purpose, we imaged the dominant, lower leg (from the ankle to the distal end of the femur) using a 3T MRI scanner (Magnetom Prisma, Siemens, Germany). Participants were lying in supine position with the ankle positioned at 90° and the hip extended. The knee was slightly flexed (<5°) using a foam wedge under the knee to avoid any muscle compression due to the weight of the leg. We placed an 18-channel body matrix coil on the participants' legs and a 32-channel spine coil was integrated in the MRI scanner for image acquisition. We used a T1-weighted MRI sequence with two-dimensional turbo spin echo (field of view = 262 × 350 mm, acquisition matrix 336 × 448 pixels [reconstructed matrix = 672 × 896 pixels], repetition time/echo time = 11.7/5.29 ms, flip angle = 10°, 260 slices, scan time = 462 s [2 sequences at 231 s each]). The slice thickness was 2 mm with no gap between slices.

The MRI images were analyzed using a combination of semi-automated (Sashimi Segmentation V1.1) and manual segmentation (ITK-SNAP V3.8.0, NIH, USA) 3D image analysis software programs. We first outlined the GM and GL on a clear slice. Then, Sashimi tracked the muscle boundaries on the adjacent slices using demons image registration. After the Sashimi process, we loaded the tracking results into ITK-SNAP. Each slice was visually checked from the distal slice to the proximal slice. We made manual corrections where the Sashimi program failed to properly segment the GM and GL. Then, we reconstructed the 3D muscle volume by

interpolated the tracking between every slice. Finally, the muscle volume was calculated for each muscle as the sum of all voxels multiplied by the voxel volume.

## 4.2. Estimation of muscle fascicle length using diffusion tensor imaging

The fascicle length at rest was estimated using DTI. DTI scans were performed in the same session, with participants in the same position, as the T1 MRI. For the DTI sequence, we used the following parameters: spin echo echoplanar imaging, field of view = 180 × 180 mm, acquisition matrix = 112 × 112, slice thickness = 5 mm, 60 slices, repetition time/echo time = 8700/52 ms, diffusion gradient timing = 22/8.9 ms, echoplanar imaging factor: 112, number of signal averages = 4, diffusion directions = 12 gradient directions on a hemisphere, b = 500 s/mm2 (reference image with b = 0 s/mm2), scan time = 480 s. We suppressed the highlighting of adipose tissue using a spectral attenuated inversion recovery. We acquired images with B0 reversed phase encoding to correct for distortion.

The DTI processing step followed previously described procedures (Bolsterlee et al., 2019). Briefly, we first applied a local principal component analysis filter (Manjón et al., 2013) on the images from the DTI acquisition to correct DTI data for Eddy-current distortions. Second, we determined the eigenvalues and eigenvectors of the diffusion tensor for each voxel. Third, we determined the fiber tract using the primary eigenvector, which is aligned with muscle fibers. Finally, we used a previously described algorithm (Bolsterlee et al., 2017) to propagate fiber tracts in both directions along the primary eigenvector until the muscle boundaries. To calculate the fascicle length, we determined a local muscle coordinate system using a principal component analysis on the vertices of the muscle surface. Then, we divided each muscle into smaller regions in the local muscle frontal plane (Figure 34). We assigned muscle fascicle to the muscle region that contained the fascicle midpoint, i.e. the mean of the two endpoints of the fiber. Then, we calculated the median muscle fascicle length for each region that contains muscle fiber midpoints. Finally, we averaged the fascicle lengths from all muscle regions to obtain a single fascicle length value representative of the entire muscle.

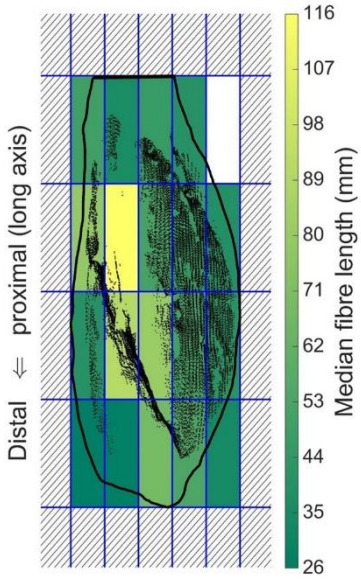


**Figure 34: Illustration of the method used to calculate muscle fiber length using diffusion tensor imaging**. The muscle is segmented in black. The grid of blue rectangle represents the different regions used to divided the muscle. The fascicle midpoints are depicted as black dots. The regions are colored according to the median fascicle length of all the fascicle from this region. From Aeles et al. (2022).

## 4.3. Estimation of dynamic muscle contractile behavior using B-mode ultrasonography

In Study #1 and Study #2, dynamic muscle contractile behavior from the GM and GL were collected using B-mode ultrasonography. The latter provides muscle images where the muscle fascicles can be tracked. This enables the calculation of time-varying fascicle length, fascicle velocity and pennation angle during walking. For this purpose, we used two flat linear ultrasound transducers (5–8 MHz, 60 mm field-of-view, LV8-5L60N-2, ArtUS, Telemed, Vilnius, Lithuania) to simultaneously image the GM and GL of the dominant leg. We placed the transducers over the muscle bellies while the participants were standing. Ultrasound gel was used between the transducer and skin to ensure the propagation of the ultrasounds sent by the transducer. We aligned the transducers with the fascicle orientation to ensure that we mostly imaged the same fascicle plane during walking. Once we were satisfied with the ultrasound transducer placement, we secured the transducers with elastic bandages to maintain a good image quality throughout the whole experiment. We collected the ultrasound videos at a frequency of 120 Hz (Echo Wave II 3.7.1, Telemed).

Post-data collection, we optimized the brightness and contrast on Echo Wave II software to improve the image quality. Then we processed five gait cycles per trial using a semi-automated

tracking algorithm (Ultratrack; Farris & Lichtwark, 2016) similarly to previous studies (Aeles et al., 2018). After we had defined the aponeuroses and the muscle fascicle on the first image, the algorithm tracked the aponeuroses and fascicle in sequential frames by implementing an affine flow model. We also used key frames at each heel-strike to correct for drift that occurs in the tracking of cyclical data. Then, all images were visually checked and we made manual corrections where required. We calculated muscle fascicle length as the distance between the superficial and deep aponeuroses, along the fascicle orientation (Figure 35). We considered the angle between the tracked muscle fascicle and the deep aponeurosis as the pennation angle (Bolsterlee et al., 2015b). Then, using custom-written scripts in Matlab, the fascicle length and pennation angle were low-pass filtered at 12 Hz. We calculated the instantaneous fascicle velocity as the derivative of fascicle length with respect to time. We interpolated the data from each gait cycle to 100 data points in order to obtain cycles with equal length. Finally, fascicle length and fascicle velocity were normalized to the individual fascicle length at heel-strike during level walking. We expressed the change in pennation angle as the difference with the individual pennation angle at heel-strike during level walking.

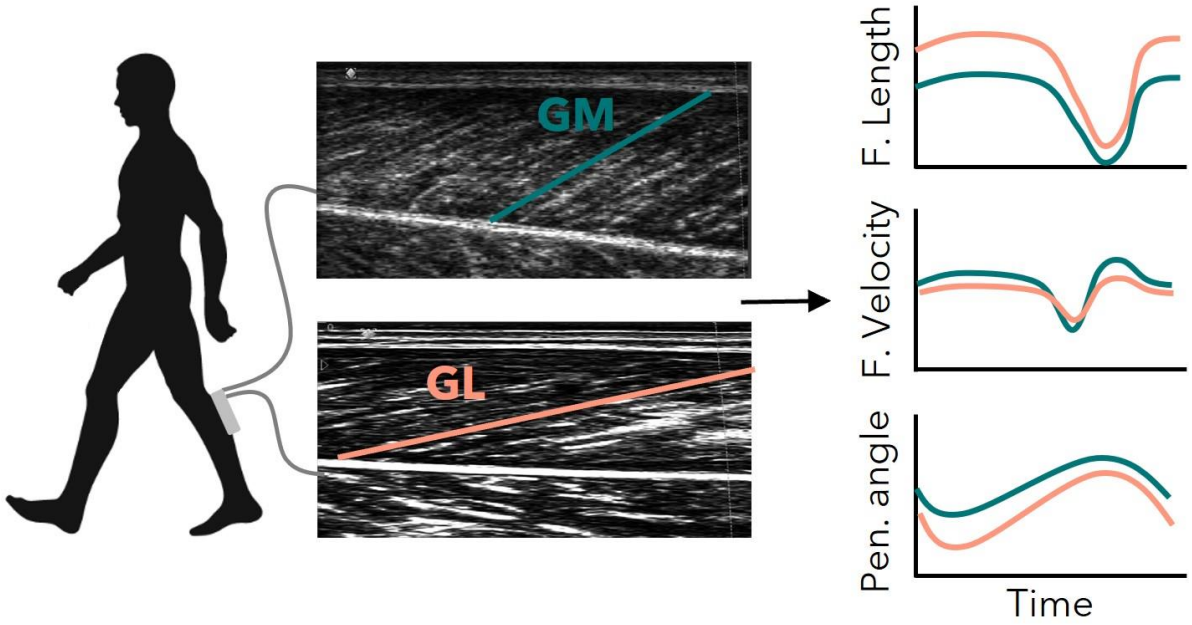


**Figure 35: Illustration of the experimental set-up used to image the muscle contractile behavior during walking.** Participants walked on a treadmill barefoot. Two ultrasounds transducers imaged simultaneously the *gastrocnemius medialis* (GM) and the *gastrocnemius lateralis* (GL). After a fascicle tracking process, the fascicle length (F. length) and pennation angle (Pen. angle) were calculated. Then, fascicle velocity (F. velocity) was calculated from the fascicle length changes.

# 5. Kinematics recordings using 3D motion capture

We used a 3D motion capture system composed of 12 cameras (Flex 13, OptiTrack, Corvallis, OR, USA) in the experimental session of Study #1 and Study #2 for three purposes. First, we recorded a static calibration trial with 8 marker clusters and 16 individual markers placed bilaterally on the lower limbs and pelvis. This static trial was then used in Opensim (V3.3; Delp et al., 2007) to scale the musculoskeletal model (Rajagopal et al., 2016) used in Study #2 for each participant.

Second, we used a 3D motion capture system to determine the timing of the gait events, i.e. heel-strike and toe-off. To do this, we placed reflective markers on the calcaneus and the fifth metatarsophalangeal joint of each foot. The motion capture system recorded the foot position at a frequency of 120 Hz. Post data collection, we labeled, gap filled, and smoothed the data using a 10 Hz low-pass second-order Butterworth filter (Motive, OptiTrack, Corvallis, OR, USA). Then, we determined heel-strike and toe-off using previously published procedures (O'Connor et al., 2007). Briefly, we determined the foot center signal by calculated the mid-point between the heel and toe marker locations. We calculated the foot vertical velocity using the first derivative of the vertical coordinates of this foot center. We used the maximal value of the vertical velocity to determine the toe-off timing. Finally, to determine the heel-strike timing, we used the second local minimum after the toe-off event. We used these gait events to determine the gait cycle (i.e. from a heel-strike to the following heel-strike) but also to split the gait cycle into stance (i.e. from heel-strike to the following toe-off) and swing (i.e. from toe-off to the following heel-strike) phases.

Finally, the 3D motion capture system was also used to synchronize either the bipolar EMG data or the ultrasound data with the kinematics. The 3D motion capture system generated a trigger that launches simultaneously the EMG or ultrasound recording and the kinematics recording. This synchronization, combined with the determination of heel-strike and toe-off, enabled us to partition the EMG and ultrasound data into gait cycles.

# 6. Estimation of force using a musculoskeletal model

For Study #2, we aimed to estimate the forces produced by the GM and GL during walking. To do this, we used the data collected in the experimental session for Study #1 previously described, into a conventional Hill-type model (Zajac, 1989).

$$F_{\mathrm{m}} = F_{\max}\left[\hat{a}(t)\hat{F}_{\mathrm{a}}\left(\hat{l}_{\mathrm{f}}\right)\hat{F}_{\mathrm{a}}(\hat{v}) + \hat{F}_{\mathrm{p}}\left(\hat{l}_{\mathrm{f}}\right)\right] \times \cos\beta.$$

This model predicted a muscle force $F_{\mathrm{m}}$ (N), which depends on the maximal force-generating capacity $F_{\max}$, expressed in N; the time-varying activation $\hat{a}(t)$; the active ($\hat{F}_{\mathrm{a}}\left(\hat{l}_{\mathrm{f}}\right)$) and passive ($\hat{F}_{\mathrm{p}}\left(\hat{l}_{\mathrm{f}}\right)$) forces as determined from the force-length relationship; the force $\hat{F}_{\mathrm{a}}(\hat{v})$ as determined from the force-velocity relationship; and the cosine of the time-varying pennation angle $\beta$. The time-varying activation, active force and passive force are normalized values between 0 and 1.

The normalized active force-length curve (Otten, 1987), was modelled as:

$$\hat{F}_{\mathrm{a}}\left(\hat{l}_{\mathrm{f}}\right) = e^{-\left(\frac{\hat{l}_{\mathrm{f}}^{0.6}-1}{0.3}\right)^{2.3}}.$$

The normalized passive force-length curve (Otten, 1987) was modelled as:

$$\hat{F}_{\mathrm{p}} = 2.64\hat{l}_{\mathrm{f}}^{\,2} - 5.30\hat{l}_{\mathrm{f}} + 2.66 \text{ for} \qquad \hat{l}_{\mathrm{f}} > 1,$$

$$\hat{F}_{\mathrm{P}}\left(\hat{l}_{\mathrm{f}}\right) = 0 \qquad \text{for} \qquad \hat{l}_{\mathrm{f}} \leq 1,$$

Where $\hat{l}_{\mathrm{f}}$ is the time-varying normalized fascicle length measured during walking. Theoretically, the fiber length should be normalized to the optimal length. The optimal length corresponds to the fiber length where the maximal active force is produced. It can be determined from the force-length relationship. However, as described in Part 1, section 1.2.2.3, it is challenging to determine the force-length relationship *in vivo* (Maganaris, 2003; Rubenson et al., 2012). Therefore, we used the fascicle length at heel-strike as a substitute.

The normalized force-velocity curve was modelled as:

$$\hat{F}_{\mathrm{a}}(\hat{v}) = \frac{1+\left(\frac{\hat{v}}{\hat{v}_0}\right)}{1-\left(\frac{\hat{v}}{v_0\alpha}\right)} \qquad \text{for} \qquad \hat{v} \leq 0,$$

$$\hat{F}_{\mathrm{a}}(\hat{v}) = 1.5 - 0.5\frac{1-\left(\frac{\hat{v}}{\hat{v}_0}\right)}{1+\left(\frac{7.56\hat{v}}{v_0\alpha}\right)} \qquad \text{for} \qquad \hat{v} > 0,$$

Where $\hat{v}$ is the time-varying normalized fascicle velocity recorded during walking. α describes the curvature of the force velocity relationship and $v_0$ is the maximum unloaded shortening velocity. We used intermediate values accounting for slow and fast muscle fibers from numerous terrestrial species of 0.235 and -7.5 $s^{-1}$ for α and $\hat{v}_0$ , respectively (Wakeling et al., 2012).

Finally, $F_{\max}$ is a function of the muscle's volume $Vol$, the optimal fiber length $l_{\mathrm{f,opt}}$ and the maximum isometric stress of a muscle fiber $\sigma_0$.

$$F_{\max} = \left(\frac{Vol}{l_{\mathrm{f,opt}}}\right)\sigma_0.$$

$\sigma_0$ was taken from the literature (22.5 N.cm$^{-2}$, Powell et al., 1984; Roy et al., 1982; Spector et al., 1980). As described in the review of literature, the specific tension mainly depends on the muscle fiber composition of the muscle. Similar muscle fiber compositions have been reported between the GM and GL (Edgerton et al., 1975; Johnson et al., 1973). Therefore, we assumed that the GM and GL have similar specific tension and we used the same value for both muscles.

In Study #2, we compared two inputs for the $F_{\max}$. We first used a scaling method to inform the Hill-type model. The scaling method estimated the optimal fiber length using a musculoskeletal model containing 37 degrees-of-freedom with 97 muscle-tendon complex actuators (Delp et al., 2007; Rajagopal et al., 2016). This model was scaled to the individual anthropometry of the participants based on the mass of the participant and markers positions recorded during the static trial. From this scaled model, we extracted the optimal fascicle length of both the GM and GL.

For the muscle volume, we used a regression equation based on body mass from Handsfield et al. (2014):

$$Vol = b1 \times BM + b2$$

Where $Vol$ (cm$^3$) is a function of body mass, $BM$ (kg) and two coefficients $b1$ and $b2$. Coefficient $b1$ is 3.41 and 2.19 for the GM and GL, respectively, and $b2$ is 12.60 and -7.59 for GM and GL, respectively (Handsfield et al., 2014). This study imaged the lower limb muscles in 24 young and healthy individuals (Handsfield et al. 2014). The two coefficients $b1$ and $b2$ correspond to the coefficient of the linear fit of the relationship between the muscle volume and body mass.

The second approach to determine $F_{\max}$ was an experimental method. Specifically, we used experimentally-determined muscle volume and fascicle length within the model. Theoretically, the PCSA should be calculated from the muscle volume and the optimal fascicle length. However, as explained above, it is challenging to determine experimentally the optimal fascicle length. Therefore, we used, as a substitute for the optimal fascicle length, the mean muscle fascicle length estimated from DTI. For the muscle volume, we used the muscle volume determined using MRI.

Further details concerning the drawbacks and the advantage of the different EMG and imaging techniques are available in the Chapter 1 of this PhD thesis (see Part 1, section 1.1.2. for the EMG technique and Part 1, section 1.2. for the imaging techniques). In a similar way, the conceptual bases and the different parameters of the Hill-type model are described in the Part 1, sections 1.2. and Part 1, 2.3 of this PhD thesis.

# CHAPTER 3: PHD EXPERIMENTATIONS

# Study #1

---

# Does different activation between the medial and the lateral gastrocnemius during walking translate into different fascicle behavior?

---

Associated publications:

Hamard, R., Aeles, J., Kelp, N. Y., Feigean, R., Hug, F., & Dick, T. J. (2021). Does different activation between the medial and the lateral gastrocnemius during walking translate into different fascicle behavior?. *Journal of Experimental Biology*, *224*(12), jeb242626.

© 2021. Published by The Company of Biologists Ltd | Journal of Experimental Biology (2021) 224, jeb242626. doi:10.1242/jeb.242626

RESEARCH ARTICLE

# Does different activation between the medial and the lateral gastrocnemius during walking translate into different fascicle behavior?

**Raphaël Hamard[1], Jeroen Aeles[1], Nicole Y. Kelp[2], Romain Feigean[1,3], François Hug[1,2,4,*] and Taylor J. M. Dick[2]**

## ABSTRACT

The functional difference between the medial gastrocnemius (MG) and lateral gastrocnemius (LG) during walking in humans has not yet been fully established. Although evidence highlights that the MG is activated more than the LG, the link with potential differences in mechanical behavior between these muscles remains unknown. In this study, we aimed to determine whether differences in activation between the MG and LG translate into different fascicle behavior during walking. Fifteen participants walked at their preferred speed under two conditions: 0% and 10% incline treadmill grade. We used surface electromyography and B-mode ultrasound to estimate muscle activation and fascicle dynamics in the MG and LG. We observed a higher normalized activation in the MG than in the LG during stance, which did not translate into greater MG normalized fascicle shortening. However, we observed significantly less normalized fascicle lengthening in the MG than in the LG during early stance, which matched with the timing of differences in activation between muscles. This resulted in more isometric behavior of the MG, which likely influences the muscle–tendon interaction and enhances the catapult-like mechanism in the MG compared with the LG. Nevertheless, this interplay between muscle activation and fascicle behavior, evident at the group level, was not observed at the individual level, as revealed by the lack of correlation between the MG–LG differences in activation and MG–LG differences in fascicle behavior. The MG and LG are often considered as equivalent muscles but the neuromechanical differences between them suggest that they may have distinct functional roles during locomotion.

**KEY WORDS: B-mode ultrasound, Fascicle length, Electromyography, Locomotion, Muscle function**

## INTRODUCTION

The triceps surae muscle group serves an essential role in human walking, generating more than 50% of the mechanical power needed for forward propulsion and swing initiation (Neptune et al., 2001). Studies have highlighted that different activation patterns exist during walking between the monoarticular soleus and the biarticular medial gastrocnemius (MG), despite their similar role as ankle plantar flexors. Specifically, the soleus is active for a greater portion of the gait cycle (Lay et al., 2007) and has an activation pattern that is less influenced by the grade of the walking surface, when compared with the MG (Franz and Kram, 2012). The few studies that have compared the gastrocnemii have shown that the MG activation is both greater and longer in duration than the lateral gastrocnemius (LG) activation during walking (Ahn et al., 2011), with large differences in the MG to LG activation ratio between individuals (Crouzier et al., 2019). This echoes recent work showing that these two muscles share minimal common neural drive (Hug et al., 2021). Together with studies suggesting that the MG and LG may produce different ankle moments in the frontal plane (Lee and Piazza, 2008), the differences in activation suggest that these muscles may have unique functional roles during walking. Other factors, such as the muscle fascicle length and contraction velocity also contribute to a muscle's force-generating capacity. This means activation alone does not provide us with all of the information necessary to understand muscle function. Concurrent information on muscle fascicle behavior is therefore needed.

Ultrasound studies have revealed different fascicle behavior between the soleus and the MG during walking, with soleus fascicles shortening less than MG fascicles (Ishikawa et al., 2005), and exhibiting a lower shortening velocity (Cronin et al., 2013). However, we know very little about how the MG and LG differ in their fascicle behavior during locomotor tasks such as walking. Studies have reported differences in resting muscle architecture between the MG and LG, such as shorter fascicle length and greater pennation angle for the MG (Charles et al., 2019). In addition, the LG is composed of different neuromuscular compartments with specific muscle architecture and innervation (Segal et al., 1991; Wolf et al., 1993). Moreover, the Achilles tendon is composed of three subtendons arising from the three muscles of the triceps surae (Edama et al., 2015). These factors may enable different neuromechanical behaviors of the three muscles.

While muscle activation and fascicle behavior each influence force generation, understanding the interplay between these factors allows for a more comprehensive assessment of muscle function. For instance, the higher mechanical work required during incline versus level walking is associated with higher activation and a greater amount of fascicle shortening in the MG muscle (Lichtwark and Wilson, 2006). However, to date, no study has combined both electromyography (EMG) and ultrasound imaging to explore the functional differences between the MG and LG muscles during locomotor tasks. The aforementioned differences in activation between the MG and LG muscles suggest that the mechanical behavior of the fascicles may also differ, requiring caution for making inferences based on measures of only one of the two muscles. In addition, a high level of inter-individual variability

[1]Nantes University, Laboratory 'Movement, Interactions, Performance' (EA 4334), 44000 Nantes, France. [2]The University of Queensland, School of Biomedical Sciences, Brisbane, QLD 4072, Australia. [3]Laboratoire de Physiologie et Evaluation Neuromusculaire, Institut de Myologie, 75013 Paris, France. [4]Institut Universitaire de France (IUF), 75231 Paris, France.

*Author for correspondence (francois.hug@univ-nantes.fr)

J.A., 0000-0003-1514-4958; F.H., 0000-0002-6432-558X

**Received 24 March 2021; Accepted 28 May 2021**

exists in the distribution of activation between these muscles (Ahn et al., 2011; Crouzier et al., 2019), but it remains unclear whether this translates into similar inter-individual variability in fascicle behavior.

The overall aim of this study was to determine whether the differences in activation strategies between the MG and LG during walking translate into different fascicle behavior. We used an experimental approach that combined surface EMG measurements and ultrasound imaging during level and incline walking. We further aimed to interpret our data at both the population level and the individual level. Based on previous work that illustrated greater activation in the MG compared with the LG (Ahn et al., 2011; Crouzier et al., 2019), we expected the higher activation to translate into a greater amount of fascicle shortening in the MG than in the LG. Additionally, at the individual level, we hypothesized that the MG to LG activation ratio would be correlated with the difference in fascicle shortening between the two muscles.

## MATERIALS AND METHODS

### Participants

Twenty participants with no recent (<6 months) lower limb pain or injury were recruited. They provided informed written consent. After a quality check of the ultrasound data (see 'Ultrasound', below), 5 participants were excluded from the analysis and therefore data are reported for 15 participants (5 females and 10 males, mean±s.d. age: 25.9±3.9 years, body mass: 75.2±14.6 kg, height: 1.73±0.10 m). The study was approved by the institutional ethics review committee at The University of Queensland (approval #2013001448) and adhered to the Declaration of Helsinki.

### Experimental protocol

Following a period of familiarization, participants performed three isometric plantar flexion maximal voluntary contractions (MVCs) with 120 s rest between each. Then, participants walked on a treadmill (Nautilus Trimline T345) while we used surface EMG, B-mode ultrasound and motion capture to measure muscle activity, fascicle behavior and foot position, respectively. The last of these was done using reflective markers attached bilaterally to the calcaneus and the metatarsophalangeal joint and a 12-camera motion capture system (Flex 13, OptiTrack, Corvallis, OR, USA), operating at 120 Hz. Participants walked under two conditions in a randomized order: (i) 0% treadmill grade (level walking) and (ii) 10% treadmill grade (incline walking). In both conditions, participants walked for 60 s at their preferred walking speed (1.1±0.1 m $s^{-1}$), which was determined at the beginning of the protocol during level walking using standardized procedures (Dal et al., 2010). The experimental protocol was composed of eight walking trials. Participants performed two trials for each condition and repeated this twice, first to record myoelectrical activity of the MG and LG and second to measure fascicle behavior of both muscles. The recording duration was 30 s and 15 s for EMG and ultrasound trials, respectively.

### EMG

We shaved, abraded and cleaned the participant's skin with alcohol to reduce the skin–electrode impedance. For the EMG trials, we placed surface electrodes (Trigno Delsys Inc., Natick, MA, USA; 10 mm inter-electrode distance) over the MG and LG muscle bellies, aligned along the direction of the muscle fascicles, determined using B-mode ultrasound imaging. Elastic bandages secured the electrodes to the skin to avoid movement artefacts. The EMG signals were amplified, digitized at 2048 Hz, band-pass filtered (20–500 Hz) and recorded in Spike2 (V7, CED Ltd, Cambridge, UK). An external trigger generated by the motion capture system was used to synchronize the motion capture data with the EMG recordings.

### B-mode ultrasound

For the ultrasound trials, we positioned two linear ultrasound probes (5–8 MHz, 60 mm field-of-view, LV8-5L60N-2, ArtUS, Telemed, Vilnius, Lithuania) over the MG and LG muscle bellies, at the same location where the EMG electrodes were placed in the previous trial. Although the fascicle plane may change during walking, we optimized the probe orientation to be aligned with the muscle fascicle plane during static standing and secured the probes with elastic bandages. Ultrasound data were captured at 120 Hz (Echo Wave II 3.7.1, Telemed). An external trigger generated by the motion capture system was used to synchronize the motion capture with the two ultrasound systems.

### Data analysis

#### 3D motion capture

Motion capture data were labeled, gap filled and smoothed with a 10 Hz low-pass second-order Butterworth filter (Motive, OptiTrack, Corvallis, OR, USA). Using custom-written scripts in Matlab (R2018b, The Mathworks, Natick, MD, USA), we identified heel-strike and toe-off based on foot vertical velocity, as described previously (O'Connor et al., 2007). Heel-strike and toe-off were used to determine the timing of each gait cycle for each individual and split the data into stance and swing phases for further analyses.

#### EMG

EMG and ultrasound analyses were conducted in Matlab R2018b. The EMG data analysis considered 15 gait cycles per trial. First, the signals were band-pass filtered using a second-order Butterworth filter (20–500 Hz). We visually checked all raw EMG data to detect movement artefacts or noise. In two trials for two different participants, we processed only 6 and 12 cycles instead of 15 because of movement artefacts. Then, we rectified and low-pass filtered (12 Hz) the EMG signal measured during the MVC trials and the maximal value was considered as the maximal EMG amplitude ($EMG_{max}$). The rectified EMG signals from 15 gait cycles were low-pass filtered at 12 Hz to determine the EMG envelope and then normalized to $EMG_{max}$. Finally, we interpolated the data from each gait cycle to 100 data points.

#### Ultrasound

Where required, we optimized the ultrasound image properties, such as brightness and contrast, post-data collection in the Echo Wave II software. Then, the image quality was checked to exclude videos whose quality was not sufficient (e.g. when fascicles were not clearly visible or when the fascicles moved entirely out of the imaging plane). After this quality check, we excluded five participants and we left out one trial for the MG and LG of another participant. We processed five gait cycles of ultrasound data per trial using a validated (Cronin et al., 2011; Gillett et al., 2013) semi-automated tracking algorithm (Ultratrack; Farris and Lichtwark, 2016), combined with manual corrections. We manually selected a region of interest surrounding the entire muscle belly and two regions of interest for each aponeurosis on the initial frame. Then, we drew a fascicle that represented the average fascicle orientation in the mid-region of the muscle belly and two straight lines in the inner limits of each aponeurosis. We used this to assess the changes in

Journal of Experimental Biology (2021) 224, jeb242626. doi:10.1242/jeb.242626

fascicle length and pennation angle, similar to previous methods (Dick and Wakeling, 2017; Aeles et al., 2018). The algorithm then tracked the fascicle and aponeuroses in sequential frames by implementing an affine flow model. Key frames were implemented at each heel-strike to help the algorithm account for tracking drift. Manual changes to the tracking were made where required, which was in most trials, mostly during shortening of the fascicles. The same investigator (R.H.) processed all videos to exclude inter-investigator variability (Aeles et al., 2017b) and the final tracking accuracy in all videos was then confirmed by another experienced operator (J.A.). Muscle fascicle length was calculated as the distance between the superficial and deep aponeuroses, along the fascicle orientation (Aeles et al., 2018). In limited cases, the fascicle extended outside the field of view. When this occurred, extrapolation was used to extend the fascicle and aponeuroses outside the image's field of view. The angle between the tracked muscle fascicle and the deep aponeurosis was defined as the pennation angle (Bolsterlee et al., 2015). We subsequently low-pass filtered all ultrasound data at 12 Hz, and calculated instantaneous fascicle velocity as the derivative of fascicle length with respect to time. Data from each gait cycle were interpolated to 100 data points. We normalized fascicle length and fascicle velocity to the mean fascicle length at heel-strike during level walking ($L_{HS}$; mean±s.d. group value: 55.4±7.6 mm and 65.3±10.0 mm for the MG and LG, respectively). The change in pennation angle was expressed as the absolute difference of the mean pennation angle at heel-strike during level walking (mean±s.d. group value: 20.9±3.0 deg and 13.6±2.3 deg for the MG and LG, respectively). For further reference, positive values indicate fascicle lengthening and negative values indicate fascicle shortening. Similarly, positive pennation angle values indicate an increase in pennation angle.

### Data reduction

From the processed EMG data, we extracted peak and average EMG amplitude during stance and during the whole cycle. For fascicle length, we calculated the amount of fascicle lengthening during stance ($L_{length}$) by subtracting the minimal fascicle length during early stance from the subsequent maximal fascicle length during stance (Fig. 1). This method takes into account the brief fascicle shortening that occurs directly following heel-strike, evident in most participants. We also determined the amount of fascicle shortening ($L_{short}$) following this initial lengthening period by taking the difference between the maximal fascicle length during the lengthening period and the fascicle length at toe-off. Similarly, the change in pennation angle was calculated for the lengthening period ($\beta_{length}$) and for the shortening period ($\beta_{short}$) by subtracting the maximal and the minimal values during each of these phases. The peak fascicle shortening velocity was also extracted during the shortening period ($V_{short}$). We analyzed 30 cycles per condition (15 per trial) for EMG and 10 cycles per condition (5 per trial) for ultrasound. We first extracted these parameters from each cycle and then averaged the resulting values over all cycles within a trial. Finally, we averaged the two trial values.

### Statistics

Statistical analyses were performed in Statistica v8.0 (Statsoft, Tulsa, OK, USA). All data were confirmed to be normally distributed using a Kolmogorov–Smirnov test. We used a two-way repeated-measures ANOVA (factor: muscle [MG, LG] and condition [level, incline]) to determine whether EMG amplitude (peak and average) and fascicle behavior ($L_{length}$, $L_{short}$, $\beta_{length}$, $\beta_{short}$ and $V_{short}$) differed between muscles and between conditions.

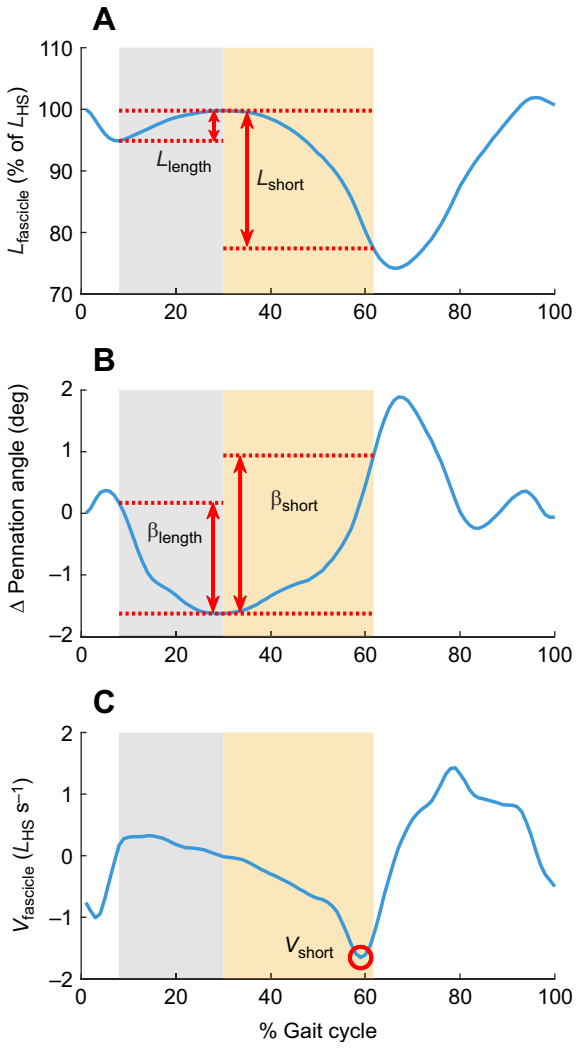


**Fig. 1. Illustration of the methods used to calculate ultrasound parameters.** Representative fascicle length ($L_{fascicle}$; A), change in pennation angle (B) and fascicle velocity ($V_{fascicle}$; C) data (mean group pattern) for the lateral gastrocnemius (LG) during level walking (blue curves), through the lengthening period (gray area) and the shortening period (orange area). $L_{fascicle}$ and $V_{fascicle}$ were normalized to the fascicle length at heel-strike during level walking ($L_{HS}$). Heel-strike occurs at 0% on the *x*-axis. The end of the orange area corresponds to the toe-off event, which we considered as the end of the shortening period. The red horizontal dotted lines represent the minimum or the maximum value within a period. The red arrows indicate the extracted parameters, i.e. the amount of fascicle lengthening ($L_{length}$) and fascicle shortening ($L_{short}$) (A), and the pennation angle decrease ($\beta_{length}$) and increase ($\beta_{short}$) (B). The red circle in C corresponds to the peak shortening velocity ($V_{short}$).

We used statistical parametric mapping (SPM) with a two-way repeated-measures ANOVA to compare the EMG profiles between muscles and conditions. To assess the inter-individual variability in muscle activation distribution, we used descriptive statistics (mean±s.d.) of the normalized EMG amplitude ratios calculated as MG/(MG+LG) (Crouzier et al., 2019). Finally, to test whether the differences in activation between muscles translated to differences in fascicle behavior, we performed correlations for both conditions between the difference in MG–LG average EMG amplitude during the lengthening period and the difference in MG–LG fascicle length and pennation angle changes during the same lengthening period. We ran similar correlations for the shortening period. A Bonferroni

Journal of Experimental Biology (2021) 224, jeb242626. doi:10.1242/jeb.242626

**Table 1. Normalized myoelectrical activity in the medial and lateral gastrocnemius during level and incline walking**

| | Level walking | | Incline walking | |
|---|---|---|---|---|
| EMG parameters | MG | LG | MG | LG |
| Peak EMG amplitude (% of $EMG_{max}$) | 45.0±13.2 | 34.3±14.1* | 68.3±18.1‡ | 62.0±19.3*,‡ |
| Average EMG amplitude during stance (% of $EMG_{max}$) | 16.2±4.8 | 11.0±3.5* | 22.4±6.6‡ | 18.1±5.2*,‡ |
| Average EMG amplitude during whole cycle (% of $EMG_{max}$) | 11.2±2.9 | 7.9±2.6* | 15.1±4.1‡ | 12.3±3.4*,‡ |

MG, medial gastrocnemius; LG, lateral gastrocnemius; EMG, electromyography; $EMG_{max}$, EMG amplitude during maximal isometric voluntary contraction. Values were normalized to maximal isometric contraction and are reported as means±s.d. *Significant difference from MG. ‡Significant difference from level walking. $n$=15.

correction for multiple comparisons was applied. The level of significance was set at $P$<0.05.

## RESULTS

### Myoelectrical activity

There was a main effect of muscle and condition on peak EMG amplitude (muscle: $P$=0.049; condition: $P$<0.001), average EMG amplitude during stance (muscle and condition: $P$<0.001), and average EMG amplitude during the whole cycle (muscle and condition: $P$<0.001), with no significant muscle×condition interactions (all $P$≥0.616). Specifically, MG peak EMG was higher than LG peak EMG, regardless of the condition (Table 1). Similarly, average EMG amplitude during stance and during the whole cycle was higher for the MG than for the LG, regardless of the condition (Fig. 2). All EMG parameters, i.e. peak and average EMG amplitude during stance and during the whole cycle, were higher during incline walking than during level walking, in both the MG and LG.

The SPM analysis revealed a main effect of muscle from 18% to 36% of the gait cycle ($P$<0.001) and a main effect of condition from 25% to 56% ($P$<0.001), from 64% to 78% ($P$<0.001) and from 89% to 92% ($P$=0.023) of the gait cycle. There was no significant interaction between muscle and condition. Specifically, the MG had higher EMG amplitude than the LG from 18% to 36% of the gait cycle and the EMG amplitude was higher for the incline condition than for the level condition during the 25–56%, 64–78% and 89–92% phases of the gait cycle.

### Muscle fascicle behavior

Inspection of the time-varying profiles of muscle fascicle behavior (Figs 3 and 4) revealed that the MG and LG fascicles, after a brief shortening in most of the individuals, lengthened after heel-strike (hereafter referred to as ‘fascicle lengthening period’). Following this, the fascicles shortened and rotated to steeper pennation angles until toe-off (hereafter referred to as ‘fascicle shortening period’).

There was a main effect of muscle on $L_{length}$ ($P$=0.017) and $\beta_{length}$ ($P$<0.001), but no main effect of condition (both $P$≥0.193) nor a muscle×condition interaction (both $P$≥0.490). Specifically, the MG fascicles lengthened less than the LG fascicles, regardless of the condition (Fig. 3A,B, Table 2). Similarly, the pennation angle decreased less for the MG than for the LG, regardless of the condition (Fig. 3C,D).

There was a main effect of condition on $L_{short}$ ($P$<0.001) with no main effect of muscle ($P$=0.309) nor a muscle×condition interaction ($P$=0.414). Specifically, $L_{short}$ was higher during incline walking than during level walking, regardless of the muscle (Fig. 3A,B, Table 2). Furthermore, for $\beta_{short}$, there was a main effect of muscle ($P$=0.038) and condition ($P$=0.009), but there was no significant muscle×condition interaction ($P$=0.532). Specifically, the MG muscle underwent a greater increase in pennation angle than the LG, regardless of the condition. Moreover, the increase in pennation angle was greater during incline walking than during level walking, regardless of the muscle (Fig. 3C,D).

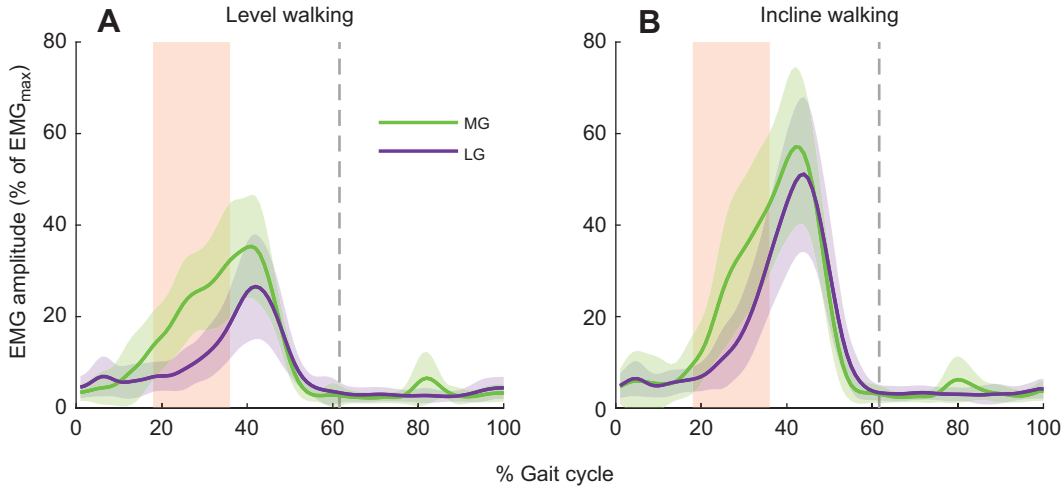


**Fig. 2. Average time-varying electromyography (EMG) patterns measured during walking.** EMG amplitude data during level walking (A) and incline walking (B) are presented as the mean (thick line) and standard deviation (shaded area) of all participants. EMG amplitude was normalized to that measured during a maximal isometric voluntary contraction ($EMG_{max}$). Heel-strike occurs at 0% on the $x$-axis. The dashed vertical lines correspond to the average timing of toe-off during the gait cycle. The red area represents the period of the gait cycle where the statistical parametric mapping indicates a significant difference in EMG amplitude between muscles (18–36% of the gait cycle). Peak EMG and average EMG amplitude measured during stance and during the whole cycle were: (i) significantly higher for the medial gastrocnemius (MG) than for the LG, regardless of the condition and (ii) significantly higher for incline walking (B) than for level walking (A), regardless of the muscle. $n$=15.

Journal of Experimental Biology (2021) 224, jeb242626. doi:10.1242/jeb.242626

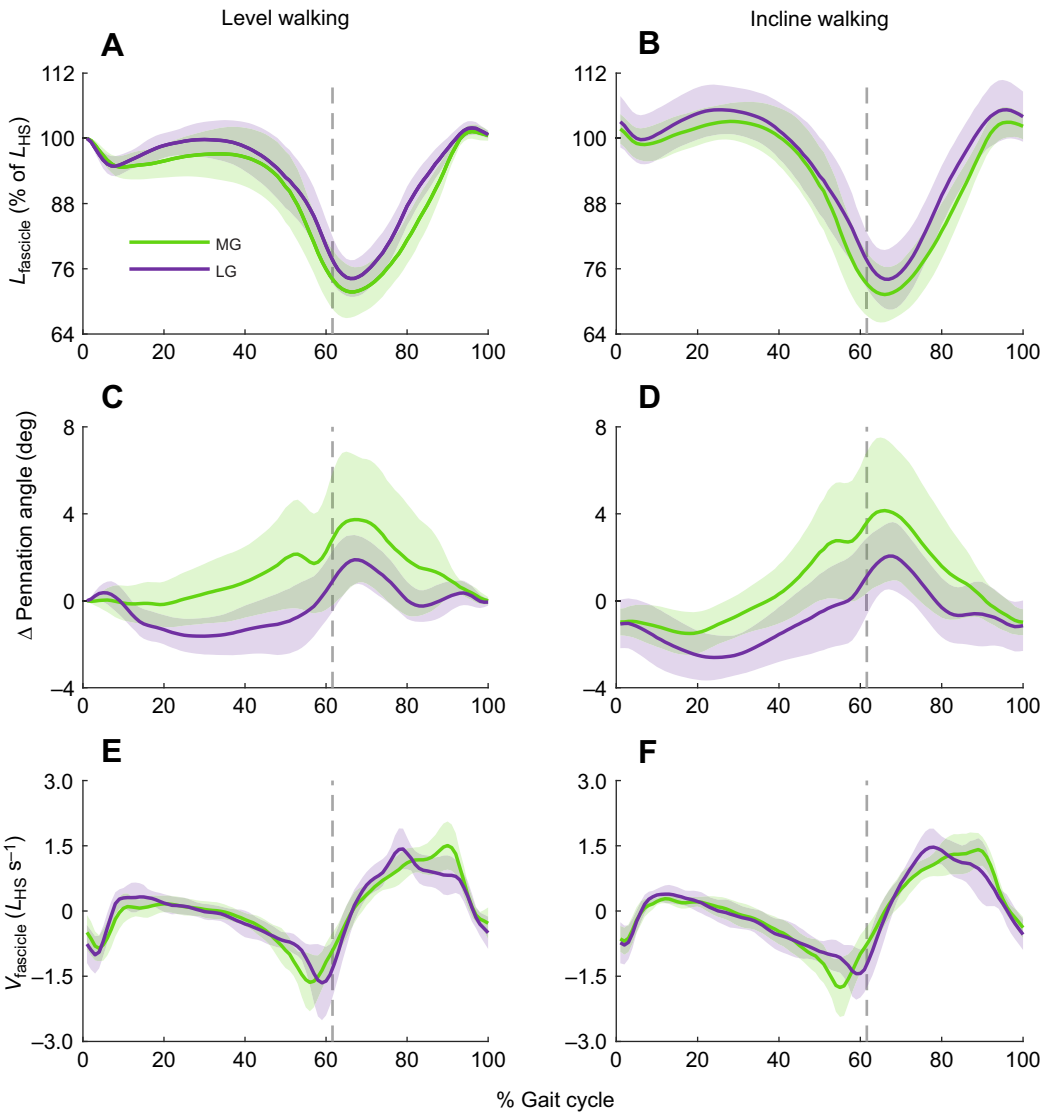


**Fig. 3. Average time-varying fascicle behavior measured during walking.** $L_{fascicle}$ (A,B), change in pennation angle (C,D) and $V_{fascicle}$ (E,F) data during level (left) and incline (right) walking are presented as the mean (thick line) and standard deviation (shaded area) of all participants. $L_{fascicle}$ and $V_{fascicle}$ were normalized to $L_{HS}$ during level walking. Heel-strike occurs at 0% on the *x*-axis. The dashed vertical lines correspond to the average timing of toe-off during the gait cycle. During the lengthening period, fascicle lengthening and the decrease in pennation angle were significantly lower for the MG than for the LG, regardless of the condition. During the shortening period, there was a greater increase in pennation angle for the MG than for the LG. Moreover, during the shortening period, fascicle shortening and the change in pennation angle were higher for incline walking (right panels) than for level walking (left panels), regardless of the muscle. $n$=15.

We found no main effect of muscle ($P$=0.927), condition ($P$=0.793) or muscle×condition interaction ($P$=0.689) on $V_{short}$ (Fig. 3E,F).

### Relationship between myoelectrical activity and muscle fascicle behavior

Fig. 4 shows the individual time-varying profiles for both EMG and fascicle behavior for all participants during level walking. The EMG time-varying profiles revealed a high amount of variability between participants in terms of both shape and amplitude. For example, across participants, the MG/(MG+LG) ratio of peak EMG amplitude ranged from 44.3% to 68.6% with a mean (±s.d.) value of 57.6±8.0%. To determine whether these inter-individual differences translated into different muscle fascicle behavior, we assessed the relationship between the MG–LG differences in average EMG amplitude during the lengthening or the shortening period and the respective MG–LG differences in fascicle behavior, i.e. $L_{length}$, $L_{short}$, $\beta_{length}$ and $\beta_{short}$ during level walking and incline walking. Out of the eight correlations, only one significant negative correlation between MG–LG differences in average EMG amplitude during lengthening and MG–LG differences in $\beta_{length}$ during level walking was observed ($R^2$=0.42, $P$=0.009). This correlation revealed that the greater the bias of activation to the MG during stance, the lower the bias of change in pennation angle to the MG. Of note, there was no correlation between MG–LG differences in average EMG amplitude during lengthening and the MG–LG differences in $L_{length}$ ($R^2$=0.14, $P$=0.177 and $R^2$=0.17, $P$=0.127 for level and incline walking, respectively).

## DISCUSSION

We combined EMG and ultrasound measurements to determine whether the observed differences in activation between the MG and

Journal of Experimental Biology (2021) 224, jeb242626. doi:10.1242/jeb.242626

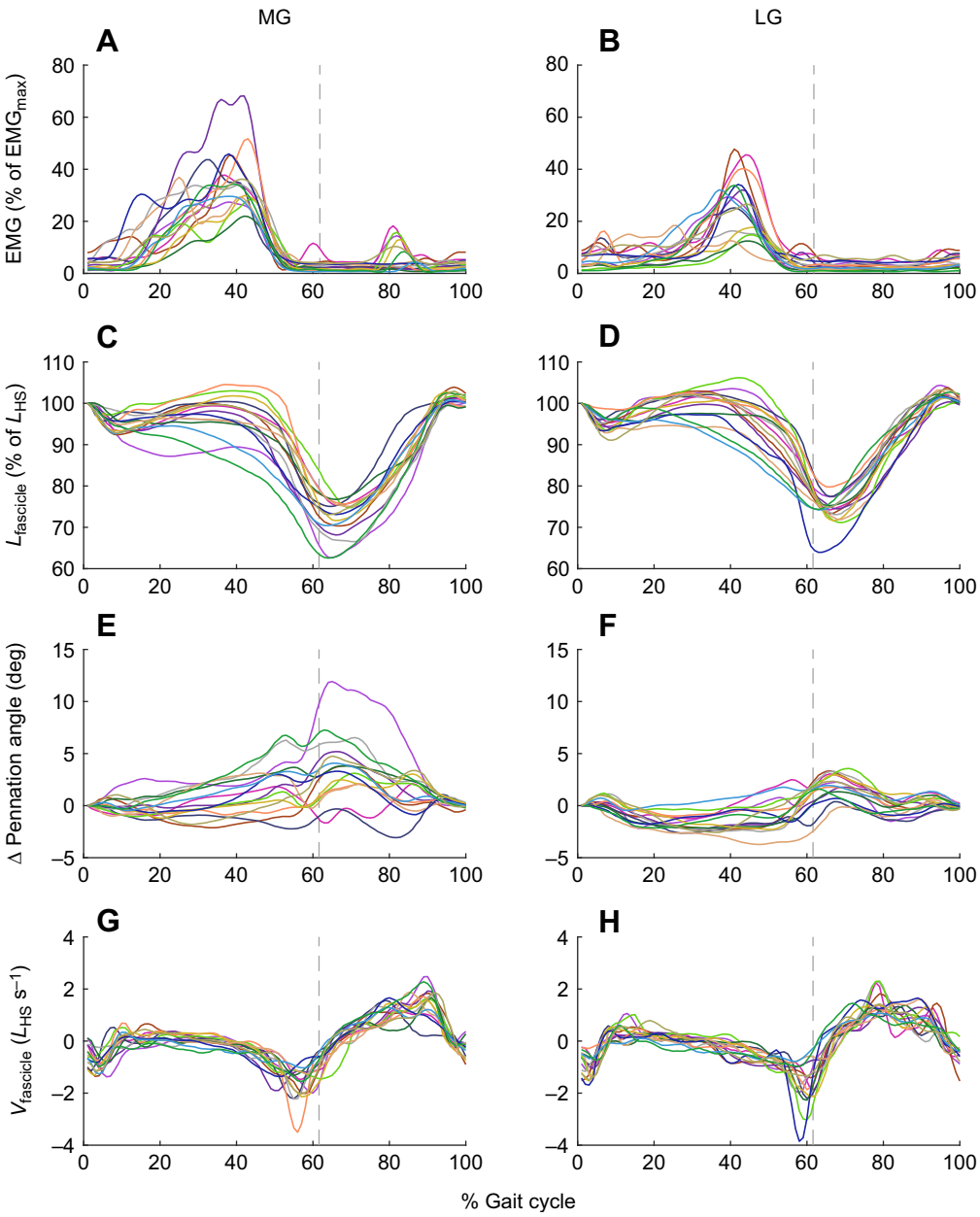


**Fig. 4. Individual time-varying EMG and fascicle behavior estimated during level walking.** EMG amplitude (A,B), $L_{fascicle}$ (C,D), change in pennation angle (E,F) and $V_{fascicle}$ (G,H) data for each participant (represented by different colors) for the MG (left) and LG (right). EMG amplitude was normalized to $EMG_{max}$; $L_{fascicle}$ and $V_{fascicle}$ were normalized to $L_{HS}$ during level walking. Heel-strike occurs at 0% on the *x*-axis. The dashed vertical lines correspond to the average timing of toe-off during the gait cycle. Approximately one-third of the participants exhibited a second MG EMG burst during the swing phase (A) similar to previous reports (Hug et al., 2019). This pattern did not occur in the LG (B). *n*=15.

the LG during walking translate into different fascicle behavior. We found that the MG was more active than the LG but, in contrast to our hypothesis, this did not translate into greater MG fascicle shortening during the stance phase. However, we observed less MG fascicle lengthening during early stance, when compared with the LG. Additionally, the inter-individual variability in the distribution of activation between the MG and LG did not explain the variability in fascicle behavior between individuals.

The higher muscle activation for the MG than for the LG, consistent with previous reports (Ahn et al., 2011; Crouzier et al., 2019), was greatest during early stance, which coincides with the period where between-muscle differences in fascicle behavior were most apparent (Fig. 2). Specifically, we observed that the MG underwent less active lengthening than the LG during early stance by approximately 2.3% of $L_{HS}$ (2.0 mm), corresponding to more than 30% of the total lengthening during stance. These differences in fascicle behavior that occurred early in the gait cycle are likely related to the highly tuned interaction between the gastrocnemii and their partially independent Achilles subtendons, which are able to undergo non-uniform displacement (Franz et al., 2015). During the early stance phase of walking, the MG and LG actively resist lengthening while the whole muscle–tendon unit (MTU) lengthens (Farris and Sawicki, 2012; Lichtwark and Wilson, 2006). During late stance, muscle activation decreases and the muscle–tendon interaction enables the series-elastic element to undergo rapid shortening (Lichtwark and Wilson, 2006). The smaller difference between the MG and LG activation during late stance combined with the rapid shortening of the series-elastic element likely explains why we did not observe a muscle difference in fascicle shortening or fascicle shortening velocity.

The higher muscle activation during early stance enables the MG fascicles to remain in a more isometric state, compared with the LG fascicles. It is well established that this isometric behavior of the plantar flexor muscle fascicles enables their tendon to stretch and store elastic strain energy, which is subsequently released in late push-off (Farris and Raiteri, 2017; Fukunaga et al., 2001; Ishikawa

Journal of Experimental Biology (2021) 224, jeb242626. doi:10.1242/jeb.242626

**Table 2. Muscle fascicle parameters for the medial and lateral gastrocnemius during level and incline walking**

| | Level walking | | Incline walking | |
|---|---|---|---|---|
| Muscle fascicle parameter | MG | LG | MG | LG |
| $L_{length}$ (% of $L_{HS}$) | 4.6±3.1 | 6.9±3.5* | 5.9±3.0 | 7.4±2.3* |
| $\beta_{length}$ (deg) | −1.3±0.9 | −2.1±0.8* | −1.2±0.5 | −1.8±0.6* |
| $L_{short}$ (% of $L_{HS}$) | −24.2±3.2 | −24.0±3.4 | −30.9±4.7‡ | −28.9±5.1‡ |
| $\beta_{short}$ (deg) | 3.9±1.8 | 3.2±1.1* | 5.4±2.5‡ | 4.1±1.2*,‡ |
| $V_{short}$ ($L_{HS}$ $s^{-1}$) | −2.1±0.6 | −2.1±0.8 | −2.2±0.6 | −2.1±0.4 |

MG, medial gastrocnemius; LG, lateral gastrocnemius; $L_{length}$, amount of fascicle lengthening; $\beta_{length}$, change in pennation angle during the fascicle lengthening period; $L_{short}$, amount of fascicle shortening; $\beta_{short}$, change in pennation angle during the fascicle shortening period; $V_{short}$, peak shortening velocity; $L_{HS}$, fascicle length at heel-strike during level walking. Values are reported as means±s.d. *Significant difference from MG. ‡Significant difference from level walking. $n$=15.

et al., 2005; Lichtwark and Wilson, 2006). While a similar catapult-like mechanism occurs in the LG, our results suggest that it may occur to a lesser extent because the lower activation results in a reduced ability to maintain the LG fascicles isometrically. Thus, the MG muscle–tendon interaction may be better tuned to store and return elastic strain energy for effective push-off. These findings are inconsistent with results from a modeling study, which predicts that, during walking, MG muscle fibers undergo alternating periods of negative and positive work to act like a spring, whereas LG muscle fibers behave more isometrically to function in a strut-like manner (Lai et al., 2019). Our *in vivo* data displayed smaller active length changes in the MG fascicles, corresponding more to strut-like behavior, and a greater active lengthening in the LG, likely resulting in more negative work production and corresponding to spring-like behavior. This discrepancy may, in part, arise from differences between measured muscle activation and model-predicted muscle excitation for the MG and LG, and from the use of generic data in Lai et al. (2019). Nonetheless, the combination of experimental data with predictions from neuro-musculoskeletal models provides a powerful and promising approach to understand human and animal locomotor function.

In addition to muscle activation, differences in tissue properties may also contribute to the reduced lengthening of the MG fascicles during walking. For example, the MG muscle has, on average, a higher passive shear modulus (Le Sant et al., 2017; Lindemann et al., 2020) and a larger volume (Crouzier et al., 2018) than the LG, likely providing more resistance to lengthening. Moreover, the subtendon stiffness seems to match the muscle passive stiffness with a stiffer MG subtendon compared with the LG subtendon (Yin et al., 2021). The nervous system may choose to activate the MG more than the LG to enhance the catapult-like mechanism of the stiffer MTU and larger muscle and thus to decrease the overall activation cost (Biewener and Roberts, 2000; Crouzier et al., 2018; Crowninshield and Brand, 1981). Furthermore, it has been suggested that the MG and LG may have different roles in the frontal plane, with the MG having a greater inversion moment arm (Lee and Piazza, 2008). These differences may lead to a higher exploitation of the MG than the LG to contribute the necessary inversion in the second part of the stance phase (Arnold et al., 2014) and to allow an efficient push-off. Taken together, the differences in tissue properties and anatomy between the MG and LG MTUs and the bias of activation towards the larger MG likely results in a greater use of elastic energy – enabling more economical walking.

Despite differences in muscle activation between level and incline walking, we did not find any difference in the amount of lengthening between these conditions. There are at least three possible explanations. First, incline walking predominantly influences peak activation (25–56% of the gait cycle), when the fascicles have already stopped lengthening. This may explain the difference in fascicle shortening but not in fascicle lengthening between level and incline walking. Second, incline walking limits the ankle plantarflexion immediately after heel-strike and increases the following ankle dorsiflexion. This, in turn, increases MTU length during stance (Lichtwark and Wilson, 2006), which, by stretching the tendon, increases the tension in the tendon. This process likely supports fascicle lengthening despite the higher activation. Finally, the increased MTU length during stance caused by incline walking likely results in greater energy storing potential in the tendon. Thus, at the muscle level, the higher mechanical demand for incline walking is achieved via higher activation and greater fascicle shortening but with a similar amount of fascicle lengthening.

We found that the greater MG than LG activation was only true ‘on average’, as 4 out of the 15 participants exhibited either a balanced MG–LG peak activation (MG to LG peak activation ratio between 49% and 51%) or an activation biased towards the LG (MG to LG ratio <49%). A study performed on 85 participants observed similar inter-individual variability, repeatable between days, despite the group data also revealing that the MG was activated more than the LG (Crouzier et al., 2019). However, the MG–LG activation ratios seem more biased towards the MG in that study as only 3 out of 85 participants had a MG to LG ratio <49% and 4 out of the 85 participants had a MG to LG ratio between 49% and 51%. This discrepancy is likely due to the higher walking speed in our study (1.1 m $s^{-1}$) compared with that in Crouzier et al. (2019) (0.9 m $s^{-1}$). Indeed, when walking speed increases, the MG–LG activation ratios tend to be closer to 50% (Ahn et al., 2011). Regardless, our results show that the MG–LG differences in activation level are not related to the inter-individual variability in MG–LG differences in fascicle behavior. Several factors could explain the absence of correlations, including different tendon and muscle mechanical properties across participants. For instance, a large variability in subtendon stiffness (Yin et al., 2021) and Achilles tendon twist (Edama et al., 2015; Knaus and Blemker, 2021) has been observed between individuals. It is therefore possible that activation varies between participants to account for known differences in mechanical and architectural properties of the muscle and tendon (Aeles et al., 2017a), and enable similar movement kinetics and kinematics during motor tasks.

Some limitations in the experimental approach used in this study need to be considered. First, the ultrasound measurements were made in 2D with a limited field of view whereas muscle is a 3D complex object with non-uniform deformations (Rana and Wakeling, 2011). While it is possible that there are 3D shape changes that are affected by the activation, our analysis focused on the primary movement plane of the muscle fascicles. Moreover, to track fascicles in the same plane during locomotion is challenging. To limit the impact of this issue, we tracked the average movement of the fascicles within the field of view instead of a single fascicle

and we followed guidelines to minimize errors in fascicle tracking (Aeles et al., 2017b; Aggeloussis et al., 2010; Bolsterlee et al., 2016). Finally, EMG and ultrasound measurements were performed on the same day but during different walking trials. It is challenging to maintain both EMG electrodes and the ultrasound probe at appropriate locations for simultaneous recordings on an individual muscle. However, we averaged the data over 30 (EMG) and 10 (ultrasound) cycles, and are confident that the EMG and ultrasound patterns are representative of the walking conditions.

## Conclusion

In this study, we found that, during walking, the higher activation of the MG was associated with less fascicle lengthening than for the LG. This enabled the MG fascicles to remain more isometric and may enhance the catapult-like muscle–tendon interaction in the MG, compared with the LG, and decrease the overall activation cost. At the individual level, we found no relationship between the MG–LG differences in activation and the between-muscle differences in fascicle behavior, which may be linked to potential inter-individual variability in muscle and tendon properties of the gastrocnemii. Our results highlight that slightly different neuromuscular behavior may be provided by these two synergist muscles that are often considered as equivalent muscles with the same function. These findings show that we cannot derive information from experimental measurements on one muscle to infer the behavior or the function of its synergist muscles. Empirical data from *in vivo* experiments that combine EMG and B-mode ultrasound in multiple muscles will provide insights for the evaluation of neuro-musculoskeletal models and simulations.

### Acknowledgements

The authors thank James Williamson and Aurélie Sarcher for their assistance in data analysis.

### Competing interests

The authors declare no competing or financial interests.

### Author contributions

Conceptualization: F.H., T.J.M.D.; Methodology: R.H., J.A., N.Y.K., R.F., F.H., T.J.M.D.; Software: R.H., J.A., F.H.; Validation: R.H., J.A., N.Y.K., R.F., F.H., T.J.M.D.; Formal analysis: R.H., J.A.; Investigation: N.Y.K., R.F., F.H., T.J.M.D.; Resources: T.J.M.D.; Data curation: R.H., J.A., N.Y.K., R.F., T.J.M.D.; Writing - original draft: R.H., J.A.; Writing - review & editing: R.H., J.A., F.H., T.J.M.D.; Visualization: R.H.; Supervision: J.A., F.H., T.J.M.D.; Project administration: T.J.M.D.; Funding acquisition: F.H., T.J.M.D.

### Funding

This work was supported by a University of Queensland Early Career Research Grant to T.J.M.D. F.H. is supported by a fellowship from the Institut Universitaire de France (IUF) and a travel grant from the Société de Biomécanique. Support was received from the Agence Nationale de la Recherche (ANR-19-CE17-002-01, COMMODE project; to F.H.).

### Data availability

The EMG and ultrasound data are available from figshare: https://doi.org/10.6084/m9.figshare.14251130.v4

### References

**Aeles, J., Lenchant, S., Vanlommel, L. and Vanwanseele, B.** (2017a). Bilateral differences in muscle fascicle architecture are not related to the preferred leg in jumping athletes. *Eur. J. Appl. Physiol.*, **117**, 1453-1461. doi:10.1007/s00421-017-3638-5

**Aeles, J., Lichtwark, G. A., Lenchant, S., Vanlommel, L., Delabastita, T. and Vanwanseele, B.** (2017b). Information from dynamic length changes improves reliability of static ultrasound fascicle length measurements. *PeerJ*, **5**, e4164. doi:10.7717/peerj.4164

**Aeles, J., Lichtwark, G. A., Peeters, D., Delecluse, C., Jonkers, I. and Vanwanseele, B.** (2018). Effect of a prehop on the muscle-tendon interaction during vertical jumps. *J. Appl. Physiol.*, **124**, 1203-1211. doi:10.1152/japplphysiol.00462.2017

**Aggeloussis, N., Giannakou, E., Albracht, K. and Arampatzis, A.** (2010). Reproducibility of fascicle length and pennation angle of gastrocnemius medialis in human gait in vivo. *Gait Posture*, **31**, 73-77. doi:10.1016/j.gaitpost.2009.08.249

**Ahn, A. N., Kang, J. K., Quitt, M. A., Davidson, B. C. and Nguyen, C. T.** (2011). Variability of neural activation during walking in humans: short heels and big calves. *Biol. Lett.*, **7**, 539-542. doi:10.1098/rsbl.2010.1169

**Arnold, J. B., Mackintosh, S., Jones, S. and Thewlis, D.** (2014). Differences in foot kinematics between young and older adults during walking. *Gait Posture*, **39**, 689-694. doi:10.1016/j.gaitpost.2013.09.021

**Biewener, A. A. and Roberts, T. J.** (2000). Muscle and tendon contributions to force, work, and elastic energy savings : A comparative perspective. *Exerc. Sport Sci. Rev.*, **28**, 99-107.

**Bolsterlee, B., Veeger, H. E., van der Helm, F. C. T., Gandevia, S. C. and Herbert, R. D.** (2015). Comparison of measurements of medial gastrocnemius architectural parameters from ultrasound and diffusion tensor images. *J. Biomech.*, **48**, 1133-1140. doi:10.1016/j.jbiomech.2015.01.012

**Bolsterlee, B., Gandevia, S. C. and Herbert, R. D.** (2016). Effect of transducer orientation on errors in ultrasound image-based measurements of human medial gastrocnemius muscle fascicle length and pennation. *PloS One*, **11**, e0157273. doi:10.1371/journal.pone.0157273

**Charles, J. P., Suntaxi, F. and Anderst, W. J.** (2019). In vivo human lower limb muscle architecture dataset obtained using diffusion tensor imaging. *PLoS One*, **14**, e0223531. doi:10.1371/journal.pone.0223531

**Cronin, N. J., Carty, C. P., Barrett, R. S. and Lichtwark, G. A.** (2011). Automatic tracking of medial gastrocnemius fascicle length during human locomotion. *J. Appl. Physiol.*, **111**, 1491-1496. doi:10.1152/japplphysiol.00530.2011

**Cronin, N. J., Avela, J., Finni, T. and Peltonen, J.** (2013). Differences in contractile behaviour between the soleus and medial gastrocnemius muscles during human walking. *J. Exp. Biol.*, **216**, 909-914.

**Crouzier, M., Lacourpaille, L., Nordez, A., Tucker, K. and Hug, F.** (2018). Neuromechanical coupling within the human triceps surae and its consequence on individual force-sharing strategies. *J. Exp. Biol.*, **221**, jeb187260. doi:10.1242/jeb.187260

**Crouzier, M., Hug, F., Dorel, S., Deschamps, T., Tucker, K. and Lacourpaille, L.** (2019). Do individual differences in the distribution of activation between synergist muscles reflect individual strategies? *Exp. Brain Res.*, **237**, 625-635. doi:10.1007/s00221-018-5445-6

**Crowninshield, R. D. and Brand, R. A.** (1981). A physiologically based criterion of muscle force prediction in locomotion. *J. Biomech.*, **14**, 793-801. doi:10.1016/0021-9290(81)90035-X

**Dal, U., Erdogan, T., Resitoglu, B. and Beydagi, H.** (2010). Determination of preferred walking speed on treadmill may lead to high oxygen cost on treadmill walking. *Gait Posture*, **31**, 366-369. doi:10.1016/j.gaitpost.2010.01.006

**Dick, T. J. M. and Wakeling, J. M.** (2017). Shifting gears: dynamic muscle shape changes and force-velocity behavior in the medial gastrocnemius. *J. Appl. Physiol.*, **123**, 1433-1442. doi:10.1152/japplphysiol.01050.2016

**Edama, M., Kubo, M., Onishi, H., Takabayashi, T., Inai, T., Yokoyama, E., Hiroshi, W., Satoshi, N. and Kageyama, I.** (2015). The twisted structure of the human Achilles tendon: classification by degree of twist. *Scand. J. Med. Sci. Sports*, **25**, e497-e503. doi:10.1111/sms.12342

**Farris, D. J. and Lichtwark, G. A.** (2016). UltraTrack: Software for semi-automated tracking of muscle fascicles in sequences of B-mode ultrasound images. *Comput. Methods Programs Biomed.*, **128**, 111-118. doi:10.1016/j.cmpb.2016.02.016

**Farris, D. J. and Raiteri, B. J.** (2017). Elastic ankle muscle-tendon interactions are adjusted to produce acceleration during walking in humans. *J. Exp. Biol.*, **220**, 4252-4260.

**Farris, D. J. and Sawicki, G. S.** (2012). Human medial gastrocnemius force-velocity behavior shifts with locomotion speed and gait. *Proc. Natl. Acad. Sci. U.S.A.*, **109**, 977-982. doi:10.1073/pnas.1107972109

**Franz, J. R. and Kram, R.** (2012). The effects of grade and speed on leg muscle activations during walking. *Gait Posture*, **35**, 143-147. doi:10.1016/j.gaitpost.2011.08.025

**Franz, J. R., Slane, L. C., Rasske, K. and Thelen, D. G.** (2015). Non-uniform in vivo deformations of the human Achilles tendon during walking. *Gait Posture*, **41**, 192-197. doi:10.1016/j.gaitpost.2014.10.001

**Fukunaga, T., Kubo, K., Kawakami, Y., Fukashiro, S., Kanehisa, H. and Maganaris, C. N.** (2001). In vivo behaviour of human muscle tendon during walking. *Proceedings of the Royal Society of London. Series B: Biological Sciences*, **268**, 229-233. doi:10.1098/rspb.2000.1361

**Gillett, J. G., Barrett, R. S. and Lichtwark, G. A.** (2013). Reliability and accuracy of an automated tracking algorithm to measure controlled passive and active muscle fascicle length changes from ultrasound. *Comput. Methods Biomech. Biomed. Engin.*, **16**, 678-687. doi:10.1080/10255842.2011.633516

**Hug, F., Vogel, C., Tucker, K., Dorel, S., Deschamps, T., Le Carpentier, É. and Lacourpaille, L.** (2019). Individuals have unique muscle activation signatures as revealed during gait and pedaling. *J. Appl. Physiol.*, **127**, 1165-1174. doi:10.1152/japplphysiol.01101.2018

**Hug, F., Del Vecchio, A., Avrillon, S., Farina, D. and Tucker, K.** (2021). Muscles from the same muscle group do not necessarily share common drive: evidence

from the human triceps surae. *J. Appl. Physiol.*, **130**, 342-354. doi:10.1152/japplphysiol.00635.2020

**Ishikawa, M., Komi, P. V., Grey, M. J., Lepola, V. and Bruggemann, G. P.** (2005). Muscle-tendon interaction and elastic energy usage in human walking. *J. Appl. Physiol.*, **99**, 603-608. doi:10.1152/japplphysiol.00189.2005

**Knaus, K. R. and Blemker, S. S.** (2021). 3D models reveal the influence of Achilles Subtendon twist on strain and energy storage. *Frontiers in Bioengineering and Biotechnology*, **9**, 539135. doi:10.3389/fbioe.2021.539135

**Lai, A. K. M., Biewener, A. A. and Wakeling, J. M.** (2019). Muscle-specific indices to characterise the functional behaviour of human lower-limb muscles during locomotion. *J. Biomech.*, **89**, 134-138. doi:10.1016/j.jbiomech.2019.04.027

**Lay, A. N., Hass, C. J., Richard Nichols, T. and Gregor, R. J.** (2007). The effects of sloped surfaces on locomotion: an electromyographic analysis. *J. Biomech.*, **40**, 1276-1285. doi:10.1016/j.jbiomech.2006.05.023

**Le Sant, G., Nordez, A., Andrade, R., Hug, F., Freitas, S. and Gross, R.** (2017). Stiffness mapping of lower leg muscles during passive dorsiflexion. *J. Anat.*, **230**, 639-650. doi:10.1111/joa.12589

**Lee, S. S. M. and Piazza, S. J.** (2008). Inversion–eversion moment arms of gastrocnemius and tibialis anterior measured in vivo. *J. Biomech.*, **41**, 3366-3370. doi:10.1016/j.jbiomech.2008.09.029

**Lichtwark, G. A. and Wilson, A. M.** (2006). Interactions between the human gastrocnemius muscle and the Achilles tendon during incline, level and decline locomotion. *J. Exp. Biol.*, **209**, 4379-4388. doi:10.1242/jeb.02434

**Lindemann, I., Coombes, B. K., Tucker, K., Hug, F. and Dick, T. J. M.** (2020). Age-related differences in gastrocnemii muscles and Achilles tendon mechanical properties in vivo. *J. Biomech.*, **112**, 110067. doi:10.1016/j.jbiomech.2020.110067

**Neptune, R. R., Kautz, S. A. and Zajac, F. E.** (2001). Contributions of the individual ankle plantar flexors to support, forward progression and swing initiation during walking. *J. Biomech.*, **34**, 1387-1398. doi:10.1016/S0021-9290(01)00105-1

**O'Connor, C. M., Thorpe, S. K., O'Malley, M. J. and Vaughan, C. L.** (2007). Automatic detection of gait events using kinematic data. *Gait Posture*, **25**, 469-474. doi:10.1016/j.gaitpost.2006.05.016

**Rana, M. and Wakeling, J. M.** (2011). *In-vivo* determination of 3D muscle architecture of human muscle using free hand ultrasound. *J. Biomech.*, **44**, 2129-2135. doi:10.1016/j.jbiomech.2011.05.026

**Segal, R. L., Wolf, S. L., DeCamp, M. J., Chopp, M. T. and English, A. W.** (1991). Anatomical partitioning of three multiarticular human muscles. *Cells Tissues Organs*, **142**, 261-266. doi:10.1159/000147199

**Wolf, S. L., Segal, R. L. and English, A. W.** (1993). Task-oriented EMG activity recorded from partitions in human lateral gastrocnemius muscle. *J. Electromyogr. Kinesiol.*, **3**, 87-94. doi:10.1016/1050-6411(93)90003-F

**Yin, N.-H., Fromme, P., McCarthy, I. and Birch, H. L.** (2021). Individual variation in Achilles tendon morphology and geometry changes susceptibility to injury. *eLife*, **10**, e63204. doi:10.7554/eLife.63204

# Study #2

---

# Inclusion of image-based in vivo experimental data into the Hill-type muscle model affects the estimation of individual force-sharing strategies during walking.

---

Associated publications:

Hamard, R., Hug, F., Kelp, N. Y., Feigean, R., Aeles, J., & Dick, T. J. (2022). Inclusion of image-based in vivo experimental data into the Hill-type muscle model affects the estimation of individual force-sharing strategies during walking. *Journal of Biomechanics*, *135*, 111033.

Journal of Biomechanics 135 (2022) 111033

Contents lists available at ScienceDirect

Journal of Biomechanics

journal homepage: www.elsevier.com/locate/jbiomech

# Inclusion of image-based *in vivo* experimental data into the Hill-type muscle model affects the estimation of individual force-sharing strategies during walking

Raphaël Hamard [a], François Hug [a,b,c,d,*], Nicole Y. Kelp [b], Romain Feigean [e], Jeroen Aeles [a], Taylor J.M. Dick [b]

[a] Nantes Université, Movement - Interactions - Performance, MIP, UR 4334, F-44000 Nantes, France
[b] The University of Queensland, School of Biomedical Sciences, Brisbane, Queensland, Australia
[c] Institut Universitaire de France (IUF), Paris, France
[d] Université Côte d'Azur, LAMHESS, Nice, France
[e] Laboratoire de Physiologie et Évaluation Neuromusculaire, Institut de Myologie, Paris, France

ARTICLE INFO

*Keywords:*
B-mode ultrasound
Electromyography
Gastrocnemius
MRI
Muscle coordination

ABSTRACT

The study of muscle coordination requires knowledge of the force produced by individual muscles, which can be estimated using Hill-type models. Predicted forces from Hill-type models are sensitive to the muscle's maximal force-generating capacity ($F_{max}$), however, to our knowledge, no study has investigated the effect of different $F_{max}$ personalization methods on predicted muscle forces. The aim of this study was to determine the influence of two personalization methods on predicted force-sharing strategies between the human gastrocnemii during walking. Twelve participants performed a walking protocol where we estimated muscle activation using surface electromyography and fascicle length, velocity, and pennation angle using B-mode ultrasound to inform the Hill-type model. $F_{max}$ was determined using either a scaling method or experimental method. The scaling method used anthropometric scaling to determine both muscle volume and fiber length, which were used to estimate the $F_{max}$ of the gastrocnemius medialis and lateralis. The experimental method used muscle volume and fascicle length obtained from magnetic resonance imaging and diffusion tensor imaging, respectively. We found that the scaling and the experimental method predicted similar gastrocnemii force-sharing strategies at the group level (mean over the participants). However, substantial differences between methods in predicted force-sharing strategies was apparent for some participants revealing the limited ability of the scaling method to predict force-sharing strategies at the level of individual participants. Further personalization of muscle models using *in vivo* experimental data from imaging techniques is therefore likely important when using force predictions to inform the diagnosis and management of neurological and orthopedic conditions.

## 1. Introduction

Knowledge of the forces that individual muscles produce provides important insights into muscle coordination, and this information can be used to improve the diagnosis and management of many neurological and orthopedic conditions (Hug and Tucker, 2017). However, directly measuring human muscle force requires highly invasive techniques (Finni et al., 1998; Gregor et al., 1987; Komi, 1990), which are not feasible in clinical environments and remain limited in most research settings. To overcome this limitation, muscle models for predicting muscle forces have been developed.

The Hill-type model is the most ubiquitous muscle model in biomechanics (Eq. (1); Zajac, 1989). It takes into account most of the known determinants of muscle force, i.e. the activation, the instantaneous length and velocity of the contracting muscle fibers, and the maximal force-generating capacity ($F_{max}$). The Hill-type model can be

*Abbreviations:* DTI, Diffusion Tensor Imaging; EMG, Electromyography; $EMG_{max}$, Maximal electromyography amplitude; $F_{max}$, Maximal force-generating capacity; GL, Gastrocnemius Lateralis; GM, Gastrocnemius Medialis; MRI, Magnetic Resonance Imaging; MVC, Maximal Voluntary Contraction; RMSE, Root Mean Square Error.

* Corresponding author at: Université Côte d'Azur, LAMHESS, Campus STAPS, 261 boulevard du Mercantour, 06200 Nice, France.
*E-mail address:* francois.hug@univ-cotedazur.fr (F. Hug).

https://doi.org/10.1016/j.jbiomech.2022.111033
Accepted 28 February 2022
Available online 4 March 2022

personalized with subject-specific data, such as time-varying muscle activation assessed using surface electromyography (EMG) (Perreault et al., 2003) or time-varying fascicle length, fascicle velocity, and pennation angle recorded using ultrasound imaging (Dick et al., 2017). An important determinant of muscle force is $F_{max}$ (Bujalski et al., 2018; Scovil and Ronsky, 2006), for which the vast majority of studies rely on scaled data using different methods. For example, muscle volume, a determinant of $F_{max}$, has been personalized through values scaled to the participant's body mass (Dick et al., 2017). Furthermore, optimal muscle fiber length, which is another determinant of $F_{max}$, is often scaled from generic musculoskeletal models (Millard et al., 2013). An important limitation of these approaches is that they use the same underlying equations to scale all individuals. This conceals the well-described inter-individual variability in the distribution of $F_{max}$ across muscles (Crouzier et al., 2018; Hug et al., 2015).

The aim of this study was to compare two different personalization methods of a Hill-type model to predict human gastrocnemii forces during level and incline walking. The first personalization method, herein referred to as the "scaling method", used anthropometric scaling to determine both muscle volume and muscle fiber length to estimate $F_{max}$ of the gastrocnemius medialis (GM) and lateralis (GL). The second method, named hereafter the "experimental method", used muscle volume and fascicle length obtained from magnetic resonance imaging (MRI) and diffusion tensor imaging (DTI), respectively. We specifically investigated the force-sharing strategy between the two gastrocnemii muscles. Because the scaling method inevitably conceals inter-individual variability in the distribution of $F_{max}$ between the GM and GL, we expected to observe substantial differences between methods when comparing the gastrocnemii force-sharing strategy at the individual level. However, we hypothesized that the two methods would predict similar force-sharing strategies at the group level.

## 2. Materials and methods

### 2.1. Participants

Twelve adults with no recent (<6 months) lower limb pain or injury gave informed written consent to participate in the study (5 females, 7 males, age: 25 ± 3.5 years, body mass: 75.4 ± 16.4 kg, height: 1.71 ± 0.10 m; mean ± standard deviation). This study was approved by the institutional ethics review committee at The University of Queensland (#2013001448).

### 2.2. Experimental data acquisition

Data were collected over two experimental sessions. The first session consisted of two consecutive scanning sequences of the participant's dominant leg: a T1-weighted MRI scan to determine muscle volume, and a DTI scan to determine muscle fascicle lengths.

For the second session, participants walked on a treadmill (Nautilus Trimline T345, TX, USA) at their preferred walking speed (1.1 ± 0.1 $m{\cdot}s^{-1}$), which was determined at the beginning of the protocol (Dal et al., 2010). During walking, we recorded surface EMG and B-mode ultrasound of the GM and GL of the dominant leg to measure muscle activation and fascicle behavior, respectively. Foot position was measured using motion capture to identify phases of the gait cycle. Participants walked under two conditions presented in a randomized order: (i) 0% treadmill grade (level walking) and (ii) 10% treadmill grade (incline walking). They performed two trials at each walking condition and repeated each condition a second time, first to record EMG and second to measure fascicle behavior. The EMG and the ultrasound recordings were conducted in separate trials to ensure that the measures were taken on the same mid-region of the muscle belly. Participants also performed three isometric plantar flexion maximal voluntary contractions (MVCs), with 120 s rest between contractions, to determine maximal GM and GL EMG amplitude for EMG normalization. The EMG and ultrasound data have been published elsewhere (Hamard et al., 2021).

#### 2.2.1. MRI

Participants were placed in a 3T MRI scanner (Magnetom Prisma, Siemens, Germany) in a supine position. The dominant foot was secured into a custom-built MRI-compatible foot plate with the hip extended and the ankle positioned at a 90° angle. The dominant knee was positioned in slight flexion (<5°) by using a foam wedge under the knee. Details on the MRI parameters have been described elsewhere (Pinel et al., 2021). The T1-weighted MRI images were analyzed using a combination of semi-automated (Sashimi V1.1; Bolsterlee, 2020) and manual segmentation software (ITK-SNAP v3.8.0, NIH, USA). We calculated total muscle volume for the GM and GL as the sum of the volume of all voxels in each muscle (ITK-SNAP v3.8.0, NIH, USA). These muscle volumes were included in the Hill-type model (see 2.3) for the experimental method.

#### 2.2.2. DTI

DTI scans were performed with the same scanner as for the MRI. Detailed information on the DTI parameters, processing and data analyses has been described elsewhere (Aeles et al., 2021). Briefly, the muscle was divided into smaller muscle regions in the local muscle frontal plane. Then, fascicles were assigned to the muscle region that contained the fascicle midpoint and the median muscle fascicle length was calculated for each region. Finally, the mean of all muscle regions was calculated and used as an input for optimal fiber length.

#### 2.2.3. 3D motion capture

3D motion capture (Flex 13, OptiTrack, Corvallis, OR, USA) was used to record a static calibration trial with 8 marker clusters and 16 individual markers placed bilaterally on the lower limbs and pelvis to scale a musculoskeletal model (Rajagopal et al., 2016) for each participant (OpenSim v3.3). Then, during the walking protocol, we used the markers attached bilaterally to the calcaneus and the fifth metatarsophalangeal joint to determine the timing of the heel-strike and toe-off events using custom-written scripts based on foot vertical velocity (O'Connor et al., 2007). Motion capture data were collected at 120 Hz (Motive, OptiTrack, Corvallis, OR, USA) and raw marker positions were filtered using a second-order low-pass Butterworth filter with a cut-off frequency of 10 Hz.

#### 2.2.4. Electromyography

We shaved, abraded and cleaned the participant's skin with alcohol to reduce the skin-electrode impedance. We placed surface electrodes (Trigno Delsys Inc., Natick, USA; 10 mm inter-electrode distance) over the GM and GL muscle bellies, aligned along the direction of the muscle fascicles, determined using B-mode ultrasound. The EMG signals were amplified, digitized at 2048 Hz, band-pass filtered (20–500 Hz), and recorded in Spike2 (V7, CED Ltd, Cambridge, UK). During post-processing, the MVC and walking EMG signals were band-pass filtered using a second-order Butterworth filter (20–500 Hz), rectified, and low-pass filtered at 12 Hz. The maximal value of the EMG signal measured during the MVC trials was considered as the maximal EMG amplitude ($EMG_{max}$). Then, the EMG signals from 15 gait cycles were normalized to $EMG_{max}$. Finally, we interpolated the data from each gait cycle to 100 data points. We averaged all the cycles within a trial and then we averaged the resulting two mean cycles from each trial to finally obtain a single mean cycle for each condition and participant.

#### 2.2.5. B-mode ultrasound

To image the GM and GL during walking, we placed two linear ultrasound probes (5–8 MHz, 60 mm field-of-view, LV8-5L60N-2, ArtUS, Telemed, Vilnius, Lithuania) on the same location as used for the EMG electrodes. The probe orientation was optimized to be aligned in the fascicle plane and secured with elastic bandages. Ultrasound data were

recorded at 120 Hz for 15 s of walking. Post data collection, we analyzed five gait cycles of ultrasound data per trial using a validated (Cronin et al., 2011; Gillett et al., 2013) semi-automated tracking algorithm (UltraTrack; Farris and Lichtwark, 2016), combined with manual corrections (for details, see Hamard et al., 2021). Ultrasound data were low-pass filtered at 12 Hz and fascicle velocity was calculated as the first time derivative of fascicle length. We normalized fascicle length to the mean fascicle length at heel-strike during level walking ($L_{HS}$; average group value: 56.6 ± 8.0 mm and 65.4 ± 10.1 mm for the GM and GL, respectively). Similarly, fascicle velocity was expressed as the normalized fascicle length per second. Ultrasound data from each gait cycle were interpolated to 100 data points and we averaged the cycles within a trial and then between both trials to create a mean cycle for each condition and participant.

### 2.3. Estimation of time-varying muscle force during walking

We estimated the time-varying forces produced by the GM and GL muscles during walking using a Hill-type model (Zajac, 1989):

$$F_m = F_{max}\left[\hat{a}(t)\hat{F}_a\left(\hat{l}_f\right)\hat{F}_a(\hat{v}) + \hat{F}_p\left(\hat{l}_f\right)\right]\cos\beta. \quad (1)$$

The muscle force $F_m$ (N) was calculated from the maximal force-generating capacity $F_{max}$, expressed in N, the time-varying normalized activation $\hat{a}(t)$, the normalized active ($\hat{F}_a(\hat{l}_f)$) and passive ($\hat{F}_p(\hat{l}_f)$) forces as determined from the force-length relationship, the normalized force $\hat{F}_a(\hat{v})$ as determined from the force-velocity relationship and the cosine of the time-varying pennation angle $\beta$ (°).

The normalized active force-length curve (Otten, 1987), was modelled as:

$$\hat{F}_a\left(\hat{l}_f\right) = e^{-\left(\frac{\hat{l}_f^{0.6}-1}{0.3}\right)^{2.3}} \quad (2)$$

The normalized passive force-length curve (Otten, 1987) was modelled as:

$$\hat{F}_p = 2.64\hat{l}_f^{\,2} - 5.30\hat{l}_f + 2.66 \quad \text{for } \hat{l}_f > 1, \quad (3)$$

$$\hat{F}_p\left(\hat{l}_f\right) = 0 \quad \text{for } \hat{l}_f \le 1 \quad (4)$$

where $\hat{l}_f$ is the time-varying normalized fascicle length measured during walking.

The normalized force-velocity curve was modelled as:

$$\hat{F}_a(\hat{v}) = \frac{1+\left(\frac{\hat{v}}{\hat{v}_0}\right)}{1-\left(\frac{\hat{v}}{v_0\alpha}\right)} \quad \text{for } \hat{v} \le 0, \quad (5)$$

$$\hat{F}_a(\hat{v}) = 1.5 - 0.5\frac{1-\left(\frac{\hat{v}}{\hat{v}_0}\right)}{1+\left(\frac{7.56\hat{v}}{v_0\alpha}\right)} \quad \text{for } \hat{v} > 0 \quad (6)$$

where $\hat{v}$ is the time-varying normalized fascicle velocity recorded during walking. α describes the curvature of the force velocity relationship and $v_0$ is the maximum unloaded shortening velocity. We used intermediate values accounting for slow and fast muscle fibers from numerous terrestrial species of 0.235 and −7.5 $s^{-1}$ for α and $\hat{v}_0$, respectively (Wakeling et al., 2012).

Finally, $F_{max}$ is a function of the muscle's volume *Vol*, the optimal fiber length $l_{f,opt}$ and the maximum isometric stress of a muscle fiber $\sigma_0$.

$$F_{max} = \left(\frac{Vol}{l_{f,opt}}\right)\sigma_0 \quad (7)$$

$\sigma_0$ was estimated from the literature (22.5 N·$cm^{-2}$, Powell et al., 1984; Roy et al., 1982; Spector et al., 1980). For the scaling method, $l_{f,opt}$ was estimated from a subject-specific musculoskeletal model (Delp et al., 2007; Rajagopal et al., 2016). This 37 degrees of freedom model with 97 muscle-tendon complex actuators was scaled to the individual anthropometry of the participants based on the mass of the participant and markers positions recorded during the static trial. For the scaling method, muscle volume was calculated using the regression equations from Handsfield et al. (2014):

$$Vol = b1 \times BM + b2 \quad (8)$$

where *Vol* ($cm^3$) is a function of body mass, *BM* (kg) and two coefficients *b*1 and *b*2. Coefficient *b*1 is 3.41 and 2.19 for the GM and GL, respectively, and *b*2 is 12.60 and −7.59 for GM and GL, respectively (Handsfield et al., 2014). Concerning the experimental method, we used, as a substitute for the $l_{f,opt}$, the mean muscle fascicle length estimated from DTI and we used the muscle volume measured from MRI for the GM and GL.

### 2.4. Statistics

We conducted the statistical analyses in Statistica v8.0 (Statsoft, Tulsa, OK, USA). All data passed the Kolmogorov-Smirnov test for normality. First, we compared the muscle volume, fascicle length and $F_{max}$ between the two methods and the two muscles using 2-way repeated-measures ANOVAs (factor: method [scaling, experimental], muscle [GM, GL]). Additionally, the GM/(GM + GL) ratios of muscle volume, fascicle length and $F_{max}$ were calculated and we used paired t-tests to determine whether these ratios differed between the two methods. We also assessed the relationship between the two estimation methods for muscle volume, fascicle length and $F_{max}$ using Pearson's correlation coefficient. Finally, we used the root mean square error (RMSE) to determine the discrepancy between methods for muscle volume, fascicle length and $F_{max}$.

From the predicted force output, we extracted the peak force, corresponding to the maximal force value during the gait cycle and the force integral, corresponding to the integral of the time-varying force. To test our first hypothesis, we used 3-way repeated-measures ANOVAs (factor: method [scaling, experimental], muscle [GM, GL] and condition [level, incline]) to determine whether the peak force or the force integral systematically differed between methods, muscles or conditions. Then, the GM/(GM + GL) ratios for peak force and force integral were calculated to estimate the force-sharing strategy between the gastrocnemii. We performed 2-way repeated-measures ANOVAs (factor: method [scaling, experimental] and condition [level, incline]) on these ratios to assess whether they systematically differed between methods and between conditions. Finally, we compared the peak force and force integral between the two methods using the RMSE. For all tests, the level of significance was set at $P < 0.05$.

## 3. Results

### 3.1. Maximal force-generating capacity

Fig. 1 depicts the results for volume, fascicle length and $F_{max}$. This paragraph, however, presents only the results for $F_{max}$ as they are more closely related to our aim. There was a main effect of muscle ($P < 0.001$) on $F_{max}$, with no main effect of method ($P = 0.744$), nor a muscle × method interaction ($P = 0.265$). Specifically, the GM had a larger $F_{max}$ (1072 ± 240 N) than the GL (587 ± 166 N) regardless of the method. Moreover, the correlation between $F_{max}$ estimated from the scaling method and $F_{max}$ estimated from experimental data was strong for both the GM ($R = 0.871$; $P < 0.001$) and the GL ($R = 0.739$; $P = 0.006$). Even though there was no statistical difference in the GM/(GM + GL) ratio of $F_{max}$ between the methods (66.5 ± 0.5% for the scaling method and 63.0

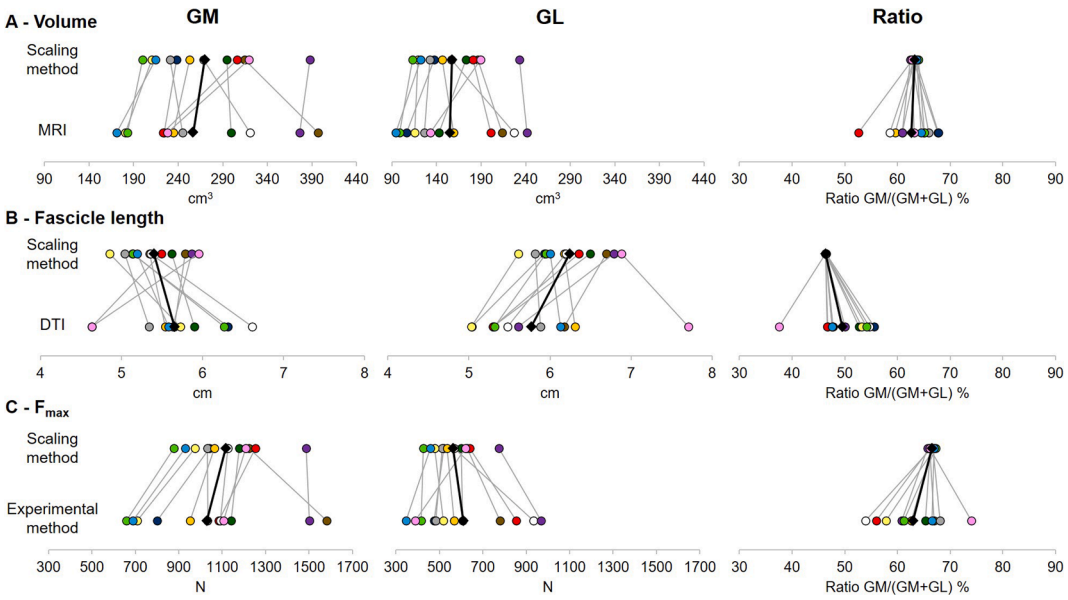


**Fig. 1.** Individual data for muscle volume (A), fascicle length (B) and maximal force-generating capacity ($F_{max}$; C) determined using the scaling and experimental methods. Data are depicted for both the gastrocnemius medialis (GM) and gastrocnemius lateralis (GL). The ratio between these muscles [GM/(GM + GL)] is also depicted for each variable. Each graph depicts individual data obtained with the scaling method (top) and experimental method (bottom). Each color represents an individual participant and the mean group value is presented as a black diamond. Because the scaling method uses the same underlying equations to scale all individuals, we can observe that the inter-individual variability in ratios between muscles is concealed.

± 5.6% for the experimental method; $P = 0.056$), inspection of individual data indicated large differences between methods for some participants, with the difference being up to 12.5% (Fig. 1). We found high RMSE values between methods for the $F_{max}$, i.e. 186 N for the GM and 160 N for the GL corresponding to 18.1% and 26.3% of the average $F_{max}$, respectively. Moreover, a discrepancy between calculation methods for $F_{max}$ was also observed for the GM/(GM + GL) ratios as indicated by a RMSE of 6.5%.

### 3.2. Force output

When considering the peak force, which occurred during the stance phase (Fig. 2), there was a main effect of muscle ($P < 0.001$) and condition ($P = 0.001$), with no main effect of method ($P = 0.513$), nor any interaction (all $P \geq 0.303$) (Table 1). Similarly, when considering the force integral calculated over the whole gait cycle, we observed a main effect of muscle ($P < 0.001$) and condition ($P = 0.003$), with no main effect of method ($P = 0.557$), nor any interaction (all $P \geq 0.333$). Overall, the GM produced more force compared to the GL during

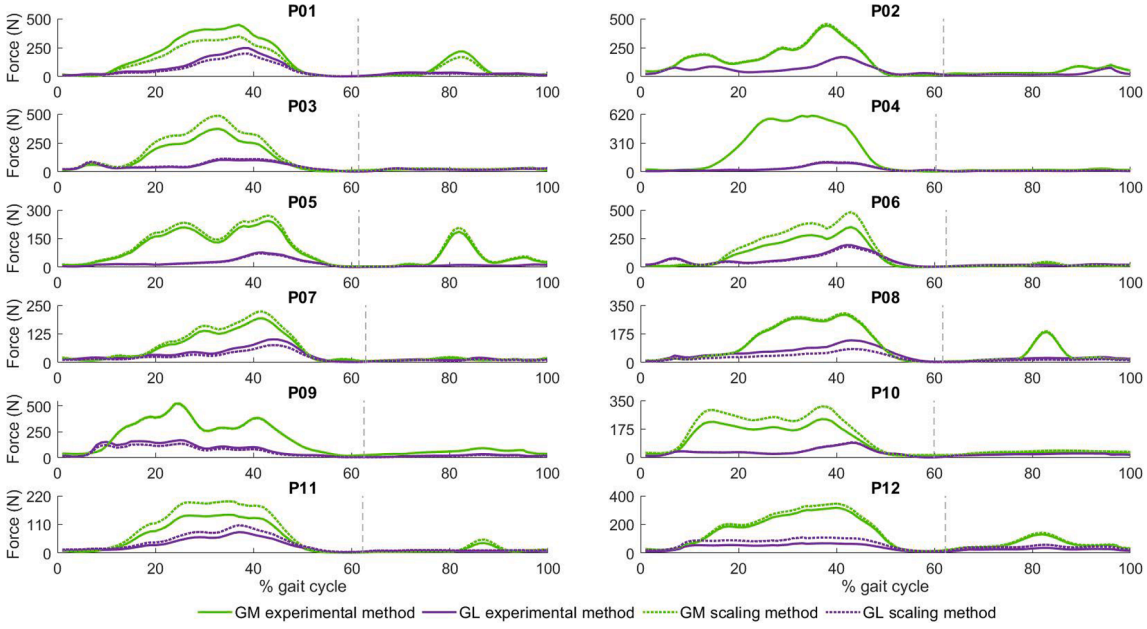


**Fig. 2.** Individual time-varying forces estimated by the Hill-type model during level walking for each participant (P). The GM (green) and GL (purple) forces are depicted by solid lines (experimental method) and dashed lines (scaling method). Heel-strike occurred at 0% on the x-axis and the dashed vertical lines represent the timing of toe-off during the gait cycle. Each plot represents an individual participant. Predicted forces for incline walking are presented in Fig. S1. (For interpretation of the references to color in this figure legend, the reader is referred to the web version of this article.)

**Table 1**
Force parameters estimated using the Hill-type model during level and incline walking.

| | Level walking | | | | Incline walking | | | |
|---|---|---|---|---|---|---|---|---|
| | GM | | GL | | GM | | GL | |
| | Scaling | Experimental | Scaling | Experimental | Scaling | Experimental | Scaling | Experimental |
| Peak force (N) | 378 ± 127 | 346 ± 137 | 120 ± 41* | 128 ± 55* | 467 ± 152† | 423 ± 155† | 186 ± 64*† | 195 ± 74*† |
| Force integral (N.s) | 123 ± 36 | 114 ± 43 | 43 ± 15* | 45 ± 17* | 149 ± 48† | 136 ± 52† | 61 ± 21*† | 65 ± 26*† |

Values are presented for the gastrocnemius medialis and lateralis during both level and incline walking. The maximal force-generating capacity was estimated using either the scaling or experimental method. GM, gastrocnemius medialis, GL, gastrocnemius lateralis. Values are reported as mean ± standard deviation. *Indicates a significant difference with GM. †Indicates a significant difference with level walking. $n = 12$. No difference between methods was found for any muscle or condition.

walking (+170 ± 96% and +159 ± 100% for peak force and force integral, respectively), regardless of the method. In addition, higher peak force (+34 ± 18%) and force integral (+27 ± 14%) were predicted during incline walking compared to level walking, regardless of the muscle and method.

When considering the peak force ratio (i.e. the force-sharing strategy between muscles), there was a main effect of condition ($P = 0.046$), with no main effect of method ($P = 0.163$) or a method × condition interaction ($P = 0.984$). Specifically, the ratio of peak force was lower (closer to 50%) during incline walking compared to level walking (Table 2). When considering the ratio of the force integral, there was no main effect of method ($P = 0.137$), nor an effect of condition ($P = 0.071$) or a method × condition interaction ($P = 0.971$).

Even though the group data did not exhibit significant differences between methods, inspection of Figs. 2 and 3 revealed noteworthy differences between methods for some participants. The difference in model-predicted forces between the methods was greater than 30% for four participants for GM and for three participants for GL during level walking. When considering the ratios (i.e. the force-sharing strategy between muscles), similar observations were made, i.e. despite the between-methods difference being lower than 1% in four participants for both peak force and force integral, the between-methods difference was substantial (greater than 6%) for four participants. These individual differences led to relatively high RMSE group values. When considering the peak force during level walking, the RMSE between the two methods was 66 N for the GM and 28 N for the GL corresponding to 19.0% and 22.1% of the group-averaged peak force, respectively. We also found high RMSE values for the force integral, i.e. 20 N.s for the GM and 12 N.s for the GL corresponding to 18.0% and 25.9% of the average force integral, respectively. Moreover, discrepancy between methods was also observed for the GM/(GM + GL) ratios of peak force and force integral. The RMSE between methods was 5.4% for peak force and 5.7% for the force integral during level walking.

## 4. Discussion

We determined the influence of two different personalization methods on a Hill-type model's predicted force-sharing strategy between the gastrocnemii during walking. We found substantial differences between the scaling method and the experimental method in the predicted force-sharing strategies at the individual level. Therefore, generic scaling methods may be unable to estimate the force-sharing strategy at the level of individual participants.

Our main results indicate substantial differences between methods for some participants. This is consistent with previous studies, which highlight that inclusion of subject-specific musculoskeletal geometry (Wesseling et al., 2016) or muscle-tendon origin and insertion (Bosmans et al., 2015) affects a model's force estimation. Furthermore, our results are similar to previous studies that report high inter-individual variability in the distribution of maximal force-generating capacity between synergist muscles from either the triceps surae (Crouzier et al., 2018) or the quadriceps (Hug et al., 2015). However, here we also highlight that the force-sharing strategy varies markedly between individuals during walking - a dynamic task whereby forces are submaximal. Furthermore, during walking, a substantial difference between the scaling method and the experimental method (greater than 6%) for GM/(GM + GL) ratio of either peak force or the force integral was observed in one third of the participants. Similar levels of differences in the GM/(GM + GL) ratio (+6–10%) were shown in patients with Achilles tendinopathy compared to asymptomatic individuals during submaximal isometric contractions (Crouzier et al., 2019b). It is therefore possible that the use of generic scaling methods may reduce the ability to detect pathological force-sharing strategies for individuals who deviate from the generic maximal force-generating capacity distribution, which is often the case in clinical populations (Barber et al., 2011).

We compared model-predicted forces when using two different methods to estimate a muscle's maximal force-generating capacity. However, an inherent limitation of such an approach is the inability to evaluate our model against direct measurements of *in vivo* force. We compared our predicted forces with forces previously estimated or measured using different approaches during similar walking conditions. For the GM, we found similar peak force levels (346 N) to those estimated using inverse dynamics analysis combined with moment arm and PCSA calculations (~305 N in Farris and Sawicki, 2012). In addition, our predicted forces are in agreement with tendon forces directly measured *in vivo*. Finni et al. (1998) reported a peak Achilles tendon force of 1320 N for the triceps surae during an analogous walking speed (1.1 $m \cdot s^{-1}$). Similar to previous methods (Dick et al., 2016), we combined this peak force with the relative PCSA of the gastrocnemii within the triceps surae (~26% for the GM and 12% for the GL; Ward et al., 2009) and accounted for the relative gastrocnemii activation levels during walking relative to the triceps surae (~40% MG, 20% LG; Crouzier et al., 2019a) to calculate a peak force of 365 N for the GM and 84 N for the GL – which is consistent with our predicted forces (346 N for

**Table 2**
Gastrocnemius medialis to gastrocnemius lateralis [GM/(GM + GL)] force ratio estimated using the Hill-type model during level and incline walking.

| | Level walking | | Incline walking | |
|---|---|---|---|---|
| | Scaling method | Experimental method | Scaling method | Experimental method |
| Peak force ratio (%) | 75.4 ± 6.2 | 72.4 ± 7.3 | 71.1 ± 7.8† | 68.0 ± 7.9† |
| Force integral ratio (%) | 74.1 ± 6.2 | 71.2 ± 7.3 | 70.5 ± 7.0 | 67.4 ± 7.5 |

Values are presented for both level and incline walking. The maximal force-generating capacity was estimated using either a scaling or experimental method. Values are reported as mean ± standard deviation. †Indicates significant difference with level walking. $n = 12$. No difference between methods was found for any muscle or condition.

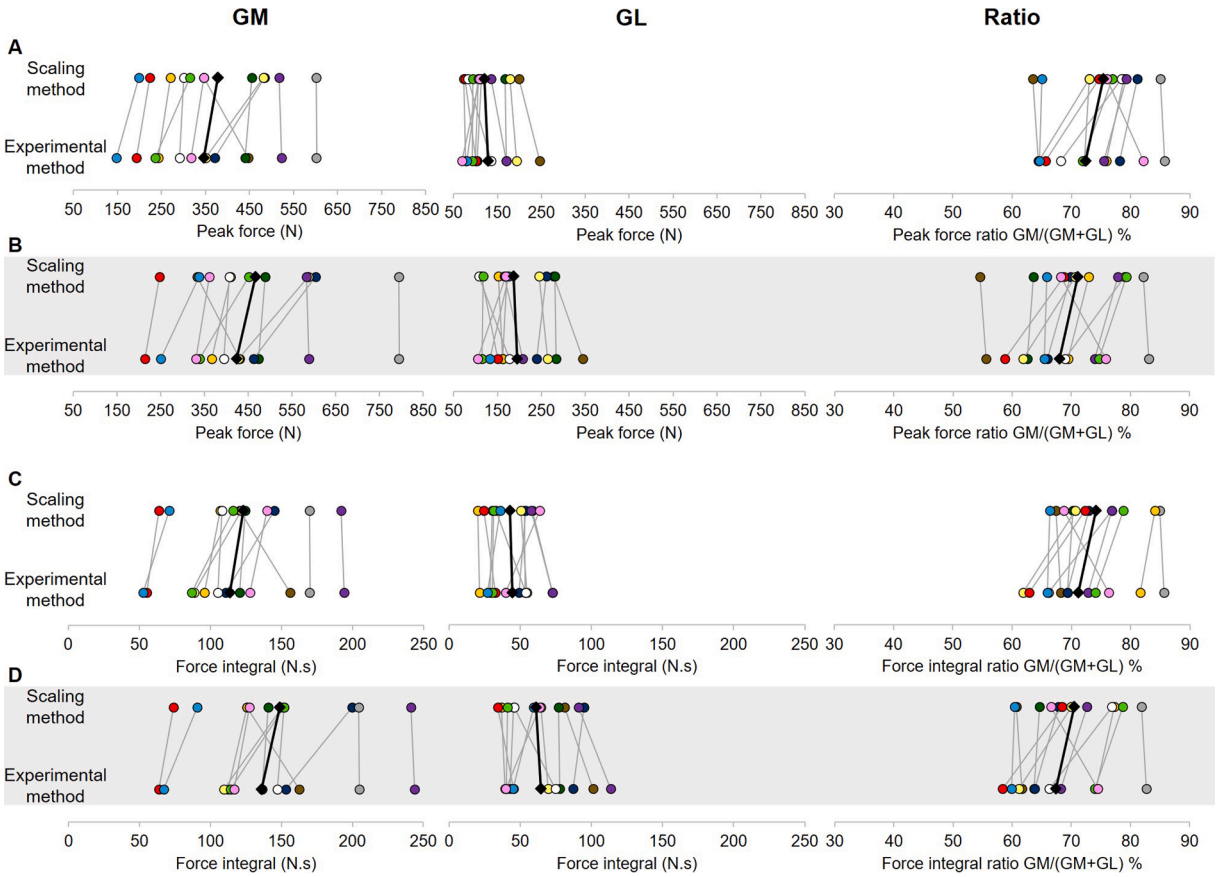


**Fig. 3.** Individual data for peak force (A and B) and force integral (C and D) for level walking (white area; A and C) and incline walking (grey area; B and D), determined using the scaling and experimental methods. Data are depicted for both the gastrocnemius medialis (GM) and gastrocnemius lateralis (GL). The ratio [GM/(GM + GL)] is also depicted for each variable. Each graph depicts individual data obtained with the scaling method and experimental method. Each color represents an individual participant and the mean group value is presented as a black diamond. The scaling method and the experimental method seem to predict similar muscle force and force-sharing strategy during walking at the group level but substantial differences between methods was apparent for some participants.

the GM and 128 N for the GL for the experimental method).

Although our results revealed no difference between methods at the group level, this result is difficult to generalize to other groups such as clinical populations. Moreover, we found a similar estimation of muscle volume for group averages when using a scaling method (Handsfield et al., 2014) versus MRI-derived muscle volumes (Fig. 1A) but, on the other hand, the estimation of fascicle length varied more between the scaling and DTI methods (Fig. 1B). This is likely because the scaling method uses subject-specific musculoskeletal models that provide the theoretical optimal fiber length based on a constant muscle-tendon geometry across all participants, whereas the DTI method provides the resting fascicle length at 90° of plantarflexion and <5° of knee flexion, which accounts for individual differences in resting fascicle lengths. Despite personalizing the maximal force-generating capacity, activation, fascicle length and velocity, and pennation angle, some model parameters remained generic. For example, the shape of the force-length and force-velocity relationships were consistent across models and individuals whereas the inter-individual variability in these relationships has been suggested in human GM (Hager et al., 2020) and vastus lateralis muscles (Brennan et al., 2018). However, the influence of these parameters on predicted forces is likely small given the relatively low sensitivity of Hill-type models to, for example, the curvature of the force-velocity relationship and the maximum unloaded shortening velocity (Dick et al., 2017). On the other hand, previous studies have shown that the Hill-type model is also sensitive to tendon slack length and optimal fiber length (Bujalski et al., 2018; Scovil & Ronsky, 2006). Further work is needed to test the effect of personalising these parameters on muscle force estimation, although directly measuring these parameters in humans *in vivo* is currently not possible.

In conclusion, when predicting individual muscle force-sharing strategies, our results highlight the importance for Hill-type models to be personalized with *in vivo* imaging data. Future research is necessary to determine the sensitivity of Hill-type models to additional subject-specific inputs, for example by using elastography to estimate the fascicle slack length and the muscle's passive force-length properties (Hug et al., 2013) or by estimating subject-specific force-length relationships (Maganaris, 2003).

## Funding

This work was supported by a University of Queensland Early Career Research Grant to Taylor JM Dick. François Hug is supported by a fellowship from the Institut Universitaire de France (IUF) and a travel grant from the Société de Biomécanique. Support was received from the French national research agency (ANR-19-CE17-002, COMMODE project; to FH).

**Data availability:**

The predicted force data are available from figshare: https://doi.org/10.6084/m9.figshare.17099864

### *CRediT authorship contribution statement*

**Raphaël Hamard:** Writing – review & editing, Writing – original draft, Visualization, Validation, Software, Methodology, Formal analysis. **François Hug:** Writing – review & editing, Validation, Supervision, Project administration, Investigation, Funding acquisition,

Conceptualization. **Nicole Y. Kelp:** Writing – review & editing, Project administration, Methodology, Investigation, Data curation. **Romain Feigean:** Writing – review & editing, Investigation, Data curation. **Jeroen Aeles:** Writing – review & editing, Supervision, Software, Formal analysis. **Taylor J.M. Dick:** Writing – review & editing, Validation, Supervision, Resources, Project administration, Methodology, Investigation, Funding acquisition, Formal analysis, Conceptualization.

## Declaration of Competing Interest

The authors declare that they have no known competing financial interests or personal relationships that could have appeared to influence the work reported in this paper.

## Acknowledgements

We thank Aiman Al-Najjar, Nicole Atcheson, and Donald Maillet from the UQ Centre for Advanced Imaging (CAI) for their support and expertise in MR imaging. We further thank Bart Bolsterlee (NeuRA & University of New-South Wales) for assistance in MRI and DTI processing.

## Appendix A. Supplementary data

Supplementary data to this article can be found online at https://doi.org/10.1016/j.jbiomech.2022.111033.

## References

Aeles, J., Bolsterlee, B., Kelp, N.Y., Dick, T.J.M., Hug, F., 2021. Regional variation in lateral and medial gastrocnemius muscle fibre lengths obtained from diffusion tensor imaging. J. Anat. https://doi.org/10.1111/joa.13539.

Barber, L., Barrett, R., Lichtwark, G., 2011. Passive muscle mechanical properties of the medial gastrocnemius in young adults with spastic cerebral palsy. J. Biomech. 44 (13), 2496–2500. https://doi.org/10.1016/j.jbiomech.2011.06.008.

Bolsterlee, 2020. GitHub—Bartbols/SASHIMI: SASHIMI segmentation is a Matlab App for semi-automatic interactive segmentation of multi-slice images. https://github.com/bartbols/SASHIMI.

Bosmans, L., Valente, G., Wesseling, M., Van Campen, A., De Groote, F., De Schutter, J., Jonkers, I., 2015. Sensitivity of predicted muscle forces during gait to anatomical variability in musculotendon geometry. J. Biomech. 48 (10), 2116–2123. https://doi.org/10.1016/j.jbiomech.2015.02.052.

Brennan, S.F., Cresswell, A.G., Farris, D.J., Lichtwark, G.A., 2018. The effect of muscle-tendon unit vs. Fascicle analyses on vastus lateralis force-generating capacity during constant power output cycling with variable cadence. J. Appl. Physiol. 124 (4), 993–1002. https://doi.org/10.1152/japplphysiol.00356.2017.

Bujalski, P., Martins, J., Stirling, L., 2018. A Monte Carlo analysis of muscle force estimation sensitivity to muscle-tendon properties using a Hill-based muscle model. J. Biomech. 79, 67–77. https://doi.org/10.1016/j.jbiomech.2018.07.045.

Cronin, N.J., Carty, C.P., Barrett, R.S., Lichtwark, G., 2011. Automatic tracking of medial gastrocnemius fascicle length during human locomotion. J. Appl. Physiol. 111 (5), 1491–1496.

Crouzier, M., Hug, F., Dorel, S., Deschamps, T., Tucker, K., Lacourpaille, L., 2019a. Do individual differences in the distribution of activation between synergist muscles reflect individual strategies? Exp. Brain Res. 237 (3), 625–635. https://doi.org/10.1007/s00221-018-5445-6.

Crouzier, M., Lacourpaille, L., Nordez, A., Tucker, K., Hug, F., 2018. Neuromechanical coupling within the human triceps surae and its consequence on individual force-sharing strategies. J. Exp. Biol. 221 (21), jeb187260. https://doi.org/10.1242/jeb.187260.

Crouzier, M., Tucker, K., Lacourpaille, L., Doguet, V., Fayet, G., Dauty, M., Hug, F., 2019b. Force-sharing within the Triceps Surae: An Achilles Heel in Achilles Tendinopathy. Med. Sci. Sports Exercise. https://doi.org/10.1249/MSS.0000000000002229.

Dal, U., Erdogan, T., Resitoglu, B., Beydagi, H., 2010. Determination of preferred walking speed on treadmill may lead to high oxygen cost on treadmill walking. Gait & Posture 31 (3), 366–369. https://doi.org/10.1016/j.gaitpost.2010.01.006.

Delp, S.L., Anderson, F.C., Arnold, A.S., Loan, P., Habib, A., John, C.T., Guendelman, E., Thelen, D.G., 2007. OpenSim : Open-source software to create and analyze dynamic simulations of movement. IEEE Trans. Bio-Med. Eng. 54 (11), 1940–1950. https://doi.org/10.1109/TBME.2007.901024.

Dick, T.J.M., Biewener, A.A., Wakeling, J.M., 2017. Comparison of human gastrocnemius forces predicted by Hill-type muscle models and estimated from ultrasound images. J. Exp. Biol. 220 (9), 1643–1653. https://doi.org/10.1242/jeb.154807.

Dick, T.J.M., Arnold, A.S., Wakeling, J.M., 2016. Quantifying Achilles Tendon Force In Vivo from Ultrasound Images. J. Biomech. 49 (14), 3200–3207. https://doi.org/10.1016/j.jbiomech.2016.07.036.

Farris, D.J., Lichtwark, G.A., 2016. UltraTrack : Software for semi-automated tracking of muscle fascicles in sequences of B-mode ultrasound images. Comput. Methods Programs Biomed. 128, 111–118. https://doi.org/10.1016/j.cmpb.2016.02.016.

Farris, D.J., Sawicki, G.S., 2012. Human medial gastrocnemius force-velocity behavior shifts with locomotion speed and gait. PNAS 109 (3), 977–982. https://doi.org/10.1073/pnas.1107972109.

Finni, T., Komi, P.V., Lukkariniemi, J., 1998. Achilles tendon loading during walking : Application of a novel optic fiber technique. Eur. J. Appl. Physiol. 77 (3), 289–291. https://doi.org/10.1007/s004210050335.

Gillett, J.G., Barrett, R.S., Lichtwark, G.A., 2013. Reliability and accuracy of an automated tracking algorithm to measure controlled passive and active muscle fascicle length changes from ultrasound. Comput. Methods Biomech. Biomed. Eng. 16 (6), 678–687. https://doi.org/10.1080/10255842.2011.633516.

Gregor, R.J., Komi, P.V., Järvinen, M., 1987. Achilles Tendon Forces During Cycling. Int. J. Sports Med. 08 (S 1), S9–S14. https://doi.org/10.1055/s-2008-1025698.

Hager, R., Poulard, T., Nordez, A., Dorel, S., Guilhem, G., 2020. Influence of joint angle on muscle fascicle dynamics and rate of torque development during isometric explosive contractions. J. Appl. Physiol. 129 (3), 569–579. https://doi.org/10.1152/japplphysiol.00143.2019.

Hamard, R., Aeles, J., Kelp, N.Y., Feigean, R., Hug, F., Dick, T.J.M., 2021. Does different activation between the medial and the lateral gastrocnemius during walking translate into different fascicle behavior? J. Exp. Biol. 224 (12), jeb242626. https://doi.org/10.1242/jeb.242626.

Handsfield, G.G., Meyer, C.H., Hart, J.M., Abel, M.F., Blemker, S.S., 2014. Relationships of 35 lower limb muscles to height and body mass quantified using MRI. J. Biomech. 47 (3), 631–638. https://doi.org/10.1016/j.jbiomech.2013.12.002.

Hug, F., Goupille, C., Baum, D., Raiteri, B.J., Hodges, P.W., Tucker, K., 2015. Nature of the coupling between neural drive and force-generating capacity in the human quadriceps muscle. Proc. Biol. Sci. 282 (1819) https://doi.org/10.1098/rspb.2015.1908.

Hug, F., Lacourpaille, L., Maïsetti, O., Nordez, A., 2013. Slack length of gastrocnemius medialis and Achilles tendon occurs at different ankle angles. J. Biomech. 46 (14), 2534–2538. https://doi.org/10.1016/j.jbiomech.2013.07.015.

Hug, F., Tucker, K., 2017. Muscle Coordination and the Development of Musculoskeletal Disorders. Exerc. Sport Sci. Rev. 45 (4), 201–208. https://doi.org/10.1249/JES.0000000000000122.

Komi, P.V., 1990. Relevance of in vivo force measurements to human biomechanics. J. Biomech. 23, 23–34. https://doi.org/10.1016/0021-9290(90)90038-5.

Maganaris, C.N., 2003. Force-length characteristics of the in vivo human gastrocnemius muscle. Clin. Anat. 16 (3), 215–223. https://doi.org/10.1002/ca.10064.

Millard, M., Uchida, T., Seth, A., Delp, S.L., 2013. Flexing Computational Muscle : Modeling and Simulation of Musculotendon Dynamics. J. Biomech. Eng. 135 (2) https://doi.org/10.1115/1.4023390.

O'Connor, C.M., Thorpe, S.K., O'Malley, M.J., Vaughan, C.L., 2007. Automatic detection of gait events using kinematic data. Gait & Posture 25 (3), 469–474. https://doi.org/10.1016/j.gaitpost.2006.05.016.

Otten, E., 1987. A myocybernetic model of the jaw system of the rat. J. Neurosci. Methods 21 (2), 287–302. https://doi.org/10.1016/0165-0270(87)90123-3.

Perreault, E.J., Heckman, C.J., Sandercock, T.G., 2003. Hill muscle model errors during movement are greatest within the physiologically relevant range of motor unit firing rates. J. Biomech. 36 (2), 211–218. https://doi.org/10.1016/s0021-9290(02)00332-9.

Pinel, S., Kelp, N.Y., Bugeja, J.M., Bolsterlee, B., Hug, F., Dick, T.J.M., 2021. Quantity versus quality : Age-related differences in muscle volume, intramuscular fat, and mechanical properties in the triceps surae. Exp. Gerontol. 156, 111594 https://doi.org/10.1016/j.exger.2021.111594.

Powell, P.L., Roy, R.R., Kanim, P., Bello, M.A., Edgerton, V.R., 1984. Predictability of skeletal muscle tension from architectural determinations in guinea pig hindlimbs. J. Appl. Physiol. 57 (6), 1715–1721. https://doi.org/10.1152/jappl.1984.57.6.1715.

Rajagopal, A., Dembia, C.L., DeMers, M.S., Delp, D.D., Hicks, J.L., Delp, S.L., 2016. Full-Body Musculoskeletal Model for Muscle-Driven Simulation of Human Gait. IEEE Trans. Biomed. Eng. 63 (10), 2068–2079. https://doi.org/10.1109/TBME.2016.2586891.

Roy, R.R., Meadows, I.D., Baldwin, K.M., Edgerton, V.R., 1982. Functional significance of compensatory overloaded rat fast muscle. J. Appl. Physiol. 52 (2), 473–478. https://doi.org/10.1152/jappl.1982.52.2.473.

Scovil, C.Y., Ronsky, J.L., 2006. Sensitivity of a Hill-based muscle model to perturbations in model parameters. J. Biomech. 39 (11), 2055–2063. https://doi.org/10.1016/j.jbiomech.2005.06.005.

Spector, S.A., Gardiner, P.F., Zernicke, R.F., Roy, R.R., Edgerton, V.R., 1980. Muscle architecture and force-velocity characteristics of cat soleus and medial gastrocnemius : Implications for motor control. J. Neurophysiol. 44 (5), 951–960. https://doi.org/10.1152/jn.1980.44.5.951.

Wakeling, J.M., Lee, S.S.M., Arnold, A.S., de Boef Miara, M., Biewener, A.A., 2012. A Muscle's Force Depends on the Recruitment Patterns of Its Fibers. Ann. Biomed. Eng. 40 (8), 1708–1720. https://doi.org/10.1007/s10439-012-0531-6.

Ward, S.R., Eng, C.M., Smallwood, L.H., Lieber, R.L., 2009. Are Current Measurements of Lower Extremity Muscle Architecture Accurate? Clin. Orthop. Relat. Res. 467 (4), 1074–1082. https://doi.org/10.1007/s11999-008-0594-8.

Wesseling, M., De Groote, F., Bosmans, L., Bartels, W., Meyer, C., Desloovere, K., Jonkers, I., 2016. Subject-specific geometrical detail rather than cost function formulation affects hip loading calculation. Comput. Methods Biomech. Biomed. Eng. 19 (14), 1475–1488. https://doi.org/10.1080/10255842.2016.1154547.

Zajac, F.E., 1989. Muscle and tendon : Properties, models, scaling, and application to biomechanics and motor control. Crit. Rev. Biomed. Eng. 17 (4), 359–411.

# Study #3

---

# A comparison of neural control of the biarticular *gastrocnemius* muscles between knee flexion and ankle plantar flexion.

---

Associated submitted article:

**Hamard, R.**, Aeles, J., Avrillon, S., Dick, T. J. & Hug, F. A comparison of neural control of the biarticular gastrocnemius muscles between knee flexion and ankle plantar flexion. *Journal of Applied Physiology* (submitted).

# A comparison of neural control of the biarticular *gastrocnemius* muscles between knee flexion and ankle plantar flexion

Raphaël Hamard[1], Jeroen Aeles[1,2,3], Simon Avrillon[4], Taylor J. M. Dick[5], François Hug[5,6]*

[1] Nantes Université, Movement - Interactions - Performance, MIP UR 4334, Nantes, France

[2] University of Antwerp, Laboratory of Functional Morphology, Department of Biology, Antwerp, Belgium

[3] Vrije Universiteit Brussel, Department of Movement and Sport Sciences, Brussels, Belgium

[4] Department of Bioengineering, Faculty of Engineering, Imperial College, London, UK

[5] School of Biomedical Sciences, The University of Queensland, Brisbane, Australia

[6] Université Côte d'Azur, LAMHESS, Nice, France

*Corresponding author:
Prof. François Hug
Université Côte d'Azur, France
E-mail: francois.hug@univ-cotedazur.fr

**RUNNING TITLE:** Control of the *gastrocnemii* during their two main functions

**ABSTRACT**

We aimed to determine whether the neural control of the biarticular *gastrocnemius medialis* (GM) and *lateralis* (GL) muscles is joint-specific, that is, whether their control differs between isolated knee flexion and ankle plantar flexion tasks. Twenty-one male participants performed isometric knee flexion and ankle plantar flexion tasks while we recorded high-density surface electromyography (HDsEMG). First, we estimated the distribution of activation both within- and between-muscles using two complementary approaches: surface EMG amplitude and motor unit activity identified from HDsEMG decomposition. Second, we estimated the level of common synaptic input between GM and GL motor units using a coherence analysis. Neither the EMG amplitude nor the motor unit discharge rate differed significantly between tasks. Even though there was a significant proximal shift in GM and GL EMG amplitude during knee flexion compared to ankle plantar flexion, the magnitude of this shift was small (1 mm) and not confirmed via the inspection of the spatial distribution of motor unit action potentials. A significant coherence between GM and GL motor units was only observed for four (knee flexion) and three (ankle plantarflexion) participants, with no difference in the level of coherence between the two tasks. We were able to track only a few motor units across tasks, which might be related to methodological limitations of the decomposition techniques. However, future work is needed to determine whether the same motor units are activated across tasks. Together, our results suggest that the neural control of the GM and GL muscles is similar across their two main functions.

**KEYWORDS:** activation; coherence; common drive; electromyography; motor units; *triceps surae*.

**NEW & NOTEWORTHY**

Several studies have focused on the neural strategies used to control the *gastrocnemius medialis* (GM) and *lateralis* (GL) during ankle plantar flexion. However, their second function, i.e. knee flexion, is not often explored. Here, we showed that the bias of activation towards GM, previously reported during ankle plantar flexion, persisted during knee flexion. The robustness of the GM and GL activation strategy across tasks was further confirmed with an analysis of the motor unit discharge rates. The level of common synaptic input between GM and GL motor units was relatively low, with no significant differences between the tasks. These results demonstrate the neural control of the *gastrocnemii* muscles is robust across their two main functions.

## INTRODUCTION

Muscle coordination is for a large part determined by how skeletal muscles are activated by the central nervous system. It appears that muscle activation is not always evenly distributed among muscles from the same anatomical group. For example, within the quadriceps, during submaximal isometric knee extension, some individuals activate the *vastus lateralis* (VL) more than the *vastus medialis* (VM), whereas others use the reverse strategy (Avrillon et al., 2021; Crouzier et al., 2018, 2019; Hug et al., 2015). This distribution of muscle activation between VL and VM is robust across different tasks such as walking and pedalling (Crouzier et al., 2019). An imbalance in the distribution of activation also exists between the biarticular *gastrocnemius medialis* (GM) and *gastrocnemius lateralis* (GL) during ankle plantar flexion. In this case, the activation is almost always biased towards the GM, with a large amount of variation in the degree of this imbalance across individuals (Crouzier et al., 2018, 2019). The imbalance of activation between GM and GL is related to their differences in maximal force-generating capacity (Crouzier et al., 2018). Specifically, the greater the physiological cross-sectional area (PCSA) of GM compared to the PCSA of the GL, the stronger the bias in muscle activation towards the GM. In contrast to what is observed across different tasks for VL and VM (Crouzier et al., 2019), the strategy used to control the biarticular GM and GL seems more variable across tasks. For example, foot position (i.e. external versus internal rotation) induces a modification in the distribution of activation between the *gastrocnemii* (Cibulka et al., 2017; Marcori et al., 2017; Riemann et al., 2011). This more flexible control of the GM and GL muscles is associated with a relatively low level of, if any, common synaptic input between these muscles (Hug et al., 2021; Rossato et al., 2022). Even though such a flexible control may be needed to manipulate the ankle joint in the frontal plane where the GM and GL generate opposite moment (Lee & Piazza, 2008; Vieira et al., 2013), it occurs at the expense of the number of dimensions that need to be controlled by the nervous system.

Previous studies have focused on the neural strategies used to control the GM and GL during ankle plantar flexion (Kinugasa et al., 2005; Masood et al., 2014; Segal & Song, 2005). However, as biarticular muscles, they also cross the knee joint and contribute to the knee flexion moment (Li et al., 2002). This second function is not often explored, leaving a knowledge gap in our understanding of the control and function of the *gastrocnemii*, and more broadly of biarticular muscles. There is evidence that the activation of biarticular muscles is joint-specific. For example, hip flexion is associated with a preferentially recruitment of the proximal portion of the *rectus femoris* muscle whereas knee extension is associated with more distal activation

of the *rectus femoris* (Miyamoto et al., 2012; Watanabe et al., 2016, 2021). There is no consensus on whether such task-specific regional activation occurs in the human GL and GM muscles. Region-specific functional roles of GM have been suggested in some (Watanabe et al., 2021), but not all studies (Héroux et al., 2015). Yet, the task-specific modulation of common synaptic input has not been examined in biarticular muscles. Specifically, if the low level of common synaptic input between GM and GL observed during ankle plantar flexion (Hug et al., 2021) is necessary to control additional degrees of freedom of the ankle, then it is possible that these muscles receive a higher level of common input during a task whereby these muscles control only one degree of freedom, e.g. knee flexion.

The overall aim of this study was to determine whether the neural control of the GM and GL differs between a knee flexion and an ankle plantar flexion task performed at the same relative activation level and at the same joint configuration. First, we estimated the distribution of activation between the GM and GL using two complementary approaches: the amplitude of surface high-density electromyographic signals (HDsEMG) and the discharge rate of individual motor units identified from decomposed HDsEMG signals. Based on the observation that there is a coupling between the distribution of activation and the distribution of force-generating capacity (Crouzier et al., 2018), we hypothesized that the distribution of activation would be robust across tasks where no specific control of moment in the frontal plane is required. Second, we investigated the regional activation within *gastrocnemii* from the amplitude of HDsEMG signals and from the spatial location of the motor units action potentials. We hypothesized that the regional activation would remain similar across knee flexion and ankle plantar flexion based on the limited possibility to regionally recruit motor units over the *gastrocnemius* muscle (Héroux et al., 2015). Third, we compared the level of common synaptic input between GM and GL across tasks using a coherence analysis applied to motor unit spike trains. We hypothesized that the common synaptic input would be higher during knee flexion compared to ankle plantar flexion, which would reduce the number of dimensions to be controlled.

# METHODS

## Participants

Twenty-one physically active males participated in this study (mean ± standard deviation; age: 27.3 ± 4.3 years, height: 176 ± 24 cm, body mass: 77.1 ± 12.9 kg). Of note, we recruited only males because we failed to identify enough GL motor units on females during our pilot testing. Participants had no history of lower leg pain that had limited function that required time off work or sport, or a consultation with a health practitioner in the previous six months. They provided informed written consent prior to the experimental session. The study was approved by the institutional research ethics committee of Nantes University (CERNI n°28022022-1).

## Experimental design

The experimental protocol consisted of isometric knee flexion and ankle plantar flexion contractions. For both knee flexion and ankle plantar flexion, participants laid prone on a dynamometer bed (Biodex System 3 Pro, Biodex Medical, Shirley, NY) with their right knee and ankle secured at 160° (180° degrees equals a fully-extended knee) and 90° (foot perpendicular to the shank), respectively. During the knee flexion task, we used a custom brace to secure the ankle at 90°. Two inextensible straps immobilized the back and the right knee of the participants.

Participants performed the knee flexion and ankle plantar flexion tasks in a randomized order. The procedure was similar for knee flexion and ankle plantar flexion tasks. Participants began with a standardized and progressive warm-up which consists in isometric knee flexion or ankle plantar flexion. After 2 min of rest, they performed three maximal isometric voluntary contractions (MVC), held for 3 s, with 120 s of rest between each contraction. Peak torque was considered as the maximal torque value obtained through a moving average with a window of 250 ms. To compare the neural control of GM and GL between the knee flexion and ankle plantar flexion tasks, it was important to match the averaged activation between tasks. We observed during our pilot testing that these muscles exhibit a lower activation during knee flexion than ankle plantar flexion for the same relative task-specific peak torque. Then, it was necessary to use higher contraction intensities for knee flexion. Therefore, participants performed submaximal isometric contractions, presented in a randomized order, at the following intensities: 30%, 40%, and 50% of peak torque for knee flexion and 20%, 30%, and 40% of peak torque for ankle plantar flexion, and the best match of activation between these relative torque levels was determined *a posteriori* as further described below. Of note, we chose

to match the average GM-GL activation *a posteriori* instead of asking the participants to produce a specific activation level using biofeedback as it would have likely modified the natural coordination strategies. For each intensity, participants performed three trapezoidal isometric contractions with 60 s of rest between each contraction. The contraction consisted of a 5 s ramp-up, 20 s steady contraction at the torque target and a 5 s ramp-down. A monitor displayed the target torque levels and the real-time torque output to the participants, digitized at 2048 Hz and provided by the HDsEMG acquisition system (EMG-Quattrocento; 400-channel EMG amplifier, OT Bioelettronica, Italy).

## Surface electromyography recordings

HDsEMG signals from the GM and the GL of the right leg were recorded using two-dimensional adhesive grids of 64 electrodes (13×5 electrodes with one electrode absent on a corner, gold-coated, interelectrode distance: 8 mm; GR08MM1305 OT Bioelettronica, Italy). First, we identified the muscle boundaries using B-mode ultrasound (Aixplorer, Supersonic Imagine, France) such that we could place the HDsEMG grid in the center of the muscle belly to minimize crosstalk. B-mode ultrasound was also used to define the fascicle orientation and align the grid in the direction of the fascicles. Then we shaved, cleansed, and abraded the skin using abrasive gel to reduce the skin-electrode impedance. A reference electrode (Kendall Medi-Trace, Canada) and a strap ground electrode were placed over the right tibia and around the left ankle, respectively. Finally, we secured the electrodes with elastic bandages to ensure good skin-electrode contact throughout the experiment. The multichannel HDsEMG acquisition system (EMG-Quattrocento, 400 channel EMG amplifier; OT Bioelettronica, Italy) band-pass filtered (10-500 Hz) and digitized the recorded monopolar signals at a sampling rate of 2048 Hz.

## Data analysis

### *Global surface electromyography*

Analyses were performed offline following the experiment in Matlab (R2018b, The MathWorks, Natick, MA) using custom-written scripts. First, the signals were band-pass filtered (20-500 Hz). Then, we visually checked the HDsEMG signals to remove channels with excessive noise or artefacts. To estimate the normalized electromyography (EMG) amplitude from the HDsEMG signals, we calculated the differential signals by taking the difference between adjacent electrodes in the proximo-distal direction, which resulted in 59 differential signals. When the signal from an electrode was excluded because of noise or artefacts, we

linearly interpolated the EMG amplitude from all the adjacent electrodes. For the MVC trials, we averaged the rectified signals over the whole grid and the maximal value of a 500 ms moving mean from the three MVC was considered as the maximal EMG value ($EMG_{max}$). For the submaximal contractions, each differential signal was rectified and then normalized to $EMG_{max}$ measured during ankle plantar flexion. We used $EMG_{max}$ measured during ankle plantar flexion as this value was systematically higher than that measured during knee flexion. Of note, as our aim was to compare EMG amplitude across tasks within a person and muscle, without removing electrodes, the value used to normalize the signals does not impact the outcomes (Besomi et al., 2020). Finally, we calculated the average of these submaximal, normalized EMG values first over the 3 plateaus for each channel and then over the 59 signals to get one representative value per muscle.

Normalized HDsEMG values were used to find an appropriate match for the comparison between knee flexion and ankle plantar flexion. To this end, we averaged the normalized HDsEMG value between the GM and GL for each intensity and each task, to obtain a single *'gastrocnemius* activation value' per intensity and per task. For further analyses, we only used the knee flexion intensity and the ankle plantar flexion intensity that exhibited the closest normalized *gastrocnemius* activation between the two tasks. Second, we used the HDsEMG normalized values to calculate the GM/(GM+GL) ratio of activation during both the knee flexion and the ankle plantar flexion tasks. Third, we assessed the regional activation for each muscle and for each task by calculating the barycenter of the normalized EMG amplitude across the 2D EMG grid (Fig. 1).

*EMG decomposition*

We used the convolutive blind source separation method to decompose the HDsEMG signals into individual motor unit spiking activity (Negro et al., 2016). Of note, this analysis was only performed on the contractions that were matched between tasks in terms of normalized EMG amplitude (see above). The automatic decomposition was performed on the plateau of the trapezoidal contraction that exhibited the highest EMG amplitude. Then, we manually edited all the motor units according to previously published procedures (Del Vecchio et al., 2020; Hug et al., 2021). The goal of this manual editing was to remove the false positive spikes identified by the automatic processing and to add the false negative spikes that were not identified by the automatic selection process. The motor unit filters derived from the processing of this plateau were then reapplied on the other plateaus. Consistent with previous studies, for further analyses,

we retained the motor units that had a pulse-to-noise ratio above 30 dB (Holobar et al., 2014; Laine et al., 2015).

*Assessment of crosstalk*

We ensured that each motor unit identified in a HDsEMG grid did not originate from crosstalk, that is, if any unit identified in one muscle actually belonged to the other recorded muscle. To do this, the firing times of each motor unit of the testing muscle were used to extract the waveform of each motor unit potential in all 59 differential EMG channels of the grid for each of the two muscles (Del Vecchio, Germer, et al., 2019). For each channel and each grid separately, peak-to-peak amplitude of the motor unit action potential was determined. We then compared the maximal amplitude between the grids, under the assumption that the action potential amplitude should be largest in the signal obtained from the electrodes closest to the discharging muscle fibres. If the amplitude in the other grid exceeded the amplitude of the testing muscle, it was deemed that the motor unit was identified due to crosstalk, and it was removed from the analyses (Aeles et al., 2023; Del Vecchio, Germer, et al., 2019).

*Assessment of motor unit discharge rate and spatial location*

For this specific analysis, we retained only the participants that had at least three motor units identified per muscle and per task. Only nine participants met this requirement, mainly because of the inability to identify motor units within the GL muscle during the knee flexion task. First, we calculated the average discharge rate of each motor unit over each plateau for both the knee flexion and ankle plantar flexion tasks. Then, we averaged the values across the three contractions to obtain a single value for each task. Second, we determined the spatial location of the action potential of each motor unit over the grid of electrodes. For this purpose, we used the shape of the motor unit action potentials obtained from the spike-trigger averaged differential EMG signals of the 59 channels. Then, we calculated the peak-to-peak amplitude of the motor unit action potential for each channel and we determined the barycenter of the peak-to-peak amplitude for each grid, i.e. muscle.

*Estimation of common synaptic input between GM and GL*

To estimate the amount of common synaptic input between muscles, we performed a coherence analysis on their cumulative motor unit spike trains. We first maximized the number of motor units and the duration used for the coherence analysis for each participant. Specifically, we discarded the portions of the signal where not enough motor units were discharging simultaneously, and we also discarded the motor units that had discharge patterns that were too intermittent during the torque plateau (interspike interval > 500 ms). As coherence is affected

by the duration on which it is calculated, we used the same duration for both tasks, i.e. on average 17 ± 7 s, within a participant. The coherence was performed on 11 ± 6 and 5 ± 3 motor units for GM and GL, respectively during knee flexion and on 17 ± 6 and 9 ± 7 motor units for GM and GL, respectively during ankle plantar flexion.

We calculated the magnitude-squared coherence using the Welch periodogram with nonoverlapping windows of 1 s. This analysis was performed on two equal-sized groups of cumulative spike trains constructed as the sum of the binary spike trains of three motor units. We used a constant number (n=3) of motor units to calculate the cumulative spike trains of each muscle as the number of motor units affects the level of coherence. However, to consider all the identified motor units in our analysis, we tested all the unique combinations of three motor units from each participant's entire available motor unit pool, with the maximal number of permutations set to 100. We considered the pooled coherence of these 100 random permutations for further analysis and we focused on the coherence within the delta band (0-5 Hz), which reflects the presence of common synaptic input relevant for force modulation (Del Vecchio, Germer, et al., 2019; Laine et al., 2015). Consistent with previous studies (Del Vecchio, Germer, et al., 2019; Laine et al., 2015; Laine & Valero-Cuevas, 2017), we transformed the coherence values to a standard z-score:

$$\mathrm{COH}\ z\ \mathrm{score} = \sqrt{2L} \times \alpha\tanh\sqrt{\mathrm{COH}} - \mathrm{bias} \qquad \text{Eq. 1}$$

Where COH is coherence, L is the number of time segments considered for the coherence analysis, and bias is calculated as the mean COH z score between 250 and 500 Hz where no coherence is expected. As classically done, the significance threshold for the Z-score transformed coherence was set at 1.65, based on a one-tailed 95% confidence interval (Laine et al., 2015).

*Motor unit matching*

We assessed the proportion of motor units which were identified during both tasks. To do this, we tracked motor units across knee flexion and ankle plantar flexion tasks using the spatio-temporal properties of the action potential waveforms within the 2D grids similar to previous studies (Del Vecchio & Farina, 2019; Martinez-Valdes et al., 2017). Briefly, we first identified the motor unit action potential waveform from differential signals for each electrode using the spike-triggered averaging technique previously described. The motor unit waveforms from the 59 electrodes were concatenated. We then performed normalized 2D cross-correlations between the waveforms of motor units. We considered motor units within a pairs as matched across tasks

when they exhibited a coefficient of correlation higher than 0.75 (Martinez-Valdes et al., 2017). We visually checked the matched motor unit action potentials to ensure the quality of the matching and removed incorrectly matched units when necessary (Fig. 1).

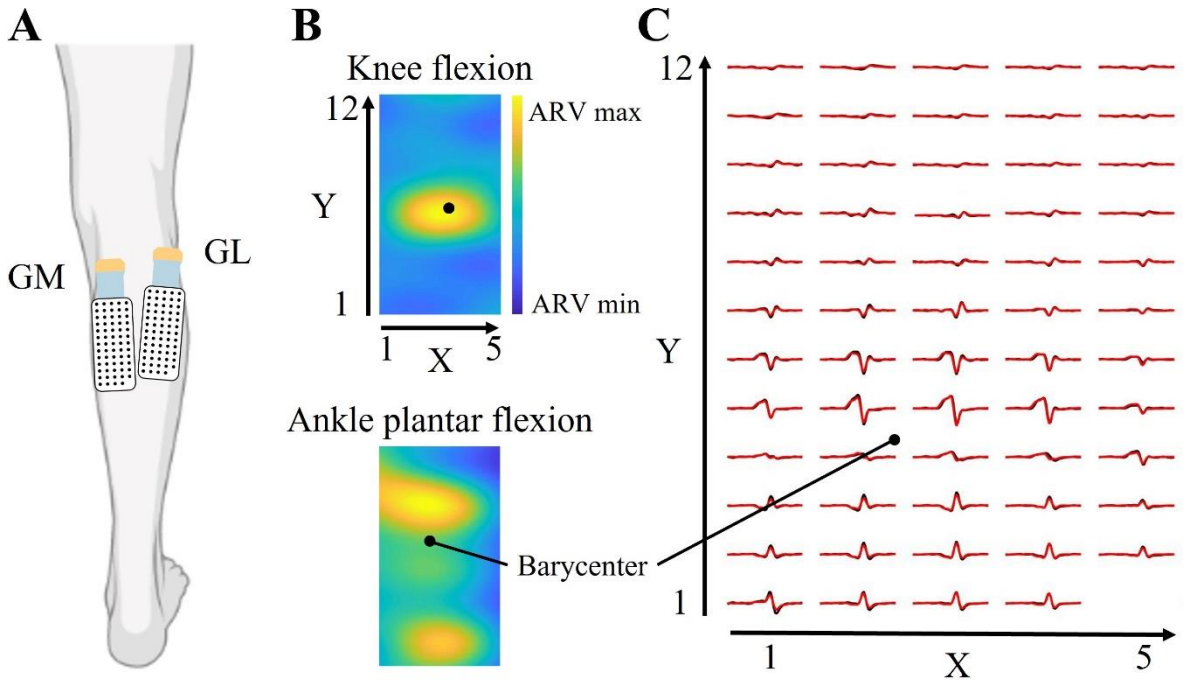


**Figure 1: HDsEMG electrode location, regional activation estimation and motor units matching.** Panel A depicts the location of the grids of electrodes over the *gastrocnemius medialis* and *gastrocnemius lateralis* muscles. Panel B depicts an individual example of the distribution of GM EMG amplitude over the grid of electrodes for both knee flexion and ankle plantar flexion. Panel C depicts an individual example of the distribution of the motor unit action potentials over the grid of electrodes during knee flexion (black) and ankle plantar flexion (red). In this specific example, the same motor unit was identified during both tasks, which was only possible for 5.1 ± 7.8% of the GM motor units and 7.5 ± 11.8% of the GM motor units and. GM, *gastrocnemius medialis*; GL, *gastrocnemius lateralis*; ARV, average and rectified EMG.

## Statistical analysis

All statistical analyses were performed with Statistica v8.0 (Statsoft, Tulsa, OK, USA). First, we confirmed whether all the data were normally distributed using Kolgomorov-Smirnoff test. To compare the average *gastrocnemius* activation across the matched knee flexion and ankle plantar flexion tasks, we performed a two-tailed paired t-test. To compare the normalized EMG amplitude between muscles and between tasks, we ran two-way repeated-measures ANOVAs (within-subject factor: muscle [GM, GL] and task [knee flexion, ankle plantar flexion]). To

determine whether the distribution of activation was correlated across tasks at the population level, we calculated the Pearson correlation coefficient on the GM/(GM+GL) ratio of activation. To compare the mean discharge rate between muscles and between tasks, we ran two-way repeated-measures ANOVAs (within-subject factor: muscle [GM, GL] and task [knee flexion, ankle plantar flexion]). To compare the regional activation between knee flexion and ankle plantar flexion, we performed two separate two-way repeated-measures ANOVAs (within-subject factor: muscle [GM, GL] and task [knee flexion, ankle plantar flexion]) on the x and on the y coordinate of the barycenter of EMG amplitude. This analysis was repeated to compare the spatial location of the motor unit action potentials across tasks. Of note, we did not interpret the main effect of muscle from these ANOVAs as the barycenter‘s coordinates were determined with respect to the grid location, which precludes any meaningful comparison between muscles. Finally, to compare the level of common synaptic input between tasks, we used a two-tailed paired t-test on the mean z-score values between 0 and 5 Hz. For all tests, the level of significance was set at $p < 0.05$.

# RESULTS

## Global surface EMG

### *EMG amplitude*

We first matched the knee flexion and ankle plantar flexion tasks based on the average *gastrocnemius* activation. In most of the participants (n=6/21), the best match was obtained by using an intensity of 40% and 30% of the task-relative peak torque for knee flexion and ankle plantar flexion, respectively. This led to an average *gastrocnemius* EMG amplitude of 16.1 ± 6.3% of $EMG_{max}$ for knee flexion and 17.1 ± 5.1% of $EMG_{max}$ for ankle plantar flexion ($p$ = 0.061; Fig. 2). The average within-participant difference in average *gastrocnemius* EMG amplitude between knee flexion and ankle plantar flexion was 2.0 ± 1.7% of $EMG_{max}$.

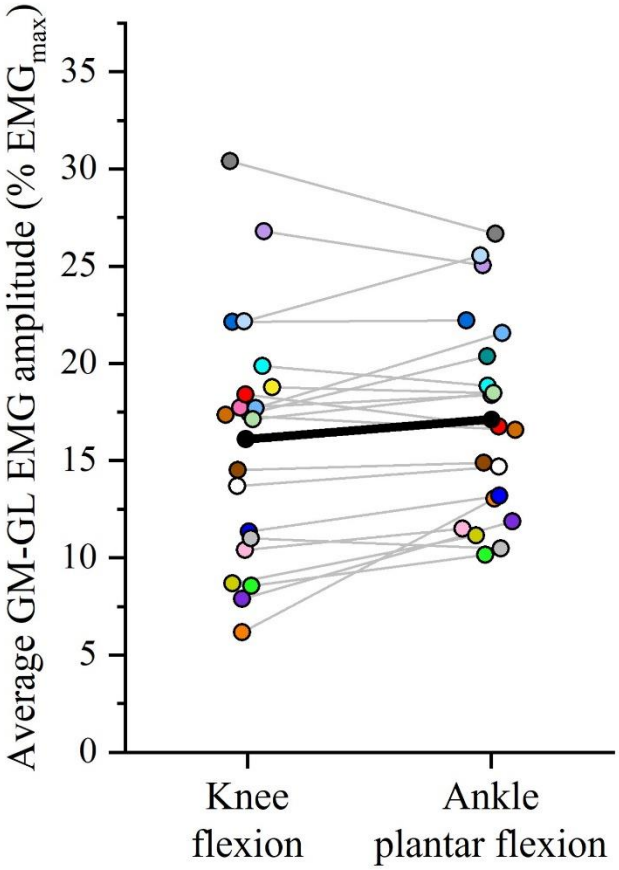


**Figure 2: Average *gastrocnemius* activation during the matched submaximal knee flexion and ankle plantar flexion.** The EMG amplitude was estimated during the submaximal torque plateaus. EMG was normalized to the maximal EMG value during maximal isometric voluntary contractions. Each color represents a participant, with the mean shown in black. The individual data points are displaced along the x axis for visual purposes. A paired t-test revealed that the mean GM-GL EMG was not different between knee flexion and ankle plantar flexion ($p$ = 0.061). n = 21.

For the separate muscles, the GM EMG amplitude was 21.9 ± 8.0% and 21.8 ± 5.6% of $EMG_{max}$ during knee flexion and ankle plantar flexion, respectively (Fig. 3). The GL EMG amplitude was 10.3 ± 7.2% and 12.4 ± 6.2% of $EMG_{max}$ during knee flexion and ankle plantar flexion, respectively. There was a main effect of muscle ($p < 0.001$) but no main effect of task ($p = 0.489$) nor a muscle×task interaction ($p = 0.448$). Specifically, normalized GM EMG amplitude was significantly higher than normalized GL EMG amplitude, leading to a GM/(GM+GL) ratio of 65.0 ± 10.0% and 70,7 ± 12.9% in knee flexion and ankle plantar flexion, respectively. The GM/(GM+GL) ratio measured during knee flexion was correlated to that measured during plantarflexion ($R = 0.604$; $p = 0.004$; Fig. 4). This demonstrates that participants who exhibited a greater bias of activation to GM during knee flexion also exhibited a greater bias of activation to GM during ankle plantar flexion.

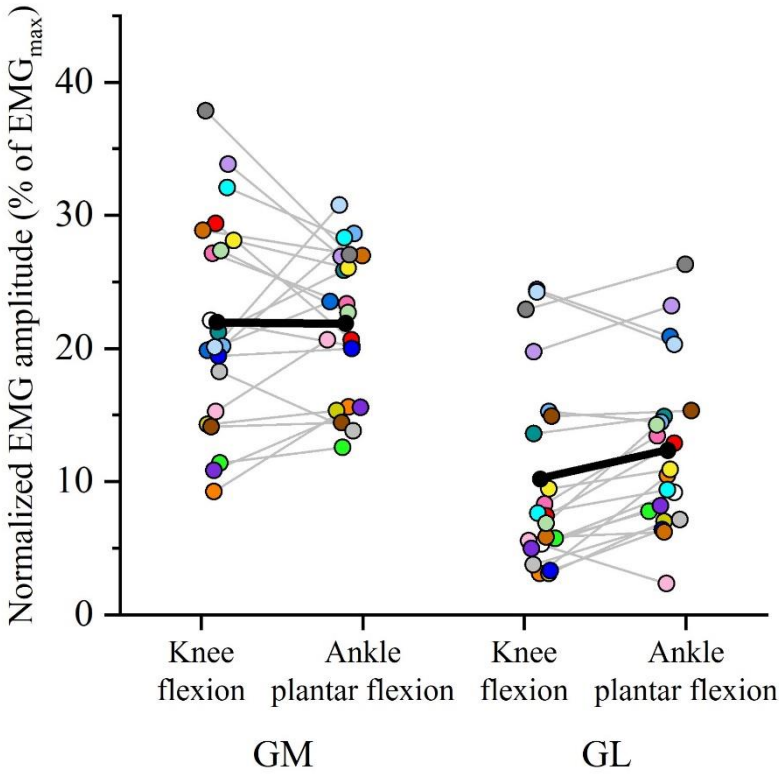


**Figure 3: GM and GL EMG amplitude measured during submaximal knee flexion and ankle plantar flexion.** The EMG amplitude was estimated using the average and rectified value of the EMG during the submaximal torque plateau. EMG was normalized to the maximal isometric voluntary contraction. Each color represents a participant, with the mean shown in black. The individual data points are displaced along the abscissa axis for a visual purpose. The ANOVA revealed that GM EMG was higher than GL EMG ($p < 0.001$), but there was no main effect of task ($p = 0.489$) nor muscle×task interaction ($p = 0.448$). GM: *Gastrocnemius medialis*; GL: *Gastrocnemius lateralis*. n = 21.

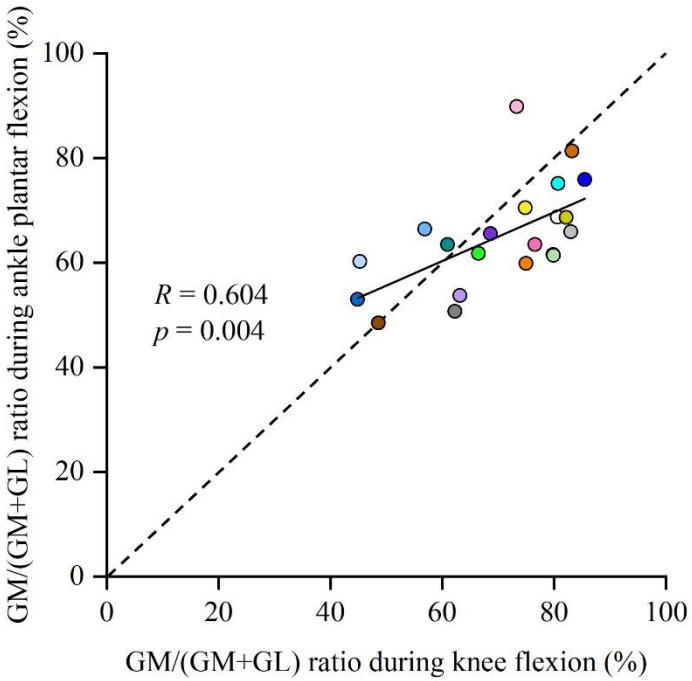


**Figure 4: Relationship between the distribution of activation during knee flexion and the distribution of activation during ankle plantar flexion.** The distribution of activation was estimated using the GM/(GM+GL) ratio of activation. The dashed line corresponds to the x=y equation. Each datapoint represents a participant. The Pearson correlation coefficient was statistically significant ($R$ = 0.604; $p$ = 0.004). GM: *Gastrocnemius medialis*; GL: *Gastrocnemius lateralis*. n = 21.

As indicated in the methods section, the aforementioned results were derived from values averaged over the entire torque plateaus. Even though GM and GL EMG amplitude was relatively constant during the plateau for ankle plantar flexion, GM and GL EMG amplitude increased over the torque plateau for knee flexion (Fig. 5). To ensure that these different profiles did not impact the results, we repeated the analysis for the knee flexion task considering only the second half of each plateau, where EMG amplitude was the highest during knee flexion. Results were similar to those presented above, with an average difference in average *gastrocnemius* EMG amplitude between the matched knee flexion and ankle plantar flexion task of 3.1 ± 2.8% of $EMG_{max}$. The GM/(GM+GL) ratio of EMG amplitude was correlated between tasks ($R$ = 0.591; $p$ = 0.005). Results was therefore consistent between the initial method and this revised method that only considered the part of the knee flexion plateau where GM and GL are substantially activated.

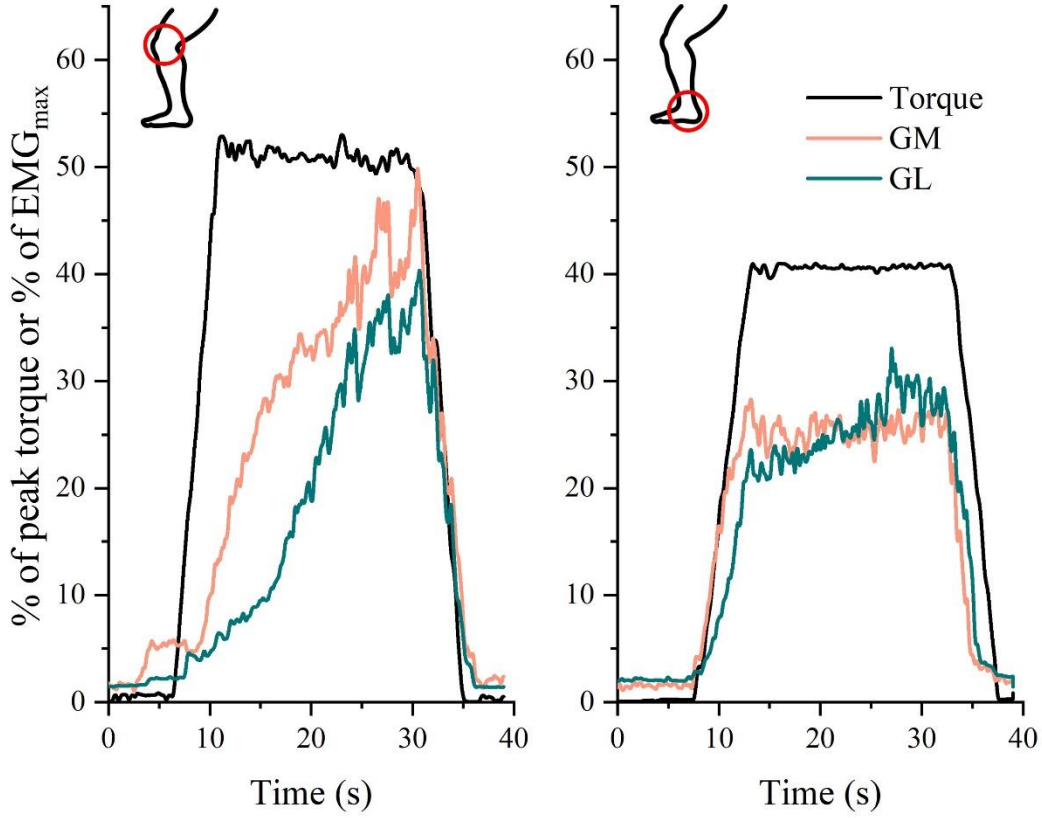


**Figure 5: GM and GL EMG patterns during knee flexion (left panel) and ankle plantar flexion (right panel) for one representative participant.** Y axis displays both the EMG amplitude (% of $EMG_{max}$) and the torque (% of task-specific peak torque). Even though GM and GL EMG amplitude was relatively constant during the plateau for ankle plantar flexion, GM and GL EMG amplitude increased over the torque plateau for knee flexion in most of the participants. GM: *Gastrocnemius medialis*; GL: *Gastrocnemius lateralis.*

*Regional activation*

When considering the proximo-distal (y axis) distribution of EMG amplitude, there was a main effect of task ($p$ = 0.028) but no muscle×task interaction ($p$ = 0.145). Specifically, the EMG amplitude was located 1.0 ± 1.4 mm more proximally on the EMG grid during knee flexion than during ankle plantar flexion, regardless of the muscle. Of note, this difference of 1 mm, albeit significant, is relatively small. When considering the medio-lateral (x axis) distribution of EMG amplitude, there was no main effect of task ($p$ = 0.155) nor a muscle×task interaction ($p$ = 0.251).

## Motor unit discharge characteristics

Global surface EMG amplitude provides indirect information on the level of muscle activation. To get more direct information about the neural drive sent to the muscles, we decomposed the HDsEMG signals into the activity of individual motor units. After the crosstalk assessment, four GL motor units were considered as crosstalk motor units and therefore discarded for further analyses. For the GM, we identified on average 14.1 ± 7.3 (range: 5-27) motor units and 18.6 ± 7.8 (range: 6-32) motor units per participant during knee flexion and ankle plantar flexion, respectively. For the GL, we identified on average 7.2 ± 6.6 (range: 3-24) motor units and 9.9 ± 7.8 (range: 3-23) motor units per participant for knee flexion and ankle plantar flexion, respectively. Among these motor units, only a small proportion were identified during both tasks: 5.1 ± 7.8% for GM (n= 0.9 ± 1.5 motor units) and 7.5 ± 11.8% for GL (n=1.0 ± 2.0 motor units). As this proportion is small, the following results are reported for the whole population of identified units, regardless of whether they could be matched between conditions.

### *Average discharge rate*

The discharge rate of GM motor units was 11.3 ± 3.1 pps and 9.8 ± 1.6 pps during knee flexion and ankle plantar flexion, respectively. The discharge rate of GL motor units was 9.9 ± 2.3 pps and 10.2 ± 1.7 pps during knee flexion and ankle plantar flexion, respectively. There was no significant main effect of muscle ($p = 0.616$) or task ($p = 0.357$), nor a muscle×task interaction ($p = 0.259$).

### *Spatial localization of identified motor units*

The ANOVA did not reveal a main effect of task ($p = 0.826$) or a muscle×task interaction ($p=0.452$) on the proximo-distal location of the identified motor units. Similar results were observed for the medio-lateral location of motor units, with no main effect of task ($p = 0.082$) or a muscle×task interaction ($p = 0.373$).

## Between muscle coherence

We considered the mean coherence value over the delta band (0-5 Hz) as an index of the level of common synaptic input received by GM and GL. A significant z-score was only observed for four and three participants (out of nine participants) during the knee flexion and ankle plantar flexion task, respectively (Fig. 6). This indicates that most of the participants did not

exhibit a significant level of common synaptic input between motor neurons innervating the GM and GL muscles. The mean coherence value over the delta band (as a z-score) was not different between tasks (knee flexion: 1.7 ± 1.2, and ankle plantar flexion: 1.4 ± 1.3; $p$=0.570).

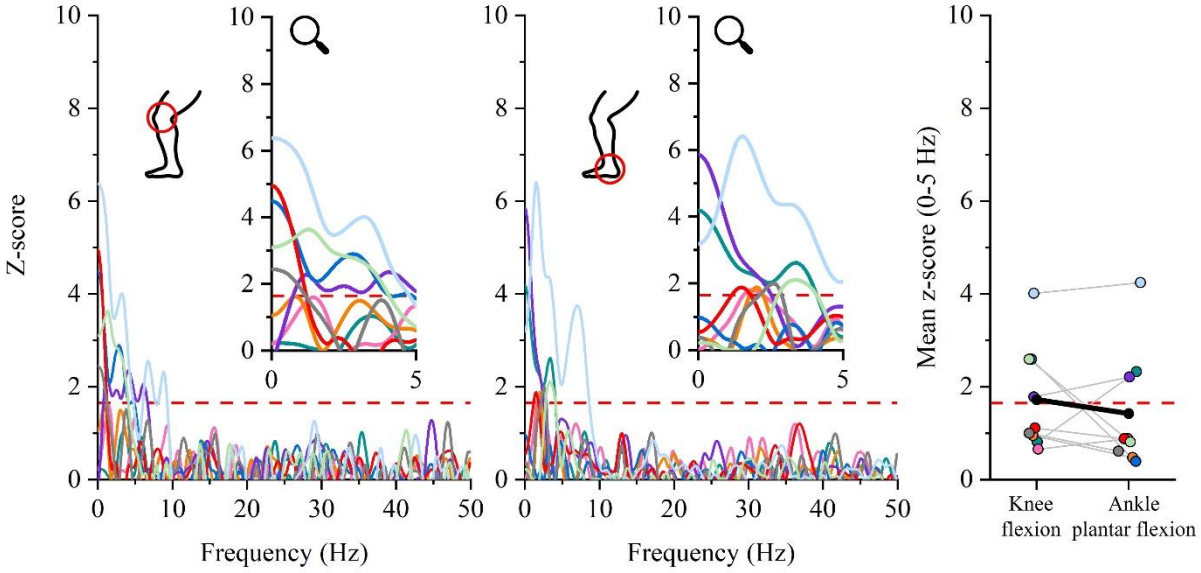


**Figure 6: Between-muscle coherence during knee flexion and ankle plantar flexion.** The left and middle panels represent the z-scores between 0 and 50 Hz during knee flexion and ankle plantar flexion respectively for each participant. The magnified inset depicts the z-score between 0 and 5 Hz. The right panel represents the average z-score value between 0 and 5 Hz for each participant for the two tasks. Each color corresponds to one participant. The red horizontal dashed line indicates the significant threshold, which is set at 1.65 (95% confidence limit). Within the right panel, the mean group is depicted in black. n=9.

## DISCUSSION

We aimed to determine whether the neural control of GM and GL differs between their two main functions in the sagittal plane, i.e., isolated knee flexion and ankle plantar flexion. In accordance with our first hypothesis, we observed that the bias of activation towards GM, already reported during ankle plantar flexion (Crouzier et al., 2019; Kinugasa et al., 2005), persisted during knee flexion. The robustness of the GM and GL activation strategy across knee flexion and ankle plantar flexion was further confirmed by the analyses of the motor unit discharge rate and the spatial location of EMG amplitude and identified motor units. Contrary to our hypothesis, the level of common synaptic input between GM and GL remained relatively low during knee flexion, with no significant difference between the tasks. Overall, our results suggest that the neural control of the *gastrocnemius* muscles at a similar overall level of activation, is consistent across their two main functions.

We observed a higher normalized EMG amplitude for GM compared to GL during ankle plantar flexion, with a GM/(GM+GL) ratio of 65.0 ± 10.0%, which is consistent with previous studies (68.8 ± 11.9% in Crouzier et al., 2019; 65.0 ± 13.2% in Crouzier et al., 2018). The current study extends this observation to knee flexion, during which this imbalance of activation persisted. Interestingly, the distribution of activation, assessed through the GM/(GM+GL) ratio, was correlated between tasks, providing further support for the existence of an individual muscle activation strategy, robust across time and tasks (Crouzier et al., 2019; Hug et al., 2019). Even though the origin of this individual strategy is mostly unknown, preliminary evidence suggests that it could be explained by a neuromechanical coupling between the activation a muscle receives and its biomechanical characteristics (Crouzier et al., 2018; Hudson et al., 2009; Hug et al., 2015). Specifically, previous studies reported a significant positive correlation between the distribution of activation across synergist muscles and their distribution of PCSA (Crouzier et al., 2018; Hug et al., 2015). Considering that muscle PCSA provides an index of muscle force-generating capacity (Powell et al., 1984), this observation aligns particularly well with the theory that activation strategies are selected such that the sum of muscle stresses cubed is minimized (Crowninshield & Brand, 1981). The consistency of the distribution of muscle activation that we observed between knee flexion and ankle plantar flexion may be explained by this coupling with the distribution of PCSA, which remained unchanged across tasks.

To further probe the neural strategy, we confirmed our results with a more direct estimate of the neural drive sent to the muscles. To this end, we decomposed HDsEMG signals into individual motor units activity. Of note, the difference in discharge rate between GM and GL

motor units cannot be interpreted as a difference in the strength of neural drive as it is not possible to verify that we compared motor units with similar intrinsic properties. Therefore, we only interpreted the main effect of task and the muscle×task interaction, which were both non-significant. Overall, it confirms that activation strategies were not different between tasks.

Previous studies have suggested that the regional activation of biarticular muscles may be task dependent (Watanabe et al., 2016, 2021). At first glance, our results seem in agreement with this hypothesis, with a significant proximal shift of EMG amplitude during knee flexion compared to ankle plantar flexion, regardless of the muscle. However, the difference was relatively small (1 mm) in comparison with the inter-electrode distance (8 mm), casting doubt about the physiological meaningfulness of this shift of EMG amplitude. Given the lack of selectivity of global surface EMG (Farina et al., 2006), it is important to ensure that this small, albeit significant, shift was not induced by crosstalk from distant muscles, such as the monoarticular hip extensor muscles. Different gearing or fascicle shortening between knee flexion and ankle plantar flexion can also explain these small differences. Importantly, a similar analysis performed at the motor unit level did not confirm the existence of a significant shift, as observed from global surface EMG. Even though the number of identified motor units is relatively modest in regard to the total number of active units, such an analysis provides a more direct estimate of the spatial location of muscle activation. This result aligns with data obtained from direct recording of motor unit activity made using fine-wire EMG, where motor units recruited in knee flexion or in ankle plantar flexion did not have a specific regional location (Héroux et al., 2015). Moreover, the absence of regional activation is consistent with the high level of common synaptic input within each muscle (Hug et al., 2021; Levine et al., 2022), which likely limits the possibility of joint-specific motor units recruitment. Taken together, our results suggest that the distribution of activation between and within GM and GL is robust regardless of the main function for which they are used, *i.e.* knee flexion or ankle plantarflexion.

In addition to the distribution of activation, understanding the control of synergist muscles requires knowledge of the level of common synaptic input received by their motor units. To explore this, we calculated the coherence between cumulative spike trains. In accordance with recent work (Hug et al., 2021; Rossato et al., 2022), we observed an absence of significant coherence between GM and GL motor units for most of the participants during ankle plantar flexion, which is interpreted as the presence of little, if any, common input. Of note, when the coherence exceeded the significative threshold in some participants, its amplitude was relatively modest when compared to other muscles such as the VL and VM (Avrillon et al., 2021). It is

thought that this low level of common synaptic input is required to dissociate GM and GL activation to comply with secondary roles such as modulation of the ankle moment in the frontal plane (Hug et al., 2021). Because such a secondary role is likely not required for knee flexion, we hypothesized that the level of common synaptic input would be higher in knee flexion compared to ankle plantar flexion. However, this was not observed which is consistent with recent results showing a robust level of common synaptic input to motor neurons innervating the GM and GL across ankle plantar flexion tasks performed at different ankle angles (Levine et al., 2022). Together, this suggests that the nervous system has a limited ability to modify the level of common synaptic input to motor neurons across tasks, even when such a change would reduce the dimensions to be controlled independently.

In this study, we also attempted to determine whether the same motor units were activated between knee flexion and ankle plantar flexion. Given that the activation level was matched between tasks, and based on the size principle (Henneman, 1957), one would expect that the same units were active during both tasks. However, our approach was able to track only a small proportion of units between tasks (< 8%). There are three potential explanations. First, even though we matched the mean *gastrocnemius* activation level across tasks, small (~2%) inevitable differences were observed, which could have led to the recruitment of different motor units across tasks. However, given the small differences in activation between tasks, only a very small proportion of units would have differed across tasks. Second, the small number of tracked units may be explained by limitations of our approach to track motor units. However, this approach was used in previous studies whereby motor units were matched across days (Del Vecchio et al., 2019; Martinez-Valdes et al., 2017). For instance, at 30% of knee extension MVC, more than 40% of the motor units from the VL and VM muscles were matched between days (Martinez-Valdes et al., 2017). Despite the lower leg position remaining similar between tasks, we cannot rule out the possibility that the muscles moved with respect to the EMG grids, for example, owing to complex force transmission processes with other synergist muscles such as the soleus. However, it is unlikely that it substantially affected the relative muscles' position. This is confirmed by the absence of change in the barycenter of motor unit action potentials across tasks (e.g. Fig. 1). Thus, we believe that our experimental procedures provided the ideal conditions to track motor units across tasks. To be sure that we did not fail to identify motor units, we performed a supplementary matching round with a lower threshold (0.60). Even with this lower threshold, the proportion of matched motor units remained low; i.e. 16.8 ± 11.0% for the GM and 13.5 ± 13.2% for the GL. In addition, we used a secondary analysis whereby we

reapplied the motor unit filters obtained in one task to the other task (Frančič & Holobar, 2021). The use of this approach led to very similar results, that is, motor units that were successfully tracked across tasks were also identified by application of the motor unit filter, but motor units that were not tracked across tasks could not be identified by the application of the motor unit filter. Finally, even though we cannot rule out that the small proportion of tracked motor units is explained by methodological limitations, it remains possible that different motor units were recruited in knee flexion and in ankle plantar flexion. In this way, using a more direct approach (fine-wire EMG) a previous study observed that only 42% of the GM motor units were recruited during both knee flexion and ankle plantar flexion isometric contractions (Héroux et al., 2015). This echoes previous work which challenges Heneman's size principle by reporting divergent recruitment orders across motor neurons innervating the same muscle (Desmedt & Godaux, 1977; Marshall et al., 2022; Tucker et al., 2009). This is also consistent with a recently proposed framework whereby motor units are grouped into functional clusters such that motor units from the same pool (muscle) can receive different common inputs (Hug et al., 2023). However, given the methodological limitations mentioned above, further studies are needed to explore whether different motor units are recruited during knee flexion and ankle plantar flexion.

In conclusion, our results demonstrate that the within- and between-muscle distribution of activation is robust regardless of the function for which the GM and GL muscles are used, that is, knee flexion or ankle plantar flexion. Specifically, the GM muscle was activated at a higher level than the GL muscle during submaximal contractions, regardless of the task. Even though this strategy leads to a force imbalance between these muscles, it likely contributes to minimize the overall muscle stress, a well-established motor control strategy. Although the presence of strong common input between GM and GL motor units would serve to reduce the computational load associated with the control of these muscles, it was not observed. This low level of common input could allow GM and GL to be independently controlled during ankle plantar flexion to comply with secondary goals, such as producing opposing ankle moments in the frontal plane. However, the functional benefit of a low level of common input in knee flexion remains unclear.

**ACKNOWLEDGEMENTS**

Dr Jeroen Aeles is supported by a Marie Skłodowska-Curie Actions Individual Fellowship funded by the European Union (I-MUSCLE, 101063675). Prof François Hug was supported by the French national research agency (ANR-19-CE17-002-01, COMMODE project).

**REFERENCES**

Aeles, J., Sarcher, A., & Hug, F. (2023). Common synaptic input between motor units from the lateral and medial posterior soleus compartments does not differ from that within each compartment. *Journal of Applied Physiology*, *134*(1), 105-115. https://doi.org/10.1152/japplphysiol.00587.2022

Avrillon, S., Del Vecchio, A., Farina, D., Pons, J. L., Vogel, C., Umehara, J., & Hug, F. (2021). Individual differences in the neural strategies to control the lateral and medial head of the quadriceps during a mechanically constrained task. *Journal of Applied Physiology*, *130*(1), 269-281. https://doi.org/10.1152/japplphysiol.00653.2020

Besomi, M., Hodges, P. W., Clancy, E. A., Van Dieën, J., Hug, F., Lowery, M., Merletti, R., Søgaard, K., Wrigley, T., Besier, T., Carson, R. G., Disselhorst-Klug, C., Enoka, R. M., Falla, D., Farina, D., Gandevia, S., Holobar, A., Kiernan, M. C., McGill, K., … Tucker, K. (2020). Consensus for experimental design in electromyography (CEDE) project : Amplitude normalization matrix. *Journal of Electromyography and Kinesiology*, *53*, 102438. https://doi.org/10.1016/j.jelekin.2020.102438

Cibulka, M., Wenthe, A., Boyle, Z., Callier, D., Schwerdt, A., Jarman, D., & Strube, M. J. (2017). VARIATION IN MEDIAL AND LATERAL GASTROCNEMIUS MUSCLE ACTIVITY WITH FOOT POSITION. *International Journal of Sports Physical Therapy*, *12*(2), 233-241.

Crouzier, M., Hug, F., Dorel, S., Deschamps, T., Tucker, K., & Lacourpaille, L. (2019). Do individual differences in the distribution of activation between synergist muscles reflect individual strategies? *Experimental Brain Research*, *237*(3), 625-635. https://doi.org/10.1007/s00221-018-5445-6

Crouzier, M., Lacourpaille, L., Nordez, A., Tucker, K., & Hug, F. (2018). Neuromechanical coupling within the human triceps surae and its consequence on individual force-sharing strategies. *The Journal of Experimental Biology*, *221*(21), jeb187260. https://doi.org/10.1242/jeb.187260

Crowninshield, R. D., & Brand, R. A. (1981). A physiologically based criterion of muscle force prediction in locomotion. *Journal of Biomechanics*, *14*(11), 793-801. https://doi.org/10.1016/0021-9290(81)90035-X

Del Vecchio, A., Casolo, A., Negro, F., Scorcelletti, M., Bazzucchi, I., Enoka, R., Felici, F., & Farina, D. (2019). The increase in muscle force after 4 weeks of strength training is mediated by adaptations in motor unit recruitment and rate coding. *The Journal of Physiology*, *597*(7), 1873-1887. https://doi.org/10.1113/JP277250

Del Vecchio, A., & Farina, D. (2019). Interfacing the neural output of the spinal cord : Robust and reliable longitudinal identification of motor neurons in humans. *Journal of neural engineering*, *17*(1), 016003.

Del Vecchio, A., Germer, C. M., Elias, L. A., Fu, Q., Fine, J., Santello, M., & Farina, D. (2019). The human central nervous system transmits common synaptic inputs to distinct motor

neuron pools during non-synergistic digit actions. *The Journal of Physiology*, *597*(24), 5935-5948. https://doi.org/10.1113/JP278623

Del Vecchio, A., Holobar, A., Falla, D., Felici, F., Enoka, R. M., & Farina, D. (2020). Tutorial : Analysis of motor unit discharge characteristics from high-density surface EMG signals. *Journal of Electromyography and Kinesiology*, *53*, 102426. https://doi.org/10.1016/j.jelekin.2020.102426

Desmedt, J. E., & Godaux, E. (1977). Ballistic contractions in man : Characteristic recruitment pattern of single motor units of the tibialis anterior muscle. *The Journal of physiology*, *264*(3), 673-693.

Farina, D., Zennaro, D., Pozzo, M., Merletti, R., & Läubli, T. (2006). Single motor unit and spectral surface EMG analysis during low-force, sustained contractions of the upper trapezius muscle. *European Journal of Applied Physiology*, *96*(2), 157-164. https://doi.org/10.1007/s00421-004-1261-8

Frančič, A., & Holobar, A. (2021). On the Reuse of Motor Unit Filters in High Density Surface Electromyograms Recorded at Different Contraction Levels. *IEEE Access*, *9*, 115227-115236. https://doi.org/10.1109/ACCESS.2021.3104762

Henneman, E. (1957). Relation between size of neurons and their susceptibility to discharge. *Science*, *126*(3287), 1345-1347.

Héroux, M. E., Brown, H. J., Inglis, J. T., Siegmund, G. P., & Blouin, J.-S. (2015). Motor units in the human medial gastrocnemius muscle are not spatially localized or functionally grouped. *The Journal of Physiology*, *593*(16), 3711-3726. https://doi.org/10.1113/JP270307

Holobar, A., Minetto, M. A., & Farina, D. (2014). Accurate identification of motor unit discharge patterns from high-density surface EMG and validation with a novel signal-based performance metric. *Journal of neural engineering*, *11*(1), 016008.

Hudson, A. L., Taylor, J. L., Gandevia, S. C., & Butler, J. E. (2009). Coupling between mechanical and neural behaviour in the human first dorsal interosseous muscle. *The Journal of Physiology*, *587*(4), 917-925. https://doi.org/10.1113/jphysiol.2008.165043

Hug, F., Avrillon, S., Del Vecchio, A., Casolo, A., Ibanez, J., Nuccio, S., Rossato, J., Holobar, A., & Farina, D. (2021). Analysis of motor unit spike trains estimated from high-density surface electromyography is highly reliable across operators. *Journal of Electromyography and Kinesiology*, *58*, 102548. https://doi.org/10.1016/j.jelekin.2021.102548

Hug, F., Avrillon, S., Ibáñez, J., & Farina, D. (2023). Common synaptic input, synergies and size principle : Control of spinal motor neurons for movement generation. *The Journal of Physiology*, *601*(1), 11-20. https://doi.org/10.1113/JP283698

Hug, F., Del Vecchio, A., Avrillon, S., Farina, D., & Tucker, K. (2021). Muscles from the same muscle group do not necessarily share common drive : Evidence from the human triceps surae. *Journal of Applied Physiology*, *130*(2), 342-354. https://doi.org/10.1152/japplphysiol.00635.2020

Hug, F., Goupille, C., Baum, D., Raiteri, B. J., Hodges, P. W., & Tucker, K. (2015). Nature of the coupling between neural drive and force-generating capacity in the human quadriceps muscle. *Proceedings. Biological Sciences*, *282*(1819). https://doi.org/10.1098/rspb.2015.1908

Hug, F., Vogel, C., Tucker, K., Dorel, S., Deschamps, T., Le Carpentier, É., & Lacourpaille, L. (2019). Individuals have unique muscle activation signatures as revealed during gait and

pedaling. *Journal of Applied Physiology*, *127*(4), 1165-1174. https://doi.org/10.1152/japplphysiol.01101.2018

Kinugasa, R., Kawakami, Y., & Fukunaga, T. (2005). Muscle activation and its distribution within human triceps surae muscles. *Journal of Applied Physiology*, *99*(3), 1149-1156. https://doi.org/10.1152/japplphysiol.01160.2004

Laine, C. M., Martinez-Valdes, E., Falla, D., Mayer, F., & Farina, D. (2015). Motor Neuron Pools of Synergistic Thigh Muscles Share Most of Their Synaptic Input. *Journal of Neuroscience*, *35*(35), 12207-12216. https://doi.org/10.1523/JNEUROSCI.0240-15.2015

Laine, C. M., & Valero-Cuevas, F. J. (2017). Intermuscular coherence reflects functional coordination. *Journal of Neurophysiology*, *118*(3), 1775-1783. https://doi.org/10.1152/jn.00204.2017

Lee, S. S. M., & Piazza, S. J. (2008). Inversion–eversion moment arms of gastrocnemius and tibialis anterior measured in vivo. *Journal of Biomechanics*, *41*(16), 3366-3370. https://doi.org/10.1016/j.jbiomech.2008.09.029

Levine, J., Avrillon, S., Farina, D., Hug, F., & Pons, J. L. (2022). *Two motor neuron synergies, invariant across ankle joint angles, activate the triceps surae during plantarflexion* (p. 2022.11.11.516183). bioRxiv. https://doi.org/10.1101/2022.11.11.516183

Li, L., Landin, D., Grodesky, J., & Myers, J. (2002). The function of gastrocnemius as a knee flexor at selected knee and ankle angles. *Journal of Electromyography and Kinesiology*, *12*(5), 385-390. https://doi.org/10.1016/S1050-6411(02)00049-4

Marcori, A. J., Moura, T. B. M. A., & Okazaki, V. H. A. (2017). Gastrocnemius muscle activation during plantar flexion with different feet positioning in physically active young men. *Isokinetics and Exercise Science*, *25*(2), 121-125. https://doi.org/10.3233/IES-160654

Marshall, N. J., Glaser, J. I., Trautmann, E. M., Amematsro, E. A., Perkins, S. M., Shadlen, M. N., Abbott, L. F., Cunningham, J. P., & Churchland, M. M. (2022). Flexible neural control of motor units. *Nature neuroscience*, *25*(11), 1492-1504.

Martinez-Valdes, E., Negro, F., Laine, C. M., Falla, D., Mayer, F., & Farina, D. (2017). Tracking motor units longitudinally across experimental sessions with high-density surface electromyography. *The Journal of physiology*, *595*(5), 1479-1496.

Masood, T., Bojsen-Møller, J., Kalliokoski, K. K., Kirjavainen, A., Äärimaa, V., Peter Magnusson, S., & Finni, T. (2014). Differential contributions of ankle plantarflexors during submaximal isometric muscle action : A PET and EMG study. *Journal of Electromyography and Kinesiology*, *24*(3), 367-374. https://doi.org/10.1016/j.jelekin.2014.03.002

Miyamoto, N., Wakahara, T., & Kawakami, Y. (2012). Task-dependent inhomogeneous muscle activities within the bi-articular human rectus femoris muscle. *Plos one*, *7*(3), e34269.

Negro, F., Muceli, S., Castronovo, A. M., Holobar, A., & Farina, D. (2016). *Multi-channel intramuscular and surface EMG decomposition by convolutive blind source separation*. *13*(2), 026027. https://doi.org/10.1088/1741-2560/13/2/026027

Powell, P. L., Roy, R. R., Kanim, P., Bello, M. A., & Edgerton, V. R. (1984). Predictability of skeletal muscle tension from architectural determinations in guinea pig hindlimbs. *Journal of Applied Physiology*, *57*(6), 1715-1721. https://doi.org/10.1152/jappl.1984.57.6.1715

Riemann, B. L., Limbaugh, G. K., Eitner, J. D., & LeFavi, R. G. (2011). Medial and Lateral Gastrocnemius Activation Differences During Heel-Raise Exercise with Three

Different Foot Positions. *The Journal of Strength & Conditioning Research*, *25*(3), 634-639. https://doi.org/10.1519/JSC.0b013e3181cc22b8

Rossato, J., Tucker, K., Avrillon, S., Lacourpaille, L., Holobar, A., & Hug, F. (2022). Less common synaptic input between muscles from the same group allows for more flexible coordination strategies during a fatiguing task. *Journal of Neurophysiology*, *127*(2), 421-433. https://doi.org/10.1152/jn.00453.2021

Segal, R. L., & Song, A. W. (2005). Nonuniform Activity of Human Calf Muscles During an Exercise Task. *Archives of Physical Medicine and Rehabilitation*, *86*(10), 2013-2017. https://doi.org/10.1016/j.apmr.2005.04.012

Tucker, K., Butler, J., Graven-Nielsen, T., Riek, S., & Hodges, P. (2009). Motor unit recruitment strategies are altered during deep-tissue pain. *Journal of Neuroscience*, *29*(35), 10820-10826.

Vieira, T. M. M., Minetto, M. A., Hodson-Tole, E. F., & Botter, A. (2013). How much does the human medial gastrocnemius muscle contribute to ankle torques outside the sagittal plane? *Human Movement Science*, *32*(4), 753-767. https://doi.org/10.1016/j.humov.2013.03.003

Watanabe, K., Kouzaki, M., & Moritani, T. (2016). Regional neuromuscular regulation within human rectus femoris muscle during gait in young and elderly men. *Journal of Biomechanics*, *49*(1), 19-25.

Watanabe, K., Vieira, T. M., Gallina, A., Kouzaki, M., & Moritani, T. (2021). Novel Insights Into Biarticular Muscle Actions Gained From High-Density Electromyogram. *Exercise and Sport Sciences Reviews*, *49*(3), 179-187. https://doi.org/10.1249/JES.0000000000000254

# CHAPTER 4: GENERAL DISCUSSION

The overall aim of this PhD thesis was to provide a deeper understanding of muscle coordination between the GM and GL, two muscles from the same anatomical group with the same general function (i.e. knee flexion and ankle plantar flexion). Study #1 and Study #2 examined the mechanical consequences of the distribution of activation between these two muscles in terms of contractile behavior and muscle force production during walking. Study #3 investigated the influence of different mechanical constraints (i.e. knee flexion versus ankle plantar flexion) on muscle coordination between the GM and GL. To achieve this, we used an integrative neuromechanical approach that combined imaging of *in vivo* contractile behavior, EMG recordings and a muscle model.

In Study #1, we aimed to determine the neuromechanical difference between the GM and GL and more specifically the difference in the interplay between muscle activation and fascicle contractile behavior during walking. Our results showed that the GM and GL each had a distinct muscle activation which resulted in specific fascicle contractile behavior. This likely enhances the catapult-like mechanism in the GM compared to the GL.

In Study #2, we aimed to estimate the individual distribution of force between the GM and GL during walking using an experimentally-informed Hill-type muscle model. We demonstrated that the GM produces more force compared to the GL with a high level of variability in the magnitude of this distribution of force between participants. Moreover, we showed that the use of *in vivo* experimental data to personalize Hill-type muscle models is necessary to assess the distribution of muscle force at an individual level.

In Study #3, we aimed to determine whether the distribution of muscle activation and the level of common synaptic input between the GM and GL differs between their two primary functions, i.e. knee flexion and ankle plantar flexion. Our results revealed that the mechanical constraints induced by knee flexion or ankle plantar flexion seem to influence only in a small extent the distribution of activation between the GM and GL. Further, the common synaptic input between the GM and GL appears robust across the two tasks.

The discussion of the results obtained from these three studies is organized into four main sections. In the first section, we describe the methodological points that should be considered to make a general interpretation about the results of this PhD thesis. In the second section we present a synthesis of the results from this PhD. In the third section, we elaborate on the functional implication of these results. Finally, in the fourth section, we present the general conclusion and discuss future directions of this PhD thesis.

# 1. Methodological considerations

## 1.1. Estimation of the neural command

### 1.1.1. Crosstalk

The three studies of this PhD thesis aimed to estimate the muscle activation, either with the more conventional surface EMG in bipolar mode (Study #1 and Study #2) or with high-density EMG (Study #3). We were particularly interested in the distribution of activation between the GM and GL, which could have been influenced by crosstalk. For example, crosstalk from the GM and *soleus* muscles may lead to an overestimation of the GL muscle activation (Germer et al., 2021). It is challenging to determine the presence of crosstalk within a surface EMG signal. A previous study aimed to indirectly quantify the crosstalk by comparing surface EMG to another approach less prone to crosstalk such as intra-muscular EMG (Péter et al., 2019). This approach was used to estimate the crosstalk within lower limb muscles during walking. The results revealed an absence of difference between the time-varying profile of surface EMG and intra-muscular EMG for both the GM and GL at preferred walking speed, the condition that we used in Study #1 and Study #2 in this thesis (Figure 36). This suggests a limited amount of crosstalk within the GM and GL EMG signals. In this study, both the intra-muscular EMG and the surface EMG were normalized to the peak EMG during walking. This is likely due to the fact that intra-muscular EMG makes the MVC very uncomfortable. However, it is possible that crosstalk influences also the peak EMG which could limit the ability to detect crosstalk. As a consequence, the absence of difference between intra-muscular EMG and surface EMG for the GM and GL during walking reported by this study should be considered with caution. To limit crosstalk, for each study, we used B-mode ultrasound to determine the muscle boundaries of the GM and GL. With this precaution, we ensured electrodes were placed in the center of the muscle and away from neighboring muscles. The muscle fiber action potentials from the neighboring muscles were therefore more distant and their detection by our electrodes should thus have been limited.

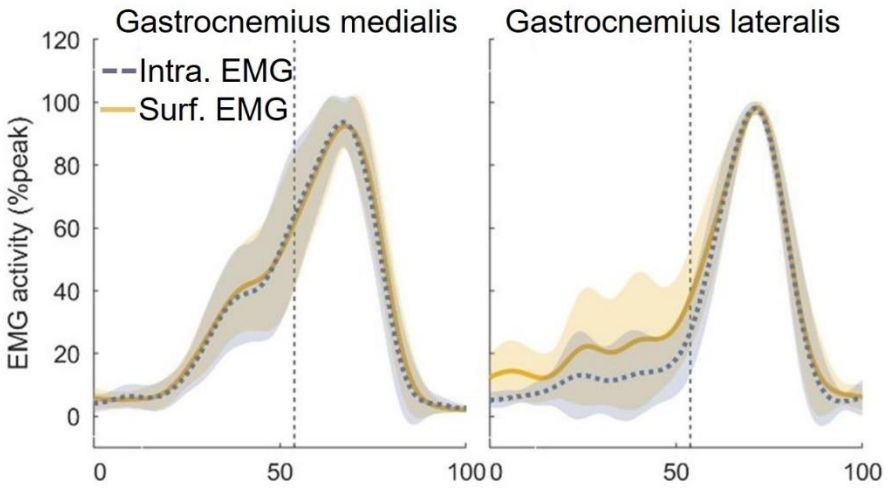


**Figure 36: Comparison of surface electromyography and intra-muscular electromyography for the *gastrocnemius medialis* and *gastrocnemius lateralis* during preferred walking speed.** No differences were found between the two methods for both the the *gastrocnemius medialis* and *gastrocnemius lateralis*. Intra. EMG, intra-muscular electromyography; Surf. electromyography, surface EMG. From Péter et al. (2019).

### 1.1.2. EMG normalization procedure

The estimation of the distribution of activation between the GM and GL also requires submaximal EMG of each muscle to be expressed relative to its maximal activity level (Besomi et al., 2020). To do this, we normalized the EMG signals to those measured during an isometric MVC. However, this normalization procedure may be limited for Study #1 and Study #2. To this end, we used a MVC during an isometric task. However, the submaximal task of interest was a dynamic task (i.e. walking) whereby the muscle fibers have isometric, concentric and eccentric behaviors. In this dynamic task, the muscle can move underneath the electrodes and a new region of the muscle can be recorded. As the muscle activation is not homogeneously distributed in a muscle (Hodson-Tole et al., 2013; Segal & Song, 2005; Wolf et al., 1993), this could lead to discrepancies such as a relatively high normalized EMG amplitude. For example, during incline walking, one participant had a GM normalized peak EMG around 90%. However, the determination of maximal EMG activity level is challenging for dynamic tasks. Previous studies have used the peak EMG within the gait cycle to normalize EMG during walking (Péter et al., 2019). Nevertheless, this results in maximal activation during walking which did not correspond to the physiological muscle activation. Unfortunately, all the known procedures have drawbacks to normalize EMG during walking and the use of isometric MVC to normalize submaximal dynamic task is considered appropriate in a recent expert consensus statement (Besomi et al., 2020). Moreover, we found a similar distribution of activation in Study #1 and Study #2 (i.e. a GM/(GM+GL) ratio of EMG of 59.6% for the average EMG during

stance at level walking) compared to Study #3 (i.e. a GM/(GM+GL) ratio of EMG of 65.0% during ankle plantar flexion) where the MVC modality matched the modality of the submaximal task of interest, i.e. same contraction type and same muscle length. Thus we are confident that the isometric MVC used in the Study #1 and Study #2 did not influence our interpretation.

## 1.2. Estimation of the contractile behavior during walking

In Study #1 and Study #2, we aimed to examine the interplay between muscle activation and the contractile behavior of the GM and GL during walking. For this purpose, we determined the fascicle length, fascicle velocity and pennation angle using B-mode ultrasonography. As mentioned in Part 1, section 1.2.1.2., B-mode ultrasound allows only to image the muscle in 2D whereas the muscle has a 3D contractile behavior (Raiteri et al., 2016; Rana et al., 2013, 2014). Although several methods allow to image the muscle in 3D during static conditions, 2D B-mode ultrasonography remains the only method to study the contractile behavior during dynamic tasks, such as walking (Franchi et al., 2018). To limit the influence of 3D shape changes in our results, we paid particular attention to the B-mode ultrasound transducer placement. We ensured to image the main fascicle plane during the whole walking cycle. Moreover, during the muscle fascicle tracking process, we removed the data where we observed substantial fascicle plane changes. This results in the exclusion of 5 participants out of the 20 recruited. Finally, previous studies revealed that a proper transducer orientation allows accurate measurement of the fascicle length (Bolsterlee et al., 2016) and pennation angle (Bolsterlee et al., 2016; Rana et al., 2013) for the *gastrocnemii*. For example, the difference between a pennation angle calculated from a 2D imaging and the 3D pennation angle is around 1° when the 2D transducer is correctly positioned (Bolsterlee et al., 2016; Rana et al., 2013). As a consequence, we are confident that our use of B-mode ultrasound led to only minor error measurements and did not influence substantially our interpretation that the GM undergoes less fascicle lengthening during mid stance compared to the GL .

Another consideration when using B-mode ultrasound to image the skeletal muscle behavior is that the ultrasound transducer images a limited region of the muscle. However, it is well established that the muscle from the *triceps surae* have heterogeneous deformation during walking (Hodson-Tole & Lai, 2019; Lichtwark et al., 2007). For example, Lichtwark et al. (2007) revealed that the distal fascicles shortened more and had greater pennation angles compare to the proximal fascicle during walking (Figure 37). However these authors highlighted that a measure from the center of the muscle belly enables representative data of

the average muscle architecture changes during walking (Lichtwark et al., 2007). In our study we positioned the ultrasound probe in the mid-region of the muscle belly. We are thus confident that it represents the average contractile behavior. Moreover, our time-varying fascicle length, fascicle velocity and pennation angle are consistent with the literature (Clark et al., 2020; Farris & Raiteri, 2017; Fukunaga et al., 2001; Ishikawa et al., 2005; Lichtwark & Wilson, 2006). Taken together, the imaging of the main fascicle plane throughout the gait cycle and the imaging of the center of the muscle belly should limit the influence of the B-mode ultrasound drawbacks on our results.

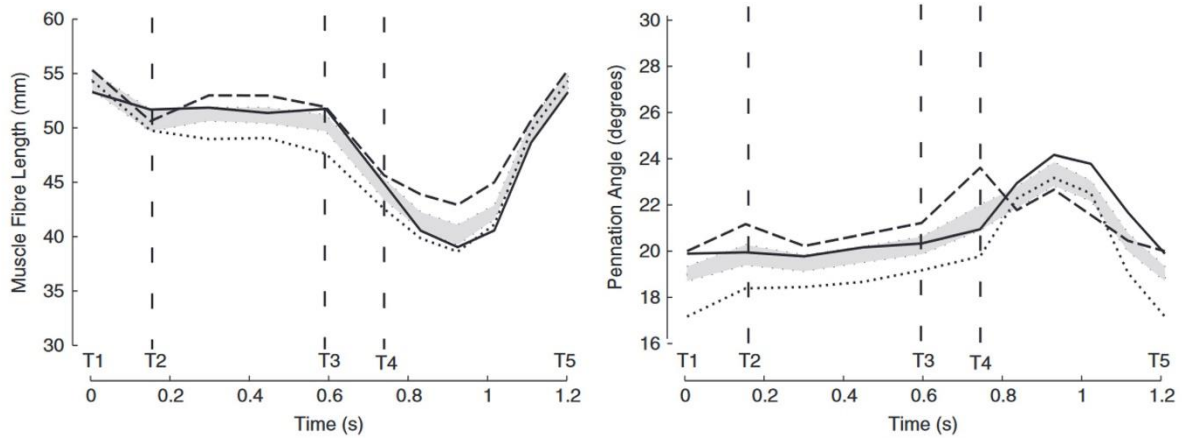


**Figure 37: Specific fascicle contractile behavior of different muscle region of the *gastrocnemius medialis* during walking**. The data presented corresponds to a complete gait cycle from heel-strike (T1) to the following heel-strike (T5). The dotted, solid and dashed curves correspond to the measurement from distal, middle and proximal region of the muscle, respectively. The authors suggested that the measure of the middle region of the muscle provides a good approximation of the average fascicle length change. From Lichtwark et al. (2007).

## 1.3. Estimation of muscle force

### 1.3.1. Generic Hill-type model parameters

In Study #2, we aimed to estimate the force produced by the GM and GL using a Hill-type muscle model informed with subject-specific inputs. However, some generic parameters were required within the models and should be considered. Due to the lack of methods to measure individual muscle forces in humans, we used generic properties for force-length relationship shape, force-velocity relationship shape and specific tension (Otten, 1987; Powell et al., 1984; Wakeling et al., 2012). The use of generic parameters for both the GM and GL and for all the participants could influence the between-participants comparison and the between-muscles comparison. As we were interested in the distribution of force between the GM and GL, here,

we discuss only the influence of these generic parameters on the between-muscles comparison. First, the consideration of a similar force-length shape for the GM and GL seems plausible. The force-length shape is, in part, due to the sarcomere structure which is likely similar across muscles. Moreover, a study estimating the force-length relationship from ankle plantar flexion torque and B-mode ultrasound-based measurements of moment arm and fascicle length suggested that the shape of the force-length relationship is similar between the *gastrocnemii* (Maganaris, 2003). The force-length relationship is also influenced by the level of activation (de Brito Fontana & Herzog, 2016; Holt & Azizi, 2014, 2016). Although the level of activation is different between the GM (peak force of 45.0% of $EMG_{max}$ during level walking) and GL (peak force at 34.3% of $EMG_{max}$ during level walking), this difference is relatively low. Therefore, the muscle-difference in the force-length relationship shape related to the muscle-specific activation should be limited. Second, the non-normalized force-velocity relationship shape is influenced, among other parameters, by the fiber length. Most of the studies reported a shorter fiber length for the GM compared to the GL (Albracht et al., 2008; Geremia et al., 2019) which could result in different force-velocity shape (Figure 38). Nevertheless, we normalized the velocity to the fiber length which should cancel out the difference in force-velocity shape between the GM and GL. Moreover, the Hill-type model sensitivity to the force-velocity relationship shape is relatively small (Bujalski et al., 2018; Dick et al., 2017; Scovil & Ronsky, 2006) which limits the influence of a generic force-velocity shape on the distribution of force between the GM and GL. For example, Dick et al., (2017) performed a sensitivity analysis on the maximum shortening velocity (from 4 to 10 optimal fiber length per s while we used a generic value of 7.5 optimal fiber length per s) and force-velocity curvature (from 0.155 to 0.315 while we used a generic value of 0.235). The results of this sensitivity analysis showed that the maximal shortening velocity had a negligeable influence on the prediction of force. The Hill-type model was sensitive to the curvature of the force-velocity relationship but we used the value that predict the most accurate force compared to a force estimated using tendon length changes (Dick et al., 2017). Third we used a generic specific tension of 22.5 $N.cm^2$. Based on the data from guinea pig muscles combined with the similarities of muscle fiber composition between the GM and GL in humans demonstrate, it seems plausible to assume a similar specific tension between the GM and GL. Taken together, the methodological considerations relative to the use of the same generic input for the GM and GL would influence only in a small extent the distribution of force between these muscles within a participant.

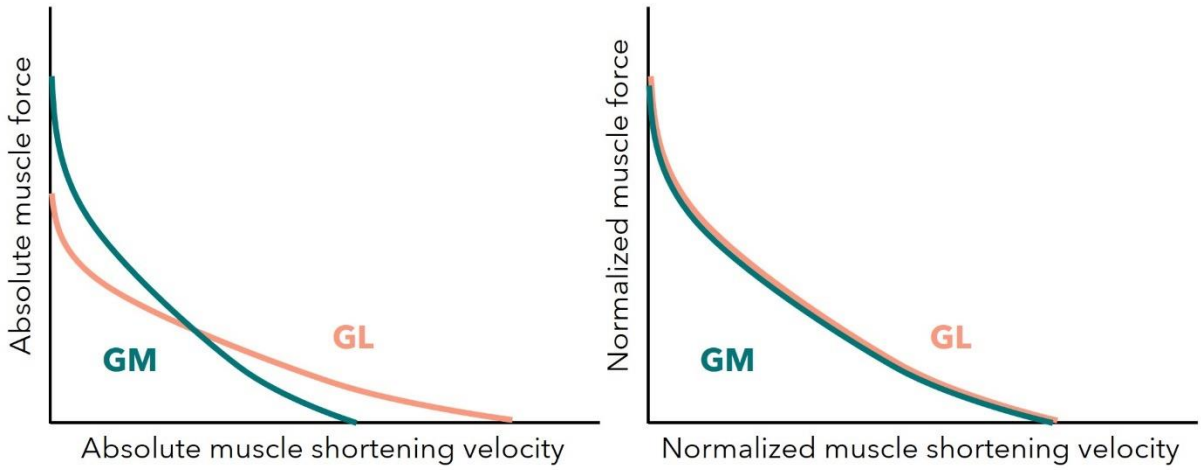


**Figure 38: Illustration of the hypothetical differences between the *gastrocnemius medialis* and *gastrocnemius lateralis* force-velocity shapes.** The *gastrocnemius medialis* (GM) has generally shorter fiber length compared to the *gastrocnemius lateralis* (GL). This results in a lower shortening velocity potential for the GM compared to the GL. Nevertheless, the normalization of the fascicle velocity to the fiber length cancel out the difference between the GM and GL.

### 1.3.2. Optimal fiber length

Within the Hill-type model, we also used experimental substitutes for optimal fiber length owing to experimental limitations in measuring this parameter. As explained above, the experimental determination of the force-length relationship is challenging and we did not determine this relationship for each individual in our study. Therefore, the optimal fiber length, which corresponds to the fiber length that enables maximal active force, was unknown. Using torque-based measures, a study estimated that the optimal fiber length of the GM occurs at relatively long muscle length in humans, specifically at 15° of knee angle and 19° of ankle dorsiflexion (Hoffman et al., 2012). In the Hill-type model considered in Study #2, the optimal fiber length is used to normalize the dynamic fascicle length and velocity values. For this purpose, we used the length at heel-strike as a substitute, as done by Clark et al. (2020). During walking, at heel-strike, the knee is flexed at ~8° whereas the ankle is slightly dorsiflexed ~8° (Arnold & Delp, 2011). As the knee angle influences the *gastrocnemii* fascicle length to a lesser extend compared to the ankle angle (Kawakami et al., 1998), fascicle length at heel-strike could slightly underestimate the optimal fiber length (Hoffman et al., 2012). Nevertheless, the studies using buckle-type force transducer and optic fiber techniques during walking showed that the Achilles tendon force began to rise quickly after heel-strike while the *triceps surae* muscles was not yet active (Finni et al., 1998; Komi, 1990). This suggests that the fiber length at heel-strike is close to optimal fiber length. More importantly, evidences suggested similarities

between the GM and GL force-length relationships. For instance, a previous work estimating the optimal fiber length from torque-length relationship suggested that the optimal fiber length of the GM and GL occurred at similar angle (Maganaris, 2003). Later another study found results that go in the same direction using shear wave elastography (Le Sant et al., 2017). This study measured the slack angle, i.e. the angle from where passive tension begins to rises (Herbert et al., 2002) for the GM and GL. As theoretically the passive force begins to rise at the optimal fiber length, the slack angle is sometimes considered as an indicator of the optimal fiber length. The authors reported that the slack angles of the GM (24° of ankle plantar flexion with the knee extended) and GL (23.5° of ankle plantar flexion with the knee extended) are very similar (Le Sant et al., 2017). Together these studies suggests that the optimal fiber lengths of the GM and GL occur at the same joint angle. Therefore, at heel-strike, both muscles are likely at the same relative length with respect to their force-length relationship. As a consequence, the GM and GL could be influenced to the same extent by this estimation which should not greatly affect our main results focusing on the distribution of force between these two muscles.

Theoretically, the optimal fascicle length is also used to determine the PCSA. For the PCSA calculation, we used the fiber length obtained using DTI as a substitute for optimal fiber length. For the DTI measurement, participants had the knee slightly flexed (< 5°) and the ankle angle in a neutral position (0° of dorsiflexion). In a similar way to the fascicle length at heel-strike, the fascicle length measured using the DTI might slightly underestimate the optimal fascicle length (Hoffman et al., 2012; Maganaris, 2003). This could result in a overestimation of the PCSA and interfere with our muscle force prediction. Nevertheless, as explained above, the GM and GL are likely at the same relative length during the DTI measurement. This approximation should affect the GM and GL PCSA to the same extent. In other words, the absolute value of force predicted can be affected by this estimation but the ratio of force between the two muscles in which we were interested should be influenced in a smaller extent. Besides, our PCSA data (47.6 ± 10.7 $cm^2$ and 26.1 ± 7.4 $cm^2$ for the GM and GL, respectively) are comparable to those found in the literature (~ 50 $cm^2$ and ~ 27 $cm^2$ for the GM and GL, respectively; Table 1). Together, the limitation related to the lack of experimental method available to measure the optimal fiber length should be considered to interpret our absolute data. Although, our estimations can be different to the optimal fiber length, the GM and GL are likely at similar relative lengths which limits the influence on our interpretation concerning the distribution of force between the GM and GL.

# 2. Synthesis of the results

## *2.1.* The neural control of the *gastrocnemii*

### 2.1.1. Neural control of the *gastrocnemius medialis* and *gastrocnemius lateralis*

The central nervous system uses the neural command to generate a particular muscle coordination strategy and thereby to reach a required joint moment. It is often considered that the GM and GL are activated in a similar way. For example, previous modelling and simulation studies used a single *gastrocnemius* component without distinguishing the GM and the GL (Kutch & Valero-Cuevas, 2011; Neptune et al., 2001; van Ingen Schenau et al., 1987). The results from this PhD thesis further confirm that the activation between muscles from the same anatomical group are not evenly distributed, even between similar muscles such as the GM and GL. Specifically, we found that activation levels in the GM are nearly twice as high as the GL during isometric ankle plantar flexion tasks and walking. The extent of this muscle difference is consistent with previous studies (Ahn et al., 2011; Crouzier et al., 2019a; Kinugasa et al., 2005; Masood et al., 2014). Here, we further showed that the higher GM activation compared to the GL persisted during isometric knee flexion. The different activation levels between the two muscles highlight that the GM and GL are distinct muscles which is confirmed by the analyses of fascicle contractile behavior and muscle force.

The consideration of the common synaptic input between the *gastrocnemii* further suggested that the GM and GL can be controlled (partly) independently by the central nervous system. Importantly, the common synaptic input and the distribution of activation are not necessarily related. Specifically, two muscles can receive different amplitude of muscle activation while they receive an important level of common synaptic input and *vice versa*, as shown in the *vastus lateralis* and *vastus medialis* (Avrillon et al., 2021). Our results confirmed recent studies that reported a low level of common synaptic input between the GM and GL during ankle plantar flexion (Hug et al., 2021b; Levine et al., 2022; Rossato et al., 2022). We extended these studies by showing that the level of common synaptic input between the GM and GL remained low during knee flexion. Despite a minority of participants (4 out of 9 participants) exhibited a significant coherence during either knee flexion or ankle plantar flexion, the average level coherence was relatively low compared to the high coherence values observed for other anatomically-defined synergist muscles, e.g. the *vastus lateralis* and *medialis*. (Avrillon et al., 2021). Our data can also informed on the modulation of common synaptic input across tasks.

A recent study reported data on common synaptic input across different motor tasks (Levine et al., 2022). However, these motor tasks were ankle plantar flexion at different ankle angle. Of note, this study observed a robust level of common synaptic between input the GM and GL across different ankle angle (Levine et al., 2022) which is consistent with our results. The two tasks considered in the Study #3, i.e. knee flexion and ankle plantar flexion are more different than the tasks used Levine et al., (2022). This suggests that the study of biarticular muscles is a powerful model to examine the modulation of common synaptic input during different tasks with substantially different mechanical constraints. Further studies could be performed on other biarticular synergist, such as the hamstrings muscles, to determine whether the robustness of common synaptic input across tasks is common to all biarticular muscles or specific to the *gastrocnemii*.

### 2.1.2. Inter-individual variability in the neural control of the gas*trocnemius medialis* and *gastrocnemius lateralis*

We reported a high level of inter-individual variability in the distribution of activation between the GM and GL during walking, isometric ankle plantar flexion and isometric knee flexion. For example, during submaximal isometric contractions, the GM/(GM+GL) ratio of activation ranged from 44.8% to 85.5% and from 48.5% to 89.9% for knee flexion and ankle plantar flexion, respectively. Most of the participants activated their GM more, sometimes to a very large extent, whereas other participants activated their GL more. Previous studies reported that the distribution of activation is correlated to the distribution of PCSA (Crouzier et al., 2018; Hug et al., 2015a). Therefore, the origin of the inter-individual variability in the distribution of activation can be linked to the individual distribution of muscle force-generating capacity. The neuromechanical coupling could also explain that the distribution of activation persists across knee flexion and ankle plantar flexion. Indeed, the distribution of PCSA between the GM and GL remained unchanged across knee flexion and ankle plantar flexion which could result in a consistent distribution of activation. However, to provide further support for the existence of a neuromechanical coupling, it is important to develop studies where the distribution of force-generating capacity will be experimentally modified through, for example, a chronic electro-myo-stimulation protocol targeted to one of the two synergist muscles.

In addition to the highly individual distribution of muscle activation, we observed a relatively high level of inter-individual variability in the common synaptic input between the GM and GL. A previous study had initially reported large inter-individual variability in the common

synaptic input between the *vastus lateralis* and *vastus medialis muscle* (Avrillon et al., 2021). Importantly, this study also revealed that the individual level of common synaptic input was reliable across two sessions separated by 20 month. This suggested that the inter-individual variability reported was a physiological variability and was not related to noise or methodological considerations. The origin of the inter-individual variability in the common synaptic input remains unclear. It is possible that the motor history experienced by each individual determines in part the inter-individual variability observed. However, to date, no data are available to support this hypothesis. Furthermore, we revealed that the changes in common synaptic input between knee flexion and ankle plantar flexion was highly variable between participants. For example, among the 9 participants, two participants exhibited a significant level of coherence across tasks, four participants had a non-significant level of coherence regardless of the task, two participants had a significant level of coherence in knee flexion but not in ankle plantar flexion and one had a significant level of coherence in ankle plantar flexion but not in knee flexion. Therefore, a third of the participants exhibited a flexible common synaptic input across tasks. To the best of our knowledge, this is the first report of inter-individual variability in the modulation of common synaptic input across different tasks.

## 2.2. Mechanical consequences of the distribution of activation

### 2.2.1. Fascicle contractile behavior

One of the main aims of this PhD thesis was to contribute to the understanding of the muscle-specific contractile behavior in the *triceps surae* during walking. Previous works reported differences in contractile behavior between the GM and the *soleus* (Cronin et al., 2013; Ishikawa et al., 2005). Nevertheless, these established differences are likely influenced by the fact that the GM behavior depends on both the knee angle and the ankle angle during walking whereas the *soleus* behavior depends only on the ankle angle. To extend these studies, we examined the contractile behavior of the GM and GL which have similar anatomical function. Our results showed that the contractile behavior, just like muscle activation, is different between the GM and GL. Moreover, we found that the timing of the between muscles difference in fascicle length changes (i.e. the fascicle lengthening period, from around 10% to 30% of the walking cycle) matches the timing of the between muscles difference in muscle activation (i.e. from 18% to 36% of the walking cycle). As a consequence, our results revealed that two *triceps surae* muscles can have distinct contractile behaviors despite a similar anatomical function.

One of the novelties of this PhD thesis lies in the description of large inter-individual variability across multiple scales of muscle coordination. Although inter-individual variability in muscle activation have been previously reported (Ahn et al., 2011; Crouzier et al., 2019a), we have shown that this extends to the contractile behavior of the muscle. For example, some participants demonstrated a concentric behavior of the fascicles from the GM and GL during the stance phase of walking whereas fascicles from other participants exhibited a stretch-shortening cycle (Figure 39). This large inter-individual variability in fascicle contractile behavior likely originates from various factors. First, the muscle activation influences the fascicle behavior and tends to cause a fascicle shortening. The large inter-individual variability in the distribution of activation likely results in individual-specific fascicle contractile behavior. Second, the muscle fascicle behavior is affected by the mechanical properties of the tendon to which it is attached (Griffiths, 1991). For example, a stiffer tendon limits the shortening of an activated muscle fascicle compared to a compliant tendon. Previous studies reported that the Achilles tendon stiffness varies greatly between individuals (Yin et al., 2021). This likely plays a role in the observed inter-individual variability in muscle contractile behavior. The muscle behavior is also affected by the joint angle and more generally the overall kinematics (Kawakami et al., 1998). This kinematics is also highly individual (Horst et al., 2016) and could contributes to the inter-individual variability in fascicle contractile behavior.

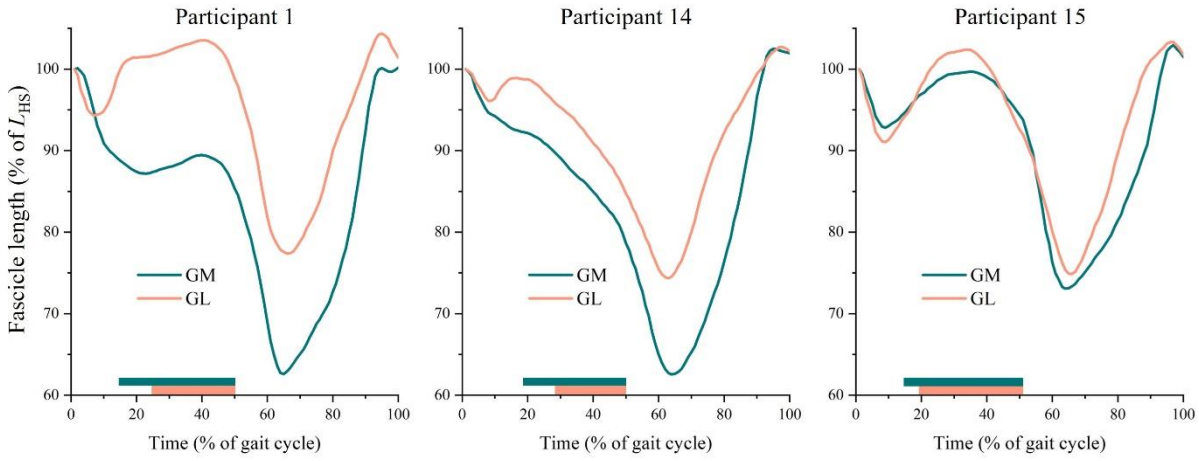


**Figure 39: Illustration of the inter-individual variability in fascicle contractile behavior.** The three panels represent three different participants. For each participant, the fascicle length of the *gastrocnemius medialis* (GM; green curve) and *gastrocnemius lateralis* (GL; orange curve) are displayed. The rectangles at the bottom of the panel represent the period where the normalized electromyography of the GM (green rectangle) and GL (orange rectangle) exceed 10% of maximal electromyography value determined during maximal voluntary contraction. The participant 1 exhibits substantial difference between the GM and GL fascicle length changes. The GM and GL fascicles of the participant 14 exhibit a concentric behavior during

the activation period. On the contrary, the GM and GL fascicles of the participant 14 undergo a stretch-shortening cycle during the activation period. $L_{HS}$, fascicle length at heel-strike.

## 2.2.2. Production of force

We also examined the consequence of the distribution of activation in terms of distribution of force. It appears important to consider the distribution of force rather than the distribution of activation to avoid any misinterpretation of muscle coordination (Hug et al., 2015b). The Figure 40 displays an example where a wrong interpretation could be done based on EMG data alone. Specifically, for this participant, the EMG signal suggest a balanced activation while the subject-specific Hill-type model reveals a large difference of muscle force towards the GM.

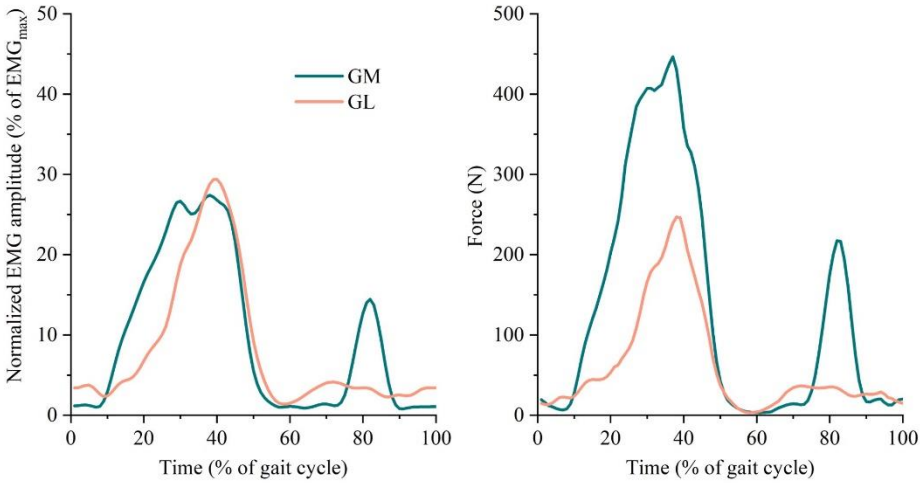


**Figure 40: Muscle activation and force of the *gastrocnemius medialis* and *gastrocnemius lateralis* during walking for a single participant.** The left panel represents the normalized electromyography (EMG) of the *gastrocnemius medialis* (GM; green curve) and *gastrocnemius lateralis* (GL; orange curve). The right panel represents the predicted force of the *gastrocnemius medialis* (GM) and *gastrocnemius lateralis* (GL) for the same participant (Participant 1).These two panels illustrate that the muscle force cannot be inferred from activation. Based on activation only, an evenly distributed muscle coordination between the GM and GL could be hypothesized. Nevertheless, when considering the main force determinants via a Hill-type model, it appears that the muscle coordination is largely biased towards the GM. $EMG_{max}$, maximal EMG level estimated during maximal isometric contraction.

Our results showed that the distribution of force between the GM and GL during walking was biased towards the GM for all the participants. The systematic higher GM force compared to the GL is related to the distribution of activation between the *gastrocnemii* but also to the distribution of maximal force-generating capacity which was higher in the GM compared to the GL for all the participants. We showed that the GM had a substantial functional role during

walking producing on average a peak force of 346 ± 137 N during the stance phase, whereas the contribution of GL was much less, producing on average a peak force of 128 ± 55 N of force during the stance phase of preferred speed walking. Combining our results with the overall Achilles tendon force previously measured during walking using a buckle-type force transducer (Finni et al., 1998), we can estimate that the GM and GL likely contributes to 27% and 10% of the Achilles tendon force, respectively. Taken together, these results suggest a limited involvement of the GL during walking at preferred speed.

The combination of the inter-individual variability in muscle activation, maximal force-generating capacity and contractile behavior results in highly individual muscle coordination between the GM and GL during walking. Specifically, we observed very different time-varying patterns of force and distributions of force between the GM and GL during walking (Figure 41). This extends previous work that suggested, based on muscle activation and PCSA, that the muscle coordination varied greatly between participants during isometric tasks (Avrillon et al., 2018; Crouzier et al., 2019a).

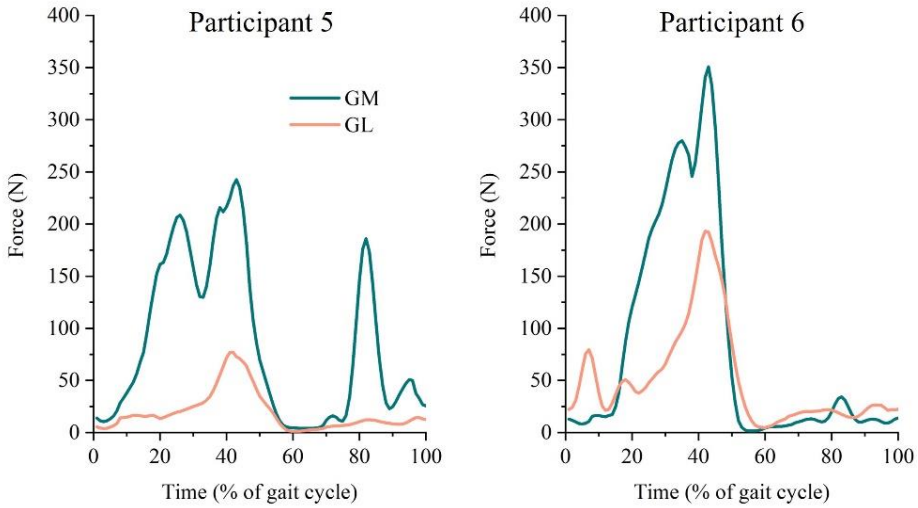


**Figure 41: Illustration of different patterns of force during walking for two participants.** For each participant, the panel depicts the force produced by the *gastrocnemius medialis* (GM; green) and the force produced by the *gastrocnemius lateralis* (GL; orange). Each participant exhibits a specific time-varying force pattern. For example, the Participant 5 produces very low amount of force with its GL. Interestingly, he produces also a second burst of force during swing phase for the GM. The Participant 6 has a more evenly distributed force between the GM and the GL.

# 3. Functional implication of muscle coordination

## 3.1. The relationship between individual muscle coordination and musculoskeletal disorders

The majority of studies in human movement focused on group mean values and neglect the individual data which limits our understanding of such levels of inter-individual variability. Our results together with previous studies demonstrate that muscle coordination is specific to an individual (Aeles et al., 2021b; Crouzier et al., 2019a; Hug et al., 2019). This raises the question of the functional consequences of the individual muscle coordination strategy. Researchers have hypothesized that individual muscle coordination might play a role in the development or persistence of musculoskeletal disorders (Hug & Tucker, 2017). They suggested that the individual muscle coordination can have specific mechanical effects on the structures of the musculoskeletal system. For example, the individual muscle coordination between the *triceps surae* muscles or between the *vastii* could induce specific mechanical effect on the Achilles tendon and patella, respectively (Hug & Tucker, 2017). Despite some individuals could have a muscle coordination strategy which is optimal and which preserves the musculoskeletal system, other individuals could adopt a muscle coordination strategy which make them at risk of developing musculoskeletal disorders. This echoes other works that have reported distinct muscle activation strategies in participant with musculoskeletal disorders compared to controls (MacDonald et al., 2009; Pal et al., 2012; Witvrouw et al., 2014). For example, the patellar tilt correlated with the ratio of activation between the *vastus lateralis* and *vastus medialis* in patient suffering from patellofemoral pain (Pal et al., 2012). This suggested that the distribution of activation between the *vastii* could influence the load applied on the patella. However, as shown in the Figure 40, the muscle activation provides only a crude estimation of muscle coordination (Hug et al., 2015b).

Recent studies provided more robust evidence on the relationship between muscle coordination and musculoskeletal disorder (Avrillon et al., 2020; Crouzier et al., 2019b). For example, Crouzier et al. (2019b), revealed that patients suffering from Achilles tendinopathy had a specific muscle coordination strategy within the *triceps surae* compared to healthy controls. Specifically, the GL contributed even less to the *triceps surae* force in participants with Achilles tendinopathy compared to controls (Figure 42). Previous evidences suggested that the distribution of force within the *triceps surae* muscles have a specific influence on the Achilles

subtendon displacements, strains and loads (Arndt et al., 1999; Arndt et al., 1998; Finni et al., 2018; Handsfield et al., 2017). As a consequence, the specific muscle coordination strategy observed in Achilles tendinopathy patients could induce a sub-optimal distribution of load or shear forces between subtendons. This could lead to the development of an Achilles tendinopathy (Bojsen-Møller & Magnusson, 2015; Magnusson et al., 2010; Sun et al., 2015). Together, these studies suggest that the muscle coordination within the *triceps surae* might play a role in the development and persistence of the Achilles tendinopathy. Nevertheless, it remains unknown whether the muscle coordination was the cause or the consequence of the Achilles tendinopathy. In other words, the cross-sectional study of Crouzier et al. (2019b) cannot determine whether muscle coordination has generated the Achilles tendinopathy or whether the Achilles tendinopathy have altered an initial muscle coordination strategy. The subject-specific modelling approach that we used in Study #2 could be a powerful approach to study the relationship between muscle coordination and musculoskeletal disorder. For example, longitudinal and prospective studies using a subject-specific approach are able to provide useful information to determine whether the altered muscle coordination strategy is a cause or a consequence of the musculoskeletal disorder.

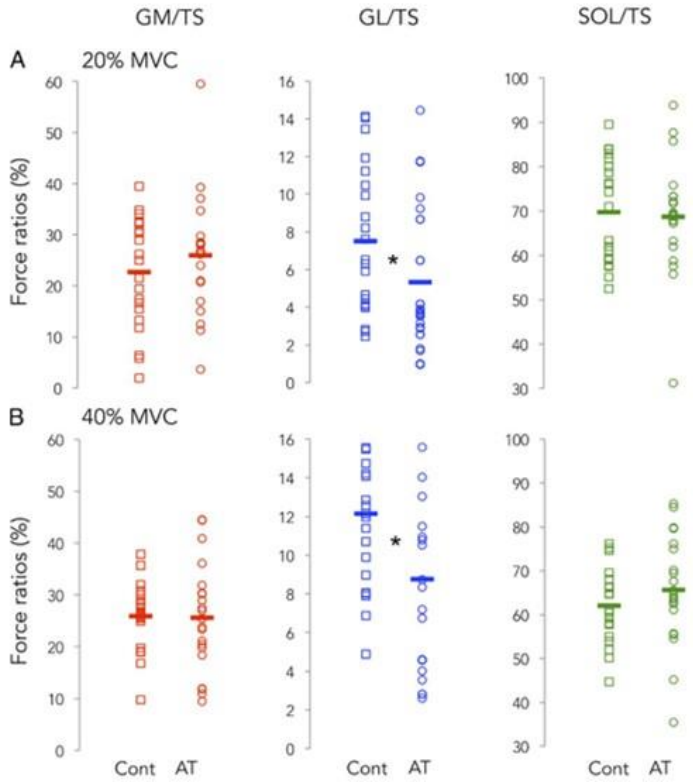


**Figure 42: Contribution to the *gastrocnemius medialis*, *gastrocnemius lateralis* and *soleus* to muscle coordination within the *triceps surae* in Achilles tendinopathy patients and healthy controls.** A and B represent muscle coordination at 20% and 40% of ankle plantar flexion maximal voluntary contraction, respectively. The force is calculated from the muscle activation recorded during the submaximal isometric contraction and the physiological cross-

sectional area. The authors found a significant difference between Achilles tendinopathy patients and healthy controls for the *gastrocnemius lateralis* contribution. AT, Achilles tendinopathy group, Cont, control group; GL, *gastrocnemius lateralis*; GM, ga*strocnemius medialis*; MVC, maximal voluntary contraction; SOL, *soleus*; TS, *triceps surae*. From Crouzier et al., (2019b).

## 3.2. The role of the *gastrocnemius lateralis*

The relatively low contribution of GL to the force produced by the *triceps surae* during submaximal tasks raises the question of the functional role of the GL. Although its PCSA is small compared to the GM and *soleus*, the GL has a higher PCSA compared to other lower limb muscles such as the *tibialis anterior* or *tibialis posterior* (Charles et al., 2019; Fukunaga et al., 1992; Ward et al., 2009). It is very unlikely that humans kept such muscle over the evolution process if it has a negligible functional role. The relatively low activation of the GL almost always observed might be related to the task features that we classically use in human research, i.e. submaximal isometric tasks or locomotor tasks. During these tasks, the central nervous system might favor the GM and *soleus* activation compared to the GL to generate the required joint moment in an economical way. Specifically, a distribution of activation biased towards the GM and *soleus* rather than towards the GL enables to reach the required joint moment while minimizing the overall activation cost and fatigue (Crouzier et al., 2018). The GL architecture has rather a greater velocity potential compared to the GM and *soleus* (Lieber & Fridén, 2000). It could be interesting to determine whether the GL has more important role during tasks that require more velocity. Furthermore, the commonly used tasks in human research (i.e. treadmill walking or isometric contraction) generally limit the need to control the ankle torque in the frontal plane. The GL plays a key role in this modulation of the torque in the frontal plane (Lee & Piazza, 2008; Wolfram, 2017). As a consequence, more various locomotor tasks that requires change of directions would reveal a more substantial role of the GL.

## 3.3. The biarticular action of the *gastrocnemii*

This PhD thesis also aimed to examine the functional role of the GM and GL during knee flexion. Although the GM and GL are biarticular muscles, the large majority of previous studies have focused on their role in ankle plantar flexion. This is likely because the *gastrocnemii* are able to produce higher torques during ankle plantar flexion compared to knee flexion (Landin et al., 2016). This difference in torque-generating capacity between knee flexion and ankle plantar flexion originates from different mechanical advantages of the *gastrocnemii* across the

joints. At the knee, the *gastrocnemii* act as a third-class lever with a lower mechanical advantage compared to their second-class lever action at the ankle. This results in very different moment arm at the knee (i.e.~15-30 mm depending on the knee angle) and at the ankle (i.e. 40-60 mm depending on the ankle angle; Buford et al., 1997; Spoor et al., 1990). Therefore, it is sometimes considered that the GM and GL are mostly useful at the knee to make the joint more stable and to prevent injuries (Li et al., 2002). Nevertheless, our data revealed that the *gastrocnemii*, especially the GM, are substantially activated during a knee flexion task. For instance, at 40% of knee flexion MVC, the *gastrocnemii* are activated at 16.9% ± 12.2% of maximal EMG determined during MVC. In comparison, the *gastrocnemii* are activated at 22.4% ± 8.6% for the same relative torque during ankle plantar flexion. Further studies are required to better understand the functional role of the GM and GL at the knee.

The study of knee flexion also enables a better understanding on the joint-specific neural control of the GM and GL. Previous studies have reported joint-specific regional activation in biarticular muscles. Specifically, evidence suggested that the proximal region of the *rectus femoris* is preferentially activated during hip flexion whereas the distal part is more activated during knee extension (Miyamoto et al., 2012; Watanabe et al., 2016). A recent study hypothesized that the activation of the GM can be regionally modulated between knee flexion and ankle plantar flexion in a similar way (Watanabe et al., 2021b). This hypothesis was based on data suggesting possible regional activation in the *gastrocnemii* (Hodson-Tole et al., 2013; Vieira et al., 2011; Wolf et al., 1993). Our results are not in line with this hypothesis. Despite we found a difference between knee flexion and ankle plantar flexion in the regional activation of the *gastrocnemii*, the effect size of this difference was very small. Moreover, the analysis at the motor unit level did not confirm the difference. As a consequence, we concluded that there was no substantial joint-specific regional activation in the GM and GL. This conclusion is in line with a previous intra-muscular EMG study revealing that the GM motor units recruited either in knee flexion or ankle plantar flexion had no specific regional location (Héroux et al., 2015). The discrepancy between the *rectus femoris* and the *gastrocnemii* could be related to the compartmentalization of the biarticular muscle. Previous studies reported the presence of distinct neuromuscular compartments in human muscles (Segal et al., 1991; Wolf & Kim, 1997). These different neuromuscular compartments have specific muscle architecture and are innervated by distinct nerve branch that can enable a muscle activation specific to the compartments. For example, the *rectus femoris* has different neuromuscular compartments that can be favor regional activation specific to the joint used (Watanabe et al., 2021b). Although

previous studies reported regional activation in the GM and GL (Hodson-Tole et al., 2013; Vieira et al., 2011; Wolf et al., 1993), the GM is not compartmentalized (Wolf & Kim, 1997) and the architectural compartments of the GL are not necessarily innervated in an independent manner (Segal et al., 1991). Moreover, the architectural compartments does not separate the GL into proximal and distal subsections but rather in medial and lateral or deep and superficial subsections (Segal et al., 1991). This could be the reason why we did not find joint-specific regional activation in this muscle. Together, our results suggest that a biarticular muscle does not have necessarily a joint-specific regional activation, even when it has architectural compartments such as the GL.

## 3.4. The determinants of muscle coordination

In this PhD thesis, we examined the influence of different mechanical constraints such as knee flexion and ankle plantar flexion on muscle coordination between the GM and GL. The investigation of muscle coordination under different mechanical constraints can provide information about the factors considered by the central nervous system to choose a specific coordination strategy. Our data revealed that the neural control of the GM and GL was robust across knee flexion and ankle plantar flexion tasks. This confirms a previous study that report consistent distribution of muscle activation between the GM and GL across a submaximal isometric task, walking and pedaling (Crouzier et al., 2019a). We hypothesized that such robustness is due to the neuromechanical coupling. The neuromechanical coupling could be a strategy used by the central nervous system to distribute the force among synergist muscles in an economical way. Specifically, a distribution of activation which is proportional to the distribution of PCSA between muscles enables to decrease the overall activation cost and more generally the metabolic cost (Crouzier et al., 2018). This is in agreement with a previous study showing that the central nervous system is able to increase the activation of the *first dorsal interosseous* to take advantage of an higher mechanical advantage related to thumb posture (Hudson et al., 2009). Moreover, the neuromechanical coupling echoes previous theoretical works suggesting that the muscle coordination strategy is chosen such that muscle stress (Crowninshield & Brand, 1981b) or the fatigue (Dul et al., 1984) is minimized. Together, these evidences suggest that the central nervous system might consider the maximal force-generating capacity to distribute the force among synergist muscles.

Our data contradicts previous animal studies that show a large flexibility of muscle coordination between the GM and *soleus* across tasks (Herzog, 1998; Herzog et al., 1993; Walmsley et al.,

1978). This discrepancy between the muscle coordination in cats and our data likely originates for two main reasons. The first one lies in the variety of the tasks studied. Herzog and collaborators (1993, 1998) studied a wide variety of tasks such as walking at different speeds, at different incline grades, paw shaking and standing. In this PhD, we only studied muscle coordination between the GM and GL during walking and submaximal isometric tasks. The use of more diverse tasks could lead to the observation of more flexible muscle coordination between the GM and GL. As explained previously, tasks that requires more speed or more eversion and inversion of the ankle could lead to a more balanced muscle coordination between the GM and the GL. The second reason explaining the discrepancy between our data and the data from previous animal studies might be related to the difference in muscle fiber composition of the muscles. The GM of the cat has a mixed population of muscle fiber whereas the *soleus* of the cat is mainly composed of slow muscle fibers. The central nervous system of the cat likely considered this difference in muscle fiber composition to distribute the force between the GM and *soleus* (Herzog et al., 1993; Walmsley et al., 1978). On the contrary, the two muscles that we studied (i.e. GM and GL) have a similar muscle fiber composition (Edgerton et al., 1975; Johnson et al., 1973). This similarity between the GM and GL muscle fiber composition may play a role in the robustness of muscle coordination that we reported. This is in agreement with the analysis of muscle coordination between the GM and *plantaris* in the cat (Herzog et al., 1993). The GM and *plantaris* of the cat have more similar muscle fiber composition and this resulted in more robust coordination across tasks compared to muscle coordination between the GM and *soleus* (Figure 43). Taken together, these studies suggest that the central nervous system could consider different muscle properties, such as muscle fiber composition or PCSA, to distribute the force between synergist muscles. The central nervous system might favor the muscle with with the larger PCSA and with the higher proportion of slow muscle fiber to minimize the fatigue (Dul et al., 1984).

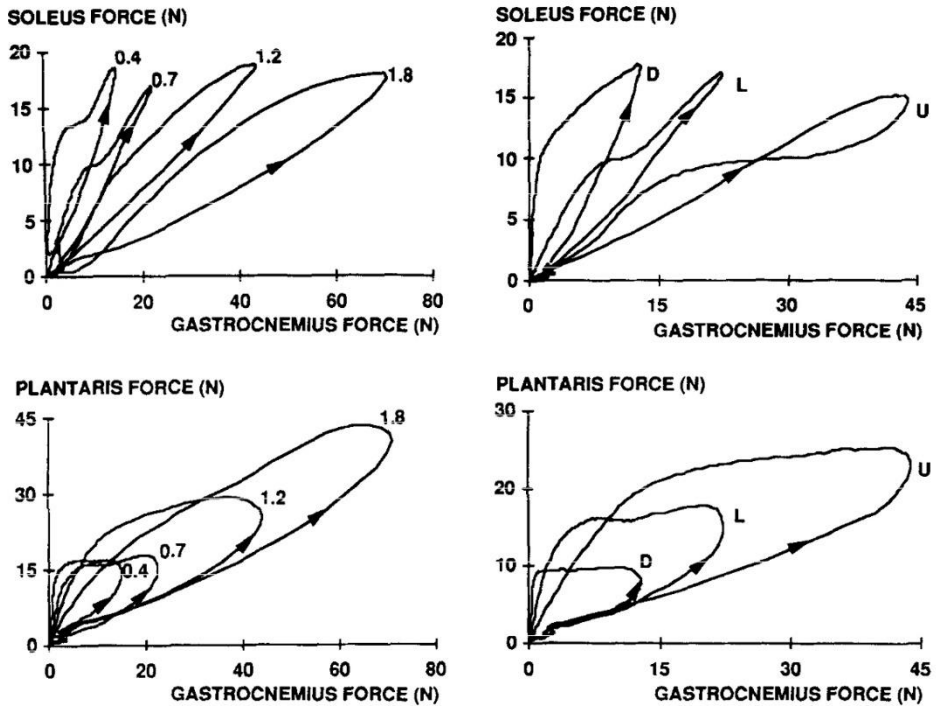


**Figure 43: Muscle coordination between the *gastrocnemius medialis* and *soleus* and between the *gastrocnemius medialis* and *plantaris* cat muscles.** The top panels represent muscle coordination between the *gastrocnemius medialis* and *soleus* at different walking speed (left panel) and different incline grades (right panel). The bottom panels represent muscle coordination between the *gastrocnemius medialis* and *plantaris* at different walking speed (left panel) and different incline grades (right panel). The muscle coordination between the *gastrocnemius medialis* and the *soleus* is flexible depending on the task. On the contrary, the muscle coordination between the *gastrocnemius medialis* and the *plantaris* is more robust across tasks. On the left panels, 0.4, 0.7, 1.2 and 1.8 correspond to the walking speed in $m.s^{-1}$. On the right panels, D, L and U correspond to downhill, level and uphill walking. From Herzog et al. (1993).

# 4. General conclusion

In this PhD thesis, we used an approach that combined neurophysiological recordings, muscle imaging and muscle modelling to provide a deeper understanding of muscle coordination between the GM and GL under different mechanical constraints. First, the results from this PhD contribute to advance our knowledge concerning the muscle-specific neuromechanical behavior within a muscle group. Specifically, we found that two muscles with the same anatomical function (i.e knee flexion and ankle plantar flexion) can have different contractile behaviors depending on their activation patterns during walking. This specific neuromechanical behavior likely enhances the catapult-like mechanism in the GM compared to GL. Combined with the between-muscle differences in PCSA, this results in a distribution of force largely biases toward the GM compared to the GL. To better understand the functional role of the GL in human movement, more varied movement tasks should be investigated.

Second, this PhD thesis expands our knowledge regarding the inter-individual variability in human movement. We provide evidence that the individual muscle activation strategies during walking were associated with large inter-individual variability in maximal force-generating capacity, fascicle contractile behavior and muscle force distribution. As a consequence, large inter-individual variability can be observed across multiple scales of the production of movement.

Third, we presented an approach using a muscle model that aims to consider the individual variability in muscle coordination. Recent studies have suggested that individual muscle coordination can be associated with musculoskeletal disorder (Avrillon et al., 2020; Crouzier et al., 2019b). However, these studies considered only muscle activation, PCSA and isometric contraction. Here, we provide a framework that combines subject-specific experimental measures with muscle models that can be a key method to further explore whether the altered muscle coordination pattern is the cause or consequence of the musculoskeletal disorder.

Fourth, this PhD work provides insight into the influence of mechanical constraints on muscle coordination. The different mechanical constraints induced by isolated knee flexion and ankle plantar flexion had a small influence on the muscle activation strategies used to control the biarticular GM and GL. Moreover, the common synaptic input between the two muscles remained relatively low across knee flexion and ankle plantar flexion. Further work are required to determine whether a modulation of common synaptic input specific to the joint in biarticular muscle is consistent across all muscle groups or is unique to the *gastrocnemii*.

# BIBLIOGRAPHY

Adrian, E. D., & Bronk, D. W. (1929). The discharge of impulses in motor nerve fibres. *The Journal of Physiology*, *67*(2), i3-151.

Aeles, J., Bolsterlee, B., Kelp, N. Y., Dick, T. J. M., & Hug, F. (2021a). Regional variation in lateral and medial gastrocnemius muscle fibre lengths obtained from diffusion tensor imaging. *Journal of Anatomy*.

Aeles, J., Horst, F., Lapuschkin, S., Lacourpaille, L., & Hug, F. (2021b). Revealing the unique features of each individual's muscle activation signatures. *Journal of The Royal Society Interface*, *18*(174), 20200770.

Aeles, J., Lichtwark, G. A., Lenchant, S., Vanlommel, L., Delabastita, T., & Vanwanseele, B. (2017). Information from dynamic length changes improves reliability of static ultrasound fascicle length measurements. *PeerJ*, *5*, e4164.

Aeles, J., Lichtwark, G., Peeters, D., Delecluse, C., Jonkers, I., & Vanwanseele, B. (2018). Effect of a prehop on the muscle-tendon interaction during vertical jumps. *Journal of Applied Physiology*, *124*(5), 1203-1211.

Aeles, J., Sarcher, A., & Hug, F. (2023). Common synaptic input between motor units from the lateral and medial posterior soleus compartments does not differ from that within each compartment. *Journal of Applied Physiology*, *134*(1), 105-115.

Ahn, A. N., Kang, J. K., Quitt, M. A., Davidson, B. C., & Nguyen, C. T. (2011). Variability of neural activation during walking in humans : Short heels and big calves. *Biology Letters*, *7*(4), 539-542.

Ai, Q., Ding, B., Liu, Q., & Meng, W. (2016). A Subject-Specific EMG-Driven Musculoskeletal Model for Applications in Lower-Limb Rehabilitation Robotics. *International Journal of Humanoid Robotics*, *13*(03), 1650005.

Ait-Haddou, R., Jinha, A., Herzog, W., & Binding, P. (2004). Analysis of the force-sharing problem using an optimization model. *Mathematical biosciences*, *191*(2), 111-122.

Albracht, K., Arampatzis, A., & Baltzopoulos, V. (2008). Assessment of muscle volume and physiological cross-sectional area of the human triceps surae muscle in vivo. *Journal of Biomechanics*, *41*(10), 2211-2218. https://doi.org/10.1016/j.jbiomech.2008.04.020

Alexander, R. M., Maloiy, G. M. O., Ker, R. F., Jayes, A. S., & Warui, C. N. (1982). The role of tendon elasticity in the locomotion of the camel (Camelus dromedarius). *Journal of Zoology*, *198*(3), 293-313. https://doi.org/10.1111/j.1469-7998.1982.tb02077.x

Amarantini, D., & Martin, L. (2004). A method to combine numerical optimization and EMG data for the estimation of joint moments under dynamic conditions. *Journal of biomechanics*, *37*(9), 1393-1404.

Anderson, F. C., & Pandy, M. G. (2003). Individual muscle contributions to support in normal walking. *Gait & Posture*, *17*(2), 159-169.

Andrews, J. G. (1974). Biomechanical analysis of human motion. *Kinesiology*, *4*, 32-42.

Arndt, A., Bengtsson, A.-S., Peolsson, M., Thorstensson, A., & Movin, T. (2012). Non-uniform displacement within the Achilles tendon during passive ankle joint motion. *Knee Surgery, Sports Traumatology, Arthroscopy: Official Journal of the ESSKA*, *20*(9), 1868-1874. https://doi.org/10.1007/s00167-011-1801-9

Arndt, A., Brüggemann, G.-P., Koebke, J., & Segesser, B. (1999). Asymmetrical Loading of the Human Triceps Surae : I. Mediolateral Force Differences in the Achilles Tendon. *Foot & Ankle International*, *20*(7), 444-449. https://doi.org/10.1177/107110079902000709

Arndt, A. N., Komi, P. V., Brüggemann, G.-P., & Lukkariniemi, J. (1998). Individual muscle contributions to the in vivo achilles tendon force. *Clinical Biomechanics (Bristol, Avon)*, *13*(7), 532-541.

Arnold, E. M., & Delp, S. L. (2011). Fibre operating lengths of human lower limb muscles during walking. *Philosophical Transactions of the Royal Society B: Biological Sciences*, *366*(1570), 1530-1539. https://doi.org/10.1098/rstb.2010.0345

Avrillon, S., Del Vecchio, A., Farina, D., Pons, J. L., Vogel, C., Umehara, J., & Hug, F. (2021). Individual differences in the neural strategies to control the lateral and medial head of the quadriceps during a mechanically constrained task. *Journal of Applied Physiology*, *130*(1), 269-281. https://doi.org/10.1152/japplphysiol.00653.2020

Avrillon, S., Guilhem, G., Barthelemy, A., & Hug, F. (2018). Coordination of hamstrings is individual specific and is related to motor performance. *Journal of Applied Physiology*, *125*(4), 1069-1079.

Avrillon, S., Hug, F., & Guilhem, G. (2020). Bilateral differences in hamstring coordination in previously injured elite athletes. *Journal of Applied Physiology*, *128*(3), 688-697. https://doi.org/10.1152/japplphysiol.00411.2019

Barber, L., Barrett, R., & Lichtwark, G. (2009). Validation of a freehand 3D ultrasound system for morphological measures of the medial gastrocnemius muscle. *Journal of biomechanics*, *42*(9), 1313-1319.

Barrett, B. (1962). THE LENGTH AND MODE OF TERMINATION OF INDIVIDUAL MUSCLE FIBRES IN THE HUMAN SARTORIUS AND POSTERIOR FEMORAL MUSCLES. *Cells Tissues Organs*, *48*(3), 242-257. https://doi.org/10.1159/000141843

Bernstein, Nicolai A. (1967). *The co-ordination and regulation of movements*.

Besomi, M., Hodges, P. W., Clancy, E. A., Van Dieën, J., Hug, F., Lowery, M., Merletti, R., Søgaard, K., Wrigley, T., Besier, T., Carson, R. G., Disselhorst-Klug, C., Enoka, R. M., Falla, D., Farina, D., Gandevia, S., Holobar, A., Kiernan, M. C., McGill, K., … Tucker, K. (2020). Consensus for experimental design in electromyography (CEDE) project : Amplitude normalization matrix. *Journal of Electromyography and Kinesiology*, *53*, 102438. https://doi.org/10.1016/j.jelekin.2020.102438

Besomi, M., Hodges, P. W., Van Dieën, J., Carson, R. G., Clancy, E. A., Disselhorst-Klug, C., Holobar, A., Hug, F., Kiernan, M. C., Lowery, M., McGill, K., Merletti, R., Perreault,

E., Søgaard, K., Tucker, K., Besier, T., Enoka, R., Falla, D., Farina, D., … Wrigley, T. (2019). Consensus for experimental design in electromyography (CEDE) project : Electrode selection matrix. *Journal of Electromyography and Kinesiology*, *48*, 128-144. https://doi.org/10.1016/j.jelekin.2019.07.008

Biewener, A. A. (1998a). Muscle Function in vivo : A Comparison of Muscles used for Elastic Energy Savings versus Muscles Used to Generate Mechanical Power1. *Integrative and Comparative Biology*, *38*(4), 703-717. https://doi.org/10.1093/icb/38.4.703

Biewener, A. A. (2016). Locomotion as an emergent property of muscle contractile dynamics. *Journal of Experimental Biology*, *219*(2), 285-294. https://doi.org/10.1242/jeb.123935

Biewener, A. A., & Blickhan, R. (1988). Kangaroo rat locomotion : Design for elastic energy storage or acceleration? *Journal of Experimental Biology*, *140*(1), 243-255. https://doi.org/10.1242/jeb.140.1.243

Biewener, A. A., & Corning, W. R. (2001). Dynamics of mallard (Anas platyrynchos) gastrocnemius function during swimming versus terrestrial locomotion. *Journal of Experimental Biology*, *204*(10), 1745-1756. https://doi.org/10.1242/jeb.204.10.1745

Biewener, A. A., Konieczynski, D. D., & Baudinette, R. V. (1998b). In vivo muscle force-length behavior during steady-speed hopping in tammar wallabies. *Journal of Experimental Biology*, *201*(11), 1681-1694. https://doi.org/10.1242/jeb.201.11.1681

Biewener, A. A., & Roberts, T. J. (2000). Muscle and tendon contributions to force, work, and elastic energy savings : A comparative perspective. *Exerc Sport Sci Rev*, *28*(3), 99-107.

Bizzi, E., Cheung, V. C. K., d'Avella, A., Saltiel, P., & Tresch, M. (2008). Combining modules for movement. *Brain Research Reviews*, *57*(1), 125-133. https://doi.org/10.1016/j.brainresrev.2007.08.004

Blemker, S. S., Asakawa, D. S., Gold, G. E., & Delp, S. L. (2007). Image-based musculoskeletal modeling : Applications, advances, and future opportunities. *Journal of Magnetic Resonance Imaging*, *25*(2), 441-451. https://doi.org/10.1002/jmri.20805

Bojsen-Møller, J., & Magnusson, S. P. (2015). Heterogeneous Loading of the Human Achilles Tendon In Vivo. *Exercise and Sport Sciences Reviews*, *43*(4), 190-197. https://doi.org/10.1249/JES.0000000000000062

Bolsterlee, B., D'Souza, A., Gandevia, S. C., & Herbert, R. D. (2017). How does passive lengthening change the architecture of the human medial gastrocnemius muscle? *Journal of Applied Physiology (Bethesda, Md.: 1985)*, *122*(4), 727-738. https://doi.org/10.1152/japplphysiol.00976.2016

Bolsterlee, B., D'Souza, A., & Herbert, R. D. (2019). Reliability and robustness of muscle architecture measurements obtained using diffusion tensor imaging with anatomically constrained tractography. *Journal of Biomechanics*, *86*, 71-78. https://doi.org/10.1016/j.jbiomech.2019.01.043

Bolsterlee, B., Finni, T., D'Souza, A., Eguchi, J., Clarke, E. C., & Herbert, R. D. (2018). Three-dimensional architecture of the whole human soleus muscle in vivo. *PeerJ*, *6*, e4610. https://doi.org/10.7717/peerj.4610

Bolsterlee, B., Gandevia, S. C., & Herbert, R. D. (2016). Effect of Transducer Orientation on Errors in Ultrasound Image-Based Measurements of Human Medial Gastrocnemius Muscle Fascicle Length and Pennation. *PloS One*, *11*(6), e0157273. https://doi.org/10.1371/journal.pone.0157273

Bolsterlee, B., Vardy, A. N., van der Helm, F. C. T., & (DirkJan) Veeger, H. E. J. (2015a). The effect of scaling physiological cross-sectional area on musculoskeletal model predictions. *Journal of Biomechanics*, *48*(10), 1760-1768. https://doi.org/10.1016/j.jbiomech.2015.05.005

Bolsterlee, B., Veeger, H. E. J. D., van der Helm, F. C. T., Gandevia, S. C., & Herbert, R. D. (2015b). Comparison of measurements of medial gastrocnemius architectural parameters from ultrasound and diffusion tensor images. *Journal of Biomechanics*, *48*(6), 1133-1140. https://doi.org/10.1016/j.jbiomech.2015.01.012

Bottinelli, R., Canepari, M., Pellegrino, M. A., & Reggiani, C. (1996). Force-velocity properties of human skeletal muscle fibres : Myosin heavy chain isoform and temperature dependence. *The Journal of Physiology*, *495*(2), 573-586. https://doi.org/10.1113/jphysiol.1996.sp021617

Bottinelli, R., Pellegrino, M. A., Canepari, M., Rossi, R., & Reggiani, C. (1999). Specific contributions of various muscle fibre types to human muscle performance : An in vitro study. *Journal of Electromyography and Kinesiology*, *9*(2), 87-95. https://doi.org/10.1016/S1050-6411(98)00040-6

Bottinelli, R., & Reggiani, C. (2000). Human skeletal muscle fibres : Molecular and functional diversity. *Progress in Biophysics and Molecular Biology*, *73*(2), 195-262. https://doi.org/10.1016/S0079-6107(00)00006-7

Bouillard, K., Nordez, A., & Hug, F. (2011). Estimation of Individual Muscle Force Using Elastography. *PLOS ONE*, *6*(12), e29261. https://doi.org/10.1371/journal.pone.0029261

Brennan, S. F., Cresswell, A. G., Farris, D. J., & Lichtwark, G. A. (2017). In vivo fascicle length measurements via B-mode ultrasound imaging with single vs dual transducer arrangements. *Journal of Biomechanics*, *64*, 240-244. https://doi.org/10.1016/j.jbiomech.2017.09.019

Browning, R. C., Modica, J. R., Kram, R., & Goswami, A. (2007). The effects of adding mass to the legs on the energetics and biomechanics of walking. *Medicine & Science in Sports & Exercise*, *39*(3), 515-525.

Buchanan, T. S., Lloyd, D. G., Manal, K., & Besier, T. F. (2004). Neuromusculoskeletal Modeling : Estimation of Muscle Forces and Joint Moments and Movements from

Measurements of Neural Command. *Journal of Applied Biomechanics*, *20*(4), 367-395. https://doi.org/10.1123/jab.20.4.367

Buford, W. L., Ivey, F. M., Malone, J. D., Patterson, R. M., Pearce, G. L., Nguyen, D. K., & Stewart, A. A. (1997). Muscle balance at the knee-moment arms for the normal knee and the ACL-minus knee. *IEEE Transactions on Rehabilitation Engineering*, *5*(4), 367-379. https://doi.org/10.1109/86.650292

Bujalski, P., Martins, J., & Stirling, L. (2018). A Monte Carlo analysis of muscle force estimation sensitivity to muscle-tendon properties using a Hill-based muscle model. *Journal of Biomechanics*, *79*, 67-77. https://doi.org/10.1016/j.jbiomech.2018.07.045

Campanini, I., Merlo, A., Degola, P., Merletti, R., Vezzosi, G., & Farina, D. (2007). Effect of electrode location on EMG signal envelope in leg muscles during gait. *Journal of Electromyography and Kinesiology*, *17*(4), 515-526.

Challis, J. H. (1997). Producing physiologically realistic individual muscle force estimations by imposing constraints when using optimization techniques. *Medical Engineering & Physics*, *19*(3), 253-261. https://doi.org/10.1016/S1350-4533(96)00062-8

Charles, J. P., Grant, B., D'Août, K., & Bates, K. T. (2020). Subject-specific muscle properties from diffusion tensor imaging significantly improve the accuracy of musculoskeletal models. *Journal of Anatomy*, *n/a*(n/a). https://doi.org/10.1111/joa.13261

Charles, J. P., Moon, C.-H., & Anderst, W. (2018). Determining subject-specific lower-limb muscle architecture data for musculoskeletal models using diffusion tensor MRI. *Journal of Biomechanical Engineering*. https://doi.org/10.1115/1.4040946

Charles, J. P., Suntaxi, F., & Anderst, W. J. (2019). In vivo human lower limb muscle architecture dataset obtained using diffusion tensor imaging. *PLOS ONE*, *14*(10), e0223531. https://doi.org/10.1371/journal.pone.0223531

Clark, W. H., & Franz, J. R. (2018). Do triceps surae muscle dynamics govern non-uniform Achilles tendon deformations? *PeerJ*, *6*. https://doi.org/10.7717/peerj.5182

Clark, W. H., Pimentel, R. E., & Franz, J. R. (2020). Imaging and Simulation of Inter-muscular Differences in Triceps Surae Contributions to Forward Propulsion During Walking. *Annals of Biomedical Engineering*. https://doi.org/10.1007/s10439-020-02594-x

Coggan, A. R., Spina, R. J., King, D. S., Rogers, M. A., Rogers, M. A., Brown, M., Nemeth, P. M., & Holloszy, J. O. (1992). Histochemical and Enzymatic Comparison of the Gastrocnemius Muscle of Young and Elderly Men and Women. *Journal of Gerontology*, *47*(3), B71-B76. https://doi.org/10.1093/geronj/47.3.B71

Cresswell, A. G., Löscher, W. N., & Thorstensson, A. (1995). Influence of gastrocnemius muscle length on triceps surae torque development and electromyographic activity in man. *Experimental Brain Research*, *105*(2), 283-290. https://doi.org/10.1007/BF00240964

Cronin, N. J., Avela, J., Finni, T., & Peltonen, J. (2013). Differences in contractile behaviour between the soleus and medial gastrocnemius muscles during human walking. *Journal of Experimental Biology*, *216*(5), 909-914. https://doi.org/10.1242/jeb.078196

Cronin, N. J., & Lichtwark, G. (2013). The use of ultrasound to study muscle–tendon function in human posture and locomotion. *Gait & Posture*, *37*(3), 305-312. https://doi.org/10.1016/j.gaitpost.2012.07.024

Cronin, N. J., Peltonen, J., Ishikawa, M., Komi, P. V., Avela, J., Sinkjaer, T., & Voigt, M. (2008). Effects of contraction intensity on muscle fascicle and stretch reflex behavior in the human triceps surae. *Journal of Applied Physiology*, *105*(1), 226-232. https://doi.org/10.1152/japplphysiol.90432.2008

Crouzier, M., Hug, F., Dorel, S., Deschamps, T., Tucker, K., & Lacourpaille, L. (2019a). Do individual differences in the distribution of activation between synergist muscles reflect individual strategies? *Experimental Brain Research*, *237*(3), 625-635. https://doi.org/10.1007/s00221-018-5445-6

Crouzier, M., Lacourpaille, L., Nordez, A., Tucker, K., & Hug, F. (2018). Neuromechanical coupling within the human triceps surae and its consequence on individual force-sharing strategies. *The Journal of Experimental Biology*, *221*(21), jeb187260. https://doi.org/10.1242/jeb.187260

Crouzier, M., Tucker, K., Lacourpaille, L., Doguet, V., Fayet, G., Dauty, M., & Hug, F. (2019b). Force-sharing within the Triceps Surae : An Achilles Heel in Achilles Tendinopathy. *Medicine & Science in Sports & Exercise, Publish Ahead of Print*. https://doi.org/10.1249/MSS.0000000000002229

Crowninshield, R. D., & Brand, R. A. (1981a). The prediction of forces in joint structures : Distribution of intersegmental resultants. *Exercise and sport sciences reviews*, *9*(1), 159-182.

Crowninshield, R. D., & Brand, R. A. (1981b). A physiologically based criterion of muscle force prediction in locomotion. *Journal of Biomechanics*, *14*(11), 793-801. https://doi.org/10.1016/0021-9290(81)90035-X

Crowninshield, R. D., Johnston, R. C., Andrews, J. G., & Brand, R. A. (1978). A biomechanical investigation of the human hip. *Journal of Biomechanics*, *11*(1), 75-85. https://doi.org/10.1016/0021-9290(78)90045-3

Dal, U., Erdogan, T., Resitoglu, B., & Beydagi, H. (2010). Determination of preferred walking speed on treadmill may lead to high oxygen cost on treadmill walking. *Gait & Posture*, *31*(3), 366-369. https://doi.org/10.1016/j.gaitpost.2010.01.006

Daley, M. A., & Biewener, A. A. (2003). Muscle force-length dynamics during level versus incline locomotion : A comparison of in vivo performance of two guinea fowl ankle extensors. *Journal of Experimental Biology*, *206*(17), 2941-2958. https://doi.org/10.1242/jeb.00503

Daley, M. A., Usherwood, J. R., Felix, G., & Biewener, A. A. (2006). Running over rough terrain : Guinea fowl maintain dynamic stability despite a large unexpected change in substrate height. *Journal of Experimental Biology*, *209*(1), 171-187. https://doi.org/10.1242/jeb.01986

Damon, B. M., Ding, Z., Anderson, A. W., Freyer, A. S., & Gore, J. C. (2002). Validation of diffusion tensor MRI-based muscle fiber tracking. *Magnetic Resonance in Medicine*, *48*(1), 97-104. https://doi.org/10.1002/mrm.10198

Dao, T. T., & Tho, M.-C. H. B. (2018). A systematic review of continuum modeling of skeletal muscles : Current trends, limitations, and recommendations. *Applied bionics and biomechanics*, *2018*.

De Luca, C. J. (1997). The use of surface electromyography in biomechanics. *Journal of applied biomechanics*, *13*(2), 135-163.

De Luca, C. J., & Erim, Z. (1994). Common drive of motor units in regulation of muscle force. *Trends in Neurosciences*, *17*(7), 299-305. https://doi.org/10.1016/0166-2236(94)90064-7

De Luca, C. J., & Erim, Z. (2002). Common Drive in Motor Units of a Synergistic Muscle Pair. *Journal of Neurophysiology*, *87*(4), 2200-2204. https://doi.org/10.1152/jn.00793.2001

De Luca, C. J., & Merletti, R. (1988). Surface myoelectric signal cross-talk among muscles of the leg. *Electroencephalography and clinical neurophysiology*, *69*(6), 568-575.

de Brito Fontana, H., & Herzog, W. (2016). Vastus lateralis maximum force-generating potential occurs at optimal fascicle length regardless of activation level. *European Journal of Applied Physiology*, *116*(6), 1267-1277. https://doi.org/10.1007/s00421-016-3381-3

Del Vecchio, A., & Farina, D. (2019). Interfacing the neural output of the spinal cord : Robust and reliable longitudinal identification of motor neurons in humans. *Journal of neural engineering*, *17*(1), 016003.

Del Vecchio, A., Germer, C. M., Elias, L. A., Fu, Q., Fine, J., Santello, M., & Farina, D. (2019). The human central nervous system transmits common synaptic inputs to distinct motor neuron pools during non-synergistic digit actions. *The Journal of Physiology*, *597*(24), 5935-5948. https://doi.org/10.1113/JP278623

Del Vecchio, A., Holobar, A., Falla, D., Felici, F., Enoka, R. M., & Farina, D. (2020). Tutorial : Analysis of motor unit discharge characteristics from high-density surface EMG signals. *Journal of Electromyography and Kinesiology*, *53*, 102426. https://doi.org/10.1016/j.jelekin.2020.102426

Delp, S. L., Anderson, F. C., Arnold, A. S., Loan, P., Habib, A., John, C. T., Guendelman, E., & Thelen, D. G. (2007). OpenSim : Open-source software to create and analyze dynamic simulations of movement. *IEEE Transactions on Bio-Medical Engineering*, *54*(11), 1940-1950. https://doi.org/10.1109/TBME.2007.901024

de Oliveira, L. F., & Menegaldo, L. L. (2010). Individual-specific muscle maximum force estimation using ultrasound for ankle joint torque prediction using an EMG-driven Hill-type model. *Journal of Biomechanics*, *43*(14), 2816-2821. https://doi.org/10.1016/j.jbiomech.2010.05.035

Desmedt, J. E., & Godaux, E. (1977). Ballistic contractions in man : Characteristic recruitment pattern of single motor units of the tibialis anterior muscle. *The Journal of physiology*, *264*(3), 673-693.

Dick, T. J. M., Biewener, A. A., & Wakeling, J. M. (2017). Comparison of human gastrocnemius forces predicted by Hill-type muscle models and estimated from ultrasound images. *The Journal of Experimental Biology*, *220*(9), 1643-1653. https://doi.org/10.1242/jeb.154807

Dick, T. JM., Arnold, A. S., & Wakeling, J. M. (2016). Quantifying Achilles Tendon Force In Vivo from Ultrasound Images. *Journal of biomechanics*, *49*(14), 3200-3207. https://doi.org/10.1016/j.jbiomech.2016.07.036

Dickinson, M. H., Farley, C. T., Full, R. J., Koehl, M. a. R., Kram, R., & Lehman, S. (2000). How Animals Move : An Integrative View. *Science*, *288*(5463), 100-106. https://doi.org/10.1126/science.288.5463.100

Dominici, N., Ivanenko, Y. P., Cappellini, G., d'Avella, A., Mondì, V., Cicchese, M., Fabiano, A., Silei, T., Di Paolo, A., Giannini, C., Poppele, R. E., & Lacquaniti, F. (2011). Locomotor Primitives in Newborn Babies and Their Development. *Science*, *334*(6058), 997-999. https://doi.org/10.1126/science.1210617

Dorn, T. W., Schache, A. G., & Pandy, M. G. (2012). Muscular strategy shift in human running : Dependence of running speed on hip and ankle muscle performance. *Journal of Experimental Biology*, *215*(11), 1944-1956. https://doi.org/10.1242/jeb.064527

Duchateau, J., & Enoka, R. M. (2011). Human motor unit recordings : Origins and insight into the integrated motor system. *Brain research*, *1409*, 42-61.

Dul, J., Johnson, G. E., Shiavi, R., & Townsend, M. A. (1984). Muscular synergism—II. A minimum-fatigue criterion for load sharing between synergistic muscles. *Journal of biomechanics*, *17*(9), 675-684.

Ebrahimi, A., Martin, J. A., Schmitz, D. G., & Thelen, D. G. (2020). Shear Wave Tensiometry Reveals an Age-Related Deficit in Triceps Surae Work at Slow and Fast Walking Speeds. *Frontiers in Sports and Active Living*, *2*. https://doi.org/10.3389/fspor.2020.00069

Edama, M., Kubo, M., Onishi, H., Takabayashi, T., Inai, T., Yokoyama, E., Hiroshi, W., Satoshi, N., & Kageyama, I. (2015). The twisted structure of the human Achilles tendon : Classification by degree of twist. *Scandinavian Journal of Medicine & Science in Sports*, *25*(5), e497-e503. https://doi.org/10.1111/sms.12342

Edgerton, V., Smith, J., & Simpson, D. (1975). Muscle fibre type populations of human leg muscles. *The Histochemical journal*, *7*, 259-266. https://doi.org/10.1007/BF01003594

Engstrom, C. M., Loeb, G. E., Reid, J. G., Forrest, W. J., & Avruch, L. (1991). Morphometry of the human thigh muscles. A comparison between anatomical sections and computer tomographic and magnetic resonance images. *Journal of Anatomy*, *176*, 139-156.

Enoka, R. M., & Duchateau, J. (2015). Inappropriate interpretation of surface EMG signals and muscle fiber characteristics impedes understanding of the control of neuromuscular function. *Journal of Applied Physiology*, *119*(12), 1516-1518.

Enoka, R. M., & Duchateau, J. (2019). Chapter 7 - Muscle Function : Strength, Speed, and Fatigability. In J. A. Zoladz (Éd.), *Muscle and Exercise Physiology* (p. 129-157). Academic Press. https://doi.org/10.1016/B978-0-12-814593-7.00007-4

Enoka, R. M., & Fuglevand, A. J. (2001). Motor unit physiology : Some unresolved issues. *Muscle & Nerve*, *24*(1), 4-17. https://doi.org/10.1002/1097-4598(200101)24:1<4::AID-MUS13>3.0.CO;2-F

Erdemir, A., McLean, S., Herzog, W., & van den Bogert, A. J. (2007). Model-based estimation of muscle forces exerted during movements. *Clinical Biomechanics*, *22*(2), 131-154. https://doi.org/10.1016/j.clinbiomech.2006.09.005

Farina, D., Merletti, R., & Enoka, R. M. (2004a). The extraction of neural strategies from the surface EMG. *Journal of Applied Physiology*, *96*(4), 1486-1495. https://doi.org/10.1152/japplphysiol.01070.2003

Farina, D., Merletti, R., Indino, B., & Graven-Nielsen, T. (2004b). Surface EMG crosstalk evaluated from experimental recordings and simulated signals. *Methods of information in medicine*, *43*(01), 30-35.

Farina, D., Negro, F., Muceli, S., & Enoka, R. M. (2016). Principles of Motor Unit Physiology Evolve With Advances in Technology. *Physiology*, *31*(2), 83-94. https://doi.org/10.1152/physiol.00040.2015

Farris, D. J., & Lichtwark, G. A. (2016). UltraTrack : Software for semi-automated tracking of muscle fascicles in sequences of B-mode ultrasound images. *Computer Methods and Programs in Biomedicine*, *128*, 111-118. https://doi.org/10.1016/j.cmpb.2016.02.016

Farris, D. J., & Raiteri, B. J. (2017). Elastic ankle muscle-tendon interactions are adjusted to produce acceleration during walking in humans. *The Journal of Experimental Biology*, *220*(Pt 22), 4252-4260. https://doi.org/10.1242/jeb.159749

Farris, D. J., & Sawicki, G. S. (2012). Human medial gastrocnemius force-velocity behavior shifts with locomotion speed and gait. *Proceedings of the National Academy of Sciences of the United States of America*, *109*(3), 977-982. https://doi.org/10.1073/pnas.1107972109

Farris, D. J., Trewartha, G., McGuigan, M. P., & Lichtwark, G. A. (2013). Differential strain patterns of the human Achilles tendon determined in vivo with freehand three-dimensional ultrasound imaging. *The Journal of Experimental Biology*, *216*(Pt 4), 594-600. https://doi.org/10.1242/jeb.077131

Feinstein, B., Lindegård, B., Nyman, E., & Wohlfart, G. (1955). Morphologic studies of motor units in normal human muscles. *Cells Tissues Organs*, *23*(2), 127-142.

Finni, T., Bernabei, M., Baan, G. C., Noort, W., Tijs, C., & Maas, H. (2018). Non-uniform displacement and strain between the soleus and gastrocnemius subtendons of rat Achilles tendon. *Scandinavian Journal of Medicine & Science in Sports*, *28*(3), 1009-1017. https://doi.org/10.1111/sms.13001

Finni, T., Komi, P. V., & Lepola, V. (2000). In vivo human triceps surae and quadriceps femoris muscle function in a squat jump and counter movement jump. *European Journal of Applied Physiology*, *83*(4), 416-426. https://doi.org/10.1007/s004210000289

Finni, T., Komi, P. V., & Lukkariniemi, J. (1998). Achilles tendon loading during walking : Application of a novel optic fiber technique. *European Journal of Applied Physiology and Occupational Physiology*, *77*(3), 289-291. https://doi.org/10.1007/s004210050335

Franchi, M. V., Raiteri, B. J., Longo, S., Sinha, S., Narici, M. V., & Csapo, R. (2018). Muscle Architecture Assessment : Strengths, Shortcomings and New Frontiers of in Vivo Imaging Techniques. *Ultrasound in Medicine & Biology*, *44*(12), 2492-2504. https://doi.org/10.1016/j.ultrasmedbio.2018.07.010

Franz, J. R., Slane, L. C., Rasske, K., & Thelen, D. G. (2015). Non-uniform in vivo deformations of the human Achilles tendon during walking. *Gait & Posture*, *41*(1), 192-197. https://doi.org/10.1016/j.gaitpost.2014.10.001

Fukashiro, S., Komi, P. V., Järvinen, M., & Miyashita, M. (1995). In vivo achilles tendon loading' during jumping in humans. *European Journal of Applied Physiology and Occupational Physiology*, *71*(5), 453-458. https://doi.org/10.1007/BF00635880

Fukunaga, Kubo, Kawakami, Fukashiro, Kanehisa, & Maganaris. (2001). In vivo behaviour of human muscle tendon during walking. *Proceedings of the Royal Society of London. Series B: Biological Sciences*, *268*(1464), 229-233. https://doi.org/10.1098/rspb.2000.1361

Fukunaga, T., Ichinose, Y., Ito, M., Kawakami, Y., & Fukashiro, S. (1997). Determination of fascicle length and pennation in a contracting human muscle in vivo. *Journal of Applied Physiology*, *82*(1), 354-358. https://doi.org/10.1152/jappl.1997.82.1.354

Fukunaga, T., Roy, R. R., Shellock, F. G., Hodgson, J. A., Day, M. K., Lee, P. L., Kwong-Fu, H., & Edgerton, V. R. (1992). Physiological cross-sectional area of human leg muscles based on magnetic resonance imaging. *Journal of Orthopaedic Research*, *10*(6), 926-934. https://doi.org/10.1002/jor.1100100623

Fukunaga, T., Roy, R. R., Shellock, F. G., Hodgson, J. A., & Edgerton, V. R. (1996). Specific tension of human plantar flexors and dorsiflexors. *Journal of Applied Physiology (Bethesda, Md.: 1985)*, *80*(1), 158-165. https://doi.org/10.1152/jappl.1996.80.1.158

Funaro, A., Shim, V., Crouzier, M., Mylle, I., & Vanwanseele, B. (2022). Subject-Specific 3D Models to Investigate the Influence of Rehabilitation Exercises and the Twisted

Structure on Achilles Tendon Strains. *Frontiers in Bioengineering and Biotechnology*, *10*. https://www.frontiersin.org/articles/10.3389/fbioe.2022.914137

Gallina, A., Disselhorst-Klug, C., Farina, D., Merletti, R., Besomi, M., Holobar, A., Enoka, R. M., Hug, F., Falla, D., Søgaard, K., McGill, K., Clancy, E. A., Carson, R. G., van Dieën, J. H., Gandevia, S., Lowery, M., Besier, T., Kiernan, M. C., Rothwell, J. C., … Hodges, P. W. (2022). Consensus for experimental design in electromyography (CEDE) project : High-density surface electromyography matrix. *Journal of Electromyography and Kinesiology*, *64*, 102656. https://doi.org/10.1016/j.jelekin.2022.102656

Geremia, J. M., Baroni, B. M., Bini, R. R., Lanferdini, F. J., de Lima, A. R., Herzog, W., & Vaz, M. A. (2019). Triceps Surae Muscle Architecture Adaptations to Eccentric Training. *Frontiers in Physiology*, *10*. https://doi.org/10.3389/fphys.2019.01456

Germer, C. M., Farina, D., Elias, L. A., Nuccio, S., Hug, F., & Del Vecchio, A. (2021). Surface EMG cross talk quantified at the motor unit population level for muscles of the hand, thigh, and calf. *Journal of Applied Physiology*, *131*(2), 808-820. https://doi.org/10.1152/japplphysiol.01041.2020

Gerus, P., Rao, G., & Berton, E. (2012). Subject-specific tendon-aponeurosis definition in Hill-type model predicts higher muscle forces in dynamic tasks. *PloS One*, *7*(8), e44406. https://doi.org/10.1371/journal.pone.0044406

Gerus, P., Rao, G., & Berton, E. (2015). Ultrasound-based subject-specific parameters improve fascicle behaviour estimation in Hill-type muscle model. *Computer Methods in Biomechanics and Biomedical Engineering*, *18*(2), 116-123. https://doi.org/10.1080/10255842.2013.780047

Gibbs, J., Harrison, L. M., & Stephens, J. A. (1995). Organization of inputs to motoneurone pools in man. *The Journal of Physiology*, *485*(1), 245-256. https://doi.org/10.1113/jphysiol.1995.sp020727

Gillett, J. G., Barrett, R. S., & Lichtwark, G. A. (2013). Reliability and accuracy of an automated tracking algorithm to measure controlled passive and active muscle fascicle length changes from ultrasound. *Computer Methods in Biomechanics and Biomedical Engineering*, *16*(6), 678-687. https://doi.org/10.1080/10255842.2011.633516

Ginn, K., Eastburn, G., & Lee, M. (1993). Evaluation of a buckle force transducer for measuring tissue tension. *Australian Journal of Physiotherapy*, *39*(1), 31-38. https://doi.org/10.1016/S0004-9514(14)60467-0

Gollnick, P. D., Sjödin, B., Karlsson, J., Jansson, E., & Saltin, B. (1974). Human soleus muscle : A comparison of fiber composition and enzyme activities with other leg muscles. *Pflügers Archiv*, *348*(3), 247-255. https://doi.org/10.1007/BF00587415

Gordon, A. M., Huxley, A. F., & Julian, F. J. (1966). The variation in isometric tension with sarcomere length in vertebrate muscle fibres. *The Journal of Physiology*, *184*(1), 170-192. https://doi.org/10.1113/jphysiol.1966.sp007909

Green, H. J., Daub, B., Houston, M. E., Thomson, J. A., Fraser, I., & Ranney, D. (1981). Human vastus lateralis and gastrocnemius muscles : A comparative histochemical and biochemical analysis. *Journal of the Neurological Sciences*, *52*(2), 201-210. https://doi.org/10.1016/0022-510X(81)90005-8

Gregor, R. J., Komi, P. V., & Järvinen, M. (1987). Achilles Tendon Forces During Cycling. *International Journal of Sports Medicine*, *08*(S 1), S9-S14. https://doi.org/10.1055/s-2008-1025698

Griffiths, R. I. (1991). Shortening of muscle fibres during stretch of the active cat medial gastrocnemius muscle : The role of tendon compliance. *The Journal of Physiology*, *436*(1), 219-236. https://doi.org/10.1113/jphysiol.1991.sp018547

Hamner, S. R., & Delp, S. L. (2013). Muscle contributions to fore-aft and vertical body mass center accelerations over a range of running speeds. *Journal of Biomechanics*, *46*(4), 780-787. https://doi.org/10.1016/j.jbiomech.2012.11.024

Hamner, S. R., Seth, A., & Delp, S. L. (2010). Muscle contributions to propulsion and support during running. *Journal of Biomechanics*, *43*(14), 2709-2716. https://doi.org/10.1016/j.jbiomech.2010.06.025

Handsfield, G. G., Inouye, J. M., Slane, L. C., Thelen, D. G., Miller, G. W., & Blemker, S. S. (2017). A 3D Model of the Achilles Tendon to Determine The Mechanisms Underlying Nonuniform Tendon Displacements. *Journal of biomechanics*, *51*, 17-25. https://doi.org/10.1016/j.jbiomech.2016.11.062

Handsfield, G. G., Meyer, C. H., Hart, J. M., Abel, M. F., & Blemker, S. S. (2014). Relationships of 35 lower limb muscles to height and body mass quantified using MRI. *Journal of Biomechanics*, *47*(3), 631-638. https://doi.org/10.1016/j.jbiomech.2013.12.002

Handsfield, G. G., Slane, L. C., & Screen, H. R. C. (2016). Nomenclature of the tendon hierarchy : An overview of inconsistent terminology and a proposed size-based naming scheme with terminology for multi-muscle tendons. *Journal of Biomechanics*, *49*(13), 3122-3124. https://doi.org/10.1016/j.jbiomech.2016.06.028

Harridge, S. D., Bottinelli, R., Canepari, M., Pellegrino, M. A., Reggiani, C., Esbjörnsson, M., & Saltin, B. (1996). Whole-muscle and single-fibre contractile properties and myosin heavy chain isoforms in humans. *Pflugers Archiv: European Journal of Physiology*, *432*(5), 913-920. https://doi.org/10.1007/s004240050215

Hauraix, H., Dorel, S., Rabita, G., Guilhem, G., & Nordez, A. (2017). Muscle fascicle shortening behaviour of vastus lateralis during a maximal force–velocity test. *European Journal of Applied Physiology*, *117*(2), 289-299. https://doi.org/10.1007/s00421-016-3518-4

Haxton, H. A. (1944). Absolute muscle force in the ankle flexors of man. *The Journal of Physiology*, *103*(3), 267-273.

Heidlauf, T., Klotz, T., Rode, C., Siebert, T., & Röhrle, O. (2017). A continuum-mechanical skeletal muscle model including actin-titin interaction predicts stable contractions on the descending limb of the force-length relation. *PLOS Computational Biology*, *13*(10), e1005773. https://doi.org/10.1371/journal.pcbi.1005773

Henneman, E. (1957). Relation between size of neurons and their susceptibility to discharge. *Science*, *126*(3287), 1345-1347.

Herbert, R. D., Moseley, A. M., Butler, J. E., & Gandevia, S. C. (2002). Change in length of relaxed muscle fascicles and tendons with knee and ankle movement in humans. *The Journal of physiology*, *539*(2), 637-645.

Hermens, H. J., Freriks, B., Disselhorst-Klug, C., & Rau, G. (2000). Development of recommendations for SEMG sensors and sensor placement procedures. *Journal of electromyography and Kinesiology*, *10*(5), 361-374.

Héroux, M. E., Brown, H. J., Inglis, J. T., Siegmund, G. P., & Blouin, J.-S. (2015). Motor units in the human medial gastrocnemius muscle are not spatially localized or functionally grouped. *The Journal of Physiology*, *593*(16), 3711-3726. https://doi.org/10.1113/JP270307

Héroux, M. E., Stubbs, P. W., & Herbert, R. D. (2016). Behavior of human gastrocnemius muscle fascicles during ramped submaximal isometric contractions. *Physiological Reports*, *4*(17), e12947. https://doi.org/10.14814/phy2.12947

Herzog, W. (1996). Force-sharing among synergistic muscles : Theoretical considerations and experimental approaches. *Exercise and sport sciences reviews*, *24*(1), 173-202.

Herzog, W. (1998). Force-sharing among the primary cat ankle muscles. *European Journal of Morphology*, *36*(4-5), 280-287. https://doi.org/10.1076/ejom.36.4.280.5813

Herzog, W. (2017). Skeletal muscle mechanics : Questions, problems and possible solutions. *Journal of NeuroEngineering and Rehabilitation*, *14*(1), 98. https://doi.org/10.1186/s12984-017-0310-6

Herzog, W., & Leonard, T. R. (1991). Validation of optimization models that estimate the forces exerted by synergistic muscles. *Journal of biomechanics*, *24*, 31-39.

Herzog, W., Leonard, T. R., & Guimaraes, A. C. (1993). Forces in gastrocnemius, soleus, and plantaris tendons of the freely moving cat. *Journal of Biomechanics*, *26*(8), 945-953. https://doi.org/10.1016/0021-9290(93)90056-k

Hessel, A. L., Raiteri, B. J., Marsh, M. J., & Hahn, D. (2021). Rightward shift of optimal fascicle length with decreasing voluntary activity level in the soleus and lateral gastrocnemius muscles. *Journal of Experimental Biology*, *224*(jeb235614). https://doi.org/10.1242/jeb.235614

Hill, A. V. (1938). The heat of shortening and the dynamic constants of muscle. *Proceedings of the Royal Society of London. Series B - Biological Sciences*, *126*(843), 136-195. https://doi.org/10.1098/rspb.1938.0050

Hodson-Tole, E. F., & Lai, A. K. M. (2019). Ultrasound-derived changes in thickness of human ankle plantar flexor muscles during walking and running are not homogeneous along the muscle mid-belly region. *Scientific Reports*, *9*(1), 15090. https://doi.org/10.1038/s41598-019-51510-4

Hodson-Tole, E. F., Loram, I. D., & Vieira, T. M. M. (2013). Myoelectric activity along human gastrocnemius medialis : Different spatial distributions of postural and electrically elicited surface potentials. *Journal of Electromyography and Kinesiology*, *23*(1), 43-50. https://doi.org/10.1016/j.jelekin.2012.08.003

Hoffman, B. W., Lichtwark, G. A., Carroll, T. J., & Cresswell, A. G. (2012). A comparison of two Hill-type skeletal muscle models on the construction of medial gastrocnemius length-tension curves in humans in vivo. *Journal of Applied Physiology*, *113*(1), 90-96. https://doi.org/10.1152/japplphysiol.00070.2012

Holobar, A., & Farina, D. (2014). Blind source identification from the multichannel surface electromyogram. *Physiological measurement*, *35*(7), R143.

Holobar, A., Minetto, M. A., Botter, A., Negro, F., & Farina, D. (2010). Experimental analysis of accuracy in the identification of motor unit spike trains from high-density surface EMG. *IEEE Transactions on Neural Systems and Rehabilitation Engineering*, *18*(3), 221-229.

Holobar, A., & Zazula, D. (2007). Multichannel Blind Source Separation Using Convolution Kernel Compensation. *IEEE Transactions on Signal Processing*, *55*(9), 4487-4496. https://doi.org/10.1109/TSP.2007.896108

Holt, N. C., & Azizi, E. (2014). What drives activation-dependent shifts in the force–length curve? *Biology Letters*, *10*(9), 20140651. https://doi.org/10.1098/rsbl.2014.0651

Holt, N. C., & Azizi, E. (2016). The effect of activation level on muscle function during locomotion : Are optimal lengths and velocities always used? *Proceedings. Biological Sciences*, *283*(1823). https://doi.org/10.1098/rspb.2015.2832

Holt, N. C., Roberts, T. J., & Askew, G. N. (2014). The energetic benefits of tendon springs in running : Is the reduction of muscle work important? *Journal of Experimental Biology*, *217*(24), 4365-4371. https://doi.org/10.1242/jeb.112813

Horst, F., Kramer, F., Schäfer, B., Eekhoff, A., Hegen, P., Nigg, B. M., & Schöllhorn, W. I. (2016). Daily changes of individual gait patterns identified by means of support vector machines. *Gait & Posture*, *49*, 309-314. https://doi.org/10.1016/j.gaitpost.2016.07.073

Hudson, A. L., Taylor, J. L., Gandevia, S. C., & Butler, J. E. (2009). Coupling between mechanical and neural behaviour in the human first dorsal interosseous muscle. *The Journal of Physiology*, *587*(4), 917-925. https://doi.org/10.1113/jphysiol.2008.165043

Hug, F. (2011). Can muscle coordination be precisely studied by surface electromyography? *Journal of Electromyography and Kinesiology: Official Journal of the International Society of Electrophysiological Kinesiology*, *21*(1), 1-12. https://doi.org/10.1016/j.jelekin.2010.08.009

Hug, F., Avrillon, S., Del Vecchio, A., Casolo, A., Ibanez, J., Nuccio, S., Rossato, J., Holobar, A., & Farina, D. (2021a). Analysis of motor unit spike trains estimated from high-density surface electromyography is highly reliable across operators. *Journal of Electromyography and Kinesiology*, *58*, 102548. https://doi.org/10.1016/j.jelekin.2021.102548

Hug, F., Del Vecchio, A., Avrillon, S., Farina, D., & Tucker, K. (2021b). Muscles from the same muscle group do not necessarily share common drive : Evidence from the human triceps surae. *Journal of Applied Physiology*, *130*(2), 342-354. https://doi.org/10.1152/japplphysiol.00635.2020

Hug, F., Del Vecchio, A., Avrillon, S., Farina, D., & Tucker, K. (2021b). Muscles from the same muscle group do not necessarily share common drive : Evidence from the human triceps surae. *Journal of Applied Physiology*, *130*(2), 342-354. https://doi.org/10.1152/japplphysiol.00635.2020

Hug, F., Goupille, C., Baum, D., Raiteri, B. J., Hodges, P. W., & Tucker, K. (2015a). Nature of the coupling between neural drive and force-generating capacity in the human quadriceps muscle. *Proceedings. Biological Sciences*, *282*(1819). https://doi.org/10.1098/rspb.2015.1908

Hug, F., Hodges, P. W., & Tucker, K. (2015b). Muscle force cannot be directly inferred from muscle activation : Illustrated by the proposed imbalance of force between the vastus medialis and vastus lateralis in people with patellofemoral pain. *The Journal of Orthopaedic and Sports Physical Therapy*, *45*(5), 360-365. https://doi.org/10.2519/jospt.2015.5905

Hug, F., & Tucker, K. (2017). Muscle Coordination and the Development of Musculoskeletal Disorders. *Exercise and Sport Sciences Reviews*, *45*(4), 201-208. https://doi.org/10.1249/JES.0000000000000122

Hug, F., Tucker, K., Gennisson, J.-L., Tanter, M., & Nordez, A. (2015c). Elastography for Muscle Biomechanics : Toward the Estimation of Individual Muscle Force. *Exercise and Sport Sciences Reviews*, *43*(3), 125-133. https://doi.org/10.1249/JES.0000000000000049

Hug, F., Vogel, C., Tucker, K., Dorel, S., Deschamps, T., Le Carpentier, É., & Lacourpaille, L. (2019). Individuals have unique muscle activation signatures as revealed during gait and pedaling. *Journal of Applied Physiology*, *127*(4), 1165-1174. https://doi.org/10.1152/japplphysiol.01101.2018

Huxley, A. F. (1957). Muscle structure and theories of contraction. *Prog. Biophys. Biophys. Chem*, *7*, 255-318.

Huxley, A. F. (1974). Muscular contraction. *The Journal of Physiology*, *243*(1), 1-43. https://doi.org/10.1113/jphysiol.1974.sp010740

Huxley, A. F., & Niedergerke, R. (1954). Structural changes in muscle during contraction : Interference microscopy of living muscle fibres. *Nature*, *173*(4412), 971-973.

Huxley, A. F., & Simmons, R. M. (1971). Proposed mechanism of force generation in striated muscle. *Nature*, *233*(5321), 533-538.

Ichinose, Y., Kawakami, Y., Ito, M., Kanehisa, H., & Fukunaga, T. (2000). In vivo estimation of contraction velocity of human vastus lateralis muscle during "isokinetic" action. *Journal of Applied Physiology*, *88*(3), 851-856. https://doi.org/10.1152/jappl.2000.88.3.851

Ishikawa, M., Komi, P. V., Grey, M. J., Lepola, V., & Bruggemann, G.-P. (2005). Muscle-tendon interaction and elastic energy usage in human walking. *Journal of Applied Physiology*, *99*(2), 603-608. https://doi.org/10.1152/japplphysiol.00189.2005

Johnson, M. A., Polgar, J., Weightman, D., & Appleton, D. (1973). Data on the distribution of fibre types in thirty-six human muscles. An autopsy study. *Journal of the Neurological Sciences*, *18*(1), 111-129. https://doi.org/10.1016/0022-510x(73)90023-3

Kawakami, Y., Ichinose, Y., & Fukunaga, T. (1998). Architectural and functional features of human triceps surae muscles during contraction. *Journal of Applied Physiology (Bethesda, Md.: 1985)*, *85*(2), 398-404. https://doi.org/10.1152/jappl.1998.85.2.398

Kaya, M., Leonard, T., & Herzog, W. (2003). Coordination of medial gastrocnemius and soleus forces during cat locomotion. *Journal of Experimental Biology*, *206*(20), 3645-3655.

Keenan, K. G., Farina, D., Maluf, K. S., Merletti, R., & Enoka, R. M. (2005). Influence of amplitude cancellation on the simulated surface electromyogram. *Journal of Applied Physiology*, *98*(1), 120-131. https://doi.org/10.1152/japplphysiol.00894.2004

Kelp, N. Y., Gore, A., Clemente, C. J., Tucker, K., Hug, F., & Dick, T. J. M. (2021). Muscle architecture and shape changes in the gastrocnemii of active younger and older adults. *Journal of Biomechanics*, *129*, 110823. https://doi.org/10.1016/j.jbiomech.2021.110823

Kerkman, J. N., Daffertshofer, A., Gollo, L. L., Breakspear, M., & Boonstra, T. W. (2018). Network structure of the human musculoskeletal system shapes neural interactions on multiple time scales. *Science Advances*, *4*(6), eaat0497. https://doi.org/10.1126/sciadv.aat0497

Keuler, E. M., Loegering, I. F., Martin, J. A., Roth, J. D., & Thelen, D. G. (2019). Shear Wave Predictions of Achilles Tendon Loading during Human Walking. *Scientific Reports*, *9*(1), Art. 1. https://doi.org/10.1038/s41598-019-49063-7

Kinugasa, R., Kawakami, Y., & Fukunaga, T. (2005). Muscle activation and its distribution within human triceps surae muscles. *Journal of Applied Physiology*, *99*(3), 1149-1156. https://doi.org/10.1152/japplphysiol.01160.2004

Klimstra, M., Dowling, J., Durkin, J. L., & MacDonald, M. (2007). The effect of ultrasound probe orientation on muscle architecture measurement. *Journal of Electromyography and Kinesiology: Official Journal of the International Society of Electrophysiological Kinesiology*, *17*(4), 504-514. https://doi.org/10.1016/j.jelekin.2006.04.011

Komi, P. V. (1990). Relevance of in vivo force measurements to human biomechanics. *Journal of Biomechanics*, *23*, 23-34. https://doi.org/10.1016/0021-9290(90)90038-5

Komi, P. V., Belli, A., Huttunen, V., Bonnefoy, R., Geyssant, A., & Lacour, J. R. (1996). Optic fibre as a transducer of tendomuscular forces. *European Journal of Applied Physiology and Occupational Physiology*, *72*(3), 278-280. https://doi.org/10.1007/BF00838652

Komi, P. V., Fukashiro, S., & Järvinen, M. (1992). Biomechanical Loading of Achilles Tendon During Normal Locomotion. *Clinics in Sports Medicine*, *11*(3), 521-531. https://doi.org/10.1016/S0278-5919(20)30506-8

Komi, P. V., Salonen, M., & Järvinen, M. (1984). In vivo-measurements of achilles tendon forces in man. *Medicine & Science in Sports & Exercise*, *16*(2), 165.

Konow, N., Azizi, E., & Roberts, T. J. (2011). Muscle power attenuation by tendon during energy dissipation. *Proceedings of the Royal Society B: Biological Sciences*, *279*(1731), 1108-1113. https://doi.org/10.1098/rspb.2011.1435

Kutch, J. J., & Valero-Cuevas, F. J. (2011). Muscle redundancy does not imply robustness to muscle dysfunction. *Journal of Biomechanics*, *44*(7), 1264-1270. https://doi.org/10.1016/j.jbiomech.2011.02.014

Kwah, L. K., Pinto, R. Z., Diong, J., & Herbert, R. D. (2013). Reliability and validity of ultrasound measurements of muscle fascicle length and pennation in humans : A systematic review. *Journal of Applied Physiology*, *114*(6), 761-769. https://doi.org/10.1152/japplphysiol.01430.2011

Labeit, D., Watanabe, K., Witt, C., Fujita, H., Wu, Y., Lahmers, S., Funck, T., Labeit, S., & Granzier, H. (2003). Calcium-dependent molecular spring elements in the giant protein titin. *Proceedings of the National Academy of Sciences*, *100*(23), 13716-13721. https://doi.org/10.1073/pnas.2235652100

Lacourpaille, L., Nordez, A., & Hug, F. (2017). The nervous system does not compensate for an acute change in the balance of passive force between synergist muscles. *Journal of Experimental Biology*, *220*(19), 3455-3463. https://doi.org/10.1242/jeb.163303

Lai, A. K. M., Biewener, A. A., & Wakeling, J. M. (2019). Muscle-specific indices to characterise the functional behaviour of human lower-limb muscles during locomotion. *Journal of Biomechanics*, *89*, 134-138. https://doi.org/10.1016/j.jbiomech.2019.04.027

Lai, A. K. M., Lichtwark, G. A., Schache, A. G., & Pandy, M. G. (2018). Differences in in vivo muscle fascicle and tendinous tissue behavior between the ankle plantarflexors during running. *Scandinavian Journal of Medicine & Science in Sports*, *28*(7), 1828-1836. https://doi.org/10.1111/sms.13089

Lai, A., Lichtwark, G. A., Schache, A. G., Lin, Y.-C., Brown, N. A. T., & Pandy, M. G. (2015). In vivo behavior of the human soleus muscle with increasing walking and running speeds. *Journal of Applied Physiology (Bethesda, Md.: 1985)*, *118*(10), 1266-1275. https://doi.org/10.1152/japplphysiol.00128.2015

Laine, C. M., Martinez-Valdes, E., Falla, D., Mayer, F., & Farina, D. (2015). Motor Neuron Pools of Synergistic Thigh Muscles Share Most of Their Synaptic Input. *Journal of Neuroscience*, *35*(35), 12207-12216. https://doi.org/10.1523/JNEUROSCI.0240-15.2015

Laine, C. M., & Valero-Cuevas, F. J. (2017). Intermuscular coherence reflects functional coordination. *Journal of Neurophysiology*, *118*(3), 1775-1783. https://doi.org/10.1152/jn.00204.2017

Landin, D., Thompson, M., & Reid, M. (2016). Actions of Two Bi-Articular Muscles of the Lower Extremity : A Review. *Journal of Clinical Medicine Research*, *8*(7), 489-494. https://doi.org/10.14740/jocmr2478w

Larsson, L., & Moss, R. L. (1993). Maximum velocity of shortening in relation to myosin isoform composition in single fibres from human skeletal muscles. *The Journal of Physiology*, *472*(1), 595-614. https://doi.org/10.1113/jphysiol.1993.sp019964

Le Sant, G., Nordez, A., Andrade, R., Hug, F., Freitas, S., & Gross, R. (2017). Stiffness mapping of lower leg muscles during passive dorsiflexion. *Journal of Anatomy*, *230*(5), 639-650. https://doi.org/10.1111/joa.12589

Lee, S. S. M., Arnold, A. S., Miara, M. de B., Biewener, A. A., & Wakeling, J. M. (2013). Accuracy of gastrocnemius muscles forces in walking and running goats predicted by one-element and two-element Hill-type models. *Journal of Biomechanics*, *46*(13), 2288-2295. https://doi.org/10.1016/j.jbiomech.2013.06.001

Lee, S. S. M., & Piazza, S. J. (2008). Inversion–eversion moment arms of gastrocnemius and tibialis anterior measured in vivo. *Journal of Biomechanics*, *41*(16), 3366-3370. https://doi.org/10.1016/j.jbiomech.2008.09.029

Lemaire, K. K., Baan, G. C., Jaspers, R. T., & van Soest, A. J. 'Knoek'. (2016). Comparison of the validity of Hill and Huxley muscle–tendon complex models using experimental data obtained from rat m. Soleus in situ. *Journal of Experimental Biology*, *219*(7), 977-987. https://doi.org/10.1242/jeb.128280

Levine, J., Avrillon, S., Farina, D., Hug, F., & Pons, J. L. (2022). *Two motor neuron synergies, invariant across ankle joint angles, activate the triceps surae during plantarflexion* (p. 2022.11.11.516183). bioRxiv. https://doi.org/10.1101/2022.11.11.516183

Li, L., Landin, D., Grodesky, J., & Myers, J. (2002). The function of gastrocnemius as a knee flexor at selected knee and ankle angles. *Journal of Electromyography and Kinesiology*, *12*(5), 385-390. https://doi.org/10.1016/S1050-6411(02)00049-4

Lichtwark, G. A., Bougoulias, K., & Wilson, A. M. (2007). Muscle fascicle and series elastic element length changes along the length of the human gastrocnemius during walking and running. *Journal of Biomechanics*, *40*(1), 157-164. https://doi.org/10.1016/j.jbiomech.2005.10.035

Lichtwark, G. A., & Wilson, A. M. (2005). In vivo mechanical properties of the human Achilles tendon during one-legged hopping. *Journal of Experimental Biology*, *208*(24), 4715-4725. https://doi.org/10.1242/jeb.01950

Lichtwark, G. A., & Wilson, A. M. (2006). Interactions between the human gastrocnemius muscle and the Achilles tendon during incline, level and decline locomotion. *The Journal of Experimental Biology*, *209*(Pt 21), 4379-4388. https://doi.org/10.1242/jeb.02434

Lieber, R. L., & Fridén, J. (2000). Functional and clinical significance of skeletal muscle architecture. *Muscle & Nerve*, *23*(11), 1647-1666. https://doi.org/10.1002/1097-4598(200011)23:11<1647::aid-mus1>3.0.co;2-m

Lloyd, D. G., & Besier, T. F. (2003). An EMG-driven musculoskeletal model to estimate muscle forces and knee joint moments in vivo. *Journal of Biomechanics*, *36*(6), 765-776. https://doi.org/10.1016/S0021-9290(03)00010-1

Loeb, G. E., & Ghez, C. (2000). The motor unit and muscle action. *Principles of neural science*, *380*(6573), 674-694.

Loram, I. D., Maganaris, C. N., & Lakie, M. (2006). Use of ultrasound to make noninvasive in vivo measurement of continuous changes in human muscle contractile length. *Journal of Applied Physiology*, *100*(4), 1311-1323. https://doi.org/10.1152/japplphysiol.01229.2005

Maas, H., Noort, W., Baan, G. C., & Finni, T. (2020). Non-uniformity of displacement and strain within the Achilles tendon is affected by joint angle configuration and differential muscle loading. *Journal of Biomechanics*, 109634. https://doi.org/10.1016/j.jbiomech.2020.109634

MacDonald, D., Moseley, G. L., & Hodges, P. W. (2009). Why do some patients keep hurting their back? Evidence of ongoing back muscle dysfunction during remission from recurrent back pain. *PAIN®*, *142*(3), 183-188. https://doi.org/10.1016/j.pain.2008.12.002

Maganaris, C. N. (2003). Force-length characteristics of the in vivo human gastrocnemius muscle. *Clinical Anatomy*, *16*(3), 215-223. https://doi.org/10.1002/ca.10064

Maganaris, C. N., Baltzopoulos, V., Ball, D., & Sargeant, A. J. (2001). In vivo specific tension of human skeletal muscle. *Journal of Applied Physiology*, *90*(3), 865-872. https://doi.org/10.1152/jappl.2001.90.3.865

Magnusson, S. P., Langberg, H., & Kjaer, M. (2010). The pathogenesis of tendinopathy : Balancing the response to loading. *Nature Reviews. Rheumatology*, *6*(5), 262-268. https://doi.org/10.1038/nrrheum.2010.43

Manjón, J. V., Coupé, P., Concha, L., Buades, A., Collins, D. L., & Robles, M. (2013). Diffusion Weighted Image Denoising Using Overcomplete Local PCA. *PLOS ONE*, *8*(9), e73021. https://doi.org/10.1371/journal.pone.0073021

Martin, D. C., Medri, M. K., Chow, R. S., Oxorn, V., Leekam, R. N., Agur, A. M., & McKEE, N. H. (2001). Comparing human skeletal muscle architectural parameters of cadavers with in vivo ultrasonographic measurements. *The Journal of Anatomy*, *199*(4), 429-434. https://doi.org/10.1017/S0021878201008251

Martin, J. A., Brandon, S. C. E., Keuler, E. M., Hermus, J. R., Ehlers, A. C., Segalman, D. J., Allen, M. S., & Thelen, D. G. (2018). Gauging force by tapping tendons. *Nature Communications*, *9*(1), Art. 1. https://doi.org/10.1038/s41467-018-03797-6

Martinez-Valdes, E., Enoka, R. M., Holobar, A., McGill, K., Farina, D., Besomi, M., Hug, F., Falla, D., Carson, R. G., Clancy, E. A., Disselhorst-Klug, C., van Dieën, J. H., Tucker, K., Gandevia, S., Lowery, M., Søgaard, K., Besier, T., Merletti, R., Kiernan, M. C., … Hodges, P. W. (2023). Consensus for experimental design in electromyography (CEDE) project : Single motor unit matrix. *Journal of Electromyography and Kinesiology*, *68*, 102726. https://doi.org/10.1016/j.jelekin.2022.102726

Martinez-Valdes, E., Negro, F., Laine, C. M., Falla, D., Mayer, F., & Farina, D. (2017). Tracking motor units longitudinally across experimental sessions with high-density surface electromyography. *The Journal of physiology*, *595*(5), 1479-1496.

Masood, T., Bojsen-Møller, J., Kalliokoski, K. K., Kirjavainen, A., Äärimaa, V., Peter Magnusson, S., & Finni, T. (2014). Differential contributions of ankle plantarflexors during submaximal isometric muscle action : A PET and EMG study. *Journal of Electromyography and Kinesiology*, *24*(3), 367-374. https://doi.org/10.1016/j.jelekin.2014.03.002

Massey, G., Evangelidis, P., & Folland, J. (2015). Influence of contractile force on the architecture and morphology of the quadriceps femoris. *Experimental Physiology*, *100*(11), 1342-1351. https://doi.org/10.1113/EP085360

McManus, L., Lowery, M., Merletti, R., Søgaard, K., Besomi, M., Clancy, E. A., van Dieën, J. H., Hug, F., Wrigley, T., Besier, T., Carson, R. G., Disselhorst-Klug, C., Enoka, R. M., Falla, D., Farina, D., Gandevia, S., Holobar, A., Kiernan, M. C., McGill, K., … Hodges, P. W. (2021). Consensus for experimental design in electromyography (CEDE) project : Terminology matrix. *Journal of Electromyography and Kinesiology*, *59*, 102565. https://doi.org/10.1016/j.jelekin.2021.102565

McNeill Alexander, R. (2002). Tendon elasticity and muscle function. *Comparative Biochemistry and Physiology Part A: Molecular & Integrative Physiology*, *133*(4), 1001-1011. https://doi.org/10.1016/S1095-6433(02)00143-5

Menegaldo, L. L., & Oliveira, L. F. (2011). An EMG-driven model to evaluate quadriceps strengthening after an isokinetic training. *Procedia IUTAM*, *2*, 131-141. https://doi.org/10.1016/j.piutam.2011.04.014

Merletti, R., Farina, D., & Gazzoni, M. (2003). The linear electrode array : A useful tool with many applications. *Journal of Electromyography and Kinesiology*, *13*(1), 37-47.

Merletti, R., Rainoldi, A., & Farina, D. (2001). Surface electromyography for noninvasive characterization of muscle. *Exercise and sport sciences reviews*, *29*(1), 20-25.

Miyamoto, N., Wakahara, T., & Kawakami, Y. (2012). Task-Dependent Inhomogeneous Muscle Activities within the Bi-Articular Human Rectus Femoris Muscle. *PLOS ONE*, *7*(3), e34269. https://doi.org/10.1371/journal.pone.0034269

Modenese, L., Ceseracciu, E., Reggiani, M., & Lloyd, D. G. (2016). Estimation of musculotendon parameters for scaled and subject specific musculoskeletal models using an optimization technique. *Journal of Biomechanics*, *49*(2), 141-148. https://doi.org/10.1016/j.jbiomech.2015.11.006

Moritz, C. T., & Farley, C. T. (2004). Passive dynamics change leg mechanics for an unexpected surface during human hopping. *Journal of Applied Physiology*, *97*(4), 1313-1322. https://doi.org/10.1152/japplphysiol.00393.2004

Morse, C. I., Thom, J. M., Birch, K. M., & Narici, M. V. (2005a). Changes in triceps surae muscle architecture with sarcopenia. *Acta Physiologica Scandinavica*, *183*(3), 291-298. https://doi.org/10.1111/j.1365-201X.2004.01404.x

Morse, C. I., Thom, J. M., Reeves, N. D., Birch, K. M., & Narici, M. V. (2005b). In vivo physiological cross-sectional area and specific force are reduced in the gastrocnemius of elderly men. *Journal of Applied Physiology*, *99*(3), 1050-1055. https://doi.org/10.1152/japplphysiol.01186.2004

Moss, C. L. (1992). Comparison of the histochemical and contractile properties of human triceps surae. *Medical and Biological Engineering and Computing*, *30*(6), 600-604. https://doi.org/10.1007/BF02446791

Muramatsu, T., Muraoka, T., Kawakami, Y., Shibayama, A., & Fukunaga, T. (2002). In vivo determination of fascicle curvature in contracting human skeletal muscles. *Journal of Applied Physiology*, *92*(1), 129-134. https://doi.org/10.1152/jappl.2002.92.1.129

Narici, M., Franchi, M., & Maganaris, C. (2016). Muscle structural assembly and functional consequences. *Journal of Experimental Biology*, *219*(2), 276-284. https://doi.org/10.1242/jeb.128017

Narici, M. V., Binzoni, T., Hiltbrand, E., Fasel, J., Terrier, F., & Cerretelli, P. (1996). In vivo human gastrocnemius architecture with changing joint angle at rest and during graded isometric contraction. *The Journal of Physiology*, *496*(1), 287-297. https://doi.org/10.1113/jphysiol.1996.sp021685

Negro, F., Muceli, S., Castronovo, A. M., Holobar, A., & Farina, D. (2016a). *Multi-channel intramuscular and surface EMG decomposition by convolutive blind source separation*. *13*(2), 026027. https://doi.org/10.1088/1741-2560/13/2/026027

Negro, F., Yavuz, U. Ş., & Farina, D. (2016b). The human motor neuron pools receive a dominant slow-varying common synaptic input. *The Journal of physiology*, *594*(19), 5491-5505.

Neptune, R. R., Kautz, S. A., & Zajac, F. E. (2001). Contributions of the individual ankle plantar flexors to support, forward progression and swing initiation during walking. *Journal of Biomechanics*, *34*(11), 1387-1398. https://doi.org/10.1016/S0021-9290(01)00105-1

Nishikawa, K. (2020). Titin : A Tunable Spring in Active Muscle. *Physiology*, *35*(3), 209-217. https://doi.org/10.1152/physiol.00036.2019

O'Connor, C. M., Thorpe, S. K., O'Malley, M. J., & Vaughan, C. L. (2007). Automatic detection of gait events using kinematic data. *Gait & Posture*, *25*(3), 469-474. https://doi.org/10.1016/j.gaitpost.2006.05.016

Oliveira, L. F., Verneque, D., & Menegaldo, L. L. (2017). The influence of aging on the isometric torque sharing patterns among the plantar flexor muscles. *Acta of Bioengineering and Biomechanics, Vol. 19, nr 1*, 41-45. https://doi.org/10.5277/ABB-00540-2015-03

Otten, E. (1987). A myocybernetic model of the jaw system of the rat. *Journal of Neuroscience Methods*, *21*(2), 287-302. https://doi.org/10.1016/0165-0270(87)90123-3

Overduin, S. A., d'Avella, A., Carmena, J. M., & Bizzi, E. (2012). Microstimulation Activates a Handful of Muscle Synergies. *Neuron*, *76*(6), 1071-1077. https://doi.org/10.1016/j.neuron.2012.10.018

Pal, S., Besier, T. F., Draper, C. E., Fredericson, M., Gold, G. E., Beaupre, G. S., & Delp, S. L. (2012). Patellar tilt correlates with vastus lateralis : Vastus medialis activation ratio in maltracking patellofemoral pain patients. *Journal of Orthopaedic Research*, *30*(6), 927-933. https://doi.org/10.1002/jor.22008

Pang, B. S. F., & Ying, M. (2006). Sonographic Measurement of Achilles Tendons in Asymptomatic Subjects. *Journal of Ultrasound in Medicine*, *25*(10), 1291-1296. https://doi.org/10.7863/jum.2006.25.10.1291

Passmore, E., Lai, A., Sangeux, M., Schache, A. G., & Pandy, M. G. (2017). Application of ultrasound imaging to subject-specific modelling of the human musculoskeletal system. *Meccanica*, *52*(3), 665-676. https://doi.org/10.1007/s11012-016-0478-z

Pękala, P. A., Henry, B. M., Ochała, A., Kopacz, P., Tatoń, G., Młyniec, A., Walocha, J. A., & Tomaszewski, K. A. (2017). The twisted structure of the Achilles tendon unraveled : A detailed quantitative and qualitative anatomical investigation. *Scandinavian Journal of Medicine & Science in Sports*, *27*(12), 1705-1715. https://doi.org/10.1111/sms.12835

Penrod, D. D., Davy, D. T., & Singh, D. P. (1974). An optimization approach to tendon force analysis. *Journal of biomechanics*, *7*(2), 123-129.

Perreault, E. J., Heckman, C. J., & Sandercock, T. G. (2003). Hill muscle model errors during movement are greatest within the physiologically relevant range of motor unit firing rates. *Journal of Biomechanics*, *36*(2), 211-218. https://doi.org/10.1016/s0021-9290(02)00332-9

Péter, A., Andersson, E., Hegyi, A., Finni, T., Tarassova, O., Cronin, N., Grundström, H., & Arndt, A. (2019a). Comparing Surface and Fine-Wire Electromyography Activity of Lower Leg Muscles at Different Walking Speeds. *Frontiers in Physiology*, *10*. https://doi.org/10.3389/fphys.2019.01283

Péter, A., Andersson, E., Hegyi, A., Finni, T., Tarassova, O., Cronin, N., Grundström, H., & Arndt, A. (2019b). Comparing Surface and Fine-Wire Electromyography Activity of Lower Leg Muscles at Different Walking Speeds. *Frontiers in Physiology*, *10*. https://www.frontiersin.org/articles/10.3389/fphys.2019.01283

Piazza, S. J., & Delp, S. L. (1996). The influence of muscles on knee flexion during the swing phase of gait. *Journal of biomechanics*, *29*(6), 723-733.

Piazzesi, G., Reconditi, M., Linari, M., Lucii, L., Bianco, P., Brunello, E., Decostre, V., Stewart, A., Gore, D. B., Irving, T. C., Irving, M., & Lombardi, V. (2007). Skeletal Muscle Performance Determined by Modulation of Number of Myosin Motors Rather Than Motor Force or Stroke Size. *Cell*, *131*(4), 784-795. https://doi.org/10.1016/j.cell.2007.09.045

Pinel, S., Kelp, N. Y., Bugeja, J. M., Bolsterlee, B., Hug, F., & Dick, T. J. M. (2021). Quantity versus quality : Age-related differences in muscle volume, intramuscular fat, and mechanical properties in the triceps surae. *Experimental Gerontology*, *156*, 111594. https://doi.org/10.1016/j.exger.2021.111594

Powell, P. L., Roy, R. R., Kanim, P., Bello, M. A., & Edgerton, V. R. (1984). Predictability of skeletal muscle tension from architectural determinations in guinea pig hindlimbs. *Journal of Applied Physiology*, *57*(6), 1715-1721. https://doi.org/10.1152/jappl.1984.57.6.1715

Powers, K., Schappacher-Tilp, G., Jinha, A., Leonard, T., Nishikawa, K., & Herzog, W. (2014). Titin force is enhanced in actively stretched skeletal muscle. *Journal of Experimental Biology*, *217*(20), 3629-3636. https://doi.org/10.1242/jeb.105361

Prilutsky, B. I., & Zatsiorsky, V. M. (2002). Optimization-based models of muscle coordination. *Exercise and sport sciences reviews*, *30*(1), 32.

Proske, U., & Morgan, D. L. (2001). Muscle damage from eccentric exercise : Mechanism, mechanical signs, adaptation and clinical applications. *The Journal of Physiology*, *537*(2), 333-345. https://doi.org/10.1111/j.1469-7793.2001.00333.x

Raiteri, B. J., Cresswell, A. G., & Lichtwark, G. A. (2016). Three-dimensional geometrical changes of the human tibialis anterior muscle and its central aponeurosis measured with three-dimensional ultrasound during isometric contractions. *PeerJ*, *4*, e2260. https://doi.org/10.7717/peerj.2260

Rajagopal, A., Dembia, C. L., DeMers, M. S., Delp, D. D., Hicks, J. L., & Delp, S. L. (2016). Full-Body Musculoskeletal Model for Muscle-Driven Simulation of Human Gait. *IEEE Transactions on Biomedical Engineering*, *63*(10), 2068-2079. https://doi.org/10.1109/TBME.2016.2586891

Rana, M., Hamarneh, G., & Wakeling, J. M. (2013). 3D fascicle orientations in triceps surae. *Journal of Applied Physiology (Bethesda, Md.: 1985)*, *115*(1), 116-125. https://doi.org/10.1152/japplphysiol.01090.2012

Rana, M., Hamarneh, G., & Wakeling, J. M. (2014). 3D curvature of muscle fascicles in triceps surae. *Journal of Applied Physiology*, *117*(11), 1388-1397. https://doi.org/10.1152/japplphysiol.00109.2013

Rassier, D. E., MacIntosh, B. R., & Herzog, W. (1999). Length dependence of active force production in skeletal muscle. *Journal of applied physiology*, *86*(5), 1445-1457.

Reeves, N. D., & Narici, M. V. (2003). Behavior of human muscle fascicles during shortening and lengthening contractions in vivo. *Journal of Applied Physiology*, *95*(3), 1090-1096. https://doi.org/10.1152/japplphysiol.01046.2002

Rice, C. L., Cunningham, D. A., Taylor, A. W., & Paterson, D. H. (1988). Comparison of the histochemical and contractile properties of human triceps surae. *European Journal of Applied Physiology and Occupational Physiology*, *58*(1), 165-170. https://doi.org/10.1007/BF00636621

Roberts, T. J. (1997). Muscular Force in Running Turkeys : The Economy of Minimizing Work. *Science*, *275*(5303), 1113-1115. https://doi.org/10.1126/science.275.5303.1113

Roberts, T. J. (2002). The integrated function of muscles and tendons during locomotion. *Comparative Biochemistry and Physiology Part A: Molecular & Integrative Physiology*, *133*(4), 1087-1099. https://doi.org/10.1016/S1095-6433(02)00244-1

Roberts, T. J., & Azizi, E. (2011). Flexible mechanisms : The diverse roles of biological springs in vertebrate movement. *Journal of Experimental Biology*, *214*(3), 353-361. https://doi.org/10.1242/jeb.038588

Roberts, T. J., & Konow, N. (2013). How tendons buffer energy dissipation by muscle. *Exercise and sport sciences reviews*, *41*(4), 10.1097/JES.0b013e3182a4e6d5. https://doi.org/10.1097/JES.0b013e3182a4e6d5

Roberts, T. J., Kram, R., Weyand, P. G., & Taylor, C. R. (1998). Energetics of bipedal running. I. Metabolic cost of generating force. *Journal of Experimental Biology*, *201*(19), 2745-2751. https://doi.org/10.1242/jeb.201.19.2745

Rockenfeller, R., Günther, M., & Hooper, S. L. (2022). Muscle active force-length curve explained by an electrophysical model of interfilament spacing. *Biophysical Journal*, *121*(10), 1823-1855.

Rodriguez-Falces, J., Negro, F., & Farina, D. (2017). Correlation between discharge timings of pairs of motor units reveals the presence but not the proportion of common synaptic input to motor neurons. *Journal of Neurophysiology*, *117*(4), 1749-1760. https://doi.org/10.1152/jn.00497.2016

Röhrle, O., Davidson, J., & Pullan, A. (2012). A Physiologically Based, Multi-Scale Model of Skeletal Muscle Structure and Function. *Frontiers in Physiology*, *3*. https://www.frontiersin.org/articles/10.3389/fphys.2012.00358

Rossato, J., Tucker, K., Avrillon, S., Lacourpaille, L., Holobar, A., & Hug, F. (2022). Less common synaptic input between muscles from the same group allows for more flexible coordination strategies during a fatiguing task. *Journal of Neurophysiology*, *127*(2), 421-433. https://doi.org/10.1152/jn.00453.2021

Roy, R. R., Meadows, I. D., Baldwin, K. M., & Edgerton, V. R. (1982). Functional significance of compensatory overloaded rat fast muscle. *Journal of Applied Physiology*, *52*(2), 473-478. https://doi.org/10.1152/jappl.1982.52.2.473

Rubenson, J., Pires, N. J., Loi, H. O., Pinniger, G. J., & Shannon, D. G. (2012). On the ascent : The soleus operating length is conserved to the ascending limb of the force-length curve across gait mechanics in humans. *Journal of Experimental Biology*, *215*(20), 3539-3551. https://doi.org/10.1242/jeb.070466

Rutherford, O. M., & Jones, D. A. (1992). Measurement of fibre pennation using ultrasound in the human quadriceps in vivo. *European Journal of Applied Physiology and Occupational Physiology*, *65*(5), 433-437. https://doi.org/10.1007/BF00243510

Sandercock, T. G., & Heckman, C. J. (1997). Force from cat soleus muscle during imposed locomotor-like movements : Experimental data versus Hill-type model predictions. *Journal of neurophysiology*, *77*(3), 1538-1552. https://doi.org/10.1152/jn.1997.77.3.1538

Sawicki, G. S., Robertson, B. D., Azizi, E., & Roberts, T. J. (2015). Timing matters : Tuning the mechanics of a muscle–tendon unit by adjusting stimulation phase during cyclic contractions. *Journal of Experimental Biology*, *218*(19), 3150-3159. https://doi.org/10.1242/jeb.121673

Schmitt, S., Günther, M., & Häufle, D. F. B. (2019). The dynamics of the skeletal muscle : A systems biophysics perspective on muscle modeling with the focus on Hill-type muscle models. *GAMM-Mitteilungen*, *42*(3), e201900013. https://doi.org/10.1002/gamm.201900013

Scovil, C. Y., & Ronsky, J. L. (2006). Sensitivity of a Hill-based muscle model to perturbations in model parameters. *Journal of Biomechanics*, *39*(11), 2055-2063. https://doi.org/10.1016/j.jbiomech.2005.06.005

Secher, N. H., Rube, N., & Secher, O. (1982). Effect of Tubocurarine on Human Soleus and Gastrocnemius Muscles. *Acta Anaesthesiologica Scandinavica*, *26*(3), 231-234. https://doi.org/10.1111/j.1399-6576.1982.tb01760.x

Segal, R. L., & Song, A. W. (2005). Nonuniform Activity of Human Calf Muscles During an Exercise Task. *Archives of Physical Medicine and Rehabilitation*, *86*(10), 2013-2017. https://doi.org/10.1016/j.apmr.2005.04.012

Segal, R. L., Wolf, S. L., DeCamp, M. J., Chopp, M. T., & English, A. W. (1991). Anatomical Partitioning of Three Multiarticular Human Muscles. *Cells Tissues Organs*, *142*(3), 261-266. https://doi.org/10.1159/000147199

Seireg, A., & Arvikar, R. J. (1973). A mathematical model for evaluation of forces in lower extremeties of the musculo-skeletal system. *Journal of Biomechanics*, *6*(3), 313-326. https://doi.org/10.1016/0021-9290(73)90053-5

Seireg, A., & Arvikar, R. J. (1975). The prediction of muscular load sharing and joint forces in the lower extremities during walking. *Journal of Biomechanics*, *8*(2), 89-102. https://doi.org/10.1016/0021-9290(75)90089-5

Seynnes, O. R., & Cronin, N. J. (2020). Simple Muscle Architecture Analysis (SMA) : An ImageJ macro tool to automate measurements in B-mode ultrasound scans. *PLOS ONE*, *15*(2), e0229034. https://doi.org/10.1371/journal.pone.0229034

Shao, Q., Bassett, D. N., Manal, K., & Buchanan, T. S. (2009). An EMG-driven model to estimate muscle forces and joint moments in stroke patients. *Computers in Biology and Medicine*, *39*(12), 1083-1088. https://doi.org/10.1016/j.compbiomed.2009.09.002

Sherrington, C. S. (1906). *The integrative action of the nervous system* (Vol. 35). Yale University Press.

Slane, L. C., Martin, J., DeWall, R., Thelen, D., & Lee, K. (2017). Quantitative ultrasound mapping of regional variations in shear wave speeds of the aging Achilles tendon. *European radiology*, *27*(2), 474-482. https://doi.org/10.1007/s00330-016-4409-0

Slane, L. C., & Thelen, D. G. (2015). Achilles tendon displacement patterns during passive stretch and eccentric loading are altered in middle-aged adults. *Medical Engineering & Physics*, *37*(7), 712-716. https://doi.org/10.1016/j.medengphy.2015.04.004

Solomonow, M., Baratta, R., Bernardi, M., Zhou, B., Lu, Y., Zhu, M., & Acierno, S. (1994). Surface and wire EMG crosstalk in neighbouring muscles. *Journal of Electromyography and Kinesiology*, *4*(3), 131-142.

Souza de Oliveira, D., Casolo, A., Balshaw, T. G., Maeo, S., Bahia Lanza, M., Martin, N. R. W., Maffulli, N., Kinfe, T. M., Eskofier, B., Folland, J. P., Farina, D., & Del Vecchio, A. (2022). *Neural decoding from surface high-density EMG signals : Influence of anatomy and synchronization on the number of identified motor units* [Preprint]. Bioengineering. https://doi.org/10.1101/2022.02.05.479100

Spector, S. A., Gardiner, P. F., Zernicke, R. F., Roy, R. R., & Edgerton, V. R. (1980). Muscle architecture and force-velocity characteristics of cat soleus and medial gastrocnemius : Implications for motor control. *Journal of Neurophysiology*, *44*(5), 951-960. https://doi.org/10.1152/jn.1980.44.5.951

Spoor, C. W., van Leeuwen, J. L., Meskers, C. G. M., Titulaer, A. F., & Huson, A. (1990). Estimation of instantaneous moment arms of lower-leg muscles. *Journal of Biomechanics*, *23*(12), 1247-1259. https://doi.org/10.1016/0021-9290(90)90382-D

Stegeman, D., & Hermens, H. (2007). Standards for surface electromyography : The European project Surface EMG for non-invasive assessment of muscles (SENIAM). *Enschede: Roessingh Research and Development*, *10*, 8-12.

Stenroth, L., Peltonen, J., Cronin, N. J., Sipilä, S., & Finni, T. (2012). Age-related differences in Achilles tendon properties and triceps surae muscle architecture in vivo. *Journal of Applied Physiology*, *113*(10), 1537-1544. https://doi.org/10.1152/japplphysiol.00782.2012

Stienen, G. J., Kiers, J. L., Bottinelli, R., & Reggiani, C. (1996). Myofibrillar ATPase activity in skinned human skeletal muscle fibres : Fibre type and temperature dependence. *The Journal of Physiology*, *493*(2), 299-307. https://doi.org/10.1113/jphysiol.1996.sp021384

Sun, Y.-L., Wei, Z., Zhao, C., Jay, G. D., Schmid, T. M., Amadio, P. C., & An, K.-N. (2015). Lubricin in human achilles tendon : The evidence of intratendinous sliding motion and shear force in achilles tendon. *Journal of Orthopaedic Research: Official Publication of the Orthopaedic Research Society*, *33*(6), 932-937. https://doi.org/10.1002/jor.22897

Szaro, P., Cifuentes Ramirez, W., Borkmann, S., Bengtsson, A., Polaczek, M., & Ciszek, B. (2020). Distribution of the subtendons in the midportion of the Achilles tendon revealed in vivo on MRI. *Scientific Reports*, *10*(1), 16348. https://doi.org/10.1038/s41598-020-73345-0

Szaro, P., Witkowski, G., Smigielski, R., Krajewski, P., & Ciszek, B. (2009). Fascicles of the adult human Achilles tendon—An anatomical study. *Annals of Anatomy = Anatomischer Anzeiger: Official Organ of the Anatomische Gesellschaft*, *191*(6), 586-593. https://doi.org/10.1016/j.aanat.2009.07.006

Tickle, P. G., Richardson, M. F., & Codd, J. R. (2010). Load carrying during locomotion in the barnacle goose (Branta leucopsis) : The effect of load placement and size. *Comparative Biochemistry and Physiology Part A: Molecular & Integrative Physiology*, *156*(3), 309-317.

Tresch, M. C., & Bizzi, E. (1999). Responses to spinal microstimulation in the chronically spinalized rat and their relationship to spinal systems activated by low threshold cutaneous stimulation. *Experimental Brain Research*, *129*(3), 401-416. https://doi.org/10.1007/s002210050908

Tucker, K., Butler, J., Graven-Nielsen, T., Riek, S., & Hodges, P. (2009). Motor unit recruitment strategies are altered during deep-tissue pain. *Journal of Neuroscience*, *29*(35), 10820-10826.

van Ingen Schenau, G. J., Bobbert, M. F., & Rozendal, R. H. (1987). The unique action of bi-articular muscles in complex movements. *Journal of Anatomy*, *155*, 1-5.

van Ingen Schenau, G. J., Bobbert, M. F., & van Soest, A. J. (1990). The Unique Action of Bi-Articular Muscles in Leg Extensions. In J. M. Winters & S. L.-Y. Woo (Éds.), *Multiple*

*Muscle Systems : Biomechanics and Movement Organization* (p. 639-652). Springer. https://doi.org/10.1007/978-1-4613-9030-5_41

van Ingen Schenau, G. J., Dorssers, W. M., Welter, T. G., Beelen, A., de Groot, G., & Jacobs, R. (1995). The control of mono-articular muscles in multijoint leg extensions in man. *The Journal of Physiology*, *484*(1), 247-254. https://doi.org/10.1113/jphysiol.1995.sp020662

Vieira, T. M. M., Loram, I. D., Muceli, S., Merletti, R., & Farina, D. (2011). Postural activation of the human medial gastrocnemius muscle : Are the muscle units spatially localised? *The Journal of Physiology*, *589*(Pt 2), 431-443. https://doi.org/10.1113/jphysiol.2010.201806

Vieira, T. M. M., Minetto, M. A., Hodson-Tole, E. F., & Botter, A. (2013). How much does the human medial gastrocnemius muscle contribute to ankle torques outside the sagittal plane? *Human Movement Science*, *32*(4), 753-767. https://doi.org/10.1016/j.humov.2013.03.003

Wakeling, J. M., Lee, S. S. M., Arnold, A. S., de Boef Miara, M., & Biewener, A. A. (2012). A Muscle's Force Depends on the Recruitment Patterns of Its Fibers. *Annals of Biomedical Engineering*, *40*(8), 1708-1720. https://doi.org/10.1007/s10439-012-0531-6

Walmsley, B., Hodgson, J. A., & Burke, R. E. (1978). Forces produced by medial gastrocnemius and soleus muscles during locomotion in freely moving cats. *Journal of Neurophysiology*, *41*(5), 1203-1216. https://doi.org/10.1152/jn.1978.41.5.1203

Wang, K., McClure, J., & Tu, A. (1979). Titin : Major myofibrillar components of striated muscle. *Proceedings of the National Academy of Sciences*, *76*(8), 3698-3702. https://doi.org/10.1073/pnas.76.8.3698

Ward, S. R., Eng, C. M., Smallwood, L. H., & Lieber, R. L. (2009). Are Current Measurements of Lower Extremity Muscle Architecture Accurate? *Clinical Orthopaedics and Related Research*, *467*(4), 1074-1082. https://doi.org/10.1007/s11999-008-0594-8

Watanabe, K., Kouzaki, M., & Moritani, T. (2016). Regional neuromuscular regulation within human rectus femoris muscle during gait in young and elderly men. *Journal of Biomechanics*, *49*(1), 19-25.

Watanabe, K., Vieira, T. M., Gallina, A., Kouzaki, M., & Moritani, T. (2021a). Novel Insights Into Biarticular Muscle Actions Gained From High-Density Electromyogram. *Exercise and Sport Sciences Reviews*, *49*(3), 179-187. https://doi.org/10.1249/JES.0000000000000254

Watanabe, K., Vieira, T. M., Gallina, A., Kouzaki, M., & Moritani, T. (2021b). Novel Insights Into Biarticular Muscle Actions Gained From High-Density Electromyogram. *Exercise and Sport Sciences Reviews*, *49*(3), 179-187. https://doi.org/10.1249/JES.0000000000000254

Weng, L., Tirumalai, A. P., Lowery, C. M., Nock, L. F., Gustafson, D. E., Von Behren, P. L., & Kim, J. H. (1997). US extended-field-of-view imaging technology. *Radiology*, *203*(3), 877-880.

Wickiewicz, Rr, R., Pl, P., & Vr, E. (1983). Muscle architecture of the human lower limb. *Clinical Orthopaedics and Related Research*, *179*, 275-283.

Williams, C. D., Salcedo, M. K., Irving, T. C., Regnier, M., & Daniel, T. L. (2013). The length–tension curve in muscle depends on lattice spacing. *Proceedings of the Royal Society B: Biological Sciences*, *280*(1766), 20130697. https://doi.org/10.1098/rspb.2013.0697

Wilson, A. M., Watson, J. C., & Lichtwark, G. A. (2003). A catapult action for rapid limb protraction. *Nature*, *421*(6918), Art. 6918. https://doi.org/10.1038/421035a

Winter, D. A. (2009). *Biomechanics and motor control of human movement*. John Wiley & Sons.

Witvrouw, E., Callaghan, M. J., Stefanik, J. J., Noehren, B., Bazett-Jones, D. M., Willson, J. D., Earl-Boehm, J. E., Davis, I. S., Powers, C. M., McConnell, J., & Crossley, K. M. (2014). Patellofemoral pain : Consensus statement from the 3rd International Patellofemoral Pain Research Retreat held in Vancouver, September 2013. *British Journal of Sports Medicine*, *48*(6), 411-414. https://doi.org/10.1136/bjsports-2014-093450

Wolf, S. L., & Kim, J. H. (1997). Morphological Analysis of the Human Tibialis Anterior and Medial Gastrocnemius Muscles. *Cells Tissues Organs*, *158*(4), 287-295. https://doi.org/10.1159/000147942

Wolf, S. L., Segal, R. L., & English, A. W. (1993). Task-oriented EMG activity recorded from partitions in human lateral gastrocnemius muscle. *Journal of Electromyography and Kinesiology*, *3*(2), 87-94. https://doi.org/10.1016/1050-6411(93)90003-F

Wolfram, S. (2017). *Differential behaviour of the medial and lateral heads of gastrocnemius during plantarflexion : The effect of calcaneal inversion and eversion* [Doctoral, Manchester Metropolitan University]. http://e-space.mmu.ac.uk/618921/

Wolfram, S., Hodson-Tole, E. F., Morse, C. I., Winwood, K. L., & McEwan, I. M. (2020). Elongation differences between the sub-tendons of gastrocnemius medialis and lateralis during plantarflexion in different frontal plane position of the foot. *Gait & Posture*, *75*, 149-154. https://doi.org/10.1016/j.gaitpost.2019.10.020

Yin, N.-H., Fromme, P., McCarthy, I., & Birch, H. L. (2021). Individual variation in Achilles tendon morphology and geometry changes susceptibility to injury. *eLife*, *10*, e63204. https://doi.org/10.7554/eLife.63204

Yushkevich, P. A., Piven, J., Hazlett, H. C., Smith, R. G., Ho, S., Gee, J. C., & Gerig, G. (2006). User-guided 3D active contour segmentation of anatomical structures : Significantly improved efficiency and reliability. *NeuroImage*, *31*(3), 1116-1128. https://doi.org/10.1016/j.neuroimage.2006.01.015

Zajac, F. E. (1989). Muscle and tendon : Properties, models, scaling, and application to biomechanics and motor control. *Critical Reviews in Biomedical Engineering*, *17*(4), 359-411.

COLLEGE DOCTORAL PAYS DE LA LOIRE
ED EDUCATION, COGNITION, LANGAGES, INTERACTIONS, SANTE
Nantes Université

**Titre :** Une approche neuromécanique de la coordination entre les muscles *gastrocnemius medialis* et *gastrocnemius lateralis*

**Mots clés :** Distribution de la force ; Echographie B-mode ; Electromyographie de surface ; Modèle de Hill ; Neuromécanique ; Triceps Surae.

**Résumé :** Les différences fonctionnelles entre le *gastrocnemius medialis* et le *gastrocnemius lateralis* sont rarement étudiées. De plus, la majorité des recherches s'intéressant à ces deux muscles se sont focalisées sur leur rôle lors de la flexion plantaire de cheville. Ainsi, leur fonction secondaire de flexion du genou reste mal comprise. L'objectif de cette thèse est d'apporter une meilleure compréhension de la coordination musculaire entre le *gastrocnemius medialis* et le *gastrocnemius lateralis*. Nous avons utilisé une approche qui combine des mesures expérimentales et de la modélisation musculaire pour étudier les coordinations musculaires à différents niveaux, de l'unité motrice individuelle au muscle. Quatre principaux résultats peuvent être tirés de cette thèse. Premièrement, ces deux muscles ont des comportements neuromusculaires distincts lors de la marche qui induisent une production de force accrue du *gastrocnemius medialis* par rapport au *gastrocnemius lateralis.* Deuxièmement, nous avons observé une grande variabilité inter-individuelle à tous les niveaux du mouvement. Troisièmement, la modèlisation musculaire utilisant des données spécifiques aux sujets semble pertinente pour explorer la variabilité inter-individuelle. Quatrièmement, le contrôle nerveux du *gastrocnemius medialis* et du *gastrocnemius lateralis* est similaire entre la flexion de genou et la flexion plantaire de cheville.
Pris dans leur ensemble, ces résultats démontrent que ces deux muscles sont distincts, tant au niveau nerveux que biomécanique. Cela conduit à des productions de force différentes et une grande variabilité inter-individuelle.

**Title :** A neuromechanical approach to the coordination between the human *gastrocnemius medialis* and *gastrocnemius lateralis* muscles

**Keywords :** B-mode ultrasonography; Hill-type model; Muscle force distribution; Neuromechanics; Surface electromyography; *Triceps surae*.

**Abstract :** The functional differences between the *gastrocnemius medialis* and *gastrocnemius lateralis* are rarely studied. In addition, the large majority of previous research on these two muscles has focused on their ankle plantar flexion role. Their secondary role, i.e. knee flexion, remains therefore poorly understood. The aim of this thesis was to provide a deeper understanding of muscle coordination between the *gastrocnemius medialis* and *gastrocnemius lateralis*. We used an approach that combines experimental measures and basic muscle modelling to explore muscle coordination across multiple scales, from the individual motor unit to the whole muscle.
Four main results can be derived from this thesis. First, these two muscles have distinct neuromuscular behavior during walking resulting in a higher production of force in the *gastrocnemius medialis* compared to the *gastrocnemius lateralis*. Second, a large inter-individual variability can be observed across multiples scales of the movement procution. Third, a modelling approach using subject-specific data appears useful to considere this inter-individual variability. Fourth, the neural control of the *gastrocnemius medialis* and *gastrocnemius lateralis* is robust across knee flexion and ankle plantar flexion.
Together, these results demonstrate that the two muscles are distinct at the neural and biomechanical level, which results in distinct force outputs and highly inter-individual variable muscle coordination.